PHYSICAL AND NUMERICAL MODELING TO EVALUATE ASD EXHAUST DESIGN FOR ACCEPTABLE RE-ENTRAINMENT AND DISPERSION IN HOUSES

by

Dr. David E. Neff

Dr. Robert N. Meroney

Dr. Hesham El-Badry

for

Dr. Bruce Henschel, AEERL

Environmental Protection Agency

Air and Energy Engineering Research Laboratory

Research Triangle Park, NC 27711

FLUID MECHANICS AND WIND ENGINEERING PROGRAM

Colorado State University

CSU Contract No. 53-5912

CER93-94-DEN-RNM-HEB-4

March 1994

PHYSICAL AND NUMERICAL MODELING TO EVALUATE ASD EXHAUST DESIGN FOR ACCEPTABLE RE-ENTRAINMENT AND DISPERSION IN HOUSES

Prepared by

David E. Neff
Robert N. Meroney
Hesham El-Badry

FINAL REPORT
(March, 1994)

for

Dr. Bruce Henschel, AEERL
Environmental Protection Agency
Air and Energy Engineering Research Laboratory
Research Triangle Park, NC 27711

FLUID MECHANICS AND WIND ENGINEERING PROGRAM

Colorado State University

TABLE OF CONTENTS

LIST OF TABLES

LIST OF FIGURES

1 REPORT SUMMARY

Currently, EPA requires that mitigation exhaust for radon removal be discharged above the eave of a building to ensure that very little of the exhaust is re-entrained into the building, and to ensure that exposures are small to persons in the yard or neighboring buildings. This requirement often increases the cost, detracts aesthetically from the home, and can discourage some owners from installing a mitigation system. The objective of this study was to identify whether there are conditions under which the mitigation radon exhaust for typical homes can safely be released at grade level.

Drs. Bruce Henschel and Alan Huber of EPA requested Colorado State University staff to perform a wind tunnel measurement program designed to study the circulation of exhaust gases around typical suburban homes to determine if such changes are viable. And, secondly, to use the wind tunnel data to validate modules in analytic programs capable of providing a structure for parametric studies of mitigation exhaust dispersion. This report describes all work performed by Colorado State University staff.

A 1:35 scale model of four different typical suburban homes were constructed and tested in a wind tunnel facility. These tests, both visual and concentration measurements, covered four wind directions, three effluent to approach flow wind speed ratios, three release locations and 45 concentration sampling locations. The results from these tests determined that:

1) *Exhaust gases will recirculate heavily into the house wake for all three effluent sources tested whenever the stacks are located downwind of home's roof crest.*

2) *The at-grade wall release location usually leads to the highest building surface concentration values. The eave release location leads to somewhat higher concentrations than the roof release location.*

3) *Source strengths of 100 pCi/L produced concentrations greater than the design value of 1 pCi/L only for wall releases, and the maximum of these was only 1.4 pCi/L. Source strengths of 1000 pCi/L produced concentrations greater than design value of 1 pCi/L at sampling locations for all three effluent release locations.*

Full documentation of the testing is provided in this report. The organization of major topics discussed in this report are as follows:

Section 2	The fluid model design with discussion of the similarity criteria employed.
Section 3	Wind tunnel testing program and results documenting the stacks tested.
Section 4	Discussion of the instrumentation and measurement methodologies used.
Section 5	Comparison of the analytical models with the wind tunnel data.

2 FLUID MODEL DESIGN

Appendix D provides a technical discussion of general fluid model design techniques and provides a review of several fluid modeling validation studies. This section of the report addresses only specific scaling and modeling decisions appropriate for the current project.

2.1 SITE SPECIFICATIONS

A boundary layer wind tunnel fluid model was designed to assist in the mitigation of radon exhausts from typical homes. This 1:35 reduced scale model is a representation of:

1) four different generic suburban style homes; a one story home with roof slopes of 6:12 and 9:12, a two story home with roof slopes of 6:12 and 9:12,
2) generic roughness used to simulate the influence of adjacent structures within 70 meters of the site,
3) the atmospheric wind structure of interest approaching the site, and
4) the vent gas stack geometries and discharge characteristics.

Figures 1 through 4 show dimensioned drawings, in both field and model scale units, of the one story 6:12 roof slope house, one story 9:12 house, two story 6:12 house and the two story 9:12 house that were evaluated. Figures 5 and 6 are photographs of these four model homes. A model scale of 1:35 was selected with the assistance of Table 1 which lists important modeling dimensions and parameters for several different model scale ratios. Table 2 presents the same information as that in Table 1 but only for the chosen model scale ratio of 1:35.

2.2 BOUNDARY LAYER WIND TUNNEL CONFIGURATION

All model tests were performed in the Environmental Wind Tunnel (EWT) test facility at Colorado State University (CSU). This tunnel has a 3.66 m by 2.13 m cross-section, a 17.4 m length, a wind speed range of 0 to 15 m/s and a flexible test section roof. A description of this facility is provided in Appendix B Section 2. Appropriate boundary layer development techniques were utilized

to represent wind conditions approaching the suburban home site. The suburban home model was placed 13.6 meters from the start of the EWT's test section. This placement provides sufficient upwind fetch and a sufficient downwind measurement zone. The zone upwind of the turntable area was modeled with a generic roughness designed to create the desired model boundary layer. Eight 1.8 meter high vortex generators and an 18 cm floor trip were placed at the beginning of the EWT's test section.

The development of a suburban type boundary layer winds at a reduced scale of 1:35 required placement of a turbulence generating grid at the upwind edge of the model turntable. Figures 7 and 8 show a plan view and an elevation view of the wind tunnel turntable layout used for this project (note all units are model scale centimeters).

2.3 WIND SPEED VARIATION WITH HEIGHT SPECIFICATIONS

The variation of mean wind speed with height above the ground (referred to as the boundary layer) at the study site is deduced from empirical equations known to correlate atmospheric data. The log-linear velocity profile relationship should be used for heights up to 100 meters. This relationship is expressed as:

$U/u_* = 2.5*\ln[(z-d)/z_o]$; where

u_* ≡ friction velocity,

d ≡ displacement height,

z_o ≡ roughness length.

Several references suggested values of the roughness length for various types of ground cover. A roughness length of 0.2 to 0.4 meters (0.3 meters was chosen) is an appropriate value for all wind directions approaching a typical suburban site.

The mean velocity through the entire depth of the boundary layer is represented by the power law equation:

$U/U_\infty = (z/\delta)^p$; where

U ≡ mean wind speed at height z,

U_∞ ≡ wind speed at boundary layer height δ,

δ ≡ boundary layer height = 600 meters

p ≡ power law index.

A power law index of ~0.2 is an appropriate value for all wind directions approaching a typical suburban site.

2.4 WIND DIRECTION SPECIFICATIONS

Four wind directions, 0°, 45°, 90° and 180°, were chosen for study on each model suburban home. Considering the symmetries of the exhaust locations and building shape these primary wind directions should effectively map out the distribution of maximum concentrations.

2.5 EXHAUST SPECIFICATIONS

Three exhaust locations were studied; a 0.46m tall mid-roof location, a 0.3m tall at eave location and a 0.76m above grade wall location. Each of these stacks have a 0.1016m inside diameter. Figure 1 through Figure 6 show the different house shapes studied and the location of these three stacks on each building. Exhaust exit velocities ranging from 1.25 m/s to 5.84 m/s were studied. Figure 9 assists in showing the combination of exit velocities and approach flow velocities that were performed in this study.

2.6 WIND SPEED SPECIFICATIONS

Since all tests were for a neutrally buoyant plume in a neutral atmospheric stability each model test condition can be scaled to any field condition where velocity ratio equality (exhaust to approach flow, W/U) is maintained. To cover a wide range of exhaust velocities and approach flow wind speeds three W/U velocity ratios were studied, 0.25, 1.0 and 2.5. Figure 9 assists in showing the combination of exit velocities and approach flow velocities that this parameter range covered. A model testing wind speed of 400 cm/s at the equivalent field height of ten meters was selected. The model Reynolds number based on building height and wind speed was always greater than 11,000. Table 2 presents a summary of the important scaling parameter values used in this study.

3 FLUID MODEL TEST PROGRAM

3.1 WIND PROFILE MEASUREMENTS

The approach flow velocity and turbulence were to be similar to atmospheric flow over suburban type roughness conditions. Table 6 lists typical velocity and turbulence profile data from atmospheric correlations over suburban sites. Table 7 lists the model design values of these atmospheric correlations. To document the fluid model's approach flow six velocity and turbulence profiles were measured. Three of these were lateral to each other at 50 cm upwind of model center. The other three were lateral to each other at 100 cm downwind of model center. Table 3 lists the run conditions for these tests (run numbers A1-A6). Figure 13 graphically displays these velocity and turbulence profiles on linear coordinates. Figure 14 graphically displays the velocity profiles on log coordinates. Also shown in these figures are model design curves from Table 7 of typical suburban conditions.

To document the fluid model's approach flow Reynolds number invariance three velocity and turbulence profile, each at a different wind speed, were measured. Table 3 lists the run conditions for these tests (run numbers B1-B3). Figure 15 graphically displays these velocity and turbulence profiles on linear coordinates. Figure 16 graphically displays the velocity profiles on log coordinates. Also shown in these figures are model design curves from Table 7 of typical suburban conditions.

The wind tunnel reference velocity of 400 cm/s at a model height of 28.6 cm (ten meter field height) was set via a correlation between a pitot probe, 1.5 meters above model center, and measured velocities at 28.6 cm above model ground level at model center. The building model was removed during these measurements and the turntable was in the north position. Subsequent tunnel velocity settings were adjusted via the pitot probe which was present in all tests.

3.2 STACK PLUME VISUALIZATION

Flow visualization of the effluent plume motion for 96 different conditions (32 runs with each run showing 3 different release locations) was documented on the video cassette VHS tape and

included with this report in Appendix A. The run conditions specifications for these visual tests are listed as Run No. Series C in Table 3.

The camera position for runs with a wind direction of 0°, 45° and 90° was 45° away from looking upwind. The camera position for runs with a wind direction of 180° was 45° away from looking downwind. The film test observes the plume trajectories from the model stacks in the vicinity of the building only, and zooms in on each stack to document downwash and near stack plume rise characteristics.

3.3 CONCENTRATION MEASUREMENTS

3.3.1 *Atmospheric Dispersion Comparability Tests*

To document atmospheric dispersion comparability a passive ground level source was placed 100 cm upwind of the model center position. The model house was removed and the concentration sampling grid depicted in Figure 10 was placed into the wind tunnel. The run conditions for this test are listed in Table 3 (run number A7). The results from this test along with Pasquill-Gifford dispersion category calculations are shown in Tables 9 and 10 for urban and open conditions respectively. The urban condition is appropriate for near field releases into a suburban boundary layer. Figures 17 through 20 present plume profile comparisons to the Pasquill-Gifford urban dispersion model. These figures demonstrate that the model boundary layer is changing with downwind distance but that at the model position the appropriate Pasquill-Gifford C-D category is obtained.

3.3.2 *Reynolds Number Invariance Tests*

To demonstrate that the model suburban houses were Reynolds number invariant a series of three concentration tests, each at a different wind speed, were performed. The run conditions for these tests are listed in Table 3 (run number B4-B6). The results from these tests are listed in Table 8. This table also lists the error in field normalized concentration, K_p, that existed between these runs. At concentration locations where the plume is not highly intermittent the errors in K_p are generally acceptable.

3.3.3 *ASD Exhaust Release Tests*

Concentration measurements were obtained at 45 sample locations for 144 different run conditions. The sampling locations located on the building surface are shown in Figure 11. The sampling locations located downwind of the building are shown in Figure 12. The run condition specifications for all 144 runs are listed in Table 4 for the one story houses and Table 5 for the two story houses. Table 11a through Table 11p lists the concentration data in normalized field concentrations, $K_p = (\chi U_H/Q)_p$ [m^{-2}]. Figure 21a through Figure 21p display bar charts comparing the release location's influence on concentration patterns for all test runs. Figure 22 displays bar charts comparing the influence of building shape on concentration patterns for selected run conditions. Figure 23 displays bar charts comparing the influence of exit velocity ratio on concentration patterns for selected run conditions. Figure 24 displays bar charts comparing the influence of wind direction on concentration patterns for selected run conditions. Note that the values in these tables and figures are K_p*10^4.

To determine sample concentration, χ, in pCi/L for different source strengths, Q_{ss}, in pCi/L the following equation was used χ [pCi/L] = (K_p[m^{-2}])*(W/U_H)*(Area[m^2])*(Q_{ss}[pCi/L]) where "Area" is the cross-sectional area of the exhaust pipe. Table 12 lists the maximum concentrations observed at each sample location over all 48 conditions tested (4 house shapes, 4 wind directions, 3 W/U ratios). Listings for both 100 pCi/L and 1000 pCi/L are present. Whenever the maximum concentration was below the atmospheric background value of 0.4 pCi/L an entry of --BG-- was placed into the table. Figure 25 displays a bar chart comparing the release location's influence on maximum observed concentration.

4 INSTRUMENTATION AND MEASUREMENT METHODOLOGY

An overview of laboratory measurement techniques along with conversion methods used to convert measured model quantities to their meaningful field equivalents are discussed in this section. Appendix B provides a detailed discussion of the laboratory and measurement methods commonly employed.

4.1 VELOCITY MEASUREMENT AND PRESENTATION

The techniques employed in the acquisition of velocity profiles are discussed in detail in Appendix B Section 3 including basic equations and errors associated with each technique. Single-hot-film (TSI 1220 Sensor) and pitot-static probes are used to measure velocity statistics. TSI 1125 Velocity Calibrator System and Pitot-static Probes are used for velocity calibration.

The approach mean velocity and turbulent statistics profiles are obtained from velocity measurement techniques. The approach mean velocity profiles for a suburban roughness condition are regressed to find the best log-log and log-linear fit. The log-log regression will find a power law exponent, p, such that $U/U_r = (z/z_r)^p$. The log-linear regression ($U/u_* = 2.5\ln\{(z-d)/z_o\}$) will find a best fit roughness length z_o, friction velocity u_*, and displacement height d.

Velocity measurements obtained in this study are summarized and presented through plots of vertical profiles of mean velocity and longitudinal turbulence intensity. The velocity coordinates are normalized by a reference model velocity at the reference height. Since a neutral boundary layer's velocity is invariant with respect to wind speed, the normalized profiles can be converted to any field velocity at a specific height by the appropriate multiplicative constant. Each of the vertical profiles of mean velocity are plotted on linear-linear and log-linear paper to display the best fit regressions.

4.2 PLUME VISUALIZATION TECHNIQUES

Techniques employed to obtain a visible plume are discussed in Appendix B Section 4. A Smoke Generator System and a Video Camera System are used for plume visualization. Phenomena observed over the model in the wind tunnel will occur faster than that observed at full scale. As an example assume a field to model wind speed ratio of say 0.5 (=[2m/s]/[4m/s]) and a model to field length scale ratio of 35, then the time scale ratio between the model and the field is 1:70. If the TV tapes were replayed in slow motion (70 times slower than the recorded speed) the observed plume trajectories and motions would appear realistic.

4.3 CONCENTRATION MEASUREMENT AND PRESENTATION

Techniques employed to obtain the concentration data are discussed in Appendix B Section 5. A gas chromatograph with flame ionization detector is used to measure gas concentrations. Concentration data are reported in terms of field scale normalized concentration, K_p, where $K_p = (\chi U_H/Q)_p$ [m^{-2}]. This normalized format is convenient because the concentration results, χ_p [gm/m^3], from a test at one particular combination of wind speed, $(U_H)_p$ [m/s], and source mass flow rate, Q_p [gm/sec], can be extrapolated to other $(U_H)_p$ and Q_p values provided that flow physics, such as plume rise, remains the same. $(U_H)_p$ is the field wind speed at the reference height, H. The conversion from model units to field units is as follows:

$K_p = K_m * (H_m/H_p)^2$ [m^{-2}]; with $K_m = (\chi U_H/Q)_m$ [cm^{-2}].

χ_m is the source normalized model concentration ($ppm/10^6 ppm$),

$(U_H)_m$ [cm/s] is model wind speed at reference height,

Q_m [ccs] is the model stack flow rate,

H_m [cm] is the model reference height, and

H_p [m] is the field reference height.

4.4 STACK FLOW RATE AND COMPOSITION TECHNIQUES

An Omega mass flow controlling system was used to monitor and control some of the stack gas flow settings. This system has four mass flow channels with full scale responses of 0.1, 1, 10, and 100 SLPM for gases with unity gas factors. Different gases will have different gas factors, and this must be taken into account when calculating the proper meter setting. The local atmospheric pressure (~631 mmHg at CSU) must also be accounted for in these calculations.

During a visual plume test the proper plume flow rate and specific gravity would be attained by mixing metered quantities of Air (SG = 1) and Helium (SG = 0.14) or Argon (SG = 1.38). This gas mixture is then passed through the smoke generator and then out the model stack. During a plume concentration test a hydrocarbon gas must be in the source mixture so that measurements of sample concentration can be made with a flame ionization type gas chromatograph. Depending upon experimental considerations, such as plume buoyancy, background concentrations, and range of anticipated diffusion, a hydrocarbon, such as methane (SG = 0.55), ethane (SG = 1.04), or propane (SG = 1.52) will be mixed with helium (SG = 0.14), nitrogen (SG = 0.967), or argon (SG = 1.38). This mixture is passed directly into the model stack.

Since only neutrally buoyant plumes were studied the gas used for all visual testing was 100% air tagged with smoke. The gas used for all concentration tests was 100% ethane.

5 BUILDING DOWNWASH MODELING

The concentration field produced by a source located near the ground in the vicinity of buildings can be significantly modified from that predicted by conventional diffusion formulae. Such formulae contain the implicit assumptions that the flow field has straight parallel streamlines, modest velocity gradients, and distributions of turbulence energy and length scales which result from surface features that remain unchanged over long distances. Near buildings the flow field becomes highly complex. Curved streamlines, sharp velocity discontinuities, and non-homogeneous turbulence disperse effluents in a complicated manner related to source configuration and building geometry.

In the immediate lee of the building, there is a cavity region where recirculation occurs, mean velocities are reduced and the air flow is highly turbulent. The flow in the building wake farther downstream is characterized by a high turbulence intensity and mean velocity deficit that decay to background levels. The complex flow patterns induced by the building prohibit reliable determination of air quality concentrations close to buildings through the use of the basic Gaussian plume model and associated dispersion parameters without substantial modification (Huber, 1991; Huber 1984; Schulman and Scire 1993). General reviews of experimental data and mathematical models have been prepared, among others, by Meroney (1982) and Hosker (1985).

Different models were suggested for calculating the concentration in near-wake (the recirculation cavity) and in the far-wake downstream the building. In this report the Schulman and Scire model (1993) was used to predict the concentration in the near-wake, and the Huber and Snyder model (1982) was used to calculate the far-wake concentrations.

5.1 ESTIMATION OF CONCENTRATION IN THE RECIRCULATION CAVITY

In this section the Schulman and Scire (1991,1993) models to predict concentrations in the near wake (recirculation cavity) will be discussed and compared to the wind tunnel data.

5.1.1 *Background*

Schulman and Scire (1991) suggested a model that estimates the concentrations at the building roof, downwind wall and near wake recirculation cavity for winds perpendicular to the building sides. They suggest another model (Schulman and Scire, 1993) for estimating concentrations in the recirculation cavity for winds perpendicular to the building sides.

Figure 26 illustrates the flow over an isolated building and the capture of plume material by the downwind recirculation cavity.

The first model (Schulman and Scire, 1991) computed a total concentration by considering separately the contribution of the portions of the plume below and above the high turbulence region.

$$\chi = f_1 C_1 + f_2 C_2$$

where f_1 and f_2 are the fractions of the plume below and above the high turbulence region,

$$C_1 = \frac{B_o Q}{Us^2}$$

and

$$C_2 = \frac{B_o Q}{Us^2} e^{-(Hs-H+\Delta h)^2/2\sigma_z^2} \qquad \textit{for roof receptors}$$

$$C_2 = \frac{B_o Q}{Us^2} e^{-(Hs+\Delta h)^2/2\sigma_z^2} \qquad \textit{for ground-level receptors}$$

where B_o is an empirical constant approximately equal to 16 (ASHRAE, 1989), s is the stretched string distance between stack base and receptor, and the vertical dispersion coefficient σ_z is

$$\sigma_z = 0.21\ R^{0.25} x^{0.75}$$

Schulman and Scire (1993) suggest another model which computes the ground-level concentration in the down-wind recirculation cavity by considering the fraction of the plume below the cavity height H_R.

$$\chi = f_c C_c$$

with

$$C_c = \frac{B_o Q}{B_o w_o A_o + U s^2}$$

where f_c is the portion of the plume below H_R at the end of the cavity, w_o is the exhaust speed from the stack and A_o is the stack or exit face area.

5.1.2 *Model Comparison With Wind Tunnel Data*

Thirty six runs of the Schulman and Scire (1993) model were made for each combination of stack location (roof, eave and wall), wind direction (0°, 45° and 90°) (i.e. 180° wind direction was not calculated using the model since the concentrations were at back-ground level), and building dimensions (one-story 6:12, one-story 9:12, two-story 6:12 and two-story 9:12). The stretched-string distance between the stack base and the receptor is tabulated in Table 16. The fact that the stack is located in the wake of the building resulted in using a value of one for the coefficient f_c. The model results are shown in Tables 17a to 17p. Table 18 gives the maximum over all the runs for source equals to 100 pCi/L and 1000 pCi/L. Figure 27 illustrates the relase locations' influence on calculated maximum concentrations for source strength equals to 1000 pCi/L.

The model results are generally conservative estimates of the observed values in the experiments (see Figures 25 and 27). The model over predicts the concentrations, and the predicted concentrations are often one to two order of magnitude higher than the observed concentrations specially in areas closer to the stack. The model applies for rectangular buildings where the wind is perpendicular to the building sides. Applying the model for sloped roof buildings where the stack is in the recirculation cavity is not appropriate and a new model has to be developed for these conditions.

5.2 ESTIMATION OF CONCENTRATION IN THE FAR-WAKE OF BUILDINGS

In the following subsections, models that predicts the concentrations in the far wake will be reviewed, and the Huber and Snyder (1982) model will be used to predict concentrations in the far-wake of the building.

5.2.1 *Background:*

Gaussian plume models are routinely applied in studies of environmental impact. The Gaussian plume equation for estimating normalized concentration is

$$\frac{\chi U}{Q} = \frac{1}{2\pi\sigma_y\sigma_z} e^{-y^2/2\sigma_y^2}\left[e^{-(z-h)^2/2\sigma_z^2} + e^{-(z+h)^2/2\sigma_z^2}\right]$$

where

χ = pollutant concentration (g m^{-3})

U = mean wind speed affecting the plume (m s^{-1})

Q = emission rate (g s^{-1})

h = effective emission height above the ground (m)

σ_y, σ_z = the values of the horizontal and vertical dispersion given in Table 13.

This form assumes that the plume spread has a Gaussian distribution, the wind affecting the plume is uniform, and the plume is perfectly reflected at the surface.

A variety of modification to the basic Gaussian plume model have been suggested by different researchers to provide estimates of concentrations in the wake of buildings. These modifications are based on estimating enhanced dispersion parameters.

Gifford (1968) suggested two different models for enhanced dispersion. The first one is based on the concept of adding a looping component to the plume centerline. This model is defined as

$$\sigma_y' = [\sigma_y^2 + (0.7W_b/2)^2]^{1/2} ; \qquad for\ x>3H_b$$

$$\sigma_z' = [\sigma_z^2 + (0.7H_b)^2]^{1/2} ; \qquad for\ x>3H_b$$

where

x = distance downwind of the leeward edge of the influential building,

W_b = width of the region of influential buildings normal to the wind,

H_b = height of highest influential building and

σ_y, σ_z = the values of the horizontal and vertical dispersion parameters in absence of building influences.

The second model is based on dilution of the effluent into the cross-sectional area of the building and is defined as;

$$\sigma_y' = (\sigma_y^2 + CA/\pi)^{1/2}$$

$$\sigma_z' = (\sigma_z^2 + CA/\pi)^{1/2}$$

where

A = cross-sectional area of the buildings normal to the wind and

C = a constant ranges between 0.5 and 2.

Huber and snyder (1982) suggested a model which is based on the concept that the scale of mixing is related to the length scales of the building.

The modified σ_z equation for a building where ($W_b \geq H_b$)is given by:

$$\sigma_z' = 0.7H_b + 0.067(x-3H_b) \quad \text{for} \quad 3H_b \leq x < 10H_b$$

or

$$= \sigma_z\{x + x_z\} \quad \text{for} \quad x \geq 10H_b$$

where

H_b = is in meters,

x_z = the virtual source distance such that

$$\sigma_z \{0.01H_b\} = 1.2H_b$$

For a building ($W_b < H_b$), Huber (1977) suggests that the modified σ_z equation is given by:

$$\sigma_z' = 0.7W_b + 0.067(x-3W_b) \qquad \text{for} \quad 3W_b \le x < 10W_b$$

or

$$= \sigma_z\{x + x_z\} \qquad \text{for} \quad x \ge 10W_b$$

where W_b is in meters.

It is important to note that σ_z' is not permitted to be less than the point source value given in Table 13, a condition that may mathematically occur.

For ($W_b \ge H_b$) building with a building width to building height ratio W_b/H_b less than or equal to 5, the modified σ_y equation is given by:

$$\sigma_y' = 0.35W_b + 0.067(x-3H_b) \qquad \text{for} \quad 3H_b \le x < 10H_b$$

or

$$= \sigma_y\{x + x_y\} \qquad \text{for} \quad x \ge 10H_b$$

For building width to building height ratios W_b/H_b greater than 5, the presently available data are insufficient to provide general equations for σ_y. For a building that is much wider than it is tall and a stack located toward the center of the building (i.e., away form either end), only the height scale is considered to be significant. The modified σ_y equation is then given by:

$$\sigma_y' = 0.35H_b + 0.067(x-3H_b) \qquad \text{for} \quad 3H_b \le x < 10H_b$$

or

$$= \sigma_y\{x + x_y\} \qquad \text{for} \quad x \ge 10H_b$$

For W_b/H_b greater than 5 and a stack located laterally within about 2.5 H_b of the end of the building, lateral plume spread is affected by the flow around the end of the building. With end effects, the enhancement in the initial lateral spread is assumed to be given by:

$$\sigma_y' = 1.75H_b + 0.067(x-3H_b) \qquad \text{for} \quad 3H_b \le x < 10H_b$$

or

$$= \sigma_y\{x + x_y\} \qquad \text{for} \quad x \ge 10H_b$$

The modified σ_y equation for ($W_b < H_b$) building is given by:

$$\sigma_y' = 0.35W_b + 0.067(x-3W_b) \qquad \text{for} \quad 3W_b \le x < 10W_b$$

or

$$= \sigma_y\{x + x_y\} \qquad \text{for} \quad x \ge 10W_b$$

5.2.2 *Model Comparison With Wind Tunnel Data:*

The Huber and Snyder model (1982) was used to predict the concentrations for $x \ge 3\ H_b$ downwind of the building for all the experiment combinations. The input data for the model is shown in Tables 14 and 15. The model results are shown in Tables 17a to 17p. Table 18 gives the maximum over all the runs for source equals to 100 pCi/L and 1000 pCi/L. Figure 27 displays the bar charts comparing the release locations' influence on maximum calculated concentrations for source strength equals to 1000 pCi/L. The model predicts concentrations of the same order of magnitude as the wind tunnel results found in Figure 25.

5.3 ESTIMATION OF CONCENTRATIONS USING THE FLUENT COMPUTATIONAL FLUID DYNAMICS PACKAGE

Many user-friendly computational fluid dynamics (CFD) packages are now available which combine geometry definition, grid generation, flow calculations, and graphic post-processors. These packages have been successfully applied to many engineering problems at the scales of turbomachinery, heat exchangers, chemical mixers, and airfoil elements. The processors can typically incorporate conditions of steady and transient motion, laminar and turbulent flows, heat and mass transfer, chemical reaction, porous media, two-phase flow, incompressible and compressible fluids, two and three dimensionality, and dispersion of particles, bubbles, or droplets.

During this project the commercial package FLUENT Ver 4.23 solved the dispersion around two and three-dimensional representations of the houses described in Figures 1 through 4. Sources of gas were released at the noted locations, but no effort was made to scale the stack size. The purpose of these calculations is to evaluate the use of such a CFD calculation package for applications to air-pollution and infiltration problems around small buildings.

5.3.1 *FLUENT Program Characteristics*

FLUENT Version 4.23 is a general purpose computer program for modeling fluid flow, heat transfer, and chemical reaction. FLUENT models the conservation equations for mass, momentum, energy, and chemical species using a control volume based, finite difference method. The governing equations are discretized on a curvilinear grid to enable computations in complex/irregular geometries. A nonstaggered system is used for storage of discrete velocities and pressures. Interpolations are accomplished via a first-order, Power-Law scheme or via a higher order QUICK scheme. The equations are solved using the SIMPLE or SIMPLEC algorithm with an iterative line-by-line matrix solver and multigrid acceleration.

The program can calculate turbulent flows with either the standard two-equation (k-ϵ) turbulent model, the renormalized group theory two-equation (RNG k-ϵ) turbulent model, or the Reynolds stress model (RSM). Calculations using the standard and RNG k-ϵ models are examined for the dispersion around a building situation.

The FLUENT preprocessor permits construction of either Cartesian or boundary fitted coordinates (BFC). The examples considered used the FLUENT preBFC program with the option of the boundary fitted coordinate system. A typical two-dimensional boundary-fitted grid for the one-story house with 6:12 roof pitch is shown in Figure 28. To limit calculation time a two-dimensional grid 51 x 51 cells was used. For the three-dimensional case a grid 41x31x41 was examined, again small to limit calculation time. The program can calculate over as many as 500,000 nodes and 10 chemical species, but one pays a penalty in calculation time and computer memory requirements.

5.3.2 *Configuration Examined for Two-Dimensional Example*

As noted earlier a grid was constructed around a cross-section of the building looking down the ridge line. The calculation domain extends 75 meters upwind of the building forward face, 125 meters downwind of the back face and through a boundary-layer depth of 75 meters. Two alternative boundary-fitted grids created for the one-story 6:12 slope roof case are shown in Figures 28 and 29

displayed. We will focus here on velocity vector profiles, streamfunction, u-velocity contours, and species concentrations for typical results.

Figures 30 through 37 present results for the base case of a single story domestic house with roof slope of 6:12 when a standard k-epsilon turbulence model is used. The model overestimates turbulent kinetic energy in strong shear regions, which results in excessive diffusion of scalars and sometimes the elimination of separation regions. Nonetheless, the u-velocity contours and streamfunction plots (Figures 30 and 31) present a strong roof top height separation cavity downwind of the building. The upwind vortex at ground level is very small and weak.

Each source presents a different trajectory and dispersion domain. The upwind ground- level source (Figure 32) jets upwind into the ground level vortex and then carries upward over the face of the building. The upwind eave source (Figure 33) is bent parallel to the roof and disperses downwind. The upwind mid-roof source (Figure 34) disperses up over the ridge line but remains mostly outside the separation cavity.

The downwind mid-roof source (Figure 37) lofts gases upward through the cavity. Subsequently the gas moves upwind to ridge-top and disperses downwind. The downwind eave release (Figure 36) also mixes gases upwind into the recirculation region. The downwind ground level release (Figure 35) appears to jet downwind against the weak recirculation region and does not mix upward over the building face very much. Indeed the presence of the downwind ground level release seems to divide the cavity region into two counter-rotating cells.

Figures 38 through 45 contrast the 9:12 roof slope results with the 6:12 roof slope calculations. The general flow description is similar and the figures differ only in detail. The steeper roof slope tends to result in stronger blockage and larger recirculation regions up and downwind of the building.

Calculations using the RNG k-ϵ turbulence model reveals that the standard model over-estimates the dispersion of the inlet jets and consequent lateral dispersion of the plumes. Indeed given the RNG approach the upwind and downwind jets remain coherent for longer distances and markedly influence the two-dimensional flow field around the building barrier. Jet coherence is so strong that the combination of the six jets strongly influences the oncoming flow field as shown by the streamlines in Figure 46 and the concentration distribution for the upwind groundlevel inlet in Figure

(uniform and adapted grids, respectively). Calculations were performed for both the 6:12 and 9:12 roof slope configurations.

Inlet and boundary conditions were stipulated to approximate field conditions examined in the physical model experiments. The longitudinal velocity for the inlet flow boundary was set to a piece-wise linear approximation to the profile tabulated for the Snyder approach condition shown in Table 6. The inlet turbulence intensity was set to 25% (one could also set a profile if desired), and the turbulence length scale was arbitrarily set to 25 m (again inlet dissipation rate may be specified as desired). The top grid boundary was set to a symmetry condition which guarantees horizontal flow at 75 m. The outlet boundary was set to a constant pressure condition (this allows flow reentry if the separation cavity happens to extend to more than five building heights downwind. The ground surface boundary was specified to be a non-slip surface, reflective to concentration species, and with a specified equivalent surface roughness of about $Z_o \approx 0.100$ m. The effective roughness may vary depending on the local surface friction generated during calculations. The building surfaces were also non-slip, but they had a smoother surface ($Z_o \approx 0.001$ m).

The stack exhaust sources could be simulated by three alternative methods *a)* as a specified inlet cell with associated species concentration, velocity vector, density, diffusivity, and viscosity, *b)* a fixed cell set in the active calculation region which retained constant property values, or *c)* as particles injected at a given node location with specified velocity, angle, and momentum. During the calculations discussed herein sources were represented as one grid wide inlet cells located on the surface of the building at approximately ground-level, eave, and mid-roof locations. The inlet gases were uniformly chosen to have a density of 1.28 kg/m, molecular weight of 28, injection velocity of 4.0 m/sec, and transport properties similar to air.

Different species were permitted to enter the domain from source locations at upwind ground, upwind eave, upwind mid-roof, downwind mid-roof, downwind eave, and downwind ground simultaneously. It was assumed that the inlet jets would not interact since density, molecular weight and gas properties were identical.

5.3.3 *Results from Two-Dimensional Calculations*

The post-processor system permits a wide range of presentation formats including profiles, contour plots, filled contour plots, and vectors, Properties of velocity components, gas species, pressure, turbulent energy, dissipation, streamfunction, streaklines, and eddy diffusivity may be

47 (Compare to Figures 31 and 32). Hence, additional calculations for the RNG case were performed with only one inlet active. Figures 48 and 49 present typical results for the single inlet active at the downwind eave (Compare to Figures 31 and 36). Keep in mind that jets in the two-dimensional simulation can isolate various flow regions, and this over-estimates the importance of inlet flows on the background flow patterns.

5.3.4 *Configuration Examined for Three-dimensional Example*

To simplify the calculation domain only flows perpendicular to the long face of the building were examined; hence, a symmetry plane exists along a longitudinal line cutting through the center of the structure. This case lets one examine the three-dimensional influence of end effects as the flow goes around the structure in the lateral direction. The grid is set to 21 x 16 x 21 nodes in the lateral, vertical and downstream directions, respectively. The domain was constructed to extend 75 m upwind of the front building face, 125 meters downwind of the back building face, 75 meters from the side wall building face, and 75 meters vertically (total domain was a box 235 m long, 75 m tall and 100 m wide). Calculations were only performed for the 6:12 roof slope single story building. The flow domain geometry and non-adapted boundary-fitted grid used during calculations is displayed in Figure 50. Only grid lines on the central symmetry plane, flow outlet, and lower walls are shown for clarity, but internal grids are interpolated from these planes.

Flow inlet and boundary conditions were set to similar values specified during the two-dimensional exercise. Sources were located one grid dimension inside the symmetry plane.

5.3.5 *Results from Three-dimensional Calculations*

Contour plots of the u, v and w-velocity components drawn on similar planes are shown in Figures 51, 52, and 53, respectively. Streakline patterns from particles released upwind and 20 m from the symmetry plane are displayed in Figure 54. Note the lateral divergence of the streaklines caused by the lateral extent of the building and the subsequent entrainment into the building wake.

Plume contours for the downstream mid-roof release are shown in Figures 55.. Note the added influence of the finite building aspect ratio on plume behavior. Upwind ground-level plumes are displaced laterally as well as vertically over the building.

5.3.6 *Critique of FLUENT Model for Air Pollution Applications*

The commercial CFD package FLUENT Ver 4.23 was user-friendly, robust and flexible for the application considered here. The software documentation was well prepared, the tutorials were easy to understand and complete, and the software support was good. A training session at the company headquarters was very helpful and reduces the time required to learn to use the package.

The preBFC preprocessor geometry and grid construction routines were very flexible, and they can handle much more complicated building geometries than were considered herein. Grid node adjustment and re-interpolation schemes provide the user great flexibility in defining grid resolution. The program can easily accommodate very complex cylindrical or curvilinear geometries. Volume elements need not have orthogonal angles. Construction of a 3-dimensional grid is not a trivial exercise, there is definitely a learning curve associated with effective grid construction, and initial attempts are likely to be frustrating. Graphics in the preprocessor permit the presentation of the geometry as wire skeletons, shapes with hidden boundaries, and even artificial lighting to enhance the appearance of depth and 3-dimensionality.

Cartesian grid construction can also be performed directly within the FLUENT program itself; however, boundary-fitted coordinates require the use of the preprocessor. Initial and boundary conditions are specified within FLUENT itself. The program gives quite flexible control of source release including inlet injection angles, initial trajectories of particles, consideration of up to 10 species simultaneously including muilti-diffusion coefficients, chemical reaction, heat transfer, and phase change.

Only the two-equation k-ϵ turbulence models were tested; however, a Reynolds stress model was available. Without additional investment in the construction of user-defined subroutines the program cannot handle the effects of buoyancy on turbulence production and dissipation, although the effect of buoyancy on momentum is present. The wall roughness functions are also limited, and specification of extremely rough surfaces ($Z_o > 0.2$ m) seems to lead to instabilities. Currently there are no means to specify the effects of thermal stratification through specification of Monin-Obukhov length, Pasquill-Gifford stability parameter, Turner number, or Richardson number.

Convergence of the iterative solution procedure can be very dependent on the optimum selection of various solution coefficients. The correct choice of multigrid options, block corrections, direction of calculation sweep, specification of under relaxation constants, grid volume ratios, grid

angles, and surface wall functions can also influence solution stability and convergence. Luck seems to play a significant role in how quickly one obtains a converged solution.

The post-processor package is also very flexible. Many alternative presentation formats are available including property profiles, streaklines, contour lines, filled contour lines, and velocity vectors. The program will also calculate many integral conservation values (for example one can compare source mass entering and leaving the solution domain). One can evaluate surface friction, heat flux and mass flux distributions along different wall surfaces.

Given the limited nature of the evaluation of this program during this project, one cannot comment on the quantitative reliability of numbers calculated. Future analysis should include more careful specification of inlet conditions, improved specification of inflow velocity, turbulence and dissipation profiles (only piecewise continuous velocity and constant turbulence and length scales were studied herein). Additional options not used here but available include buoyancy effects, chemical reacting gas species, particle or droplet transport, and heat transfer. It would also be worthwhile to evaluate the comparative advantages and accuracies of using the k-ϵ, the RNG k-ϵ, or the RSM models for building air pollution problems.

REFERENCES

ASHRAE (1989), " Air flow around buildings," Chapter 14 in ASHRAE Handbook-Fundamentals, Atlanta, American Society of Heating, Refrigerating, and Air-Conditioning Engineers, Inc.

Gifford F. A. (1968), " An outline of theories of diffusion in the lower layers of the atmosphere," Chapter 3 in Meteorology and Atomic Energy, Slade D. H., Ed., TID-214190, available NTIS, Springfield, VA.

Hanna S. R., Briggs G. A. and Hosker R. P. (1982), "Handbook on atmospheric diffusion," Technical Information Center U. S. Department of Energy.

Hosker, R. P., Jr. (1984), "Flow and Diffusion Near Obstacles," Atmospheric Science and Power Production, DOE/TIC-27601, pp. 241-326.

Huber A. H. (1991), "Wind tunnel and qaussian plume modeling of building wake dispersion," Atmos. Environ.25A, pp. 1237.

Huber A. H. (1988), "Performance of a gaussian model for centerline concentrations in the wake of buildings," Atmos. Environ.22, pp. 1039-1050.

Huber A. H. (1984), "Evaluation of a method for estimating pollution concentrations downwind of inflencing buildings," Atmos. Environ.18, pp. 2513-2338.

Huber A. H. and Snyder W. H. (1982), " Wind tunnel investigation of the effects of a rectangular building on dispersion of effluents from short adjacent stacks," Atmos. Environ. 16, pp. 2837-2848.

Meroney R. N. (1982), " Turbulent diffusion near buildings," Chapter 11 in Engineering Meterology, Plate E. J., Ed., Elsevier Scientific Publishing Co., Amsterdam, pp. 481-525.

Schulman L. L. and Scire J. S. (1993), " Building downwash screening modeling for the downwind recirculation cavity," Air & Waste 43, pp. 1122-1127.

Schulman L. L. and Scire J. S. (1991), " The effect of stack height, exhaust speed, and wind direction on concentrations from a rooftop stack," ASHRAE Trans. 97(2), pp. 573.

Snyder, W. H. (1981), "Guidelines for Fluid Modeling of Atmospheric Diffusion," EPA Report EPA-600/8-81-009, 185 pp.

Wilson D. J. (1979), " Flow patterns over flat-roofed buildings and application to exhaust stack design," ASHRAE Trans. 85(2), pp. 284-295.

Wilson D. J. and Britter R. E. (1982)., " Estimates of building surface concentrations from nearby point sources," Atmos. Environ. 16, pp. 2631-2646.

TABLES

ASD Exhaust System Building Scale Specifications

Specification	Field Dimension	Field Units	Model Scale 1:XX						Model Units
			25	30	35	40	45	50	
ONE STORY									
Height									
wall	3.51	m	14.0	11.7	**10.0**	8.8	7.8	7.0	cm
peak 6:12 rise	6.55	m	26.2	21.8	**18.7**	16.4	14.6	13.1	cm
peak 9:12 rise	8.08	m	32.3	26.9	**23.1**	20.2	17.9	16.2	cm
Width	12.19	m	48.8	40.6	**34.8**	30.5	27.1	24.4	cm
Length	15.24	m	61.0	50.8	**43.5**	38.1	33.9	30.5	cm
TWO STORY									
Height									
wall	6.10	m	24.4	20.3	**17.4**	15.2	13.5	12.2	cm
peak 6:12 rise	8.08	m	32.3	26.9	**23.1**	20.2	17.9	16.2	cm
peak 9:12 rise	9.07	m	36.3	30.2	**25.9**	22.7	20.1	18.1	cm
Width	7.92	m	31.7	26.4	**22.6**	19.8	17.6	15.8	cm
Length	10.97	m	43.9	36.6	**31.3**	27.4	24.4	21.9	cm
APPROACH FLOW									
Roughness Length	30.00	cm	1.20	1.00	**0.86**	0.75	0.67	0.60	cm
Wind Speed#1 @10m	234	cm/s	400	400	**400**	400	400	400	cm/s
Wind Speed#2 @10m	500	cm/s	400	400	**400**	400	400	400	cm/s
STACK FLOW									
Exit Pipe ID	10.16	cm	0.41	0.34	**0.29**	0.25	0.23	0.20	cm
Exit Velocity (min)	125	cm/s	100	100	**100**	100	100	100	cm/s
Exit Velocity (max)	584	cm/s	1000	1000	**1000**	1000	1000	1000	cm/s
Stack Flow Rate (min)	10134	ccs	13.0	9.0	**6.6**	5.1	4.0	3.2	ccs
Stack Flow Rate (max)	47347	ccs	129.7	90.1	**66.2**	50.7	40.0	32.4	ccs
SCALING PARAMETERS									
min. Roughness Re#	46720		2667	2222	**1905**	1667	1481	1333	
min. House Re# (one story)	166375		31156	25963	**22254**	19472	17309	15578	
min. House Re# (two story)	289348		54184	45153	**38703**	33865	30102	27092	
Stack Re# (min)	8467		226	188	**161**	141	125	113	
Stack Re# (max)	39556		2258	1881	**1613**	1411	1254	1129	
W/U ratio (min)	0.25		0.25	0.25	**0.25**	0.25	0.25	0.25	
W/U ratio (max)	2.50		2.50	2.50	**2.50**	2.50	2.50	2.50	

Table 1 ASD Exhaust System Building Model Scale Selection Specifications

ASD Exhaust System Field-Model Specifications

Specification	Field Dimension	Field Units	Model Spec. 35	Model Units
ONE STORY				
Height				
wall	3.51	m	10.0	cm
peak 6:12 rise	6.55	m	18.7	cm
peak 9:12 rise	8.08	m	23.1	cm
Width	12.19	m	34.8	cm
Length	15.24	m	43.5	cm
TWO STORY				
Height				
wall	6.10	m	17.4	cm
peak 6:12 rise	8.08	m	23.1	cm
peak 9:12 rise	9.07	m	25.9	cm
Width	7.92	m	22.6	cm
Length	10.97	m	31.3	cm
APPROACH FLOW				
Roughness Length	30	cm	0.86	cm
Wind Speed#1 @10m	234	cm/s	400	cm/s
Wind Speed#2 @10m	292	cm/s	400	cm/s
Wind Speed#3 @10m	500	cm/s	400	cm/s
STACK FLOW				
Exit Pipe ID	10.16	cm	0.29	cm
Exit Velocity (min)	125	cm/s	100	cm/s
Exit Velocity (avg)	292	cm/s	400	cm/s
Exit Velocity (max)	584	cm/s	1000	cm/s
Stack Flow Rate (min)	10134	ccs	6.6	ccs
Stack Flow Rate (avg)	23673	ccs	26.5	ccs
Stack Flow Rate (max)	47347	ccs	66.2	ccs
SCALING PARAMETERS				
min. Roughness Re#	46720		1905	
min. House Re# (one story)	166375		22254	
min. House Re# (two story)	289348		38703	
Stack Re# (min)	8467		161	
Stack Re# (max)	39556		1613	
W/U ratio (min)	0.25		0.25	
W/U ratio (mid)	1.00		1.00	
W/U ratio (max)	2.50		2.50	

Table 2 ASD Exhaust System Field-Model Design Specifications

Test Conditions *Model Design Settings*

Measurement Type	Run No.	File Name (xx > run#)	House Type	Roof Slope	Stack Location	Wind Dir. (deg)	Velocity Ratio W/U	Ref. Velocity (cm/s)	Effluent Velocity (cm/s)	Effluent Flow Rate (ccs)
Approach Flow Tests										
Vel. Profile U,u' @ x=-0.5m,y=-0.5m	A1	EPA_xx.prf	-	-	-	0	-	400	-	-
Vel. Profile U,u' @ x=-0.5m,y=0m	A2	EPA_xx.prf	-	-	-	0	-	400	-	-
Vel. Profile U,u' @ x=-0.5m,y=0.5m	A3	EPA_xx.prf	-	-	-	0	-	400	-	-
Vel. Profile U,u' @ x=1.0m,y=-0.5m	A4	EPA_xx.prf	-	-	-	0	-	400	-	-
Vel. Profile U,u' @ x=1.0m,y=0m	A5	EPA_xx.prf	-	-	-	0	-	400	-	-
Vel. Profile U,u' @ x=1.0m,y=0.5m	A6	EPA_xx.prf	-	-	-	0	-	400	-	-
Conc. Profile (downwind)	A7	EPA_xx.gc	-	-	note (1)	0	-	400	37	26.5
Re# Invariance Tests										
Vel. Profile U,u' @ x=-0.5m,y=0m	B1	EPA_xx.prf	-	-	-	0	-	300	-	-
Vel. Profile U,u' @ x=-0.5m,y=0m	B2	EPA_xx.prf	-	-	-	0	-	400	-	-
Vel. Profile U,u' @ x=-0.5m,y=0m	B3	EPA_xx.prf	-	-	-	0	-	500	-	-
Conc. Profile (house & downwind)	B4	EPA_xx.gc	one story	6:12	roof (1)	0	1.00	300	300	19.9
Conc. Profile (house & downwind)	B5	EPA_xx.gc	one story	6:12	roof (1)	0	1.00	400	400	26.5
Conc. Profile (house & downwind)	B6	EPA_xx.gc	one story	6:12	roof (1)	0	1.00	500	500	33.1
Visual Test Series										
Visualization of Plume	C1	Tape #1	one story	6:12	note (2)	0	1.00	400	400	26.5
Visualization of Plume	C2	Tape #1	one story	6:12	note (2)	0	2.50	400	1000	66.2
Visualization of Plume	C3	Tape #1	one story	6:12	note (2)	45	1.00	400	400	26.5
Visualization of Plume	C4	Tape #1	one story	6:12	note (2)	45	2.50	400	1000	66.2
Visualization of Plume	C5	Tape #1	one story	6:12	note (2)	90	1.00	400	400	26.5
Visualization of Plume	C6	Tape #1	one story	6:12	note (2)	90	2.50	400	1000	66.2
Visualization of Plume	C7	Tape #1	one story	6:12	note (2)	180	1.00	400	400	26.5
Visualization of Plume	C8	Tape #1	one story	6:12	note (2)	180	2.50	400	1000	66.2
Visualization of Plume	C9	Tape #1	one story	9:12	note (2)	0	1.00	400	400	26.5
Visualization of Plume	C10	Tape #1	one story	9:12	note (2)	0	2.50	400	1000	66.2
Visualization of Plume	C11	Tape #1	one story	9:12	note (2)	45	1.00	400	400	26.5
Visualization of Plume	C12	Tape #1	one story	9:12	note (2)	45	2.50	400	1000	66.2
Visualization of Plume	C13	Tape #1	one story	9:12	note (2)	90	1.00	400	400	26.5
Visualization of Plume	C14	Tape #1	one story	9:12	note (2)	90	2.50	400	1000	66.2
Visualization of Plume	C15	Tape #1	one story	9:12	note (2)	180	1.00	400	400	26.5
Visualization of Plume	C16	Tape #1	one story	9:12	note (2)	180	2.50	400	1000	66.2
Visualization of Plume	C17	Tape #1	two story	6:12	note (2)	0	1.00	400	400	26.5
Visualization of Plume	C18	Tape #1	two story	6:12	note (2)	0	2.50	400	1000	66.2
Visualization of Plume	C19	Tape #1	two story	6:12	note (2)	45	1.00	400	400	26.5
Visualization of Plume	C20	Tape #1	two story	6:12	note (2)	45	2.50	400	1000	66.2
Visualization of Plume	C21	Tape #1	two story	6:12	note (2)	90	1.00	400	400	26.5
Visualization of Plume	C22	Tape #1	two story	6:12	note (2)	90	2.50	400	1000	66.2
Visualization of Plume	C23	Tape #1	two story	6:12	note (2)	180	1.00	400	400	26.5
Visualization of Plume	C24	Tape #1	two story	6:12	note (2)	180	2.50	400	1000	66.2
Visualization of Plume	C25	Tape #1	two story	9:12	note (2)	0	1.00	400	400	26.5
Visualization of Plume	C26	Tape #1	two story	9:12	note (2)	0	2.50	400	1000	66.2
Visualization of Plume	C27	Tape #1	two story	9:12	note (2)	45	1.00	400	400	26.5
Visualization of Plume	C28	Tape #1	two story	9:12	note (2)	45	2.50	400	1000	66.2
Visualization of Plume	C29	Tape #1	two story	9:12	note (2)	90	1.00	400	400	26.5
Visualization of Plume	C30	Tape #1	two story	9:12	note (2)	90	2.50	400	1000	66.2
Visualization of Plume	C31	Tape #1	two story	9:12	note (2)	180	1.00	400	400	26.5
Visualization of Plume	C32	Tape #1	two story	9:12	note (2)	180	2.50	400	1000	66.2

note (1) : passive at x = (-50cm,y=0cm,z=0cm)
note (2) : sequence smoke to all 3 stacks

Table 3 Model Conditions for Approach Flow, Re #, and Visualization Test Series

Test Conditions | *Model Design Settings*

Measurement Type	Run No.	File Name (xx > run#)	House Type	Roof Slope	Stack Location	Wind Dir. (deg)	Velocity Ratio W/U	Ref. Velocity (cm/s)	Effluent Velocity (cm/s)	Effluent Flow Rate (ccs)
Concentration Test Series (D)										
Conc. Profile (house & downwind)	D1	EPA_xx.gc	one story	6:12	roof (1)	0	0.25	400	100	6.6
Conc. Profile (house & downwind)	D2	EPA_xx.gc	one story	6:12	eave (2)	0	0.25	400	100	6.6
Conc. Profile (house & downwind)	D3	EPA_xx.gc	one story	6:12	wall (3)	0	0.25	400	100	6.6
Conc. Profile (house & downwind)	D4	EPA_xx.gc	one story	6:12	roof (1)	0	1.00	400	400	26.5
Conc. Profile (house & downwind)	D5	EPA_xx.gc	one story	6:12	eave (2)	0	1.00	400	400	26.5
Conc. Profile (house & downwind)	D6	EPA_xx.gc	one story	6:12	wall (3)	0	1.00	400	400	26.5
Conc. Profile (house & downwind)	D7	EPA_xx.gc	one story	6:12	roof (1)	0	2.50	400	1000	66.2
Conc. Profile (house & downwind)	D8	EPA_xx.gc	one story	6:12	eave (2)	0	2.50	400	1000	66.2
Conc. Profile (house & downwind)	D9	EPA_xx.gc	one story	6:12	wall (3)	0	2.50	400	1000	66.2
Conc. Profile (house & downwind)	D10	EPA_xx.gc	one story	6:12	roof (1)	45	0.25	400	100	6.6
Conc. Profile (house & downwind)	D11	EPA_xx.gc	one story	6:12	eave (2)	45	0.25	400	100	6.6
Conc. Profile (house & downwind)	D12	EPA_xx.gc	one story	6:12	wall (3)	45	0.25	400	100	6.6
Conc. Profile (house & downwind)	D13	EPA_xx.gc	one story	6:12	roof (1)	45	1.00	400	400	26.5
Conc. Profile (house & downwind)	D14	EPA_xx.gc	one story	6:12	eave (2)	45	1.00	400	400	26.5
Conc. Profile (house & downwind)	D15	EPA_xx.gc	one story	6:12	wall (3)	45	1.00	400	400	26.5
Conc. Profile (house & downwind)	D16	EPA_xx.gc	one story	6:12	roof (1)	45	2.50	400	1000	66.2
Conc. Profile (house & downwind)	D17	EPA_xx.gc	one story	6:12	eave (2)	45	2.50	400	1000	66.2
Conc. Profile (house & downwind)	D18	EPA_xx.gc	one story	6:12	wall (3)	45	2.50	400	1000	66.2
Conc. Profile (house & downwind)	D19	EPA_xx.gc	one story	6:12	roof (1)	90	0.25	400	100	6.6
Conc. Profile (house & downwind)	D20	EPA_xx.gc	one story	6:12	eave (2)	90	0.25	400	100	6.6
Conc. Profile (house & downwind)	D21	EPA_xx.gc	one story	6:12	wall (3)	90	0.25	400	100	6.6
Conc. Profile (house & downwind)	D22	EPA_xx.gc	one story	6:12	roof (1)	90	1.00	400	400	26.5
Conc. Profile (house & downwind)	D23	EPA_xx.gc	one story	6:12	eave (2)	90	1.00	400	400	26.5
Conc. Profile (house & downwind)	D24	EPA_xx.gc	one story	6:12	wall (3)	90	1.00	400	400	26.5
Conc. Profile (house & downwind)	D25	EPA_xx.gc	one story	6:12	roof (1)	90	2.50	400	1000	66.2
Conc. Profile (house & downwind)	D26	EPA_xx.gc	one story	6:12	eave (2)	90	2.50	400	1000	66.2
Conc. Profile (house & downwind)	D27	EPA_xx.gc	one story	6:12	wall (3)	90	2.50	400	1000	66.2
Conc. Profile (house & downwind)	D28	EPA_xx.gc	one story	6:12	roof (1)	180	0.25	400	100	6.6
Conc. Profile (house & downwind)	D29	EPA_xx.gc	one story	6:12	eave (2)	180	0.25	400	100	6.6
Conc. Profile (house & downwind)	D30	EPA_xx.gc	one story	6:12	wall (3)	180	0.25	400	100	6.6
Conc. Profile (house & downwind)	D31	EPA_xx.gc	one story	6:12	roof (1)	180	1.00	400	400	26.5
Conc. Profile (house & downwind)	D32	EPA_xx.gc	one story	6:12	eave (2)	180	1.00	400	400	26.5
Conc. Profile (house & downwind)	D33	EPA_xx.gc	one story	6:12	wall (3)	180	1.00	400	400	26.5
Conc. Profile (house & downwind)	D34	EPA_xx.gc	one story	6:12	roof (1)	180	2.50	400	1000	66.2
Conc. Profile (house & downwind)	D35	EPA_xx.gc	one story	6:12	eave (2)	180	2.50	400	1000	66.2
Conc. Profile (house & downwind)	D36	EPA_xx.gc	one story	6:12	wall (3)	180	2.50	400	1000	66.2
Concentration Test Series (E)										
Conc. Profile (house & downwind)	E1	EPA_xx.gc	one story	9:12	roof (1)	0	0.25	400	100	6.6
Conc. Profile (house & downwind)	E2	EPA_xx.gc	one story	9:12	eave (2)	0	0.25	400	100	6.6
Conc. Profile (house & downwind)	E3	EPA_xx.gc	one story	9:12	wall (3)	0	0.25	400	100	6.6
Conc. Profile (house & downwind)	E4	EPA_xx.gc	one story	9:12	roof (1)	0	1.00	400	400	26.5
Conc. Profile (house & downwind)	E5	EPA_xx.gc	one story	9:12	eave (2)	0	1.00	400	400	26.5
Conc. Profile (house & downwind)	E6	EPA_xx.gc	one story	9:12	wall (3)	0	1.00	400	400	26.5
Conc. Profile (house & downwind)	E7	EPA_xx.gc	one story	9:12	roof (1)	0	2.50	400	1000	66.2
Conc. Profile (house & downwind)	E8	EPA_xx.gc	one story	9:12	eave (2)	0	2.50	400	1000	66.2
Conc. Profile (house & downwind)	E9	EPA_xx.gc	one story	9:12	wall (3)	0	2.50	400	1000	66.2
Conc. Profile (house & downwind)	E10	EPA_xx.gc	one story	9:12	roof (1)	45	0.25	400	100	6.6
Conc. Profile (house & downwind)	E11	EPA_xx.gc	one story	9:12	eave (2)	45	0.25	400	100	6.6
Conc. Profile (house & downwind)	E12	EPA_xx.gc	one story	9:12	wall (3)	45	0.25	400	100	6.6
Conc. Profile (house & downwind)	E13	EPA_xx.gc	one story	9:12	roof (1)	45	1.00	400	400	26.5
Conc. Profile (house & downwind)	E14	EPA_xx.gc	one story	9:12	eave (2)	45	1.00	400	400	26.5
Conc. Profile (house & downwind)	E15	EPA_xx.gc	one story	9:12	wall (3)	45	1.00	400	400	26.5
Conc. Profile (house & downwind)	E16	EPA_xx.gc	one story	9:12	roof (1)	45	2.50	400	1000	66.2
Conc. Profile (house & downwind)	E17	EPA_xx.gc	one story	9:12	eave (2)	45	2.50	400	1000	66.2
Conc. Profile (house & downwind)	E18	EPA_xx.gc	one story	9:12	wall (3)	45	2.50	400	1000	66.2
Conc. Profile (house & downwind)	E19	EPA_xx.gc	one story	9:12	roof (1)	90	0.25	400	100	6.6
Conc. Profile (house & downwind)	E20	EPA_xx.gc	one story	9:12	eave (2)	90	0.25	400	100	6.6
Conc. Profile (house & downwind)	E21	EPA_xx.gc	one story	9:12	wall (3)	90	0.25	400	100	6.6
Conc. Profile (house & downwind)	E22	EPA_xx.gc	one story	9:12	roof (1)	90	1.00	400	400	26.5
Conc. Profile (house & downwind)	E23	EPA_xx.gc	one story	9:12	eave (2)	90	1.00	400	400	26.5
Conc. Profile (house & downwind)	E24	EPA_xx.gc	one story	9:12	wall (3)	90	1.00	400	400	26.5
Conc. Profile (house & downwind)	E25	EPA_xx.gc	one story	9:12	roof (1)	90	2.50	400	1000	66.2
Conc. Profile (house & downwind)	E26	EPA_xx.gc	one story	9:12	eave (2)	90	2.50	400	1000	66.2
Conc. Profile (house & downwind)	E27	EPA_xx.gc	one story	9:12	wall (3)	90	2.50	400	1000	66.2
Conc. Profile (house & downwind)	E28	EPA_xx.gc	one story	9:12	roof (1)	180	0.25	400	100	6.6
Conc. Profile (house & downwind)	E29	EPA_xx.gc	one story	9:12	eave (2)	180	0.25	400	100	6.6
Conc. Profile (house & downwind)	E30	EPA_xx.gc	one story	9:12	wall (3)	180	0.25	400	100	6.6
Conc. Profile (house & downwind)	E31	EPA_xx.gc	one story	9:12	roof (1)	180	1.00	400	400	26.5
Conc. Profile (house & downwind)	E32	EPA_xx.gc	one story	9:12	eave (2)	180	1.00	400	400	26.5
Conc. Profile (house & downwind)	E33	EPA_xx.gc	one story	9:12	wall (3)	180	1.00	400	400	26.5
Conc. Profile (house & downwind)	E34	EPA_xx.gc	one story	9:12	roof (1)	180	2.50	400	1000	66.2
Conc. Profile (house & downwind)	E35	EPA_xx.gc	one story	9:12	eave (2)	180	2.50	400	1000	66.2
Conc. Profile (house & downwind)	E36	EPA_xx.gc	one story	9:12	wall (3)	180	2.50	400	1000	66.2

Table 4 Model Testing Conditions for One Story Home Test Series

Test Conditions | *Model Design Settings*

Measurement Type	Run No.	File Name (xx > run#)	House Type	Roof Slope	Stack Location	Wind Dir. (deg)	Velocity Ratio W/U	Ref. Velocity (cm/s)	Effluent Velocity (cm/s)	Effluent Flow Rate (ccs)
Concentration Test Series (F)										
Conc. Profile (house & downwind)	F1	EPA_xx.gc	two story	6:12	roof (1)	0	0.25	400	100	6.6
Conc. Profile (house & downwind)	F2	EPA_xx.gc	two story	6:12	eave (2)	0	0.25	400	100	6.6
Conc. Profile (house & downwind)	F3	EPA_xx.gc	two story	6:12	wall (3)	0	0.25	400	100	6.6
Conc. Profile (house & downwind)	F4	EPA_xx.gc	two story	6:12	roof (1)	0	1.00	400	400	26.5
Conc. Profile (house & downwind)	F5	EPA_xx.gc	two story	6:12	eave (2)	0	1.00	400	400	26.5
Conc. Profile (house & downwind)	F6	EPA_xx.gc	two story	6:12	wall (3)	0	1.00	400	400	26.5
Conc. Profile (house & downwind)	F7	EPA_xx.gc	two story	6:12	roof (1)	0	2.50	400	1000	66.2
Conc. Profile (house & downwind)	F8	EPA_xx.gc	two story	6:12	eave (2)	0	2.50	400	1000	66.2
Conc. Profile (house & downwind)	F9	EPA_xx.gc	two story	6:12	wall (3)	0	2.50	400	1000	66.2
Conc. Profile (house & downwind)	F10	EPA_xx.gc	two story	6:12	roof (1)	45	0.25	400	100	6.6
Conc. Profile (house & downwind)	F11	EPA_xx.gc	two story	6:12	eave (2)	45	0.25	400	100	6.6
Conc. Profile (house & downwind)	F12	EPA_xx.gc	two story	6:12	wall (3)	45	0.25	400	100	6.6
Conc. Profile (house & downwind)	F13	EPA_xx.gc	two story	6:12	roof (1)	45	1.00	400	400	26.5
Conc. Profile (house & downwind)	F14	EPA_xx.gc	two story	6:12	eave (2)	45	1.00	400	400	26.5
Conc. Profile (house & downwind)	F15	EPA_xx.gc	two story	6:12	wall (3)	45	1.00	400	400	26.5
Conc. Profile (house & downwind)	F16	EPA_xx.gc	two story	6:12	roof (1)	45	2.50	400	1000	66.2
Conc. Profile (house & downwind)	F17	EPA_xx.gc	two story	6:12	eave (2)	45	2.50	400	1000	66.2
Conc. Profile (house & downwind)	F18	EPA_xx.gc	two story	6:12	wall (3)	45	2.50	400	1000	66.2
Conc. Profile (house & downwind)	F19	EPA_xx.gc	two story	6:12	roof (1)	90	0.25	400	100	6.6
Conc. Profile (house & downwind)	F20	EPA_xx.gc	two story	6:12	eave (2)	90	0.25	400	100	6.6
Conc. Profile (house & downwind)	F21	EPA_xx.gc	two story	6:12	wall (3)	90	0.25	400	100	6.6
Conc. Profile (house & downwind)	F22	EPA_xx.gc	two story	6:12	roof (1)	90	1.00	400	400	26.5
Conc. Profile (house & downwind)	F23	EPA_xx.gc	two story	6:12	eave (2)	90	1.00	400	400	26.5
Conc. Profile (house & downwind)	F24	EPA_xx.gc	two story	6:12	wall (3)	90	1.00	400	400	26.5
Conc. Profile (house & downwind)	F25	EPA_xx.gc	two story	6:12	roof (1)	90	2.50	400	1000	66.2
Conc. Profile (house & downwind)	F26	EPA_xx.gc	two story	6:12	eave (2)	90	2.50	400	1000	66.2
Conc. Profile (house & downwind)	F27	EPA_xx.gc	two story	6:12	wall (3)	90	2.50	400	1000	66.2
Conc. Profile (house & downwind)	F28	EPA_xx.gc	two story	6:12	roof (1)	180	0.25	400	100	6.6
Conc. Profile (house & downwind)	F29	EPA_xx.gc	two story	6:12	eave (2)	180	0.25	400	100	6.6
Conc. Profile (house & downwind)	F30	EPA_xx.gc	two story	6:12	wall (3)	180	0.25	400	100	6.6
Conc. Profile (house & downwind)	F31	EPA_xx.gc	two story	6:12	roof (1)	180	1.00	400	400	26.5
Conc. Profile (house & downwind)	F32	EPA_xx.gc	two story	6:12	eave (2)	180	1.00	400	400	26.5
Conc. Profile (house & downwind)	F33	EPA_xx.gc	two story	6:12	wall (3)	180	1.00	400	400	26.5
Conc. Profile (house & downwind)	F34	EPA_xx.gc	two story	6:12	roof (1)	180	2.50	400	1000	66.2
Conc. Profile (house & downwind)	F35	EPA_xx.gc	two story	6:12	eave (2)	180	2.50	400	1000	66.2
Conc. Profile (house & downwind)	F36	EPA_xx.gc	two story	6:12	wall (3)	180	2.50	400	1000	66.2
Concentration Test Series (G)										
Conc. Profile (house & downwind)	G1	EPA_xx.gc	two story	9:12	roof (1)	0	0.25	400	100	6.6
Conc. Profile (house & downwind)	G2	EPA_xx.gc	two story	9:12	eave (2)	0	0.25	400	100	6.6
Conc. Profile (house & downwind)	G3	EPA_xx.gc	two story	9:12	wall (3)	0	0.25	400	100	6.6
Conc. Profile (house & downwind)	G4	EPA_xx.gc	two story	9:12	roof (1)	0	1.00	400	400	26.5
Conc. Profile (house & downwind)	G5	EPA_xx.gc	two story	9:12	eave (2)	0	1.00	400	400	26.5
Conc. Profile (house & downwind)	G6	EPA_xx.gc	two story	9:12	wall (3)	0	1.00	400	400	26.5
Conc. Profile (house & downwind)	G7	EPA_xx.gc	two story	9:12	roof (1)	0	2.50	400	1000	66.2
Conc. Profile (house & downwind)	G8	EPA_xx.gc	two story	9:12	eave (2)	0	2.50	400	1000	66.2
Conc. Profile (house & downwind)	G9	EPA_xx.gc	two story	9:12	wall (3)	0	2.50	400	1000	66.2
Conc. Profile (house & downwind)	G10	EPA_xx.gc	two story	9:12	roof (1)	45	0.25	400	100	6.6
Conc. Profile (house & downwind)	G11	EPA_xx.gc	two story	9:12	eave (2)	45	0.25	400	100	6.6
Conc. Profile (house & downwind)	G12	EPA_xx.gc	two story	9:12	wall (3)	45	0.25	400	100	6.6
Conc. Profile (house & downwind)	G13	EPA_xx.gc	two story	9:12	roof (1)	45	1.00	400	400	26.5
Conc. Profile (house & downwind)	G14	EPA_xx.gc	two story	9:12	eave (2)	45	1.00	400	400	26.5
Conc. Profile (house & downwind)	G15	EPA_xx.gc	two story	9:12	wall (3)	45	1.00	400	400	26.5
Conc. Profile (house & downwind)	G16	EPA_xx.gc	two story	9:12	roof (1)	45	2.50	400	1000	66.2
Conc. Profile (house & downwind)	G17	EPA_xx.gc	two story	9:12	eave (2)	45	2.50	400	1000	66.2
Conc. Profile (house & downwind)	G18	EPA_xx.gc	two story	9:12	wall (3)	45	2.50	400	1000	66.2
Conc. Profile (house & downwind)	G19	EPA_xx.gc	two story	9:12	roof (1)	90	0.25	400	100	6.6
Conc. Profile (house & downwind)	G20	EPA_xx.gc	two story	9:12	eave (2)	90	0.25	400	100	6.6
Conc. Profile (house & downwind)	G21	EPA_xx.gc	two story	9:12	wall (3)	90	0.25	400	100	6.6
Conc. Profile (house & downwind)	G22	EPA_xx.gc	two story	9:12	roof (1)	90	1.00	400	400	26.5
Conc. Profile (house & downwind)	G23	EPA_xx.gc	two story	9:12	eave (2)	90	1.00	400	400	26.5
Conc. Profile (house & downwind)	G24	EPA_xx.gc	two story	9:12	wall (3)	90	1.00	400	400	26.5
Conc. Profile (house & downwind)	G25	EPA_xx.gc	two story	9:12	roof (1)	90	2.50	400	1000	66.2
Conc. Profile (house & downwind)	G26	EPA_xx.gc	two story	9:12	eave (2)	90	2.50	400	1000	66.2
Conc. Profile (house & downwind)	G27	EPA_xx.gc	two story	9:12	wall (3)	90	2.50	400	1000	66.2
Conc. Profile (house & downwind)	G28	EPA_xx.gc	two story	9:12	roof (1)	180	0.25	400	100	6.6
Conc. Profile (house & downwind)	G29	EPA_xx.gc	two story	9:12	eave (2)	180	0.25	400	100	6.6
Conc. Profile (house & downwind)	G30	EPA_xx.gc	two story	9:12	wall (3)	180	0.25	400	100	6.6
Conc. Profile (house & downwind)	G31	EPA_xx.gc	two story	9:12	roof (1)	180	1.00	400	400	26.5
Conc. Profile (house & downwind)	G32	EPA_xx.gc	two story	9:12	eave (2)	180	1.00	400	400	26.5
Conc. Profile (house & downwind)	G33	EPA_xx.gc	two story	9:12	wall (3)	180	1.00	400	400	26.5
Conc. Profile (house & downwind)	G34	EPA_xx.gc	two story	9:12	roof (1)	180	2.50	400	1000	66.2
Conc. Profile (house & downwind)	G35	EPA_xx.gc	two story	9:12	eave (2)	180	2.50	400	1000	66.2
Conc. Profile (house & downwind)	G36	EPA_xx.gc	two story	9:12	wall (3)	180	2.50	400	1000	66.2

Table 5 Model Testing Conditions for Two Story Home Test Series

Velocity and Turbulence Profile Design Criteria

Field Conditions

Ref. Wind Speed (m/s)=	4.0 <	Inputs
Ref. Height (m)	10.0 <	
Power Law Index =	0.20 <	
Roughness Length (m)=	0.30 <	
Displacement Height (m)=	0.00 <	
Friction Velocity (m/s)=	0.46	

Snyder Approach

Field Height (m)	Field Velocity (m/s)	Field Turb.Int. (%)
5.0	3.5	32.7
10.0	4.0	26.3
15.0	4.3	23.5
20.0	4.6	21.9
30.0	5.0	20.0
40.0	5.3	18.8
50.0	5.5	18.0
75.0	6.0	16.7
100.0	6.3	15.9
150.0	6.9	14.8
200.0	7.3	14.2
250.0	7.6	13.7
300.0	7.9	13.3
350.0	8.1	13.0
400.0	8.4	12.8
450.0	8.6	12.6

Simiu&Scanlan Approach

Field Height (m)	Field Velocity (m/s)	Field Turb.Int. (%)
5.0	3.2	32.9
10.0	4.0	26.4
15.0	4.5	23.7
20.0	4.8	22.1
30.0	5.3	20.1
40.0	5.6	18.9
50.0	5.8	18.1
75.0	6.3	16.8
100.0	6.6	16.0
150.0	7.1	14.9
200.0	7.4	14.3
250.0	7.7	13.8
300.0	7.9	13.4
350.0	8.1	13.1
400.0	8.2	12.9
450.0	8.3	12.7

Beta (fit to Simiu&Scanlan) = 5.37

note: suburban roughness zo = 30cm and d=0!

Table 6 Velocity and Turbulence Profile Design Data; Field Conditions

Velocity and Turbulence Profile Design Criteria

Model Conditions

Ref. Wind Speed (cm/s)=	400.0	
Ref. Height (cm)	28.6	
Power Law Index =	0.20	
Roughness Length (cm)=	0.86	
Displacement Height (cm)=	0.00	
Friction Velocity (cm/s)=	45.63	
Length Scale =	35.0	< Inputs
Model/Field Speed Ratio =	1.0	<

Snyder Approach

Model Height (cm)	Model Velocity (cm/s)	Model Turb.Int. (%)
14.3	348.2	32.7
28.6	400.0	26.3
42.9	433.8	23.5
57.1	459.5	21.9
85.7	498.3	20.0
114.3	527.8	18.8
142.9	551.9	18.0
214.3	598.5	16.7
285.7	634.0	15.9
428.6	687.5	14.8
571.4	728.2	14.2
714.3	761.5	13.7
857.1	789.7	13.3
1000.0	814.5	13.0
1142.9	836.5	12.8
1285.7	856.5	12.6

Simiu&Scanlan Approach

Model Height (cm)	Model Velocity (cm/s)	Model Turb.Int. (%)
14.3	320.9	32.9
28.6	400.0	26.4
42.9	446.3	23.7
57.1	479.1	22.1
85.7	525.3	20.1
114.3	558.1	18.9
142.9	583.6	18.1
214.3	629.8	16.8
285.7	662.7	16.0
428.6	708.9	14.9
571.4	741.7	14.3
714.3	767.2	13.8
857.1	788.0	13.4
1000.0	805.6	13.1
1142.9	820.8	12.9
1285.7	834.2	12.7

Table 7 Velocity and Turbulence Profile Design Data; Model Conditions

Concentration Data: One Story; 6:12 Roof Slope; Wind Dir. = 000; Roof Release

RUN Velocity (cm/s) Flow Rate (ccs)	Run# B4 303.5 19.9	Run# B5 392.6 26.5	Run# B6 500.7 33.1				
Building Position Number	Model Conc. (cm-2)	Model Conc. (cm-2)	Model Conc. (cm-2)	Minimum Conc. (cm-2)	Average Conc. (cm-2)	Maximum Conc. (cm-2)	Error in K +-(%)
1	1880	1944	2612	1880	2145	2612	17.1
2	2254	2353	2694	2254	2433	2694	9.0
3	2787	2794	2233	2233	2605	2794	10.8
4	2093	2071	2801	2071	2322	2801	15.7
5	2394	2480	2783	2394	2552	2783	7.6
6	3147	3155	2412	2412	2904	3155	12.8
7	4572	4455	5110	4455	4712	5110	6.9
8	8704	8842	12176	8704	9907	12176	17.5
9	5641	5975	5819	5641	5811	5975	2.9
10	7698	8744	7624	7624	8022	8744	7.0
11	56912	55657	51018	51018	54529	56912	5.4
12	11367	11346	10268	10268	10994	11367	5.0
13	26	25	27	25	26	27	
14	4	4	7	4	5	7	
15	1	2	5	1	2	5	
16	0	0	2	0	1	2	
17	0	0	1	0	0	1	
18	0	0	0	0	0	0	
19	0	0	0	0	0	0	
20	0	0	0	0	0	0	
21	0	0	0	0	0	0	
22	0	0	0	0	0	0	
23	0	0	0	0	0	0	
24	0	0	0	0	0	0	
25	7	3	126	3	45	126	136.1
26	0	0	46	0	15	46	150.0
27	0	0	20	0	7	20	150.0
28	6	6	109	6	41	109	126.4
29	0	0	45	0	15	45	150.0
30	0	0	18	0	6	18	150.0
31	150	95	139	95	128	150	21.4
32	0	0	0	0	0	0	
33	18	1	0	0	6	18	144.2
34	86	36	0	0	41	86	105.0
35	0	0	0	0	0	0	
36	15	2	0	0	6	15	130.9
37	89	33	2	2	41	89	105.4
38	62	32	4	4	33	62	88.1
39	2390	2211	2874	2211	2492	2874	13.3
40	2188	2129	2457	2129	2258	2457	7.3
41	1617	1597	1909	1597	1707	1909	9.1
42	1680	1683	1485	1485	1616	1683	6.1
43	1081	1060	1672	1060	1271	1672	24.0
44	1565	1500	1696	1500	1587	1696	6.2
45	1225	1246	1219	1219	1230	1246	1.1

Table 8 Reynolds Number Invariance Test Results

ADCT Stack Concentration Measurements: Urban Comparisons

Model Values (CGS)			Run A7		Field Values (MKS)			
1					35			< Length Scale
400.0					4.0			< Wind Speed
26.5					-			< Flow Rate
22.0					22.0			< Stack Gas Temp. (C)
22.0					22.0			< Ambient Temp. (C)
0.0					0.0			< Effective Stack Height

Model Position			Model	Model	Field Position			Field Est	PG-A	PG-B	PG-C	PG-D	PG-E	PG-F
X	Y	Z	Conc.	K*10^6	X	Y	Z	K*10^6	K*10^6	K*10^6	K*10^6	K*10^6	K*10^6	K*10^6
(cm)	(cm)	(cm)	(ppm)	(cm-2)	(m)	(m)	(m)	(m-2)	(m-2)	(m-2)	(m-2)	(m-2)	(m-2)	(m-2)
50.0	25.0	0.0	56	850	17.5	8.8	0.0	6937	3938	3938	1759	342	4	4
50.0	18.8	0.0	90	1360	17.5	6.6	0.0	11102	6743	6743	5489	2938	341	341
50.0	12.5	0.0	119	1802	17.5	4.4	0.0	14712	9901	9901	12373	13656	8808	8808
50.0	6.3	0.0	140	2109	17.5	2.2	0.0	17214	12468	12468	20149	34333	61945	61945
50.0	0.0	0.0	146	2208	17.5	0.0	0.0	18027	13464	13464	23705	46685	118679	118679
50.0	-6.3	0.0	142	2136	17.5	-2.2	0.0	17436	12468	12468	20149	34333	61945	61945
50.0	-12.5	0.0	134	2026	17.5	-4.4	0.0	16536	9901	9901	12373	13656	8808	8808
50.0	-18.8	0.0	116	1751	17.5	-6.6	0.0	14293	6743	6743	5489	2938	341	341
50.0	-25.0	0.0	97	1457	17.5	-8.8	0.0	11891	3938	3938	1759	342	4	4
50.0	0.0	0.0	146	2208	17.5	0.0	0.0	18027	13464	13464	23705	46685	118679	118679
50.0	0.0	6.0	120	1804	17.5	0.0	2.1	14725	11907	11907	19800	32270	38416	38416
50.0	0.0	11.0	86	1300	17.5	0.0	3.9	10609	8909	8909	12945	13494	2678	2678
50.0	0.0	16.0	55	824	17.5	0.0	5.6	6728	5620	5620	6591	3379	39	39
50.0	0.0	21.0	32	480	17.5	0.0	7.4	3918	2989	2989	2613	507	0	0
150.0	50.0	0.0	9	128	52.5	17.5	0.0	1047	851	851	822	573	123	123
150.0	37.5	0.0	17	252	52.5	13.1	0.0	2058	1085	1085	1372	1510	953	953
150.0	25.0	0.0	28	426	52.5	8.8	0.0	3475	1290	1290	1979	3017	4124	4124
150.0	12.5	0.0	37	558	52.5	4.4	0.0	4559	1431	1431	2465	4571	9932	9932
150.0	0.0	0.0	40	601	52.5	0.0	0.0	4904	1481	1481	2652	5250	13313	13313
150.0	-12.5	0.0	38	577	52.5	-4.4	0.0	4707	1431	1431	2465	4571	9932	9932
150.0	-25.0	0.0	30	454	52.5	-8.8	0.0	3709	1290	1290	1979	3017	4124	4124
150.0	-37.5	0.0	23	349	52.5	-13.1	0.0	2846	1085	1085	1372	1510	953	953
150.0	-50.0	0.0	15	225	52.5	-17.5	0.0	1836	851	851	822	573	123	123
150.0	0.0	0.0	40	601	52.5	0.0	0.0	4904	1481	1481	2652	5250	13313	13313
150.0	0.0	11.0	35	531	52.5	0.0	3.9	4337	1417	1417	2480	4567	8717	8717
150.0	0.0	21.0	25	373	52.5	0.0	7.4	3044	1260	1260	2076	3160	2845	2845
150.0	0.0	31.0	13	198	52.5	0.0	10.9	1614	1041	1041	1555	1736	461	461
150.0	0.0	41.0	4	62	52.5	0.0	14.4	505	800	800	1042	758	37	37
250.0	100.0	0.0	0	0	87.5	35.0	0.0	0	235	235	174	75	5	5
250.0	75.0	0.0	2	36	87.5	26.3	0.0	296	335	335	367	310	103	103
250.0	50.0	0.0	10	146	87.5	17.5	0.0	1195	431	431	627	852	874	874
250.0	25.0	0.0	20	297	87.5	8.8	0.0	2427	502	502	864	1563	3154	3154
250.0	0.0	0.0	23	344	87.5	0.0	0.0	2809	528	528	961	1913	4838	4838
250.0	-25.0	0.0	17	254	87.5	-8.8	0.0	2070	502	502	864	1563	3154	3154
250.0	-50.0	0.0	12	183	87.5	-17.5	0.0	1491	431	431	627	852	874	874
250.0	-75.0	0.0	6	85	87.5	-26.3	0.0	690	335	335	367	310	103	103
250.0	*******	0.0	2	35	87.5	-35.0	0.0	283	235	235	174	75	5	5
250.0	0.0	0.0	23	344	87.5	0.0	0.0	2809	528	528	961	1913	4838	4838
250.0	0.0	18.5	19	290	87.5	0.0	6.5	2366	506	506	898	1657	3136	3136
250.0	0.0	36.0	10	143	87.5	0.0	12.6	1171	448	448	742	1112	937	937
250.0	0.0	53.5	1	14	87.5	0.0	18.7	111	366	366	542	577	129	129
250.0	0.0	71.0	0	0	87.5	0.0	24.9	0	277	277	351	232	8	8

Table 9 Atm. Dispersion Comparability Test Comparisons with Urban Diff. Parameters

ADCT Stack Concentration Measurements; Open Comparisons

Model Values (CGS)	RUN #A	Field Values (MKS)	
1		35	< Length Scale
400.0		4.0	< Wind Speed
26.5		-	< Flow Rate
22.0		22.0	< Stack Gas Temp. (C)
22.0		22.0	< Ambient Temp. (C)
0.0		0.0	< Effective Stack Height

Model Position			Model	Model	Field Position			Field Est	PG-A	PG-B	PG-C	PG-D	PG-E	PG-F
X	Y	Z	Conc.	K*10^6	X	Y	Z	K*10^6	K*10^6	K*10^6	K*10^6	K*10^6	K*10^6	K*10^6
(cm)	(cm)	(cm)	(ppm)	(cm-2)	(m)	(m)	(m)	(m-2)	(m-2)	(m-2)	(m-2)	(m-2)	(m-2)	(m-2)
50.0	25.0	0.0	56	850	17.5	8.8	0.0	**6937**	1779	407	4	0	0	0
50.0	18.8	0.0	90	1360	17.5	6.6	0.0	**11102**	5517	3459	351	4	0	0
50.0	12.5	0.0	119	1802	17.5	4.4	0.0	**14712**	12382	15951	8909	1649	97	0
50.0	6.3	0.0	140	2109	17.5	2.2	0.0	**17214**	20113	39910	62020	64635	66073	12273
50.0	0.0	0.0	146	2208	17.5	0.0	0.0	**18027**	23643	54182	118421	219553	580972	1633984
50.0	-6.3	0.0	142	2136	17.5	-2.2	0.0	**17436**	20113	39910	62020	64635	66073	12273
50.0	-12.5	0.0	134	2026	17.5	-4.4	0.0	**16536**	12382	15951	8909	1649	97	0
50.0	-18.8	0.0	116	1751	17.5	-6.6	0.0	**14293**	5517	3459	351	4	0	0
50.0	-25.0	0.0	97	1457	17.5	-8.8	0.0	**11891**	1779	407	4	0	0	0
50.0	0.0	0.0	146	2208	17.5	0.0	0.0	**18027**	23643	54182	118421	219553	580972	1633984
50.0	0.0	6.0	120	1804	17.5	0.0	2.1	**14725**	19748	32863	38295	28194	179	0
50.0	0.0	11.0	86	1300	17.5	0.0	3.9	**10609**	12911	10092	2664	222	0	0
50.0	0.0	16.0	55	824	17.5	0.0	5.6	**6728**	6574	1548	39	0	0	0
50.0	0.0	21.0	32	480	17.5	0.0	7.4	**3918**	2607	119	0	0	0	0
150.0	50.0	0.0	9	128	52.5	17.5	0.0	**1047**	830	681	131	4	0	0
150.0	37.5	0.0	17	252	52.5	13.1	0.0	**2058**	1375	1768	986	185	11	0
150.0	25.0	0.0	28	426	52.5	8.8	0.0	**3475**	1972	3496	4172	2828	1352	30
150.0	12.5	0.0	37	558	52.5	4.4	0.0	**4559**	2448	5262	9912	14522	24780	20742
150.0	0.0	0.0	40	601	52.5	0.0	0.0	**4904**	2632	6031	13227	25055	65341	183770
150.0	-12.5	0.0	38	577	52.5	-4.4	0.0	**4707**	2448	5262	9912	14522	24780	20742
150.0	-25.0	0.0	30	454	52.5	-8.8	0.0	**3709**	1972	3496	4172	2828	1352	30
150.0	-37.5	0.0	23	349	52.5	-13.1	0.0	**2846**	1375	1768	986	185	11	0
150.0	-50.0	0.0	15	225	52.5	-17.5	0.0	**1836**	830	681	131	4	0	0
150.0	0.0	0.0	40	601	52.5	0.0	0.0	**4904**	2632	6031	13227	25055	65341	183770
150.0	0.0	11.0	35	531	52.5	0.0	3.9	**4337**	2460	5003	8651	11193	2995	4
150.0	0.0	21.0	25	373	52.5	0.0	7.4	**3044**	2060	3054	2815	1329	1	0
150.0	0.0	31.0	13	198	52.5	0.0	10.9	**1614**	1543	1369	454	42	0	0
150.0	0.0	41.0	4	62	52.5	0.0	14.4	**505**	1034	451	36	0	0	0
250.0	100.0	0.0	0	0	87.5	35.0	0.0	**0**	179	93	6	0	0	0
250.0	75.0	0.0	2	36	87.5	26.3	0.0	**296**	371	369	112	8	0	0
250.0	50.0	0.0	10	146	87.5	17.5	0.0	**1195**	626	989	903	396	88	0
250.0	25.0	0.0	20	297	87.5	8.8	0.0	**2427**	855	1786	3155	4207	5865	2863
250.0	0.0	0.0	23	344	87.5	0.0	0.0	**2809**	949	2175	4786	9253	23807	66957
250.0	-25.0	0.0	17	254	87.5	-8.8	0.0	**2070**	855	1786	3155	4207	5865	2863
250.0	-50.0	0.0	12	183	87.5	-17.5	0.0	**1491**	626	989	903	396	88	0
250.0	-75.0	0.0	6	85	87.5	-26.3	0.0	**690**	371	369	112	8	0	0
250.0	*******	0.0	2	35	87.5	-35.0	0.0	**283**	179	93	6	0	0	0
250.0	0.0	0.0	23	344	87.5	0.0	0.0	**2809**	949	2175	4786	9253	23807	66957
250.0	0.0	18.5	19	290	87.5	0.0	6.5	**2366**	886	1798	3097	3914	967	1
250.0	0.0	36.0	10	143	87.5	0.0	12.6	**1171**	732	1059	921	356	0	0
250.0	0.0	53.5	1	14	87.5	0.0	18.7	**111**	535	443	126	7	0	0
250.0	0.0	71.0	0	0	87.5	0.0	24.9	**0**	346	132	8	0	0	0

Table 10 Atm. Dispersion Comparability Test Comparisons with Open Diff. Parameters

Concentration Data: One Story; 6:12 Roof Slope; Wind Dir. = 000 *note: Field Conc. are K*10^4*

RUN Stack Location Vel. Ratio (W/U)	D01 roof 0.24	D02 eave 0.24	D03 wall 0.25	D04 roof 1.00	D05 eave 0.99	D06 wall 0.99	D07 roof 2.52	D08 eave 2.51	D09 wall 2.50
Building Position Number	Field Conc. (m-2)	Field Conc. (m-2)	Field Conc. (m-2)	Field Conc. (m-2)	Field Conc. (m-2)	Field Conc. (m-2)	Field Conc. (m-2)	Field Conc. (m-2)	Field Conc. (m-2)
1	81	89	2,417	82	104	1,477	81	72	581
2	103	104	12,993	113	123	5,194	108	93	1,522
3	124	119	6,205	123	132	4,353	116	110	1,664
4	89	106	1,564	90	108	1,297	90	83	634
5	107	112	3,967	115	135	4,454	112	101	1,989
6	137	140	3,966	130	156	3,360	131	122	1,924
7	297	530	651	241	336	687	189	209	561
8	559	13,592	1,087	510	4,379	1,514	440	1,025	1,474
9	318	861	1,333	239	614	1,399	219	369	1,274
10	758	1,223	471	450	652	552	266	407	549
11	10,767	4,428	748	2,535	3,112	912	1,053	1,171	1,000
12	768	2,115	857	443	1,535	984	295	655	1,035
13	4	4	2	1	3	2	1	1	2
14	2	1	1	0	1	0	0	0	1
15	1	1	0	0	1	0	0	0	0
16	0	0	0	0	1	0	0	0	0
17	0	0	0	0	0	0	0	0	0
18	0	0	0	0	1	0	0	0	0
19	0	0	0	0	0	0	0	0	0
20	0	0	0	0	1	0	0	0	0
21	0	0	0	0	0	0	0	0	0
22	0	0	0	0	0	0	0	0	0
23	0	0	0	0	0	0	0	0	0
24	0	0	0	0	0	0	0	0	0
25	0	1	10	1	1	3	0	0	1
26	0	0	1	0	0	0	0	0	0
27	0	0	0	0	0	0	0	0	0
28	1	2	8	1	2	3	0	1	2
29	0	0	0	0	0	0	0	0	0
30	0	0	0	0	0	0	0	0	0
31	4	18	10	5	9	12	2	6	10
32	0	0	1	0	0	2	0	0	0
33	1	2	6	1	1	10	0	0	3
34	3	6	27	3	3	32	2	2	10
35	0	1	1	0	0	2	0	0	0
36	1	2	4	1	1	9	0	0	2
37	3	5	18	3	3	27	1	2	10
38	2	6	6	2	2	8	1	2	5
39	105	101	268	98	110	203	100	86	150
40	92	90	127	94	101	106	92	85	99
41	69	69	77	68	77	75	70	66	70
42	82	73	76	78	74	75	76	71	69
43	47	49	66	45	55	64	43	43	58
44	0	64	67	65	70	66	65	64	64
45	56	53	50	56	55	50	54	54	48
46									

Table 11a Wind Tunnel Concentration Data

Concentration Data: One Story; 6:12 Roof Slope; Wind Dir. = 045 *note: Field Conc. are K*10^4*

RUN Stack Location Vel. Ratio (W/U)	D10 roof 0.25	D11 eave 0.25	D12 wall 0.25	D13 roof 0.99	D14 eave 1.00	D15 wall 1.00	D16 roof 2.49	D17 eave 2.48	D18 wall 2.52
Building Position Number	Field Conc. (m-2)	Field Conc. (m-2)	Field Conc. (m-2)	Field Conc. (m-2)	Field Conc. (m-2)	Field Conc. (m-2)	Field Conc. (m-2)	Field Conc. (m-2)	Field Conc. (m-2)
1	153	1,023	1,268	168	936	1,294	172	549	1,803
2	47	466	39,221	73	372	8,097	46	174	2,116
3	17	133	3,741	19	94	1,996	15	47	558
4	157	995	1,416	165	903	1,434	166	530	2,001
5	43	494	13,829	56	382	8,000	47	184	2,401
6	21	127	3,015	18	94	1,972	14	46	572
7	2,349	254	153	1,695	238	183	1,048	274	179
8	420	95	31	504	34	55	275	15	35
9	9	9	100	2	5	87	1	1	27
10	1,249	120	68	959	115	91	470	106	89
11	744	18	9	305	3	6	141	3	6
12	9	4	4	1	0	1	0	0	0
13	0	0	1	0	0	0	0	0	0
14	0	0	1	0	0	0	0	0	0
15	0	0	0	0	0	0	0	0	0
16	0	0	0	0	0	0	0	0	0
17	0	0	0	0	0	0	0	0	0
18	0	0	0	0	0	0	0	0	0
19	0	0	0	0	0	0	0	0	0
20	0	0	0	0	0	0	0	0	0
21	0	0	0	0	0	0	0	0	0
22	0	0	0	0	0	0	0	0	0
23	0	0	0	0	0	0	0	0	0
24	0	0	0	0	0	0	0	0	0
25	0	0	0	0	0	0	0	0	0
26	0	0	0	0	0	0	0	0	0
27	0	0	0	0	0	0	0	0	0
28	0	0	0	0	0	0	0	0	0
29	0	0	0	0	0	0	0	0	0
30	0	0	0	0	0	0	0	0	0
31	0	0	0	0	0	0	0	0	0
32	153	335	232	152	313	256	145	257	351
33	219	476	314	214	443	369	201	367	474
34	267	609	410	265	558	480	243	456	593
35	172	383	270	174	352	300	167	295	382
36	218	480	322	214	440	378	202	365	466
37	276	565	410	276	519	467	239	425	561
38	216	424	310	213	399	358	190	334	419
39	275	490	294	286	481	352	288	457	394
40	161	156	117	168	166	136	168	170	143
41	106	105	91	111	107	101	109	107	98
42	123	116	88	124	121	100	119	118	84
43	85	99	95	94	102	102	95	99	112
44	83	80	69	86	84	79	82	81	67
45	59	57	51	61	60	58	58	56	49
46									

Table 11b Wind Tunnel Concentration Data

Concentration Data: One Story; 6:12 Roof Slope; Wind Dir. = 090 *note: Field Conc. are K*10^4*

RUN Stack Location Vel. Ratio (W/U)	D19 roof 0.25	D20 eave 0.25	D21 wall 0.25	D22 roof 0.99	D23 eave 1.00	D24 wall 1.00	D25 roof 2.50	D26 eave 2.48	D27 wall 2.48
Building Position Number	Field Conc. (m-2)	Field Conc. (m-2)	Field Conc. (m-2)	Field Conc. (m-2)	Field Conc. (m-2)	Field Conc. (m-2)	Field Conc. (m-2)	Field Conc. (m-2)	Field Conc. (m-2)
1	18	961	1,715	8	792	1,439	4	417	1,398
2	5	483	36,236	44	232	6,224	5	112	3,063
3	1	119	5,858	5	53	3,559	2	31	1,813
4	29	1,265	1,355	13	1,082	1,426	5	585	1,348
5	4	695	8,360	8	282	4,603	3	108	2,531
6	1	99	3,994	4	44	2,910	2	25	1,632
7	4,199	654	156	2,005	562	161	556	485	122
8	5	117	136	3	60	130	1	11	94
9	1	4	106	1	1	66	0	1	49
10	763	18	14	515	20	9	192	16	11
11	1	2	7	1	0	4	0	0	3
12	0	1	3	0	0	1	0	0	0
13	0	0	1	0	0	0	0	0	0
14	0	0	1	0	0	0	0	0	0
15	0	0	1	0	0	0	0	0	0
16	0	0	2	0	0	0	0	0	0
17	0	0	1	0	0	0	0	0	0
18	0	0	1	0	0	0	0	0	0
19	0	0	1	0	0	0	0	0	0
20	0	0	0	0	0	0	0	0	0
21	0	0	0	0	0	0	0	0	0
22	0	0	0	0	0	0	0	0	0
23	0	0	0	0	0	0	0	0	0
24	0	1	0	0	0	0	0	0	0
25	0	0	0	0	0	0	0	0	0
26	0	0	0	0	0	0	0	0	0
27	0	0	0	0	0	0	0	0	0
28	0	0	0	0	0	0	0	0	0
29	0	0	0	0	0	0	0	0	0
30	0	0	0	0	0	0	0	0	0
31	0	0	0	0	0	0	0	0	0
32	122	271	208	99	250	214	66	189	228
33	134	344	266	113	323	281	74	241	294
34	141	403	313	117	373	366	77	275	361
35	130	289	224	107	266	235	69	201	248
36	136	337	266	111	312	285	75	237	298
37	147	374	292	123	343	331	84	255	336
38	152	310	240	124	294	262	85	222	281
39	117	155	116	118	153	127	88	129	133
40	77	75	55	79	69	60	59	60	62
41	82	67	50	73	63	51	66	54	51
42	46	41	29	43	38	33	38	34	32
43	142	114	82	138	111	86	127	99	81
44	88	69	50	82	66	52	73	58	50
45	56	43	33	52	44	33	48	40	33
46									

Table 11c Wind Tunnel Concentration Data

Concentration Data: One Story; 6:12 Roof Slope; Wind Dir. = 180 *note: Field Conc. are K*10^4*

RUN Stack Location Vel. Ratio (W/U)	D28 roof 0.25	D29 eave 0.25	D30 wall 0.25	D31 roof 1.01	D32 eave 1.00	D33 wall 1.01	D34 roof 2.49	D35 eave 2.49	D36 wall 2.46
Building Position Number	Field Conc. (m-2)	Field Conc. (m-2)	Field Conc. (m-2)	Field Conc. (m-2)	Field Conc. (m-2)	Field Conc. (m-2)	Field Conc. (m-2)	Field Conc. (m-2)	Field Conc. (m-2)
1	7	186	391	0	172	168	0	103	64
2	22	1,043	10,025	6	619	468	1	215	109
3	9	591	1,423	1	419	512	0	161	189
4	8	135	83	0	148	54	0	123	47
5	14	3,497	307	1	1,606	98	0	442	58
6	9	503	200	0	441	105	0	209	78
7	4	109	17	0	143	18	0	174	32
8	1	1,988	25	0	2,057	24	2	1,637	41
9	3	407	26	0	430	28	1	369	46
10	17	91	10	2	127	11	10	149	27
11	4,512	392	14	1,375	483	16	354	654	34
12	40	261	17	4	256	19	20	311	37
13	61	46	30	58	52	25	52	53	39
14	53	36	24	56	43	19	49	46	34
15	50	29	20	63	36	14	45	40	30
16	66	47	29	60	54	24	59	56	39
17	56	36	24	58	43	19	52	46	34
18	51	30	20	66	37	15	47	41	30
19	142	61	27	96	81	21	123	90	37
20	140	48	20	104	59	17	137	71	33
21	88	38	16	103	50	13	71	61	28
22	244	75	23	139	103	20	178	123	35
23	296	58	18	201	85	15	251	107	31
24	130	46	16	142	68	13	100	84	28
25	0	141	266	0	118	153	0	65	106
26	0	97	144	0	84	89	0	53	81
27	0	73	90	0	65	61	0	46	67
28	0	130	170	0	113	115	0	65	94
29	0	93	128	0	85	80	0	53	78
30	0	72	86	0	66	58	1	47	65
31	0	83	86	1	79	55	1	53	65
32	3	19	24	0	19	17	0	18	28
33	3	27	36	0	24	28	0	21	34
34	6	38	64	0	36	42	0	29	39
35	4	20	23	0	19	16	0	18	28
36	5	25	32	0	23	25	0	21	32
37	6	35	55	0	33	35	0	29	38
38	5	24	24	1	24	18	0	21	29
39	47	28	18	42	33	13	47	39	28
40	46	28	16	38	33	11	49	38	27
41	36	23	12	27	27	7	36	32	23
42	44	30	15	21	32	10	43	37	26
43	20	13	7	20	17	2	20	18	18
44	34	20	9	26	22	5	33	28	21
45	29	13	5	28	17	1	28	20	16
46									

Table 11d Wind Tunnel Concentration Data

Concentration Data: One Story; 9:12 Roof Slope; Wind Dir. = 000 *note: Field Conc. are K*10^4*

RUN Stack Location Vel. Ratio (W/U)	E01 roof 0.25	E02 eave 0.25	E03 wall 0.25	E04 roof 0.99	E05 eave 0.99	E06 wall 0.99	E07 roof 2.50	E08 eave 2.49	E09 wall 2.51
Building Position Number	Field Conc. (m-2)	Field Conc. (m-2)	Field Conc. (m-2)	Field Conc. (m-2)	Field Conc. (m-2)	Field Conc. (m-2)	Field Conc. (m-2)	Field Conc. (m-2)	Field Conc. (m-2)
1	48	41	2,243	42	40	1,828	46	37	833
2	55	47	12,351	44	41	4,299	49	37	1,492
3	55	59	4,662	51	54	4,439	62	46	2,215
4	53	45	1,643	45	43	1,495	50	41	874
5	56	49	2,768	44	44	2,809	51	39	1,768
6	61	73	2,545	58	57	3,084	68	50	2,206
7	67	454	693	67	253	695	67	120	654
8	69	15,944	719	63	4,145	992	68	450	1,186
9	99	912	779	91	388	1,065	94	132	1,245
10	1,542	1,398	473	495	1,179	501	181	700	562
11	6,985	2,362	489	1,432	2,233	564	364	1,292	681
12	2,861	2,145	536	790	1,769	627	283	995	779
13	7	6	2	2	3	1	0	1	1
14	2	2	1	0	1	0	0	0	0
15	1	1	0	0	0	0	0	0	0
16	1	1	0	0	0	0	0	0	0
17	0	0	0	0	0	0	0	0	0
18	0	0	0	0	0	0	0	0	0
19	0	0	0	0	0	0	0	0	0
20	0	0	0	0	0	0	0	0	0
21	0	0	0	0	0	0	0	0	0
22	0	0	0	0	0	0	0	0	0
23	0	0	0	0	0	0	0	0	0
24	0	0	0	0	0	0	0	0	0
25	1	2	1	0	1	0	0	0	1
26	0	1	0	0	0	0	0	0	0
27	0	0	0	0	0	0	0	0	0
28	3	5	1	1	3	1	0	1	1
29	1	1	0	0	1	0	0	0	0
30	0	1	0	0	0	0	0	0	0
31	46	60	16	25	47	20	7	23	18
32	4	2	1	0	0	0	0	0	0
33	5	3	2	0	1	0	0	0	0
34	8	6	4	1	2	1	0	1	2
35	5	3	2	0	0	0	0	0	0
36	6	4	2	1	1	0	0	0	0
37	9	8	4	1	3	2	1	2	3
38	43	51	28	18	40	23	8	29	32
39	40	37	225	31	33	177	30	31	124
40	41	41	68	32	36	63	31	32	54
41	45	43	52	38	39	50	34	38	47
42	39	41	43	32	35	41	26	30	38
43	39	37	50	33	36	46	29	34	41
44	42	41	40	36	37	41	32	35	37
45	33	31	32	31	32	32	27	29	30
46									

Table 11e Wind Tunnel Concentration Data

Concentration Data: One Story; 9:12 Roof Slope; Wind Dir. = 045 *note: Field Conc. are K*10^4*

RUN Stack Location Vel. Ratio (W/U)	E10 roof 0.25	E11 eave 0.25	E12 wall 0.25	E13 roof 1.01	E14 eave 1.00	E15 wall 1.01	E16 roof 2.50	E17 eave 2.50	E18 wall 2.50
Building Position Number	Field Conc. (m-2)	Field Conc. (m-2)	Field Conc. (m-2)	Field Conc. (m-2)	Field Conc. (m-2)	Field Conc. (m-2)	Field Conc. (m-2)	Field Conc. (m-2)	Field Conc. (m-2)
1	62	823	1,009	57	719	1,010	72	500	1,256
2	35	530	36,916	40	372	7,851	30	153	3,194
3	21	224	6,317	10	146	3,861	12	62	1,625
4	69	847	1,032	62	736	1,091	78	507	1,348
5	32	690	10,712	22	411	6,904	27	180	3,298
6	22	237	4,659	10	141	3,411	12	60	1,811
7	703	847	318	644	819	392	593	747	371
8	132	735	290	123	341	341	151	102	245
9	12	69	692	3	59	678	6	14	425
10	1,655	410	199	1,381	409	242	856	332	242
11	2,107	111	65	1,329	84	98	810	35	74
12	21	11	23	7	3	19	10	1	16
13	0	0	0	0	0	0	0	0	0
14	0	0	0	0	0	0	0	0	0
15	0	0	0	0	0	0	0	0	0
16	0	0	0	0	0	0	0	0	0
17	0	0	0	0	0	0	0	0	0
18	0	0	0	0	0	0	0	0	0
19	0	0	0	0	0	0	0	0	0
20	0	0	0	0	0	0	0	0	0
21	0	0	0	0	0	0	0	0	0
22	0	0	0	0	0	0	0	0	0
23	0	0	0	0	0	0	0	0	0
24	0	0	0	0	0	0	0	0	0
25	0	0	0	0	0	0	0	0	0
26	0	0	0	0	0	0	0	0	0
27	0	0	0	0	0	0	0	0	0
28	0	0	0	0	0	0	0	0	0
29	0	0	0	0	0	0	0	0	0
30	0	0	0	0	0	0	0	0	0
31	0	0	0	0	0	0	0	0	0
32	84	294	197	83	297	228	90	271	279
33	107	383	264	110	386	297	117	360	355
34	123	436	309	125	443	357	131	403	414
35	93	320	219	93	332	254	99	298	307
36	106	376	256	108	377	292	115	352	355
37	130	419	298	132	429	352	134	387	404
38	124	341	237	116	349	269	118	317	319
39	144	393	253	154	395	285	164	398	292
40	119	142	129	124	136	133	123	132	125
41	91	82	88	96	87	94	96	84	85
42	99	95	92	104	102	101	104	98	91
43	65	59	76	72	61	79	70	59	69
44	71	60	66	76	63	71	74	60	63
45	46	38	42	47	40	44	46	38	38
46									

Table 11f Wind Tunnel Concentration Data

Concentration Data: One Story; 9:12 Roof Slope; Wind Dir. = 090 *note: Field Conc. are K*10^4*

RUN Stack Location Vel. Ratio (W/U)	E19 roof 0.25	E20 eave 0.25	E21 wall 0.25	E22 roof 1.00	E23 eave 1.00	E24 wall 1.00	E25 roof 2.50	E26 eave 2.51	E27 wall 2.49
Building Position Number	Field Conc. (m-2)	Field Conc. (m-2)	Field Conc. (m-2)	Field Conc. (m-2)	Field Conc. (m-2)	Field Conc. (m-2)	Field Conc. (m-2)	Field Conc. (m-2)	Field Conc. (m-2)
1	16	985	2,197	3	669	2,427	2	374	2,061
2	33	339	39,853	35	143	7,601	8	47	2,775
3	15	87	3,642	2	24	2,009	1	7	899
4	23	1,393	1,911	5	1,043	2,117	3	672	1,711
5	28	469	9,773	5	177	4,310	3	49	1,799
6	18	63	2,275	1	18	1,429	1	5	678
7	2,748	569	154	1,383	566	123	465	487	62
8	8	183	122	3	15	71	1	13	44
9	6	6	69	0	1	35	0	0	28
10	619	17	15	517	9	5	537	4	4
11	4	3	9	1	0	1	1	0	1
12	1	1	2	0	0	0	0	0	0
13	0	0	1	0	0	0	0	0	0
14	0	0	1	0	0	0	0	0	0
15	0	0	0	0	0	0	0	0	0
16	0	0	0	0	0	0	0	0	0
17	0	0	0	0	0	0	0	0	0
18	0	0	0	0	0	0	0	0	0
19	0	0	0	0	0	0	0	0	0
20	0	0	0	0	0	0	0	0	0
21	0	0	0	0	0	0	0	0	0
22	0	0	0	0	0	0	0	0	0
23	0	0	0	0	0	0	0	0	0
24	0	0	0	0	0	0	0	0	0
25	0	0	0	0	0	0	0	0	0
26	0	0	0	0	0	0	0	0	0
27	0	0	0	0	0	0	0	0	0
28	0	0	0	0	0	0	0	0	0
29	0	0	0	0	0	0	0	0	0
30	0	0	0	0	0	0	0	0	0
31	0	0	0	0	0	0	0	0	0
32	97	300	287	73	258	329	54	199	321
33	103	386	378	77	323	437	52	249	414
34	103	420	425	74	347	503	51	277	482
35	101	318	314	76	264	352	58	208	342
36	102	365	360	75	304	417	53	237	387
37	109	316	396	80	325	469	56	259	432
38	120	0	327	92	273	372	69	218	351
39	115	166	155	90	155	169	70	129	168
40	60	66	60	53	61	62	39	53	63
41	81	75	68	75	73	69	69	68	67
42	38	38	33	34	35	36	31	29	35
43	133	120	107	130	119	108	104	113	103
44	65	57	48	62	53	48	54	48	49
45	63	53	44	61	52	46	53	50	44
46									

Table 11g Wind Tunnel Concentration Data

Concentration Data: One Story; 9:12 Roof Slope; Wind Dir. = 180 *note: Field Conc. are K*10^4*

RUN Stack Location Vel. Ratio (W/U)	E28 roof 0.25	E29 eave 0.25	E30 wall 0.25	E31 roof 1.00	E32 eave 1.00	E33 wall 1.00	E34 roof 2.48	E35 eave 2.53	E36 wall 2.52
Building Position Number	Field Conc. (m-2)	Field Conc. (m-2)	Field Conc. (m-2)	Field Conc. (m-2)	Field Conc. (m-2)	Field Conc. (m-2)	Field Conc. (m-2)	Field Conc. (m-2)	Field Conc. (m-2)
1	12	390	657	1	321	239	0	389	240
2	22	1,816	19,490	2	976	831	1	437	200
3	4	776	1,650	0	593	562	0	192	137
4	12	249	142	0	239	90	0	505	97
5	12	6,218	539	1	2,136	109	1	765	76
6	4	533	210	0	492	133	0	182	80
7	17	85	28	7	124	34	2	416	49
8	27	438	28	8	701	38	4	989	45
9	16	232	31	8	298	38	3	159	39
10	96	47	20	76	77	26	80	195	37
11	5,536	89	23	3,153	136	28	915	253	35
12	168	81	22	114	114	28	25	101	30
13	36	48	51	34	53	44	33	49	39
14	27	46	50	27	51	45	32	53	42
15	28	44	47	28	48	43	37	58	45
16	37	48	51	35	53	45	35	50	40
17	29	46	50	28	51	45	34	53	43
18	28	44	47	30	49	43	40	59	45
19	52	47	49	52	53	44	48	52	40
20	39	46	49	38	51	44	45	55	42
21	39	44	46	42	47	42	57	59	44
22	66	45	47	61	51	42	61	53	40
23	61	44	47	61	50	42	64	55	41
24	56	43	45	59	48	41	72	57	42
25	0	201	360	0	199	212	1	88	84
26	0	142	211	0	141	143	1	66	67
27	0	106	139	1	109	103	1	50	53
28	1	164	234	1	176	145	1	86	74
29	1	124	168	1	129	117	1	64	60
30	0	96	119	1	100	90	1	49	49
31	7	96	96	5	107	77	4	59	47
32	5	58	70	1	55	54	0	99	79
33	6	84	112	0	75	75	0	132	101
34	9	117	190	0	104	106	0	171	129
35	6	56	66	1	52	51	0	98	75
36	7	74	95	0	68	67	0	124	90
37	8	97	133	1	87	81	0	161	102
38	10	56	61	3	53	48	2	107	66
39	21	46	50	17	46	41	25	49	41
40	14	34	35	14	34	32	24	39	36
41	27	31	30	25	30	28	29	33	29
42	24	29	28	21	29	26	26	27	23
43	18	30	30	17	29	27	22	36	33
44	29	26	25	28	26	24	27	28	25
45	27	21	20	27	21	19	27	24	21
46									

Table 11h Wind Tunnel Concentration Data

Concentration Data: Two Story; 6:12 Roof Slope; Wind Dir. = 000 *note: Field Conc. are K*10^4*

RUN Stack Location Vel. Ratio (W/U)	F01 roof 0.25	F02 eave 0.25	F03 wall 0.25	F04 roof 1.00	F05 eave 1.00	F06 wall 1.00	F07 roof 2.50	F08 eave 2.50	F09 wall 2.51
Building Position Number	Field Conc. (m-2)	Field Conc. (m-2)	Field Conc. (m-2)	Field Conc. (m-2)	Field Conc. (m-2)	Field Conc. (m-2)	Field Conc. (m-2)	Field Conc. (m-2)	Field Conc. (m-2)
1	49	52	4,989	50	49	3,843	45	45	2,617
2	40	45	13,509	42	39	4,145	37	36	2,925
3	43	45	5,263	44	42	3,214	40	40	2,722
4	73	74	1,901	76	75	1,677	69	71	1,577
5	55	56	1,861	57	53	1,688	50	50	1,727
6	62	56	1,864	60	60	1,730	60	55	1,695
7	383	1,981	674	292	901	731	221	398	700
8	650	16,031	728	482	3,638	757	326	1,075	763
9	255	1,186	723	224	517	764	178	285	797
10	2,365	4,593	597	965	2,767	639	514	1,055	608
11	16,449	6,853	631	3,063	4,595	637	1,326	1,484	651
12	1,351	2,705	629	621	1,531	638	357	652	675
13	6	8	1	2	4	1	1	2	2
14	2	2	0	0	1	0	0	0	0
15	1	1	0	0	1	0	0	0	0
16	1	1	0	0	0	0	0	0	0
17	0	0	0	0	0	0	0	0	0
18	0	0	0	0	0	0	0	0	0
19	0	0	0	0	0	0	0	0	0
20	0	0	0	0	0	0	0	0	0
21	0	0	0	0	0	0	0	0	0
22	0	0	0	0	0	0	0	0	0
23	0	0	0	0	0	0	0	0	0
24	0	0	0	0	0	0	0	0	0
25	4	7	13	2	4	9	1	2	11
26	2	5	4	1	3	3	1	1	4
27	1	2	2	0	1	3	0	1	2
28	13	23	26	7	16	21	4	7	26
29	7	11	9	3	8	7	2	3	9
30	2	4	3	1	2	3	1	1	3
31	110	237	107	58	124	106	39	62	111
32	4	6	7	1	4	5	1	2	3
33	6	9	11	2	6	8	1	3	6
34	10	15	27	4	10	20	3	5	13
35	5	7	7	2	4	5	1	3	4
36	12	21	15	5	12	12	3	7	11
37	22	43	43	10	29	35	7	14	34
38	178	374	97	91	226	102	49	87	100
39	30	35	182	30	30	192	28	27	177
40	40	42	83	38	36	89	32	35	83
41	40	45	61	39	40	64	34	37	59
42	49	51	59	45	45	61	38	44	58
43	30	32	50	30	29	51	26	27	49
44	41	42	51	39	39	55	35	36	52
45	35	37	37	34	34	37	31	33	37
46									

Table 11i Wind Tunnel Concentration Data

Concentration Data: Two Story; 6:12 Roof Slope; Wind Dir. = 045 *note: Field Conc. are K*10^4*

RUN Stack Location Vel. Ratio (W/U)	F10 roof 0.25	F11 eave 0.25	F12 wall 0.25	F13 roof 1.00	F14 eave 1.00	F15 wall 1.00	F16 roof 2.51	F17 eave 2.52	F18 wall 2.51
Building Position Number	Field Conc. (m-2)	Field Conc. (m-2)	Field Conc. (m-2)	Field Conc. (m-2)	Field Conc. (m-2)	Field Conc. (m-2)	Field Conc. (m-2)	Field Conc. (m-2)	Field Conc. (m-2)
1	372	732	401	355	711	405	334	528	450
2	316	685	4,074	286	634	1,349	260	449	1,063
3	248	584	16,623	223	551	7,513	203	376	3,295
4	421	712	396	402	691	396	374	516	437
5	309	745	1,164	294	665	947	266	457	1,093
6	242	601	7,007	224	553	4,537	203	371	3,065
7	3,584	302	66	2,950	296	56	1,578	191	57
8	734	36	29	531	23	27	205	15	18
9	31	55	302	20	57	271	18	39	197
10	1,883	216	55	1,331	203	57	668	146	58
11	1,816	25	13	648	14	6	158	8	5
12	16	7	7	2	2	7	1	2	5
13	0	0	0	0	0	0	0	0	0
14	0	0	0	0	0	0	0	0	0
15	0	0	0	0	0	0	0	0	0
16	0	0	0	0	0	0	0	0	0
17	0	0	0	0	0	0	0	0	0
18	0	0	0	0	0	0	0	0	0
19	0	0	0	0	0	0	0	0	0
20	0	0	0	0	0	0	0	0	0
21	0	0	0	0	0	0	0	0	0
22	0	0	0	0	0	0	0	0	0
23	0	0	0	0	0	0	0	0	0
24	0	0	0	0	0	0	0	0	0
25	0	0	0	0	0	0	0	0	0
26	0	0	0	0	0	0	0	0	0
27	0	0	0	0	0	0	0	0	0
28	0	0	0	0	0	0	0	0	0
29	0	0	0	0	0	0	0	0	0
30	0	0	0	0	0	0	0	0	0
31	2	0	0	0	0	0	0	0	0
32	246	411	171	262	413	175	253	349	179
33	280	464	197	302	473	203	287	402	209
34	317	527	232	338	535	238	318	451	245
35	253	420	176	269	425	178	261	356	181
36	266	437	188	285	447	190	276	374	193
37	311	463	203	323	472	201	309	398	209
38	274	395	164	279	406	168	265	336	170
39	321	445	190	341	480	194	340	479	196
40	210	223	133	222	232	138	219	241	138
41	143	140	104	148	143	105	147	145	105
42	138	139	88	148	143	89	140	143	93
43	123	122	111	126	126	113	122	126	111
44	111	106	82	115	107	83	111	108	84
45	62	58	53	61	59	54	59	56	53
46									

Table 11j Wind Tunnel Concentration Data

Concentration Data: Two Story; 6:12 Roof Slope; Wind Dir. = 090 *note: Field Conc. are K*10^4*

RUN Stack Location Vel. Ratio (W/U)	F19 roof 0.25	F20 eave 0.25	F21 wall 0.25	F22 roof 1.02	F23 eave 1.01	F24 wall 1.00	F25 roof 2.51	F26 eave 2.51	F27 wall 2.50
Building Position Number	Field Conc. (m-2)	Field Conc. (m-2)	Field Conc. (m-2)	Field Conc. (m-2)	Field Conc. (m-2)	Field Conc. (m-2)	Field Conc. (m-2)	Field Conc. (m-2)	Field Conc. (m-2)
1	30	386	2,135	19	265	2,237	5	82	1,922
2	25	218	9,336	10	141	3,650	4	35	2,010
3	47	117	7,238	6	66	4,026	3	18	1,981
4	75	1,571	1,070	61	917	941	14	278	775
5	28	495	1,564	13	269	1,132	2	55	773
6	47	142	3,126	5	71	2,100	2	22	1,173
7	4,780	1,407	102	2,154	1,105	73	742	595	52
8	93	117	132	31	39	97	4	13	64
9	5	17	235	1	9	168	0	2	112
10	3,180	43	28	1,784	44	20	858	17	13
11	83	4	24	21	1	17	6	0	12
12	2	2	23	0	1	16	0	0	12
13	1	0	1	0	0	0	0	0	0
14	0	0	0	0	0	0	0	0	0
15	0	0	0	0	0	0	0	0	0
16	0	0	0	0	0	0	0	0	0
17	0	0	0	0	0	0	0	0	0
18	0	0	0	0	0	0	0	0	0
19	0	0	0	0	0	0	0	0	0
20	0	0	1	0	0	0	0	0	0
21	0	0	1	0	0	0	0	0	0
22	0	0	2	0	0	1	0	0	1
23	0	0	2	0	0	1	0	0	1
24	21	0	3	13	0	2	5	0	1
25	0	0	0	0	0	0	0	0	0
26	0	0	0	0	0	0	0	0	0
27	0	0	0	0	0	0	0	0	0
28	0	0	0	0	0	0	0	0	0
29	0	0	0	0	0	0	0	0	0
30	0	0	0	0	0	0	0	0	0
31	0	0	0	0	0	0	0	0	0
32	39	189	319	26	151	360	16	76	381
33	41	220	403	29	170	463	16	83	466
34	54	257	502	37	198	578	21	98	587
35	48	209	363	32	166	417	21	86	436
36	47	221	414	33	177	474	22	89	482
37	62	244	458	46	193	508	31	103	523
38	84	244	394	68	191	443	45	102	462
39	39	114	126	24	79	127	18	54	138
40	29	48	48	18	40	47	16	25	49
41	62	74	65	50	70	64	44	56	66
42	38	41	38	32	39	38	27	30	39
43	82	114	95	69	110	94	60	93	99
44	64	68	55	55	65	54	51	56	58
45	64	64	51	56	62	52	53	58	54
46									

Table 11k Wind Tunnel Concentration Data

Concentration Data: Two Story; 6:12 Roof Slope; Wind Dir. = 180 *note: Field Conc. are K*10^4*

RUN Stack Location Vel. Ratio (W/U)	F28 roof 0.25	F29 eave 0.25	F30 wall 0.25	F31 roof 1.00	F32 eave 1.00	F33 wall 1.00	F34 roof 2.50	F35 eave 2.48	F36 wall 2.51
Building Position Number	Field Conc. (m-2)	Field Conc. (m-2)	Field Conc. (m-2)	Field Conc. (m-2)	Field Conc. (m-2)	Field Conc. (m-2)	Field Conc. (m-2)	Field Conc. (m-2)	Field Conc. (m-2)
1	15	79	76	0	28	62	0	6	74
2	18	156	187	0	64	93	0	11	61
3	16	140	82	0	57	78	0	12	64
4	6	82	32	0	42	46	0	12	54
5	5	517	30	0	151	47	0	31	50
6	11	169	32	0	122	50	0	26	54
7	4	222	26	0	139	36	0	77	44
8	2	7,652	34	3	2,721	37	0	606	41
9	1	511	21	0	374	35	0	129	43
10	23	384	22	8	323	30	2	140	37
11	3,050	3,250	25	728	2,322	32	78	1,189	37
12	34	827	19	11	629	29	7	374	35
13	38	47	82	37	40	68	34	30	55
14	33	40	79	35	35	65	30	26	54
15	32	38	76	37	36	64	31	26	53
16	52	56	77	54	48	64	48	42	53
17	42	46	76	45	42	64	40	32	53
18	45	44	77	50	43	62	41	33	51
19	217	177	56	211	178	51	155	143	45
20	294	167	60	318	175	53	208	162	47
21	173	134	54	165	135	50	123	127	46
22	369	288	49	342	310	47	209	243	44
23	676	314	50	628	318	49	393	294	45
24	307	230	49	258	233	47	170	184	44
25	0	40	256	0	27	154	0	5	86
26	0	36	196	0	24	127	0	5	80
27	0	30	159	0	20	109	1	5	73
28	0	41	106	0	27	92	0	6	71
29	0	38	86	0	27	78	0	7	63
30	0	34	79	1	26	72	1	8	58
31	9	68	42	8	53	49	6	28	48
32	7	20	97	0	6	69	0	2	64
33	8	23	128	0	7	80	0	3	74
34	13	28	164	0	9	102	0	3	81
35	10	20	58	0	7	52	0	3	56
36	11	23	67	0	8	55	0	3	60
37	12	26	75	0	9	66	0	3	67
38	16	31	37	3	16	41	2	9	48
39	31	31	57	27	29	51	25	24	44
40	25	25	38	22	24	36	21	22	34
41	31	31	34	31	30	33	29	30	30
42	30	33	34	30	32	33	29	29	29
43	24	23	31	20	21	30	18	20	29
44	31	31	29	30	29	28	29	30	26
45	30	29	22	30	27	22	29	28	21
46									

Table 11l Wind Tunnel Concentration Data

Concentration Data: Two Story; 9:12 Roof Slope; Wind Dir. = 000 *note: Field Conc. are K*10^4*

RUN Stack Location Vel. Ratio (W/U)	G01 roof 0.25	G02 eave 0.25	G03 wall 0.25	G04 roof 1.00	G05 eave 1.00	G06 wall 1.00	G07 roof 2.51	G08 eave 2.48	G09 wall 2.50
Building Position Number	Field Conc. (m-2)	Field Conc. (m-2)	Field Conc. (m-2)	Field Conc. (m-2)	Field Conc. (m-2)	Field Conc. (m-2)	Field Conc. (m-2)	Field Conc. (m-2)	Field Conc. (m-2)
1	28	40	2,323	29	34	2,313	27	32	2,589
2	25	33	1,964	23	29	2,147	23	26	2,656
3	27	33	2,125	26	30	2,229	24	27	2,458
4	38	64	1,033	42	45	1,095	40	43	1,238
5	33	41	1,000	34	38	1,074	32	36	1,247
6	36	42	1,083	37	41	1,152	34	37	1,257
7	464	1,589	559	176	869	597	110	325	579
8	545	14,523	621	140	4,879	646	89	619	622
9	573	1,768	600	169	1,143	625	100	324	625
10	3,781	2,814	507	1,335	2,650	541	437	1,505	508
11	13,988	4,076	535	3,024	3,862	563	927	2,186	525
12	4,244	2,821	527	1,228	2,649	559	455	1,294	528
13	8	4	0	2	4	1	1	2	1
14	3	1	0	0	1	0	0	0	0
15	2	1	0	0	1	0	0	0	0
16	1	0	0	0	0	0	0	0	0
17	1	0	0	0	0	0	0	0	0
18	1	0	0	0	0	0	0	0	0
19	2	0	0	0	0	0	0	0	0
20	2	0	0	0	0	0	0	0	0
21	1	0	0	0	0	0	0	0	0
22	2	1	0	0	0	0	0	0	0
23	3	1	0	0	0	0	0	0	0
24	2	0	0	0	0	0	0	0	0
25	6	7	1	2	5	4	1	3	3
26	5	5	0	1	3	2	0	3	1
27	3	2	0	1	1	1	0	1	1
28	19	27	7	7	22	12	3	10	11
29	10	16	2	3	10	5	1	7	4
30	5	5	0	1	4	2	0	3	1
31	292	367	91	113	262	84	42	149	101
32	8	7	2	1	4	2	1	3	2
33	10	11	4	2	7	3	1	5	5
34	16	16	9	4	12	7	2	8	11
35	12	14	4	3	10	4	2	8	4
36	26	26	9	6	26	9	4	15	10
37	36	47	20	14	42	18	8	24	24
38	430	503	140	164	449	154	77	268	139
39	24	27	184	17	24	177	16	18	168
40	32	39	80	26	36	79	24	29	73
41	36	39	55	30	38	55	29	32	51
42	39	42	53	34	40	55	31	36	52
43	30	33	44	26	32	42	23	25	40
44	36	39	45	33	39	46	31	33	44
45	32	32	32	29	32	34	27	29	32
46									

Table 11m Wind Tunnel Concentration Data

Concentration Data: Two Story; 9:12 Roof Slope; Wind Dir. = 045 *note: Field Conc. are K*10^4*

RUN Stack Location Vel. Ratio (W/U)	G10 roof 0.25	G11 eave 0.25	G12 wall 0.25	G13 roof 1.00	G14 eave 1.01	G15 wall 1.01	G16 roof 2.50	G17 eave 2.49	G18 wall 2.49
Building Position Number	Field Conc. (m-2)	Field Conc. (m-2)	Field Conc. (m-2)	Field Conc. (m-2)	Field Conc. (m-2)	Field Conc. (m-2)	Field Conc. (m-2)	Field Conc. (m-2)	Field Conc. (m-2)
1	141	458	724	152	424	696	138	324	607
2	115	452	1,402	123	386	1,491	105	268	1,246
3	89	369	3,941	94	302	3,724	83	202	3,320
4	183	603	629	184	584	626	167	415	585
5	148	809	945	145	630	1,028	132	350	1,037
6	100	451	1,821	98	385	1,883	93	227	2,282
7	1,162	1,241	200	1,128	1,211	203	752	1,098	210
8	835	3,368	167	711	1,813	165	475	688	185
9	112	335	341	65	328	384	47	122	480
10	1,501	787	166	1,256	727	161	689	652	157
11	6,075	926	117	1,991	829	109	927	418	125
12	249	235	66	88	274	76	45	69	92
13	3	1	0	1	1	0	0	0	0
14	0	0	0	0	0	0	0	0	0
15	1	0	0	0	0	0	0	0	0
16	1	0	0	0	0	0	0	0	0
17	1	0	0	0	0	0	0	0	0
18	0	0	0	0	0	0	0	0	0
19	1	0	0	0	0	0	0	0	0
20	1	0	0	0	0	0	0	0	0
21	1	0	0	0	0	0	0	0	0
22	0	0	0	0	0	0	0	0	0
23	1	0	0	0	0	0	0	0	0
24	1	0	0	0	0	0	0	0	0
25	1	0	2	0	0	1	0	0	1
26	1	0	0	0	0	0	0	0	0
27	1	0	0	0	0	0	0	0	0
28	0	0	1	0	0	0	0	0	0
29	1	0	0	0	0	0	0	0	0
30	1	0	0	0	0	0	0	0	0
31	1	0	0	0	0	0	0	0	0
32	99	210	242	120	221	216	98	190	190
33	123	257	291	142	277	285	120	232	240
34	137	296	377	157	311	370	132	258	314
35	111	228	257	128	238	237	105	201	209
36	123	254	297	141	269	276	119	220	243
37	140	295	340	163	299	324	135	252	286
38	152	256	256	162	267	241	136	233	226
39	145	213	194	158	212	185	142	209	181
40	96	115	105	105	108	106	97	107	99
41	81	88	82	85	84	84	83	85	78
42	80	85	75	85	83	73	79	84	70
43	73	77	79	74	75	83	74	73	78
44	68	67	60	68	66	63	67	63	60
45	44	41	39	43	40	39	41	40	38
46									

Table 11n Wind Tunnel Concentration Data

Concentration Data: Two Story; 9:12 Roof Slope; Wind Dir. = 090 *note: Field Conc. are K*10^4*

RUN Stack Location Vel. Ratio (W/U)	G19 roof 0.25	G20 eave 0.25	G21 wall 0.25	G22 roof 0.99	G23 eave 1.00	G24 wall 0.99	G25 roof 2.46	G26 eave 2.49	G27 wall 2.48
Building Position Number	Field Conc. (m-2)	Field Conc. (m-2)	Field Conc. (m-2)	Field Conc. (m-2)	Field Conc. (m-2)	Field Conc. (m-2)	Field Conc. (m-2)	Field Conc. (m-2)	Field Conc. (m-2)
1	15	249	2,582	8	179	2,493	4	80	1,955
2	15	105	3,241	4	61	2,655	2	23	1,697
3	30	46	2,175	2	21	1,954	1	12	1,258
4	29	1,139	729	19	791	748	7	323	734
5	12	252	683	4	111	736	1	43	601
6	24	52	758	2	22	761	1	11	667
7	3,367	1,911	51	1,570	1,702	37	507	1,083	37
8	97	166	41	25	122	34	6	57	32
9	5	9	48	1	3	49	0	1	46
10	3,231	74	11	2,156	66	7	1,059	36	6
11	123	5	7	53	5	4	12	1	5
12	2	1	4	0	0	3	0	0	3
13	0	0	0	0	0	1	0	0	0
14	0	0	0	0	0	1	0	0	1
15	0	0	2	0	1	3	0	1	4
16	0	0	0	0	0	0	0	0	0
17	0	0	0	0	0	1	0	0	1
18	0	1	2	0	1	5	0	1	3
19	0	0	0	0	0	0	0	0	0
20	0	0	0	0	0	0	0	0	0
21	0	0	0	0	0	0	0	0	0
22	0	0	0	0	0	0	0	0	0
23	0	0	0	0	0	0	0	0	0
24	7	0	0	7	1	0	2	0	0
25	0	0	0	0	0	0	0	0	0
26	0	0	0	0	0	0	0	0	0
27	0	0	0	0	0	0	0	0	0
28	0	0	0	0	0	0	0	0	0
29	0	0	0	0	0	0	0	0	0
30	0	0	0	0	0	0	0	0	0
31	0	0	0	0	0	0	0	0	0
32	24	143	511	16	129	473	12	78	395
33	25	161	654	16	147	619	13	90	525
34	29	184	803	18	165	768	13	102	636
35	33	158	509	22	144	483	16	90	399
36	32	168	601	20	155	565	16	95	471
37	40	199	640	26	176	624	20	109	526
38	76	202	492	56	180	466	41	120	399
39	27	86	137	17	85	175	13	61	134
40	27	53	60	21	52	69	20	44	62
41	50	66	65	45	64	66	43	60	64
42	35	42	42	34	38	44	34	34	43
43	69	102	95	63	101	97	57	94	93
44	50	52	48	47	52	50	46	47	49
45	46	45	39	46	46	41	43	43	40
46									

Table 11o Wind Tunnel Concentration Data

Concentration Data: Two Story; 9:12 Roof Slope; Wind Dir. = 180 *note: Field Conc. are K*10^4*

RUN Stack Location Vel. Ratio (W/U)	G28 roof 0.25	G29 eave 0.24	G30 wall 0.25	G31 roof 0.99	G32 eave 1.00	G33 wall 1.00	G34 roof 2.50	G35 eave 2.47	G36 wall 2.50
Building Position Number	Field Conc. (m-2)	Field Conc. (m-2)	Field Conc. (m-2)	Field Conc. (m-2)	Field Conc. (m-2)	Field Conc. (m-2)	Field Conc. (m-2)	Field Conc. (m-2)	Field Conc. (m-2)
1	4	416	71	0	225	53	0	112	49
2	5	764	132	1	379	59	0	179	49
3	3	495	96	0	414	60	0	170	51
4	3	481	34	0	297	36	0	161	39
5	3	2,621	34	1	945	35	0	398	39
6	3	669	31	1	568	36	0	282	40
7	14	456	26	5	416	29	2	345	32
8	45	4,685	30	15	3,539	34	4	2,116	35
9	24	690	21	7	771	28	4	607	31
10	137	346	22	73	328	25	32	344	28
11	5,141	950	22	1,729	979	27	383	1,195	29
12	234	425	18	136	541	24	54	565	27
13	17	66	70	17	56	51	15	44	40
14	14	63	69	15	51	49	12	39	39
15	14	63	70	16	49	48	11	38	38
16	23	64	68	24	56	49	24	46	39
17	19	63	69	19	52	48	16	40	38
18	21	63	68	22	50	47	16	40	38
19	64	66	58	69	62	44	63	60	36
20	61	65	61	59	59	44	55	52	36
21	68	67	60	68	59	43	53	54	35
22	145	80	53	152	78	41	139	84	34
23	188	83	55	175	75	41	152	75	34
24	143	78	54	142	73	40	111	78	34
25	0	140	223	1	131	121	0	81	72
26	0	121	159	1	105	98	0	72	65
27	0	101	121	1	89	83	1	62	59
28	0	116	82	1	115	72	0	86	54
29	2	104	73	1	102	60	1	74	49
30	2	86	68	2	83	59	1	64	47
31	20	96	35	16	111	41	11	91	37
32	1	77	94	0	46	53	0	33	40
33	1	97	116	0	54	59	0	39	44
34	2	123	141	0	70	64	0	47	48
35	2	64	57	1	43	41	0	35	36
36	2	75	57	0	49	41	0	38	38
37	2	92	62	0	59	45	0	50	42
38	11	67	36	7	57	32	6	54	32
39	11	42	49	12	36	38	8	29	33
40	13	31	35	14	27	28	11	23	24
41	20	30	30	20	28	25	17	25	23
42	18	30	28	20	30	25	18	27	24
43	13	26	28	14	22	22	11	18	20
44	19	25	25	20	25	21	19	23	20
45	20	21	19	21	21	17	20	20	16
46									

Table 11p Wind Tunnel Concentration Data

Conc. Data: Max. over all Runs
Source (pCi/L) = 100

Building Position Number	Stack Location: roof Field Conc. (pCi/L)	eave Field Conc. (pCi/L)	wall Field Conc. (pCi/L)
1	--- BG ---	--- BG ---	0.5
2	--- BG ---	--- BG ---	0.8
3	--- BG ---	--- BG ---	0.7
4	--- BG ---	--- BG ---	0.4
5	--- BG ---	--- BG ---	0.7
6	--- BG ---	--- BG ---	0.6
7	--- BG ---	--- BG ---	--- BG ---
8	--- BG ---	0.4	--- BG ---
9	--- BG ---	--- BG ---	--- BG ---
10	--- BG ---	--- BG ---	--- BG ---
11	--- BG ---	0.4	--- BG ---
12	--- BG ---	--- BG ---	--- BG ---
13	--- BG ---	--- BG ---	--- BG ---
14	--- BG ---	--- BG ---	--- BG ---
15	--- BG ---	--- BG ---	--- BG ---
16	--- BG ---	--- BG ---	--- BG ---
17	--- BG ---	--- BG ---	--- BG ---
18	--- BG ---	--- BG ---	--- BG ---
19	--- BG ---	--- BG ---	--- BG ---
20	--- BG ---	--- BG ---	--- BG ---
21	--- BG ---	--- BG ---	--- BG ---
22	--- BG ---	--- BG ---	--- BG ---
23	--- BG ---	--- BG ---	--- BG ---
24	--- BG ---	--- BG ---	--- BG ---
25	--- BG ---	--- BG ---	--- BG ---
26	--- BG ---	--- BG ---	--- BG ---
27	--- BG ---	--- BG ---	--- BG ---
28	--- BG ---	--- BG ---	--- BG ---
29	--- BG ---	--- BG ---	--- BG ---
30	--- BG ---	--- BG ---	--- BG ---
31	--- BG ---	--- BG ---	--- BG ---
32	--- BG ---	--- BG ---	--- BG ---
33	--- BG ---	--- BG ---	--- BG ---
34	--- BG ---	--- BG ---	--- BG ---
35	--- BG ---	--- BG ---	--- BG ---
36	--- BG ---	--- BG ---	--- BG ---
37	--- BG ---	--- BG ---	--- BG ---
38	--- BG ---	--- BG ---	--- BG ---
39	--- BG ---	--- BG ---	--- BG ---
40	--- BG ---	--- BG ---	--- BG ---
41	--- BG ---	--- BG ---	--- BG ---
42	--- BG ---	--- BG ---	--- BG ---
43	--- BG ---	--- BG ---	--- BG ---
44	--- BG ---	--- BG ---	--- BG ---
45	--- BG ---	--- BG ---	--- BG ---
46			

Conc. Data: Max. over all Runs
Source (pCi/L) = 1,000

Building Position Number	Stack Location: roof Field Conc. (pCi/L)	eave Field Conc. (pCi/L)	wall Field Conc. (pCi/L)
1	0.7	1.1	5.3
2	0.5	0.9	8.1
3	0.4	0.8	6.7
4	0.8	1.4	4.1
5	0.5	1.7	6.7
6	0.4	0.8	6.2
7	3.2	2.2	1.4
8	1.0	4.3	3.0
9	0.4	1.2	2.6
10	2.1	3.1	1.2
11	3.3	4.4	2.0
12	1.0	2.6	2.1
13	--- BG ---	--- BG ---	--- BG ---
14	--- BG ---	--- BG ---	--- BG ---
15	--- BG ---	--- BG ---	--- BG ---
16	--- BG ---	--- BG ---	--- BG ---
17	--- BG ---	--- BG ---	--- BG ---
18	--- BG ---	--- BG ---	--- BG ---
19	--- BG ---	--- BG ---	--- BG ---
20	0.4	--- BG ---	--- BG ---
21	--- BG ---	--- BG ---	--- BG ---
22	0.4	0.5	--- BG ---
23	0.8	0.6	--- BG ---
24	--- BG ---	--- BG ---	--- BG ---
25	--- BG ---	--- BG ---	--- BG ---
26	--- BG ---	--- BG ---	--- BG ---
27	--- BG ---	--- BG ---	--- BG ---
28	--- BG ---	--- BG ---	--- BG ---
29	--- BG ---	--- BG ---	--- BG ---
30	--- BG ---	--- BG ---	--- BG ---
31	--- BG ---	--- BG ---	--- BG ---
32	0.5	0.7	0.8
33	0.6	0.8	1.1
34	0.6	0.9	1.3
35	0.5	0.7	0.9
36	0.6	0.8	1.0
37	0.6	0.9	1.1
38	0.5	0.7	0.9
39	0.7	1.0	0.8
40	0.4	0.5	--- BG ---
41	--- BG ---	--- BG ---	--- BG ---
42	--- BG ---	--- BG ---	--- BG ---
43	--- BG ---	--- BG ---	--- BG ---
44	--- BG ---	--- BG ---	--- BG ---
45	--- BG ---	--- BG ---	--- BG ---
46			

Table 12 Wind Tunnel Maximum Concentration Data Summary

Pasquill Type	σ_y (m)	σ_z (m)
	Open Country Conditions	
A	$0.22x(1+0.0001x)^{-1/2}$	$0.20x$
B	$0.16x(1+0.0001x)^{-1/2}$	$0.12x$
C	$0.11x(1+0.0001x)^{-1/2}$	$0.08x(1+0.0002x)^{-1/2}$
D	$0.08x(1+0.0001x)^{-1/2}$	$0.06x(1+0.0015x)^{-1/2}$
E	$0.06x(1+0.0001x)^{-1/2}$	$0.03x(1+0.0003x)^{-1}$
F	$0.04x(1+0.0001x)^{-1/2}$	$0.016x(1+0.0003x)^{-1}$
	Urban Conditions	
A-B	$0.32x(1+0.0004x)^{-1/2}$	$0.24x(1+0.001x)^{-1/2}$
C	$0.22x(1+0.0004x)^{-1/2}$	$0.20x$
D	$0.16x(1+0.0004x)^{-1/2}$	$0.14x(1+0.0003x)^{-1/2}$
E-F	$0.11x(1+0.0004x)^{-1/2}$	$0.08x(1+0.0015x)^{-1/2}$

Table 13 Formulas recommended by Briggs (1973) for σ_y and σ_z

Huber Model Input Data : One Story Buildings

* : indicates 9 :12 if different from 6 : 12

Downwind Distances X/Xmax — Xmax = 100 m

Building Position Number	0 deg Wind direction, Stack Location: roof	eave	wall
39	0.1180	0.0875	0.0875
40	0.2055	0.1750	0.1750
41	0.2930	0.2625	0.2625
42	0.2930	0.2625	0.2625
43	0.2930	0.2625	0.2625
44	0.3805	0.3500	0.3500
45	0.5555	0.5250	0.5250
46	0.6850	0.6550	0.6550
*46	0.8420	0.8077	0.8077

Downwind Distances X/Xmax — Xmax = 100 m

Building Position Number	45 deg Wind direction, Stack Location: roof	eave	wall
39	0.1269	0.1054	0.1054
40	0.2144	0.1929	0.1929
41	0.3019	0.2804	0.2804
42	0.3019	0.2804	0.2804
43	0.3019	0.2804	0.2804
44	0.3894	0.3679	0.3679
45	0.5644	0.5429	0.5429
46	0.6550	0.6550	0.6550
*46	0.8077	0.8077	0.8077

Downwind Distances X/Xmax — Xmax = 100 m

Building Position Number	90 deg Wind direction, Stack Location: roof	eave	wall
39	0.1485	0.1485	0.1485
40	0.2360	0.2360	0.2360
41	0.3235	0.3235	0.3235
42	0.3235	0.3235	0.3235
43	0.3235	0.3235	0.3235
44	0.4110	0.4110	0.4110
45	0.5860	0.5860	0.5860
46	0.5850	0.5850	0.5850
*46	0.6550	0.6550	0.6550

Downwind Distances X/Xmax — Xmax = 100 m

Building Position Number	180 deg Wind direction, Stack Location: roof	eave	wall
39	0.1789	0.2094	0.2094
40	0.2664	0.2969	0.2969
41	0.3539	0.3844	0.3844
42	0.3539	0.3844	0.3844
43	0.3539	0.3844	0.3844
44	0.4414	0.4719	0.4719
45	0.6164	0.6469	0.6469
46	0.7500	0.7800	0.7800
*46	0.8990	0.9300	0.9300

Lateral Distance Y/ Sigma Ymax — Sigma Ymax = 21.6 m

Building Position Number	0 deg Wind direction, Stack Location: roof	eave	wall
41	0.000	0.000	0.000
42	-0.160	-0.160	-0.160
43	0.160	0.160	0.160
44	0.000	0.000	0.000
45	0.000	0.000	0.000
46	0.000	0.000	0.000

Lateral Distance Y/ Sigma Ymax — Sigma Ymax = 21.6 m

Building Position Number	45 deg Wind direction, Stack Location: roof	eave	wall
41	-0.100	-0.200	-0.200
42	-0.260	-0.360	-0.360
43	0.060	-0.040	-0.040
44	-0.100	-0.200	-0.200
45	-0.100	-0.200	-0.200
46	-0.100	-0.200	-0.200

Lateral Distance Y/ Sigma Ymax — Sigma Ymax = 21.6 m

Building Position Number	90 deg Wind direction, Stack Location: roof	eave	wall
41	-0.140	-0.280	-0.280
42	-0.300	-0.440	-0.440
43	0.020	-0.120	-0.120
44	-0.140	-0.280	-0.280
45	-0.140	-0.280	-0.280
46	-0.140	-0.280	-0.280

Lateral Distance Y/ Sigma Ymax — Sigma Ymax = 21.6 m

Building Position Number	180 deg Wind direction, Stack Location: roof	eave	wall
41	0.000	0.000	0.000
42	-0.160	-0.160	-0.160
43	0.160	0.160	0.160
44	0.000	0.000	0.000
45	0.000	0.000	0.000
46	0.000	0.000	0.000

Stack Height (m)

Building	roof	eave	wall
6 : 12	5.330	3.960	0.760
9 : 12	6.096	3.960	0.760

Stack Lee Distance (m)

Wind Direction	Stack Location: roof	eave	wall
0	3.05	0.00	0.00
45	4.31	0.00	0.00
90	7.62	7.62	7.62
180	9.14	12.19	12.19

Building Dimensions (m)

Wind Direction	Height: 6 : 12	9 :12	Width: 6 : 12	9 :12
0	6.550	8.077	15.240	15.240
45	6.550	8.077	10.770	10.770
90	5.030	5.790	12.190	12.190
180	6.550	8.077	15.240	15.240

Table 14 Huber Model Input Data for One Story House

Huber Model Input Data : Two Story Buildings

* : indicates 9 :12 if different from 6 : 12

Downwind Distances X/Xmax — Xmax = 100 m

Building Position Number	0 deg Wind direction, Stack Location: roof	eave	wall
39	0.1286	0.1088	0.1088
40	0.2161	0.1963	0.1963
41	0.3036	0.2838	0.2838
42	0.3036	0.2838	0.2838
43	0.3036	0.2838	0.2838
44	0.3911	0.3713	0.3713
45	0.5661	0.5463	0.5463
46	0.8270	0.8077	0.8077
*46	0.9270	0.9077	0.9077

Downwind Distances X/Xmax — Xmax = 100 m

Building Position Number	45 deg Wind direction, Stack Location: roof	eave	wall
39	0.1344	0.1204	0.1054
40	0.2219	0.2079	0.1929
41	0.3094	0.2954	0.2804
42	0.3094	0.2954	0.2804
43	0.3094	0.2954	0.2804
44	0.3969	0.3829	0.3679
45	0.5719	0.5579	0.5429
46	0.8350	0.8077	0.8077
*46	0.9350	0.9077	0.9077

Downwind Distances X/Xmax — Xmax = 100 m

Building Position Number	90 deg Wind direction, Stack Location: roof	eave	wall
39	0.1485	0.1485	0.1485
40	0.2360	0.2360	0.2360
41	0.3235	0.3235	0.3235
42	0.3235	0.3235	0.3235
43	0.3235	0.3235	0.3235
44	0.4110	0.4110	0.4110
45	0.5860	0.5860	0.5860
46	0.7480	0.7480	0.7480
*46	0.7980	0.7980	0.7980

Downwind Distances X/Xmax — Xmax = 100 m

Building Position Number	180 deg Wind direction, Stack Location: roof	eave	wall
39	0.1683	0.1881	0.1881
40	0.2558	0.2756	0.2756
41	0.3433	0.3631	0.3631
42	0.3433	0.3631	0.3631
43	0.3433	0.3631	0.3631
44	0.4308	0.4506	0.4506
45	0.6058	0.6256	0.6256
46	0.8670	0.8670	0.8670
*46	0.9670	0.9670	0.9670

Lateral Distance Y/ Sigma Ymax — Sigma Ymax = 21.6 m

Building Position Number	0 deg Wind direction, Stack Location: roof	eave	wall
41	0.000	0.000	0.000
42	-0.160	-0.160	-0.160
43	0.160	0.160	0.160
44	0.000	0.000	0.000
45	0.000	0.000	0.000
46	0.000	0.000	0.000

Lateral Distance Y/ Sigma Ymax — Sigma Ymax = 21.6 m

Building Position Number	45 deg Wind direction, Stack Location: roof	eave	wall
41	-0.065	-0.130	-0.130
42	-0.225	-0.290	-0.290
43	0.095	0.030	0.030
44	-0.065	-0.130	-0.130
45	-0.065	-0.130	-0.130
46	-0.065	-0.130	-0.130

Lateral Distance Y/ Sigma Ymax — Sigma Ymax = 21.6 m

Building Position Number	90 deg Wind direction, Stack Location: roof	eave	wall
41	-0.092	-0.183	-0.183
42	-0.250	-0.343	-0.343
43	0.068	-0.023	-0.023
44	-0.092	-0.183	-0.183
45	-0.092	-0.183	-0.183
46	-0.092	-0.183	-0.183

Lateral Distance Y/ Sigma Ymax — Sigma Ymax = 21.6 m

Building Position Number	180 deg Wind direction, Stack Location: roof	eave	wall
41	0.000	0.000	0.000
42	-0.160	-0.160	-0.160
43	0.160	0.160	0.160
44	0.000	0.000	0.000
45	0.000	0.000	0.000
46	0.000	0.000	0.000

Stack Height (m)

Building	roof	eave	wall
6 : 12	7.390	6.550	0.760
9 : 12	7.582	6.550	0.760

Stack Lee Distance (m)

Wind Direction	Stack Location: roof	eave	wall
0	1.98	0.00	0.00
45	2.80	0.00	0.00
90	5.49	5.49	5.49
180	5.94	7.92	7.92

Building Dimensions (m)

Wind Direction	Height: 6 : 12	9 :12	Width: 6 :12	9 :12
0	8.077	9.068	10.970	10.970
45	8.077	9.068	7.760	7.760
90	5.790	7.580	7.930	7.930
180	8.077	9.068	10.970	10.970

Table 15 Huber Model Input Data for Two Story House

Stretched string distances (field meters) between stack base and building receptors

	1 story w/ 6:12 roof			1 story w/ 9:12 roof			2 story w/ 6:12 roof			2 story w/ 9:12 roof		
Buildin	Stack Location			Stack Location			Stack Location			Stack Location		
Pos. No	roof	eave	wall	roof	eave	wall	roof	eave	wall	roof	eave	wall
1	7.67	5.59	5.10	7.91	5.67	5.01	7.39	5.50	3.85	7.84	5.50	3.85
2	5.77	2.34	0.42	6.13	2.63	0.42	6.48	4.13	1.37	6.79	4.13	1.37
3	7.67	5.59	5.10	7.91	5.67	5.01	7.39	5.50	3.85	7.84	5.50	3.85
4	6.84	5.21	5.43	7.04	5.32	5.25	5.78	4.20	4.97	6.06	4.20	4.97
5	4.58	1.17	1.93	4.94	1.33	1.58	4.52	2.07	3.33	4.73	2.07	3.33
6	6.84	5.21	5.43	7.04	5.32	5.25	5.78	4.20	4.97	7.84	5.50	3.85
7	5.36	5.36	6.75	5.43	5.39	6.79	3.92	3.92	7.60	3.96	3.82	7.42
8	1.70	1.70	4.52	1.89	2.03	4.55	1.40	1.12	6.41	1.61	1.09	6.65
9	5.36	5.36	6.75	5.43	5.39	6.79	3.92	3.92	7.60	3.96	3.82	7.42
10	5.36	7.20	10.82	5.39	7.63	9.98	3.71	4.73	9.45	3.75	5.08	9.84
11	1.70	5.11	9.56	1.89	5.85	8.51	1.12	3.29	8.65	1.02	3.57	9.10
12	5.36	7.20	10.82	5.39	7.63	9.98	3.71	4.73	9.45	3.75	5.08	9.84
13	13.54	16.74	19.39	14.70	18.27	21.00	11.34	13.55	18.66	11.69	14.35	19.74
14	12.56	15.96	18.71	13.65	17.78	20.37	10.40	12.60	18.38	11.06	13.69	19.25
15	13.54	16.74	19.39	14.70	18.27	21.00	11.34	13.55	18.66	11.69	14.35	19.74
16	12.47	15.64	18.26	13.51	17.26	19.67	9.35	11.34	16.73	9.84	12.36	17.61
17	11.39	14.79	17.54	12.53	16.45	19.32	8.44	10.61	16.35	9.10	11.62	17.33
18	12.47	15.64	18.26	13.51	17.26	19.67	9.35	11.34	16.73	9.84	12.36	17.61
19	9.91	12.96	15.52	10.85	14.46	17.01	6.41	8.44	13.76	6.83	9.17	14.63
20	8.51	11.92	14.61	9.70	13.30	15.89	5.29	7.67	13.16	5.85	8.30	13.86
21	9.93	12.96	15.52	10.85	14.46	17.01	6.41	8.44	13.76	6.83	9.17	14.63
22	7.20	9.91	12.35	7.63	10.92	13.30	4.62	6.51	11.55	4.94	7.11	12.04
23	5.11	8.51	11.26	5.85	9.87	12.18	2.98	5.36	10.82	3.43	5.78	11.59
24	7.20	9.91	12.35	7.63	10.92	13.30	4.62	6.51	11.55	4.94	7.11	12.04
25	15.79	18.04	17.79	11.17	9.98	9.66	10.33	7.95	6.93	12.67	7.95	6.93
26	12.76	14.15	13.73	13.02	13.86	13.79	10.92	10.15	9.56	11.20	10.15	9.56
27	11.23	9.93	9.66	15.75	16.98	17.85	12.04	12.74	12.32	10.40	12.74	12.32
28	15.22	17.84	17.90	10.05	9.73	9.87	8.19	7.07	7.77	11.27	7.07	7.77
29	11.96	13.83	13.92	12.08	13.02	13.93	9.00	9.63	10.08	9.56	9.63	10.08
30	10.67	9.72	9.84	15.23	16.28	18.06	9.91	12.15	12.60	8.40	12.15	12.60
31	8.21	11.40	13.22	9.80	11.41	13.13	6.90	7.56	11.48	6.90	7.70	11.41
32	11.23	9.98	9.66	15.75	16.98	17.85	12.04	12.74	12.32	10.40	12.74	12.32
33	12.76	14.15	13.73	13.02	13.86	13.79	10.92	10.15	9.56	11.20	10.15	9.56
34	15.32	18.04	17.79	11.17	9.98	9.66	10.33	7.95	6.93	12.67	7.95	6.93
35	10.67	9.72	9.86	15.23	16.28	18.06	9.91	12.15	12.60	8.40	12.15	12.60
36	11.96	13.83	13.92	12.08	13.02	13.93	9.00	9.63	10.08	9.56	9.63	10.08
37	14.15	17.84	17.90	10.05	9.73	9.87	8.19	7.07	7.77	11.27	7.07	7.77
38	8.21	11.46	13.22	9.80	11.41	13.13	6.90	7.56	11.48	6.90	7.70	11.41

Concentration Data: One Story; 6:12 Roof Slope; Wind Dir. = 000 *note: Field Conc. are K*10^4*

RUN Stack Location Vel. Ratio (W/U)		D01 roof 0.25	D02 eave 0.25	D03 wall 0.25	D04 roof 1.00	D05 eave 1.00	D06 wall 1.00	D07 roof 2.50	D08 eave 2.50	D09 wall 2.50
Building Position Number		Field Conc. (m-2)	Field Conc. (m-2)	Field Conc. (m-2)	Field Conc. (m-2)	Field Conc. (m-2)	Field Conc. (m-2)	Field Conc. (m-2)	Field Conc. (m-2)	Field Conc. (m-2)
Schulman model	1	2,718	5,114	6,153	2,713	5,099	6,130	2,704	5,067	6,085
	2	4,842	29,045	795,786	4,827	28,544	537,165	4,799	27,586	324,873
	3	2,718	5,114	6,153	2,714	5,099	6,130	2,705	5,067	6,085
	4	3,420	5,880	5,420	3,413	5,859	5,402	3,399	5,818	5,367
	5	7,630	114,134	42,577	7,595	106,762	41,508	7,526	94,490	39,513
	6	3,420	5,880	5,420	3,413	5,859	5,402	3,399	5,818	5,367
	7	5,569	5,569	3,509	5,550	5,550	3,501	5,513	5,513	3,486
	8	54,611	54,611	8,062	52,865	52,865	8,023	49,670	49,670	7,946
	9	5,569	5,569	3,551	5,550	5,550	3,543	5,513	5,513	3,528
	10	5,569	1,366	1,366	5,550	1,365	1,365	5,513	1,362	1,362
	11	54,611	1,750	1,750	52,865	1,748	1,748	49,670	1,744	1,744
	12	5,569	1,366	1,366	5,550	1,365	1,365	5,513	1,362	1,362
	13	0	0	0	0	0	0	0	0	0
	14	0	0	0	0	0	0	0	0	0
	15	0	0	0	0	0	0	0	0	0
	16	0	0	0	0	0	0	0	0	0
	17	0	0	0	0	0	0	0	0	0
	18	0	0	0	0	0	0	0	0	0
	19	0	0	0	0	0	0	0	0	0
	20	0	0	0	0	0	0	0	0	0
	21	0	0	0	0	0	0	0	0	0
	22	0	0	0	0	0	0	0	0	0
	23	0	0	0	0	0	0	0	0	0
	24	0	0	0	0	0	0	0	0	0
	25	0	0	0	0	0	0	0	0	0
	26	0	0	0	0	0	0	0	0	0
	27	0	0	0	0	0	0	0	0	0
	28	0	0	0	0	0	0	0	0	0
	29	0	0	0	0	0	0	0	0	0
	30	0	0	0	0	0	0	0	0	0
	31	0	0	0	0	0	0	0	0	0
	32	0	0	0	0	0	0	0	0	0
	33	0	0	0	0	0	0	0	0	0
	34	0	0	0	0	0	0	0	0	0
	35	0	0	0	0	0	0	0	0	0
	36	0	0	0	0	0	0	0	0	0
	37	0	0	0	0	0	0	0	0	0
	38	0	0	0	0	0	0	0	0	0
	39	825	1,618	2,073	825	1,616	2,071	824	1,613	2,065
	40	247	401	521	247	401	521	247	401	520
Huber model	41	63	80	108	63	80	108	63	80	108
	42	52	67	91	52	67	91	52	67	91
	43	52	67	91	52	67	91	52	67	91
	44	57	69	88	57	69	88	57	69	88
	45	46	53	62	46	53	62	46	53	62
	46	40	43	49	40	43	49	40	43	49

Table 17a Schulman and Huber Model's Data

Concentration Data: One Story; 6:12 Roof Slope; Wind Dir. = 045 *note: Field Conc. are K*10^4*

RUN Stack Location Vel. Ratio (W/U)		D10 roof 0.25	D11 eave 0.25	D12 wall 0.25	D13 roof 1.00	D14 eave 1.00	D15 wall 1.00	D16 roof 2.50	D17 eave 2.50	D18 wall 2.50
Building Position Number		Field Conc. (m-2)	Field Conc. (m-2)	Field Conc. (m-2)	Field Conc. (m-2)	Field Conc. (m-2)	Field Conc. (m-2)	Field Conc. (m-2)	Field Conc. (m-2)	Field Conc. (m-2)
Schulman model	1	2,718	5,114	6,153	2,714	5,099	6,130	2,705	5,067	6,085
	2	4,842	29,045	795,786	4,827	28,544	537,165	4,799	27,586	324,873
	3	2,718	5,114	6,153	2,714	5,099	6,130	2,705	5,067	6,085
	4	3,420	5,880	5,420	3,413	5,859	5,402	3,399	5,818	5,367
	5	7,630	114,134	42,577	7,595	106,762	41,508	7,526	94,490	39,513
	6	3,420	5,880	5,420	3,413	5,859	5,402	3,399	5,818	5,367
	7	5,569	5,569	3,509	5,550	5,550	3,501	5,513	5,513	3,486
	8	54,611	54,611	8,062	52,865	52,865	8,023	49,670	49,670	7,946
	9	0	0	3,551	0	0	3,543	0	0	3,528
	10	5,569	1,366	1,366	5,550	1,365	1,365	5,513	1,362	1,362
	11	54,611	1,750	0	52,865	1,748	0	49,670	1,744	0
	12	0	0	0	0	0	0	0	0	0
	13	0	0	0	0	0	0	0	0	0
	14	0	0	0	0	0	0	0	0	0
	15	0	0	0	0	0	0	0	0	0
	16	0	0	0	0	0	0	0	0	0
	17	0	0	0	0	0	0	0	0	0
	18	0	0	0	0	0	0	0	0	0
	19	0	0	0	0	0	0	0	0	0
	20	0	0	0	0	0	0	0	0	0
	21	0	0	0	0	0	0	0	0	0
	22	0	0	0	0	0	0	0	0	0
	23	0	0	0	0	0	0	0	0	0
	24	0	0	0	0	0	0	0	0	0
	25	0	0	0	0	0	0	0	0	0
	26	0	0	0	0	0	0	0	0	0
	27	0	0	0	0	0	0	0	0	0
	28	0	0	0	0	0	0	0	0	0
	29	0	0	0	0	0	0	0	0	0
	30	0	0	0	0	0	0	0	0	0
	31	0	0	0	0	0	0	0	0	0
	32	1268	1622	1705	1267	1620	1703	1265	1617	1699
	33	981	798	848	981	798	848	980	797	847
	34	681	491	505	681	491	505	680	491	505
	35	1404	1692	1651	1403	1691	1650	1401	1687	1646
	36	1118	836	826	1117	836	825	1115	835	824
	37	798	502	499	798	502	499	797	502	498
	38	2372	1230	915	2369	1229	914	2362	1228	913
	39	624	880	977	623	879	977	623	878	976
	40	208	288	360	208	288	360	208	288	360
Huber model	41	74	65	86	74	65	86	74	65	86
	42	36	22	136	36	22	136	36	22	136
	43	81	102	29	81	102	29	81	102	29
	44	67	60	76	67	60	76	67	60	76
	45	54	50	58	54	50	58	54	50	58
	46	46	43	49	46	43	49	46	43	49

Table 17b Schulman and Huber Model's Data

Concentration Data: One Story; 6:12 Roof Slope; Wind Dir. = 090 *note: Field Conc. are K*10^4*

RUN Stack Location Vel. Ratio (W/U)		D19 roof 0.25	D20 eave 0.25	D21 wall 0.25	D22 roof 1.00	D23 eave 1.00	D24 wall 1.00	D25 roof 2.50	D26 eave 2.50	D27 wall 2.50
Building Position Number		Field Conc. (m-2)	Field Conc. (m-2)	Field Conc. (m-2)	Field Conc. (m-2)	Field Conc. (m-2)	Field Conc. (m-2)	Field Conc. (m-2)	Field Conc. (m-2)	Field Conc. (m-2)
Schulman model	1	0	5,114	6,153	0	5,099	6,130	0	5,067	6,085
	2	0	29,045	795,786	0	28,544	537,165	0	27,586	324,873
	3	0	5,114	6,153	0	5,099	6,130	0	5,067	6,085
	4	0	5,880	5,420	0	5,859	5,402	0	5,818	5,367
	5	0	114,134	42,577	0	106,762	41,508	0	94,490	39,513
	6	0	5,880	5,420	0	5,859	5,402	0	5,818	5,367
	7	5,569	5,569	3,509	5,550	5,550	3,501	5,513	5,513	3,486
	8	0	54,611	8,062	0	52,865	8,023	0	49,670	7,946
	9	0	0	3,551	0	0	3,543	0	0	3,528
	10	5,569	0	0	5,550	0	0	5,513	0	0
	11	0	0	0	0	0	0	0	0	0
	12	0	0	0	0	0	0	0	0	0
	13	0	0	0	0	0	0	0	0	0
	14	0	0	0	0	0	0	0	0	0
	15	0	0	0	0	0	0	0	0	0
	16	0	0	0	0	0	0	0	0	0
	17	0	0	0	0	0	0	0	0	0
	18	0	0	0	0	0	0	0	0	0
	19	0	0	0	0	0	0	0	0	0
	20	0	0	0	0	0	0	0	0	0
	21	0	0	0	0	0	0	0	0	0
	22	0	0	0	0	0	0	0	0	0
	23	0	0	0	0	0	0	0	0	0
	24	0	0	0	0	0	0	0	0	0
	25	0	0	0	0	0	0	0	0	0
	26	0	0	0	0	0	0	0	0	0
	27	0	0	0	0	0	0	0	0	0
	28	0	0	0	0	0	0	0	0	0
	29	0	0	0	0	0	0	0	0	0
	30	0	0	0	0	0	0	0	0	0
	31	0	0	0	0	0	0	0	0	0
	32	1268	1622	1705	1267	1620	1703	1265	1617	1699
	33	981	798	848	981	798	848	980	797	847
	34	681	491	505	681	491	505	680	491	505
	35	1404	1692	1651	1403	1691	1650	1401	1687	1646
	36	1118	836	826	1117	836	825	1115	835	824
	37	798	502	499	798	502	499	797	502	498
	38	2372	1230	915	2369	1229	914	2362	1228	913
	39	474	458	547	474	458	546	473	458	546
	40	180	203	261	180	203	261	180	203	261
Huber model	41	56	45	74	56	45	74	56	45	74
	42	27	14	22	27	14	22	27	14	22
	43	69	89	144	69	89	144	69	89	144
	44	57	47	69	57	47	69	57	47	69
	45	52	45	58	52	45	58	52	45	58
	46	55	67	84	55	67	84	55	67	84

Table 17c Schulman and Huber Model's Data

Concentration Data: One Story; 6:12 Roof Slope; Wind Dir. = 180 *note: Field Conc. are K*10^4*

RUN Stack Location Vel. Ratio (W/U)		D28 roof 0.25	D29 eave 0.25	D30 wall 0.25	D31 roof 1.00	D32 eave 1.00	D33 wall 1.00	D34 roof 2.50	D35 eave 2.50	D36 wall 2.50
Building Position Number		Field Conc. (m-2)	Field Conc. (m-2)	Field Conc. (m-2)	Field Conc. (m-2)	Field Conc. (m-2)	Field Conc. (m-2)	Field Conc. (m-2)	Field Conc. (m-2)	Field Conc. (m-2)
Schulman model	1									
	2									
	3									
	4									
	5									
	6									
	7									
	8									
	9									
	10									
	11									
	12									
	13									
	14									
	15									
	16									
	17									
	18									
	19									
	20									
	21									
	22									
	23									
	24									
	25									
	26									
	27									
	28									
	29									
	30									
	31									
	32									
	33									
	34									
	35									
	36									
	37									
	38									
	39									
	40									
Huber model	41	62	80	108	62	80	108	62	80	108
	42	52	67	91	52	67	91	52	67	91
	43	52	67	91	52	67	91	52	67	91
	44	57	69	88	57	69	88	57	69	88
	45	46	53	62	46	53	62	46	53	62
	46	39	43	49	39	43	49	39	43	49

Table 17d Schulman and Huber Model's Data

Concentration Data: One Story; 9:12 Roof Slope; Wind Dir. = 000 *note: Field Conc. are K*10^4*

RUN Stack Location Vel. Ratio (W/U)		E01 roof 0.25	E02 eave 0.25	E03 wall 0.25	E04 roof 1.00	E05 eave 1.00	E06 wall 1.00	E07 roof 2.50	E08 eave 2.50	E09 wall 2.50
Building Position Number		Field Conc. (m-2)	Field Conc. (m-2)	Field Conc. (m-2)	Field Conc. (m-2)	Field Conc. (m-2)	Field Conc. (m-2)	Field Conc. (m-2)	Field Conc. (m-2)	Field Conc. (m-2)
Schulman model	1	2,555	4,971	6,378	2,551	4,956	6,354	2,544	4,927	6,305
	2	4,261	23,109	764,237	4,250	22,790	522,602	4,228	22,175	319,488
	3	2,555	4,971	6,378	2,551	4,956	6,354	2,544	4,927	6,305
	4	3,230	5,646	5,798	3,224	5,627	5,777	3,211	5,589	5,737
	5	6,560	88,797	63,654	6,534	84,269	61,293	6,483	76,434	57,040
	6	3,230	5,646	5,798	3,224	5,627	5,777	3,211	5,589	5,737
	7	5,430	5,501	3,467	5,412	5,482	3,460	5,377	5,446	3,446
	8	44,382	38,518	7,716	43,221	37,641	7,680	41,062	35,993	7,609
	9	5,430	5,501	3,467	5,412	5,482	3,460	5,377	5,446	3,446
	10	5,501	2,746	1,607	5,482	2,742	1,605	5,446	2,733	1,602
	11	44,382	4,678	2,210	43,221	4,665	2,207	41,062	4,639	2,202
	12	5,501	2,746	1,607	5,482	2,742	1,605	5,446	2,733	1,602
	13	0	0	0	0	0	0	0	0	0
	14	0	0	0	0	0	0	0	0	0
	15	0	0	0	0	0	0	0	0	0
	16	0	0	0	0	0	0	0	0	0
	17	0	0	0	0	0	0	0	0	0
	18	0	0	0	0	0	0	0	0	0
	19	0	0	0	0	0	0	0	0	0
	20	0	0	0	0	0	0	0	0	0
	21	0	0	0	0	0	0	0	0	0
	22	0	0	0	0	0	0	0	0	0
	23	0	0	0	0	0	0	0	0	0
	24	0	0	0	0	0	0	0	0	0
	25	0	0	0	0	0	0	0	0	0
	26	0	0	0	0	0	0	0	0	0
	27	0	0	0	0	0	0	0	0	0
	28	0	0	0	0	0	0	0	0	0
	29	0	0	0	0	0	0	0	0	0
	30	0	0	0	0	0	0	0	0	0
	31	1665	1228	928	1663	1227	928	1660	1225	927
	32	0	0	0	0	0	0	0	0	0
	33	0	0	0	0	0	0	0	0	0
	34	0	0	0	0	0	0	0	0	0
	35	0	0	0	0	0	0	0	0	0
	36	0	0	0	0	0	0	0	0	0
	37	0	0	0	0	0	0	0	0	0
	38	1665	1228	928	1663	1227	928	1660	1225	927
	39	776	1,618	2,074	775	1,616	2,072	774	1,613	2,066
	40	238	401	521	238	401	521	238	401	520
Huber model	41	58	80	100	58	80	100	58	80	100
	42	47	65	82	47	65	82	47	65	82
	43	47	65	82	47	65	82	47	65	82
	44	52	68	82	52	68	82	52	68	82
	45	42	51	58	42	51	58	42	51	58
	46	31	34	37	31	34	37	31	34	37

Table 17e Schulman and Huber Model's Data

Concentration Data: One Story; 9:12 Roof Slope; Wind Dir. = 045 *note: Field Conc. are K*10^4*

RUN Stack Location Vel. Ratio (W/U)		E10 roof 0.25	E11 eave 0.25	E12 wall 0.25	E13 roof 1.00	E14 eave 1.00	E15 wall 1.00	E16 roof 2.50	E17 eave 2.50	E18 wall 2.50
Building Position Number		Field Conc. (m-2)	Field Conc. (m-2)	Field Conc. (m-2)	Field Conc. (m-2)	Field Conc. (m-2)	Field Conc. (m-2)	Field Conc. (m-2)	Field Conc. (m-2)	Field Conc. (m-2)
Schulman model	1	2,555	4,956	6,378	2,551	4,956	6,354	2,544	4,927	6,305
	2	4,261	22,790	764,237	4,250	22,790	522,602	4,228	22,175	319,488
	3	2,555	4,956	6,378	2,551	4,956	6,354	2,544	4,927	6,305
	4	3,230	5,627	5,798	3,224	5,627	5,777	3,211	5,589	5,737
	5	6,560	84,269	63,654	6,534	84,269	61,293	6,483	76,434	57,040
	6	3,230	5,627	5,798	3,224	5,627	5,777	3,211	5,589	5,737
	7	5,430	5,482	3,467	5,412	5,482	3,460	5,377	5,446	3,446
	8	44,382	37,641	7,716	43,221	37,641	7,680	41,062	35,993	7,609
	9	5,430	5,482	3,467	5,412	5,482	3,460	5,377	5,446	3,446
	10	5,501	2,742	1,607	5,482	2,742	1,605	5,446	2,733	1,602
	11	44,382	4,665	2,210	43,221	4,665	2,207	41,062	4,639	2,202
	12	5,501	0	1,607	5,482	0	1,605	5,446	0	1,602
	13	0	0	0	0	0	0	0	0	0
	14	0	0	0	0	0	0	0	0	0
	15	0	0	0	0	0	0	0	0	0
	16	0	0	0	0	0	0	0	0	0
	17	0	0	0	0	0	0	0	0	0
	18	0	0	0	0	0	0	0	0	0
	19	0	0	0	0	0	0	0	0	0
	20	0	0	0	0	0	0	0	0	0
	21	0	0	0	0	0	0	0	0	0
	22	0	0	0	0	0	0	0	0	0
	23	0	0	0	0	0	0	0	0	0
	24	0	0	0	0	0	0	0	0	0
	25	0	0	0	0	0	0	0	0	0
	26	0	0	0	0	0	0	0	0	0
	27	0	0	0	0	0	0	0	0	0
	28	0	0	0	0	0	0	0	0	0
	29	0	0	0	0	0	0	0	0	0
	30	0	0	0	0	0	0	0	0	0
	31	0	0	0	0	0	0	0	0	0
	32	644	555	502	644	555	501	644	554	501
	33	943	832	841	943	832	840	942	831	839
	34	1283	1607	1714	1282	1605	1712	1280	1602	1708
	35	690	603	490	689	603	490	689	603	490
	36	1097	943	824	1096	943	824	1094	942	823
	37	1585	1689	1641	1583	1687	1640	1580	1684	1636
	38	1665	1228	928	1663	1227	928	1660	1225	927
	39	533	817	971	533	816	970	533	816	969
	40	207	283	360	207	283	360	206	283	360
Huber model	41	70	60	75	70	60	75	70	60	75
	42	29	16	21	29	16	21	29	16	21
	43	77	105	130	77	105	130	77	105	130
	44	63	57	68	63	57	68	63	57	68
	45	51	48	54	51	48	54	51	48	54
	46	33	36	39	33	36	39	33	36	39

Table 17f Schulman and Huber Model's Data

Concentration Data: One Story; 9:12 Roof Slope; Wind Dir. = 090 *note: Field Conc. are K*10^4*

RUN Stack Location Vel. Ratio (W/U)		E19 roof 0.25	E20 eave 0.25	E21 wall 0.25	E22 roof 1.00	E23 eave 1.00	E24 wall 1.00	E25 roof 2.50	E26 eave 2.50	E27 wall 2.50
Building Position Number		Field Conc. (m-2)	Field Conc. (m-2)	Field Conc. (m-2)	Field Conc. (m-2)	Field Conc. (m-2)	Field Conc. (m-2)	Field Conc. (m-2)	Field Conc. (m-2)	Field Conc. (m-2)
Schulman model	1	2,555	4,971	6,378	2,551	4,956	6,354	2,544	4,927	6,305
	2	4,261	23,109	764,237	4,250	22,790	522,602	4,228	22,175	319,488
	3	2,555	4,971	6,378	2,551	4,956	6,354	2,544	4,927	6,305
	4	3,230	5,646	5,798	3,224	5,627	5,777	3,211	5,589	5,737
	5	6,560	88,797	63,654	6,534	84,269	61,293	6,483	76,434	57,040
	6	3,230	5,646	5,798	3,224	5,627	5,777	3,211	5,589	5,737
	7	5,430	5,501	3,467	5,412	5,482	3,460	5,377	5,446	3,446
	8	0	38,518	7,716	0	37,641	7,680	0	35,993	7,609
	9	0	0	3,467	0	0	3,460	0	0	3,446
	10	5,501	0	1,607	5,482	0	1,605	5,446	0	1,602
	11	0	0	0	0	0	0	0	0	0
	12	0	0	0	0	0	0	0	0	0
	13	0	0	0	0	0	0	0	0	0
	14	0	0	0	0	0	0	0	0	0
	15	0	0	0	0	0	0	0	0	0
	16	0	0	0	0	0	0	0	0	0
	17	0	0	0	0	0	0	0	0	0
	18	0	0	0	0	0	0	0	0	0
	19	0	0	0	0	0	0	0	0	0
	20	0	0	0	0	0	0	0	0	0
	21	0	0	0	0	0	0	0	0	0
	22	0	0	0	0	0	0	0	0	0
	23	0	0	0	0	0	0	0	0	0
	24	0	0	0	0	0	0	0	0	0
	25	0	0	0	0	0	0	0	0	0
	26	0	0	0	0	0	0	0	0	0
	27	0	0	0	0	0	0	0	0	0
	28	0	0	0	0	0	0	0	0	0
	29	0	0	0	0	0	0	0	0	0
	30	0	0	0	0	0	0	0	0	0
	31	0	0	0	0	0	0	0	0	0
	32	644	555	502	644	555	501	644	554	501
	33	943	832	841	943	832	840	942	831	839
	34	1283	1607	1714	1282	1605	1712	1280	1602	1708
	35	690	603	490	689	603	490	689	603	490
	36	1097	943	824	1096	943	824	1094	942	823
	37	1585	1689	1641	1583	1687	1640	1580	1684	1636
	38	1665	1228	928	1663	1227	928	1660	1225	927
	39	450	458	547	450	458	546	450	458	546
	40	180	203	261	180	203	261	180	203	261
Huber model	41	49	45	65	49	45	65	49	45	65
	42	24	14	20	24	14	20	24	14	20
	43	60	87	125	60	87	125	60	87	125
	44	49	46	61	49	46	61	49	46	61
	45	44	41	50	44	41	50	44	41	50
	46	45	57	67	45	57	67	45	57	67

Table 17g Schulman and Huber Model's Data

Concentration Data: One Story; 9:12 Roof Slope; Wind Dir. = 180 *note: Field Conc. are K*10^4*

RUN Stack Location Vel. Ratio (W/U)		E28 roof 0.25	E29 eave 0.25	E30 wall 0.25	E31 roof 1.00	E32 eave 1.00	E33 wall 1.00	E34 roof 2.50	E35 eave 2.50	E36 wall 2.50
Building Position Number		Field Conc. (m-2)	Field Conc. (m-2)	Field Conc. (m-2)	Field Conc. (m-2)	Field Conc. (m-2)	Field Conc. (m-2)	Field Conc. (m-2)	Field Conc. (m-2)	Field Conc. (m-2)
Schulman model	1									
	2									
	3									
	4									
	5									
	6									
	7									
	8									
	9									
	10									
	11									
	12									
	13									
	14									
	15									
	16									
	17									
	18									
	19									
	20									
	21									
	22									
	23									
	24									
	25									
	26									
	27									
	28									
	29									
	30									
	31									
	32									
	33									
	34									
	35									
	36									
	37									
	38									
	39									
	40									
Huber model	41	58	80	100	58	80	100	58	80	100
	42	47	65	82	47	65	82	47	65	82
	43	47	65	82	47	65	82	47	65	82
	44	52	68	82	52	68	82	52	68	82
	45	42	51	58	42	51	58	42	51	58
	46	30	68	39	30	68	39	30	68	39

Table 17h Schulman and Huber Model's Data

Concentration Data: Two Story; 6:12 Roof Slope; Wind Dir. = 000 *note: Field Conc. are K*10^4*

RUN Stack Location Vel. Ratio (W/U)		F01 roof 0.25	F02 eave 0.25	F03 wall 0.25	F04 roof 1.00	F05 eave 1.00	F06 wall 1.00	F07 roof 2.50	F08 eave 2.50	F09 wall 2.50
Building Position Number		Field Conc. (m-2)	Field Conc. (m-2)	Field Conc. (m-2)	Field Conc. (m-2)	Field Conc. (m-2)	Field Conc. (m-2)	Field Conc. (m-2)	Field Conc. (m-2)	Field Conc. (m-2)
Schulman model	1	2,931	5,293	10,770	2,926	5,276	10,700	2,916	5,242	10,563
	2	3,813	9,362	84,379	3,804	9,309	80,281	3,786	9,205	73,138
	3	2,931	5,293	10,770	2,926	5,276	10,700	2,916	5,242	10,563
	4	4,792	9,053	6,468	4,778	9,004	6,443	4,751	8,906	6,393
	5	7,836	37,233	14,429	7,799	36,413	14,304	7,725	34,868	14,059
	6	4,792	9,053	6,468	4,778	9,004	6,443	4,751	8,906	6,393
	7	10,390	10,390	2,772	10,325	10,325	2,767	10,197	10,197	2,758
	8	80,282	124,285	3,897	76,563	115,593	3,887	70,040	101,342	3,869
	9	10,390	10,390	2,772	10,325	10,325	2,767	10,197	10,197	2,758
	10	11,596	7,156	1,791	11,515	7,125	1,789	11,356	7,064	1,785
	11	124,285	14,736	2,139	115,593	14,606	2,137	101,342	14,351	2,131
	12	11,596	7,156	1,791	11,515	7,125	1,789	11,356	7,064	1,785
	13	0	0	0	0	0	0	0	0	0
	14	0	0	0	0	0	0	0	0	0
	15	0	0	0	0	0	0	0	0	0
	16	0	0	0	0	0	0	0	0	0
	17	0	0	0	0	0	0	0	0	0
	18	0	0	0	0	0	0	0	0	0
	19	0	0	0	0	0	0	0	0	0
	20	0	0	0	0	0	0	0	0	0
	21	0	0	0	0	0	0	0	0	0
	22	0	0	0	0	0	0	0	0	0
	23	0	0	0	0	0	0	0	0	0
	24	0	0	0	0	0	0	0	0	0
	25	0	0	0	0	0	0	0	0	0
	26	0	0	0	0	0	0	0	0	0
	27	0	0	0	0	0	0	0	0	0
	28	0	0	0	0	0	0	0	0	0
	29	0	0	0	0	0	0	0	0	0
	30	0	0	0	0	0	0	0	0	0
	31	3363	2797	1213	3356	2793	1212	3342	2783	1211
	32	0	0	0	0	0	0	0	0	0
	33	0	0	0	0	0	0	0	0	0
	34	0	0	0	0	0	0	0	0	0
	35	0	0	0	0	0	0	0	0	0
	36	0	0	0	0	0	0	0	0	0
	37	0	0	0	0	0	0	0	0	0
	38	3363	2797	1213	3356	2793	1212	3342	2783	1211
	39	582	925	1,363	581	924	1,362	581	923	1,359
	40	205	302	414	205	302	414	205	302	413
Huber model	41	42	50	91	42	50	91	42	50	91
	42	25	29	53	25	29	53	25	29	53
	43	25	29	53	25	29	53	25	29	53
	44	41	48	79	41	48	79	41	48	79
	45	37	41	59	37	41	59	37	41	59
	46	29	31	40	29	31	40	29	31	40

Table 17i Schulman and Huber Model's Data

Concentration Data: Two Story; 6:12 Roof Slope; Wind Dir. = 045 *note: Field Conc. are K*10^4*

RUN Stack Location Vel. Ratio (W/U)		F10 roof 0.25	F11 eave 0.25	F12 wall 0.25	F13 roof 1.00	F14 eave 1.00	F15 wall 1.00	F16 roof 2.50	F17 eave 2.50	F18 wall 2.50
Building Position Number		Field Conc. (m-2)	Field Conc. (m-2)	Field Conc. (m-2)	Field Conc. (m-2)	Field Conc. (m-2)	Field Conc. (m-2)	Field Conc. (m-2)	Field Conc. (m-2)	Field Conc. (m-2)
Schulman model	1	2,555	5,293	10,770	2,551	5,276	10,700	2,544	5,242	10,563
	2	4,261	9,362	84,379	4,250	9,309	80,281	4,228	9,205	73,138
	3	2,555	5,293	10,770	2,551	5,276	10,700	2,544	5,242	10,563
	4	3,230	9,053	6,468	3,224	9,004	6,443	3,211	8,906	6,393
	5	6,560	37,233	14,429	6,534	36,413	14,304	6,483	34,868	14,059
	6	3,230	9,053	6,468	3,224	9,004	6,443	3,211	8,906	6,393
	7	5,430	10,390	2,772	5,412	10,325	2,767	5,377	10,197	2,758
	8	44,382	124,285	3,897	43,221	115,593	3,887	41,062	101,342	3,869
	9	5,430	10,390	2,772	5,412	10,325	2,767	5,377	10,197	2,758
	10	5,501	7,156	1,791	5,482	7,125	1,789	5,446	7,064	1,785
	11	44,382	14,736	2,139	43,221	14,606	2,137	41,062	14,351	2,131
	12	5,501	0	0	5,482	0	0	5,446	0	0
	13	0	0	0	0	0	0	0	0	0
	14	0	0	0	0	0	0	0	0	0
	15	0	0	0	0	0	0	0	0	0
	16	0	0	0	0	0	0	0	0	0
	17	0	0	0	0	0	0	0	0	0
	18	0	0	0	0	0	0	0	0	0
	19	0	0	0	0	0	0	0	0	0
	20	0	0	0	0	0	0	0	0	0
	21	0	0	0	0	0	0	0	0	0
	22	0	0	0	0	0	0	0	0	0
	23	0	0	0	0	0	0	0	0	0
	24	0	0	0	0	0	0	0	0	0
	25	0	0	0	0	0	0	0	0	0
	26	0	0	0	0	0	0	0	0	0
	27	0	0	0	0	0	0	0	0	0
	28	0	0	0	0	0	0	0	0	0
	29	0	0	0	0	0	0	0	0	0
	30	0	0	0	0	0	0	0	0	0
	31	0	0	0	0	0	0	0	0	0
	32	644	985	1053	644	984	1053	644	983	1051
	33	943	1552	1751	943	1551	1750	942	1548	1746
	34	1283	2533	3329	1282	2529	3322	1280	2521	3309
	35	690	1084	1007	689	1083	1006	689	1082	1005
	36	1097	1726	1574	1096	1724	1572	1094	1721	1569
	37	1585	3198	2648	1583	3192	2644	1580	3180	2636
	38	1665	2797	1213	1663	2793	1212	1660	2783	1211
	39	533	874	971	533	873	970	533	872	969
	40	207	283	354	207	283		206	283	353
Huber model	41	74	63	113	74	63	113	74	63	113
	42	22	12	22	22	12	22	22	12	22
	43	65	93	167	65	93	167	65	93	167
	44	67	60	98	67	60	98	67	60	98
	45	53	50	71	53	50	71	53	50	71
	46	38	41	51	38	41	51	38	41	51

Table 17j Schulman and Huber Model's Data

Concentration Data: Two Story; 6:12 Roof Slope; Wind Dir. = 090 *note: Field Conc. are K*10^4*

RUN Stack Location Vel. Ratio (W/U)		F19 roof 0.25	F20 eave 0.25	F21 wall 0.25	F22 roof 1.00	F23 eave 1.00	F24 wall 1.00	F25 roof 2.50	F26 eave 2.50	F27 wall 2.50
Building Position Number		Field Conc. (m-2)	Field Conc. (m-2)	Field Conc. (m-2)	Field Conc. (m-2)	Field Conc. (m-2)	Field Conc. (m-2)	Field Conc. (m-2)	Field Conc. (m-2)	Field Conc. (m-2)
Schulman model	1	2,931	5,293	10,770	2,926	5,276	10,700	2,916	5,242	10,563
	2	3,813	9,362	84,379	3,804	9,309	80,281	3,786	9,205	73,138
	3	2,931	5,293	10,770	2,926	5,276	10,700	2,916	5,242	10,563
	4	4,792	9,053	6,468	4,778	9,004	6,443	4,751	8,906	6,393
	5	7,836	37,233	14,429	7,799	36,413	14,304	7,725	34,868	14,059
	6	4,792	9,053	6,468	4,778	9,004	6,443	4,751	8,906	6,393
	7	10,390	10,390	2,772	10,325	10,325	2,767	10,197	10,197	2,758
	8	80,282	124,285	3,897	76,563	115,593	3,887	70,040	101,342	3,869
	9	0	0	2,772	0	0	2,767	0	0	2,758
	10	11,596	7,156	1,791	11,515	7,125	1,789	11,356	7,064	1,785
	11	124,285	0	2,139	115,593	0	2,137	101,342	0	2,131
	12	0	0	1,791	0	0	1,789	0	0	1,785
	13	0	0	0	0	0	0	0	0	0
	14	0	0	0	0	0	0	0	0	0
	15	0	0	0	0	0	0	0	0	0
	16	0	0	0	0	0	0	0	0	0
	17	0	0	0	0	0	0	0	0	0
	18	0	0	0	0	0	0	0	0	0
	19	0	0	0	0	0	0	0	0	0
	20	0	0	0	0	0	0	0	0	0
	21	0	0	0	0	0	0	0	0	0
	22	0	0	0	0	0	0	0	0	0
	23	0	0	0	0	0	0	0	0	0
	24	0	0	0	0	0	0	0	0	0
	25	0	0	0	0	0	0	0	0	0
	26	0	0	0	0	0	0	0	0	0
	27	0	0	0	0	0	0	0	0	0
	28	0	0	0	0	0	0	0	0	0
	29	0	0	0	0	0	0	0	0	0
	30	0	0	0	0	0	0	0	0	0
	31	0	0	0	0	0	0	0	0	0
	32	1103	985	1053	1102	984	1053	1101	983	1051
	33	1341	1552	1751	1340	1551	1750	1338	1548	1746
	34	1500	2533	3329	1499	2529	3322	1496	2521	3309
	35	1630	1084	1007	1628	1083	1006	1625	1082	1005
	36	1976	1726	1574	1974	1724	1572	1969	1721	1569
	37	2384	3198	2648	2380	3192	2644	2373	3180	2636
	38	3363	2797	1213	3356	2793	1212	3342	2783	1211
	39	425	391	506	425	391	506	425	391	506
	40	174	186	250	174	186	250	174	186	250
Huber model	41	60	41	86	60	41	86	60	41	86
	42	17	6	12	17	6	12	17	6	12
	43	65	88	185	65	88	185	65	88	185
	44	57	45	82	57	45	82	57	45	82
	45	49	43	66	49	43	66	49	43	66
	46	43	47	65	43	47	65	43	47	65

Table 17k Schulman and Huber Model's Data

Concentration Data: Two Story; 6:12 Roof Slope; Wind Dir. = 180 *note: Field Conc. are K*10^4*

RUN Stack Location Vel. Ratio (W/U)		F28 roof 0.25	F29 eave 0.25	F30 wall 0.25	F31 roof 1.00	F32 eave 1.00	F33 wall 1.00	F34 roof 2.50	F35 eave 2.50	F36 wall 2.50
Building Position Number		Field Conc. (m-2)	Field Conc. (m-2)	Field Conc. (m-2)	Field Conc. (m-2)	Field Conc. (m-2)	Field Conc. (m-2)	Field Conc. (m-2)	Field Conc. (m-2)	Field Conc. (m-2)
Schulman model	1									
	2									
	3									
	4									
	5									
	6									
	7									
	8									
	9									
	10									
	11									
	12									
	13									
	14									
	15									
	16									
	17									
	18									
	19									
	20									
	21									
	22									
	23									
	24									
	25									
	26									
	27									
	28									
	29									
	30									
	31									
	32									
	33									
	34									
	35									
	36									
	37									
	38									
	39									
	40									
Huber model	41	60	71	129	60	71	129	60	71	129
	42	42	50	91	42	50	91	42	50	91
	43	42	50	91	42	50	91	42	50	91
	44	55	63	103	55	63	103	55	63	103
	45	44	49	70	44	49	70	44	49	70
	46	33	35	44	33	35	44	33	35	44

Table 17l Schulman and Huber Model's Data

Concentration Data: Two Story; 9:12 Roof Slope; Wind Dir. = 000 *note: Field Conc. are K*10^4*

RUN Stack Location Vel. Ratio (W/U)		G01 roof 0.25	G02 eave 0.25	G03 wall 0.25	G04 roof 1.00	G05 eave 1.00	G06 wall 1.00	G07 roof 2.50	G08 eave 2.50	G09 wall 2.50
Building Position Number		Field Conc. (m-2)	Field Conc. (m-2)	Field Conc. (m-2)	Field Conc. (m-2)	Field Conc. (m-2)	Field Conc. (m-2)	Field Conc. (m-2)	Field Conc. (m-2)	Field Conc. (m-2)
Schulman model	1	2,601	5,293	10,770	2,597	5,276	10,700	2,589	5,242	10,563
	2	3,467	9,362	84,379	3,460	9,309	80,281	3,446	9,205	73,138
	3	2,601	5,293	10,770	2,597	5,276	10,700	2,589	5,242	10,563
	4	4,360	9,053	6,468	4,348	9,004	6,443	4,325	8,906	6,393
	5	7,156	37,233	14,429	7,125	36,413	14,304	7,064	34,868	14,059
	6	2,601	5,293	10,770	2,597	5,276	10,700	2,589	5,242	10,563
	7	10,207	10,968	2,904	10,144	10,896	2,899	10,021	10,753	2,889
	8	60,951	132,211	3,615	58,783	122,419	3,607	54,860	106,551	3,591
	9	10,207	10,968	2,904	10,144	10,896	2,899	10,021	10,753	2,889
	10	11,381	6,204	1,653	11,303	6,181	1,651	11,150	6,134	1,648
	11	150,491	12,521	1,931	137,932	12,427	1,929	118,113	12,242	1,924
	12	11,381	6,204	1,653	11,303	6,181	1,651	11,150	6,134	1,648
	13	0	0	0	0	0	0	0	0	0
	14	0	0	0	0	0	0	0	0	0
	15	0	0	0	0	0	0	0	0	0
	16	0	0	0	0	0	0	0	0	0
	17	0	0	0	0	0	0	0	0	0
	18	0	0	0	0	0	0	0	0	0
	19	0	0	0	0	0	0	0	0	0
	20	0	0	0	0	0	0	0	0	0
	21	0	0	0	0	0	0	0	0	0
	22	0	0	0	0	0	0	0	0	0
	23	0	0	0	0	0	0	0	0	0
	24	0	0	0	0	0	0	0	0	0
	25	0	0	0	0	0	0	0	0	0
	26	0	0	0	0	0	0	0	0	0
	27	0	0	0	0	0	0	0	0	0
	28	0	0	0	0	0	0	0	0	0
	29	0	0	0	0	0	0	0	0	0
	30	0	0	0	0	0	0	0	0	0
	31	3363	2697	1228	3356	2692	1227	3342	2683	1225
	32	0	0	0	0	0	0	0	0	0
	33	0	0	0	0	0	0	0	0	0
	34	0	0	0	0	0	0	0	0	0
	35	0	0	0	0	0	0	0	0	0
	36	0	0	0	0	0	0	0	0	0
	37	0	0	0	0	0	0	0	0	0
	38	3363	2697	1228	3356	2692	1227	3342	2683	1225
	39	609	931	1,338	608	930	1,337	608	929	1,335
	40	211	302	414	211	302	414	211	302	413
Huber model	41	63	75	126	63	75	126	63	75	126
	42	43	51	85	43	51	85	43	51	85
	43	43	51	85	43	51	85	43	51	85
	44	56	65	100	56	65	100	56	65	100
	45	45	50	68	45	50	68	45	50	68
	46	29	31	37	29	31	37	29	31	37

Table 17m Schulman and Huber Model's Data

Concentration Data: Two Story; 9:12 Roof Slope; Wind Dir. = 045 *note: Field Conc. are K*10^4*

RUN Stack Location Vel. Ratio (W/U)		G10 roof 0.25	G11 eave 0.25	G12 wall 0.25	G13 roof 1.00	G14 eave 1.00	G15 wall 1.00	G16 roof 2.50	G17 eave 2.50	G18 wall 2.50
Building Position Number		Field Conc. (m-2)	Field Conc. (m-2)	Field Conc. (m-2)	Field Conc. (m-2)	Field Conc. (m-2)	Field Conc. (m-2)	Field Conc. (m-2)	Field Conc. (m-2)	Field Conc. (m-2)
Schulman model	1	2,601	5,293	10,770	2,597	5,276	10,700	2,589	5,242	10,563
	2	3,467	9,362	84,379	3,460	9,309	80,281	3,446	9,205	73,138
	3	2,601	5,293	10,770	2,597	5,276	10,700	2,589	5,242	10,563
	4	4,360	9,053	6,468	4,348	9,004	6,443	4,325	8,906	6,393
	5	7,156	37,233	14,429	7,125	36,413	14,304	7,064	34,868	14,059
	6	2,601	5,293	10,770	2,597	5,276	10,700	2,589	5,242	10,563
	7	10,207	10,968	2,904	10,144	10,896	2,899	10,021	10,753	2,889
	8	60,951	132,211	3,615	58,783	122,419	3,607	54,860	106,551	3,591
	9	10,207	10,968	2,904	10,144	10,896	2,899	10,021	10,753	2,889
	10	11,381	6,204	1,653	11,303	6,181	1,651	11,150	6,134	1,648
	11	150,491	12,521	1,931	137,932	12,427	1,929	118,113	12,242	1,924
	12	11,381	6,204	1,653	11,303	6,181	1,651	11,150	6,134	1,648
	13	0	0	0	0	0	0	0	0	0
	14	0	0	0	0	0	0	0	0	0
	15	0	0	0	0	0	0	0	0	0
	16	0	0	0	0	0	0	0	0	0
	17	0	0	0	0	0	0	0	0	0
	18	0	0	0	0	0	0	0	0	0
	19	0	0	0	0	0	0	0	0	0
	20	0	0	0	0	0	0	0	0	0
	21	0	0	0	0	0	0	0	0	0
	22	0	0	0	0	0	0	0	0	0
	23	0	0	0	0	0	0	0	0	0
	24	0	0	0	0	0	0	0	0	0
	25	0	0	0	0	0	0	0	0	0
	26	0	0	0	0	0	0	0	0	0
	27	0	0	0	0	0	0	0	0	0
	28	0	0	0	0	0	0	0	0	0
	29	0	0	0	0	0	0	0	0	0
	30	0	0	0	0	0	0	0	0	0
	31	0	0	0	0	0	0	0	0	0
	32	1480	985	1053	1478	984	1053	1476	983	1051
	33	1275	1552	1751	1274	1551	1750	1272	1548	1746
	34	996	2533	3329	995	2529	3322	994	2521	3309
	35	2266	1084	1007	2263	1083	1006	2257	1082	1005
	36	1751	1726	1574	1750	1724	1572	1746	1721	1569
	37	1259	3198	2648	1258	3192	2644	1256	3180	2636
	38	3363	2697	1228	3356	2692	1227	3342	2683	1225
	39	493	883	986	493	883	986	492	882	985
	40	186	280	350	186	280	350	186	280	350
Huber model	41	78	64	105	78	64	105	78	64	105
	42	19	10	16	19	10	16	19	10	16
	43	68	103	165	68	103	165	68	103	165
	44	69	61	93	69	61	93	69	61	93
	45	53	51	69	53	51	69	53	51	69
	46	38	36	43	38	36	43	38	36	43

Table 17n Schulman and Huber Model's Data

Concentration Data: Two Story; 9:12 Roof Slope; Wind Dir. = 090 *note: Field Conc. are K*10^4*

RUN Stack Location Vel. Ratio (W/U)		G19 roof 0.25	G20 eave 0.25	G21 wall 0.25	G22 roof 1.00	G23 eave 1.00	G24 wall 1.00	G25 roof 2.50	G26 eave 2.50	G27 wall 2.50
Building Position Number		Field Conc. (m-2)	Field Conc. (m-2)	Field Conc. (m-2)	Field Conc. (m-2)	Field Conc. (m-2)	Field Conc. (m-2)	Field Conc. (m-2)	Field Conc. (m-2)	Field Conc. (m-2)
Schulman model	1	2,601	5,293	10,770	2,597	5,276	10,700	2,589	5,242	10,563
	2	3,467	9,362	84,379	3,460	9,309	80,281	3,446	9,205	73,138
	3	2,601	5,293	10,770	2,597	5,276	10,700	2,589	5,242	10,563
	4	4,360	9,053	6,468	4,348	9,004	6,443	4,325	8,906	6,393
	5	7,156	37,233	14,429	7,125	36,413	14,304	7,064	34,868	14,059
	6	2,601	5,293	10,770	2,597	5,276	10,700	2,589	5,242	10,563
	7	10,207	10,968	2,904	10,144	10,896	2,899	10,021	10,753	2,889
	8	60,951	132,211	3,615	58,783	122,419	3,607	54,860	106,551	3,591
	9	0	0	2,904	0	0	2,899	0	0	2,889
	10	11,381	6,204	1,653	11,303	6,181	1,651	11,150	6,134	1,648
	11	150,491	0	1,931	137,932	0	1,929	118,113	0	1,924
	12	0	0	0	0	0	0	0	0	0
	13	0	0	0	0	0	0	0	0	0
	14	0	0	0	0	0	0	0	0	0
	15	0	0	0	0	0	0	0	0	0
	16	0	0	0	0	0	0	0	0	0
	17	0	0	0	0	0	0	0	0	0
	18	0	0	0	0	0	0	0	0	0
	19	0	0	0	0	0	0	0	0	0
	20	0	0	0	0	0	0	0	0	0
	21	0	0	0	0	0	0	0	0	0
	22	0	0	0	0	0	0	0	0	0
	23	0	0	0	0	0	0	0	0	0
	24	0	0	0	0	0	0	0	0	0
	25	0	0	0	0	0	0	0	0	0
	26	0	0	0	0	0	0	0	0	0
	27	0	0	0	0	0	0	0	0	0
	28	0	0	0	0	0	0	0	0	0
	29	0	0	0	0	0	0	0	0	0
	30	0	0	0	0	0	0	0	0	0
	31	0	0	0	0	0	0	0	0	0
	32	1480	985	1053	1478	984	1053	1476	983	1053
	33	1275	1552	1751	1274	1551	1750	1272	1548	1750
	34	996	2533	3329	995	2529	3322	994	2521	3322
	35	2266	1084	1007	2263	1083	1006	2257	1082	1006
	36	1751	1726	1574	1750	1724	1572	1746	1721	1572
	37	1259	3198	2648	1258	3192	2644	1256	3180	2644
	38	3363	2697	1228	3356	2692	1227	3342	2683	1227
	39	413	391	506	413	391	506	413	391	506
	40	172	186	250	172	186	250	172	186	250
Huber model	41	60	41	80	60	41	80	60	41	80
	42	16	5	10	16	5	10	16	5	10
	43	66	93	183	66	93	183	66	93	183
	44	57	45	78	57	45	78	57	45	78
	45	49	43	64	49	43	64	49	43	64
	46	43	44	58	43	44	58	43	44	58

Table 17o Schulman and Huber Model's Data

Concentration Data: Two Story; 9:12 Roof Slope; Wind Dir. = 180 *note: Field Conc. are K*10^4*

RUN Stack Location Vel. Ratio (W/U)		G28 roof 0.25	G29 eave 0.25	G30 wall 0.25	G31 roof 1.00	G32 eave 1.00	G33 wall 1.00	G34 roof 2.50	G35 eave 2.50	G36 wall 2.50
Building Position Number		Field Conc. (m-2)	Field Conc. (m-2)	Field Conc. (m-2)	Field Conc. (m-2)	Field Conc. (m-2)	Field Conc. (m-2)	Field Conc. (m-2)	Field Conc. (m-2)	Field Conc. (m-2)
Schulman model	1									
	2									
	3									
	4									
	5									
	6									
	7									
	8									
	9									
	10									
	11									
	12									
	13									
	14									
	15									
	16									
	17									
	18									
	19									
	20									
	21									
	22									
	23									
	24									
	25									
	26									
	27									
	28									
	29									
	30									
	31									
	32									
	33									
	34									
	35									
	36									
	37									
	38									
	39									
	40									
Huber model	41	63	75	126	63	75	126	63	75	126
	42	43	51	85	43	51	85	43	51	85
	43	43	51	85	43	51	85	43	51	85
	44	56	65	100	56	65	100	56	65	100
	45	45	50	68	45	50	68	45	50	68
	46	29	31	37	29	31	37	29	31	37

Table 17p Schulman and Huber Model's Data

Conc. Models: Max. over all Runs
Source (pCi/L) = 100

Building Position Number	Stack Location: roof Field Conc. (pCi/L)	eave Field Conc. (pCi/L)	wall Field Conc. (pCi/L)
1	0.6	1.1	2.1
2	1.0	5.6	65.9
3	0.6	1.1	2.1
4	1.0	1.8	1.3
5	1.6	19.2	11.6
6	1.0	1.8	2.1
7	2.1	2.2	0.7
8	14.2	21.6	1.6
9	2.1	2.2	0.7
10	2.3	1.4	--- BG ---
11	23.9	2.9	0.4
12	2.3	1.4	--- BG ---
13	--- BG ---	--- BG ---	--- BG ---
14	--- BG ---	--- BG ---	--- BG ---
15	--- BG ---	--- BG ---	--- BG ---
16	--- BG ---	--- BG ---	--- BG ---
17	--- BG ---	--- BG ---	--- BG ---
18	--- BG ---	--- BG ---	--- BG ---
19	--- BG ---	--- BG ---	--- BG ---
20	--- BG ---	--- BG ---	--- BG ---
21	--- BG ---	--- BG ---	--- BG ---
22	--- BG ---	--- BG ---	--- BG ---
23	--- BG ---	--- BG ---	--- BG ---
24	--- BG ---	--- BG ---	--- BG ---
25	--- BG ---	--- BG ---	--- BG ---
26	--- BG ---	--- BG ---	--- BG ---
27	--- BG ---	--- BG ---	--- BG ---
28	--- BG ---	--- BG ---	--- BG ---
29	--- BG ---	--- BG ---	--- BG ---
30	--- BG ---	--- BG ---	--- BG ---
31	0.7	0.6	--- BG ---
32	--- BG ---	--- BG ---	--- BG ---
33	--- BG ---	--- BG ---	--- BG ---
34	--- BG ---	0.5	0.7
35	0.5	--- BG ---	--- BG ---
36	--- BG ---	--- BG ---	--- BG ---
37	0.5	0.6	0.5
38	0.7	0.6	--- BG ---
39	--- BG ---	--- BG ---	0.4
40	--- BG ---	--- BG ---	--- BG ---
41	--- BG ---	--- BG ---	--- BG ---
42	--- BG ---	--- BG ---	--- BG ---
43	--- BG ---	--- BG ---	--- BG ---
44	--- BG ---	--- BG ---	--- BG ---
45	--- BG ---	--- BG ---	--- BG ---
46	--- BG ---	--- BG ---	--- BG ---

Conc. Models: Max. over all Runs
Source (pCi/L) = 1,000

Building Position Number	Stack Location: roof Field Conc. (pCi/L)	eave Field Conc. (pCi/L)	wall Field Conc. (pCi/L)
1	5.9	10.6	21.4
2	9.7	55.9	658.7
3	5.9	10.6	21.4
4	9.6	18.1	13.0
5	15.7	191.6	115.7
6	9.6	18.1	21.4
7	20.7	21.8	7.1
8	142.0	216.0	16.1
9	20.7	21.8	7.2
10	23.0	14.3	3.6
11	239.5	29.1	4.5
12	23.0	14.3	3.6
13	--- BG ---	--- BG ---	--- BG ---
14	--- BG ---	--- BG ---	--- BG ---
15	--- BG ---	--- BG ---	--- BG ---
16	--- BG ---	--- BG ---	--- BG ---
17	--- BG ---	--- BG ---	--- BG ---
18	--- BG ---	--- BG ---	--- BG ---
19	--- BG ---	--- BG ---	--- BG ---
20	--- BG ---	--- BG ---	--- BG ---
21	--- BG ---	--- BG ---	--- BG ---
22	--- BG ---	--- BG ---	--- BG ---
23	--- BG ---	--- BG ---	--- BG ---
24	--- BG ---	--- BG ---	--- BG ---
25	--- BG ---	--- BG ---	--- BG ---
26	--- BG ---	--- BG ---	--- BG ---
27	--- BG ---	--- BG ---	--- BG ---
28	--- BG ---	--- BG ---	--- BG ---
29	--- BG ---	--- BG ---	--- BG ---
30	--- BG ---	--- BG ---	--- BG ---
31	6.8	5.6	2.5
32	3.0	3.3	3.4
33	2.7	3.1	3.5
34	3.0	5.1	6.7
35	4.6	3.4	3.3
36	4.0	3.5	3.2
37	4.8	6.4	5.4
38	6.8	5.6	2.5
39	1.7	3.3	4.2
40	0.5	0.8	1.1
41	--- BG ---	--- BG ---	--- BG ---
42	--- BG ---	--- BG ---	--- BG ---
43	--- BG ---	--- BG ---	--- BG ---
44	--- BG ---	--- BG ---	--- BG ---
45	--- BG ---	--- BG ---	--- BG ---
46	--- BG ---	--- BG ---	--- BG ---

Table 18 Schulman and Huber Model's Maximum Data Summary

FIGURES

1 Story Dwelling w/ 6:12 Roof

Front Elevation	Side Elevation
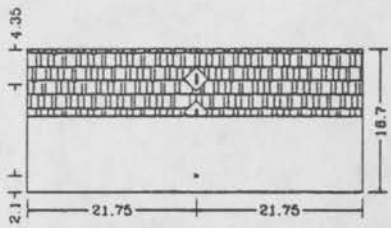	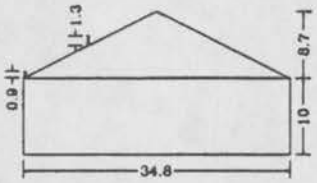
Roof Plan	**Perspective View**
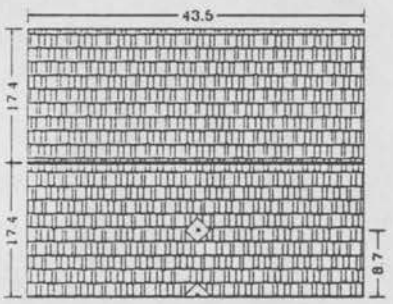	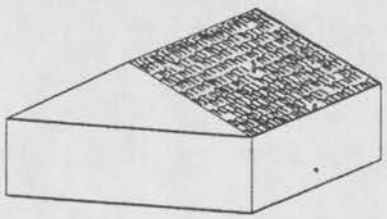

* Model dimensions shown in cm

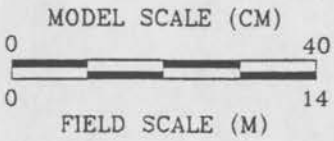

Figure 1 One Story House with 6:12 Roof Slope Dimensional Drawing

1 Story Dwelling w/ 9:12 Roof

Front Elevation	Side Elevation
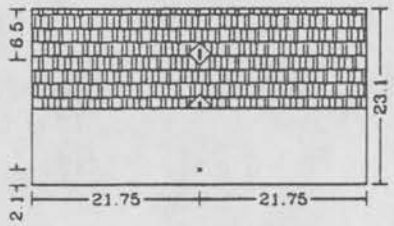	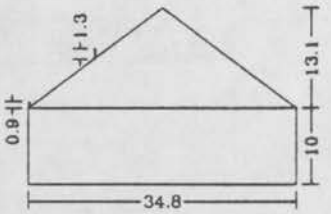
Roof Plan	**Perspective View**
	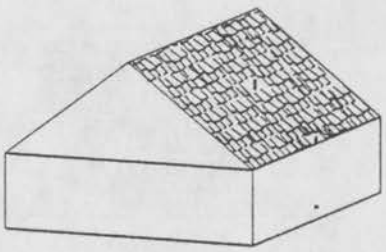

* Model dimensions shown in cm

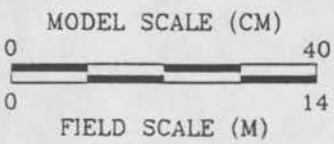

Figure 2 One Story House with 9:12 Roof Slope Dimensional Drawing

2 Story Dwelling w/ 6:12 Roof

Front Elevation	Side Elevation
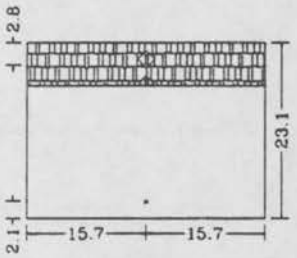	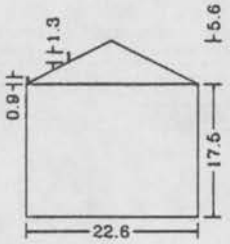
Roof Plan	**Perspective View**
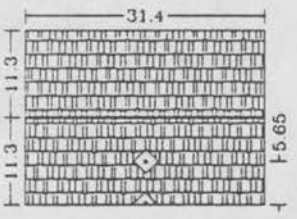	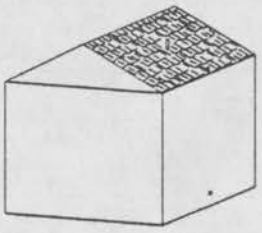

* Model dimensions shown in cm

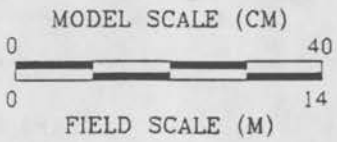

Figure 3 Two Story House with 6:12 Roof Slope Dimensional Drawing

2 Story Dwelling w/ 9:12 Roof

Front Elevation	Side Elevation
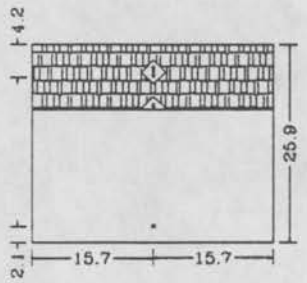	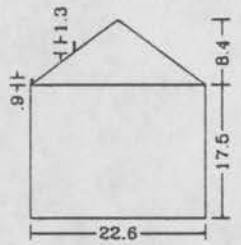
Roof Plan	**Perspective View**
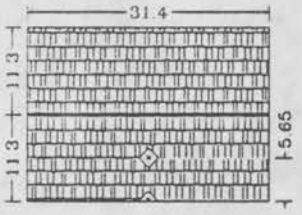	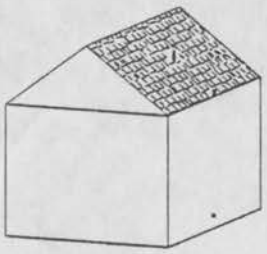

* Model dimensions shown in cm

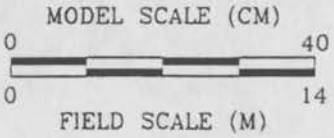

Figure 4 Two Story House with 9:12 Roof Slope Dimensional Drawing

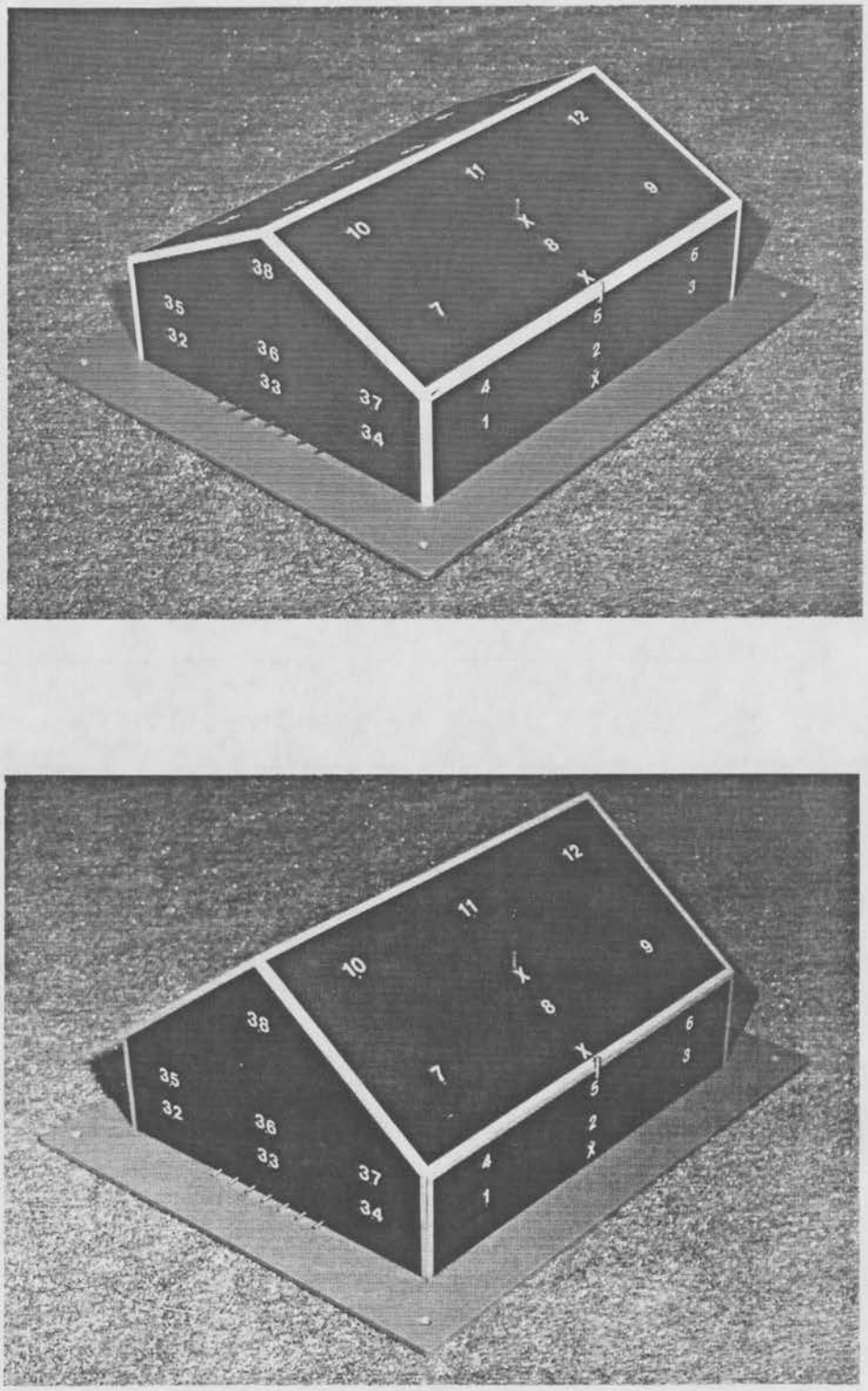

Figure 5 One Story House with 6:12 and 9:12 Roof Slope Pictures

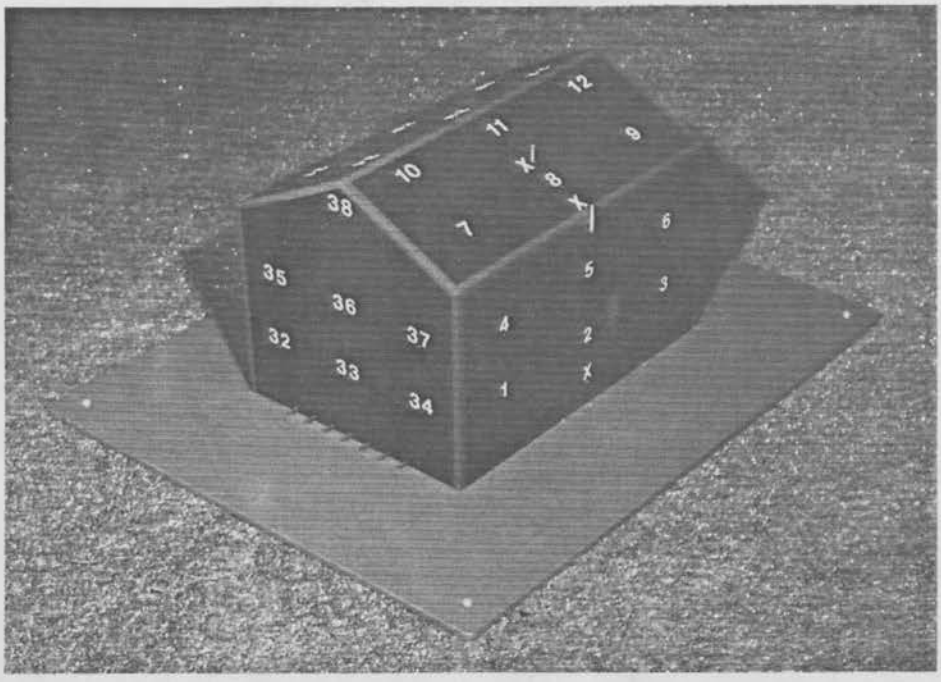

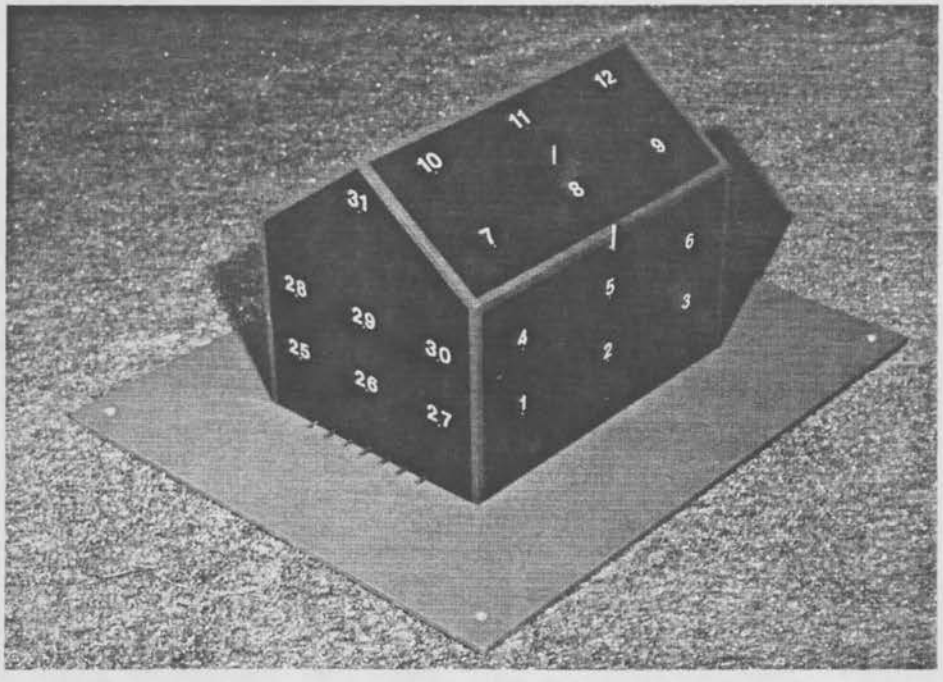

(9:12 two story house mislabeling in picture and video only numbers 27-31 should be 32-38 and visa verse, 6:12 picture is correct)

Figure 6 Two Story House with 6:12 and 9:12 Roof Slope Pictures

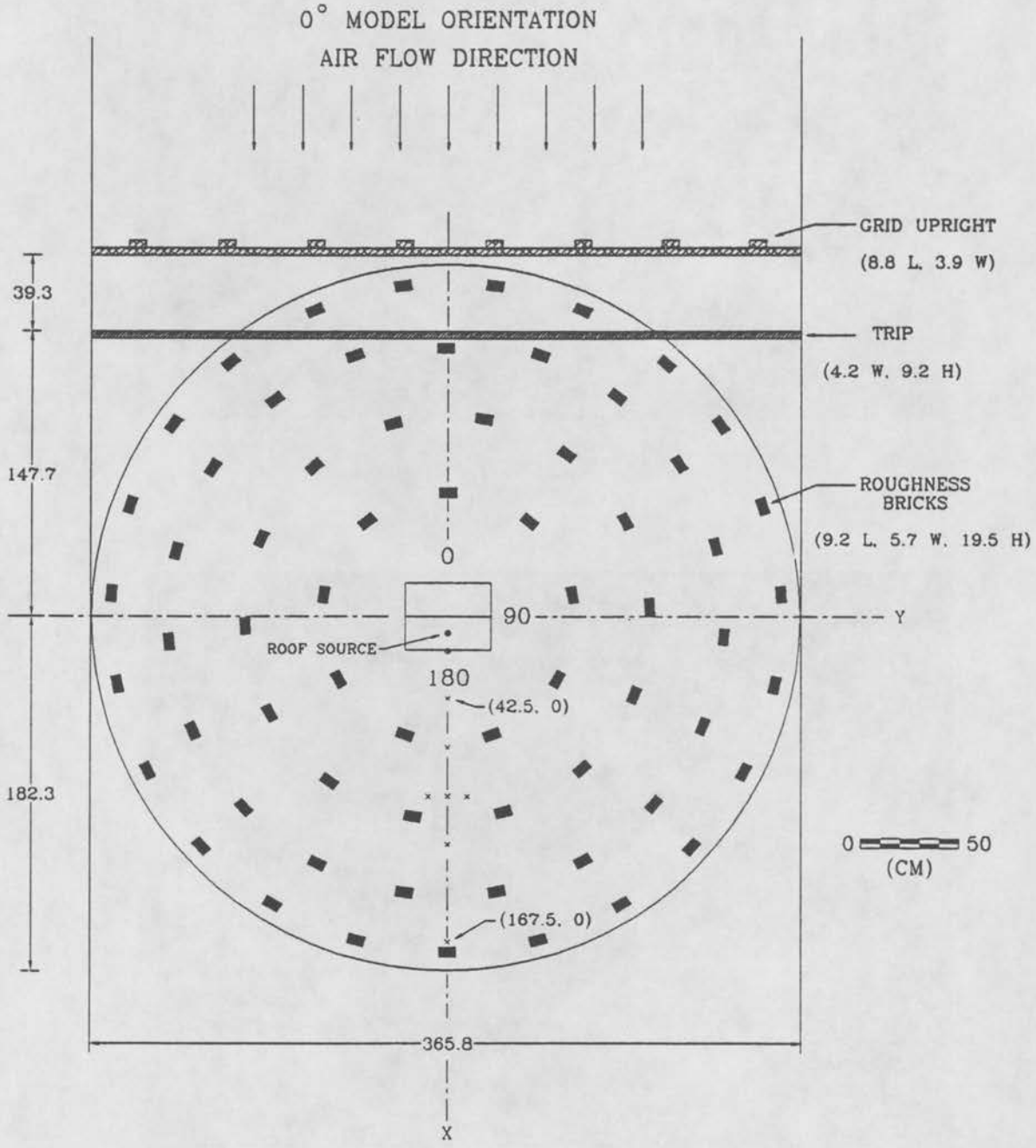

Figure 7 Exp. Model Area Plan View

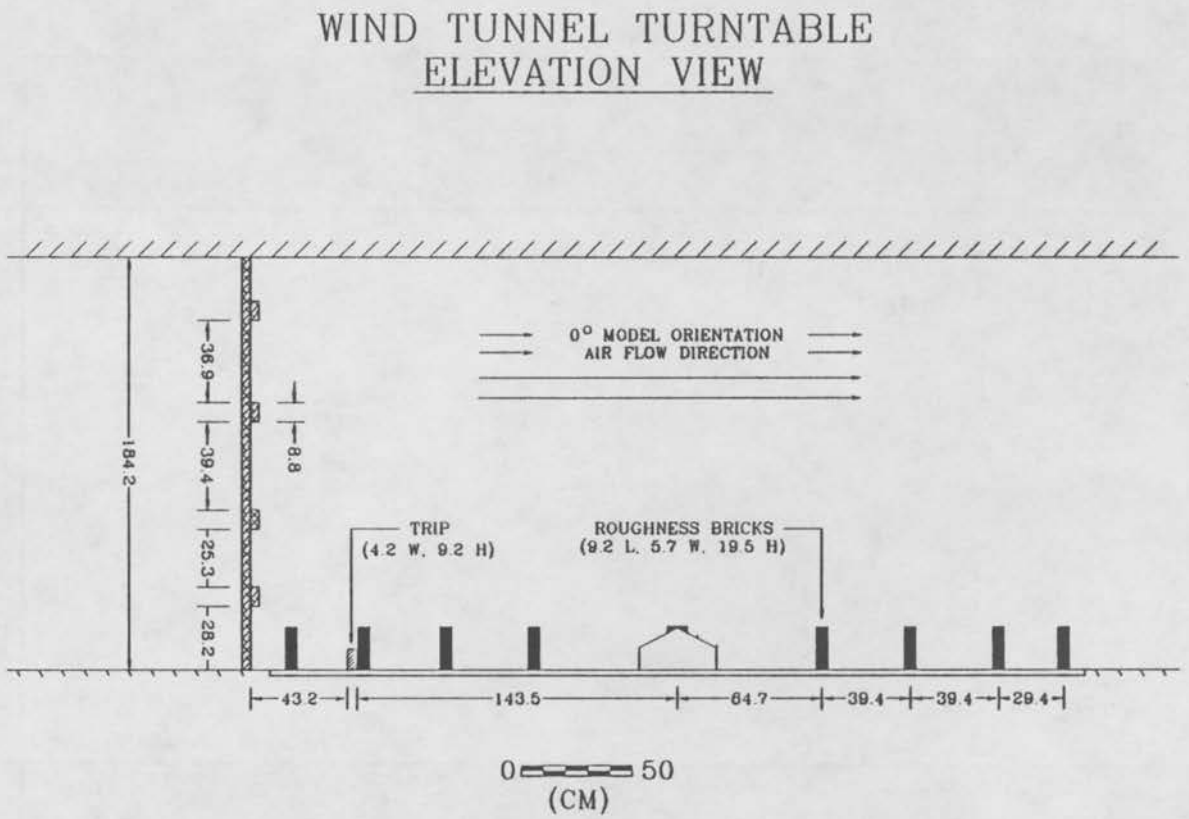

Figure 8 Exp. Model Area Elevation View

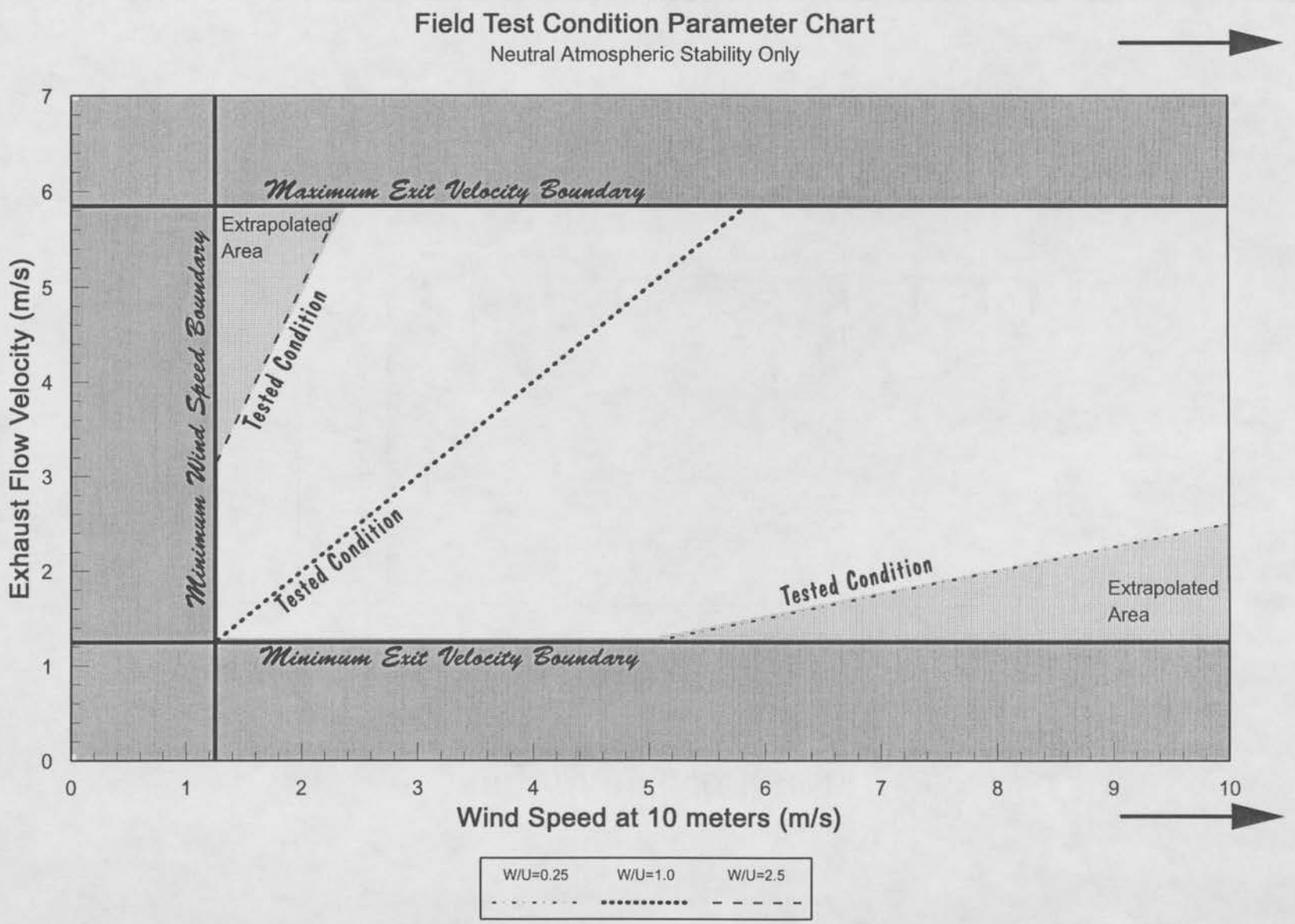

Figure 9 Parameter Range of Field Flow Conditions Tested

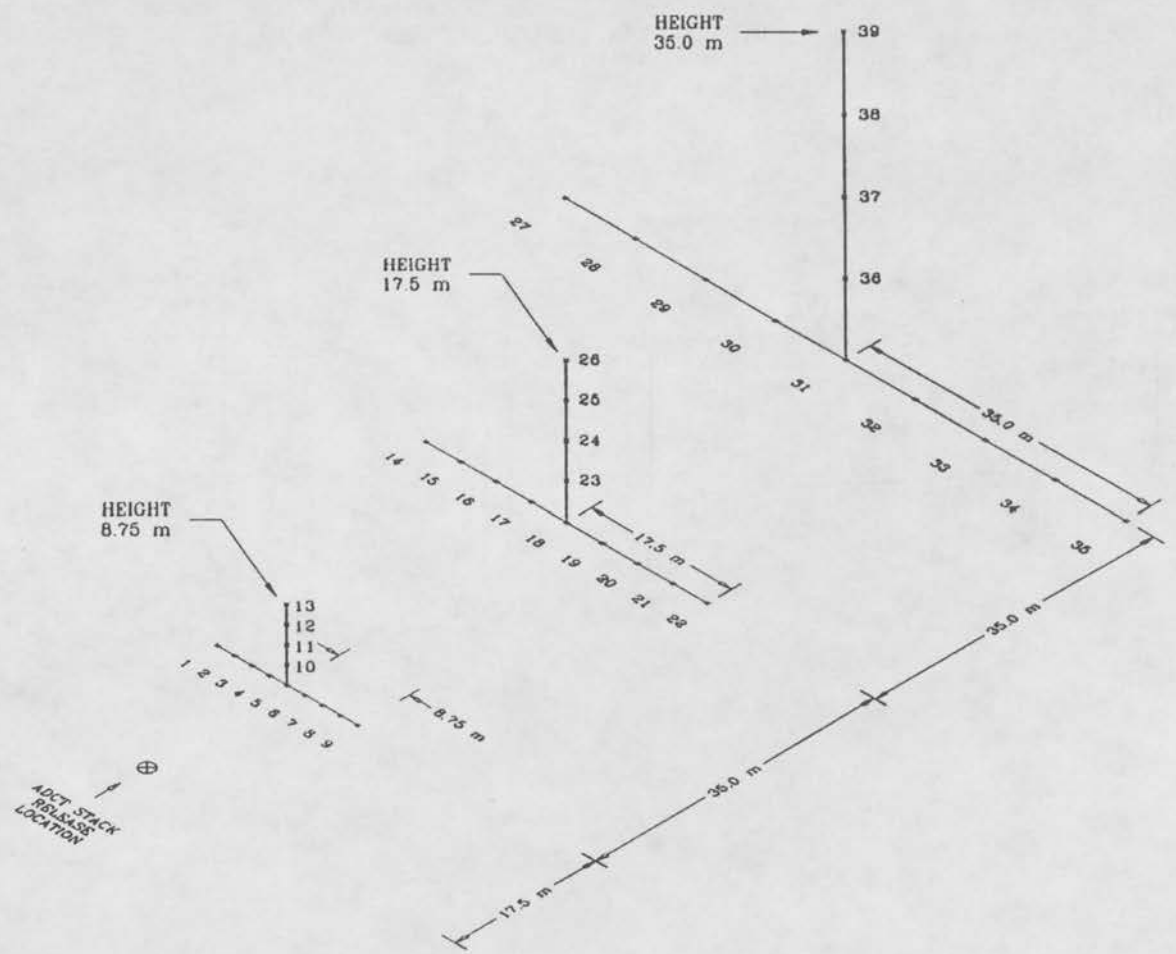

Figure 10 Atmospheric Dispersion Comparability Sampling Location Grid

BUILDING SAMPLING LOCATIONS

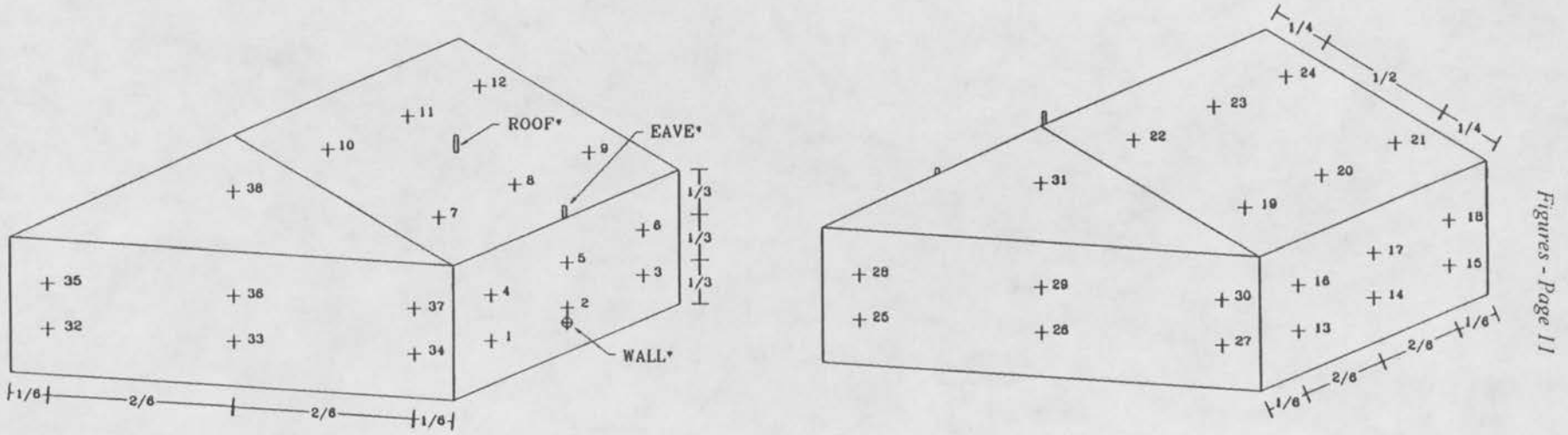

(DIMENSIONS REPRESENT RELATIVE DISTANCE)

+: SAMPLE PORT
*: EXHAUST LOCATION

Figure 11 Generic House Sampling Locations Map

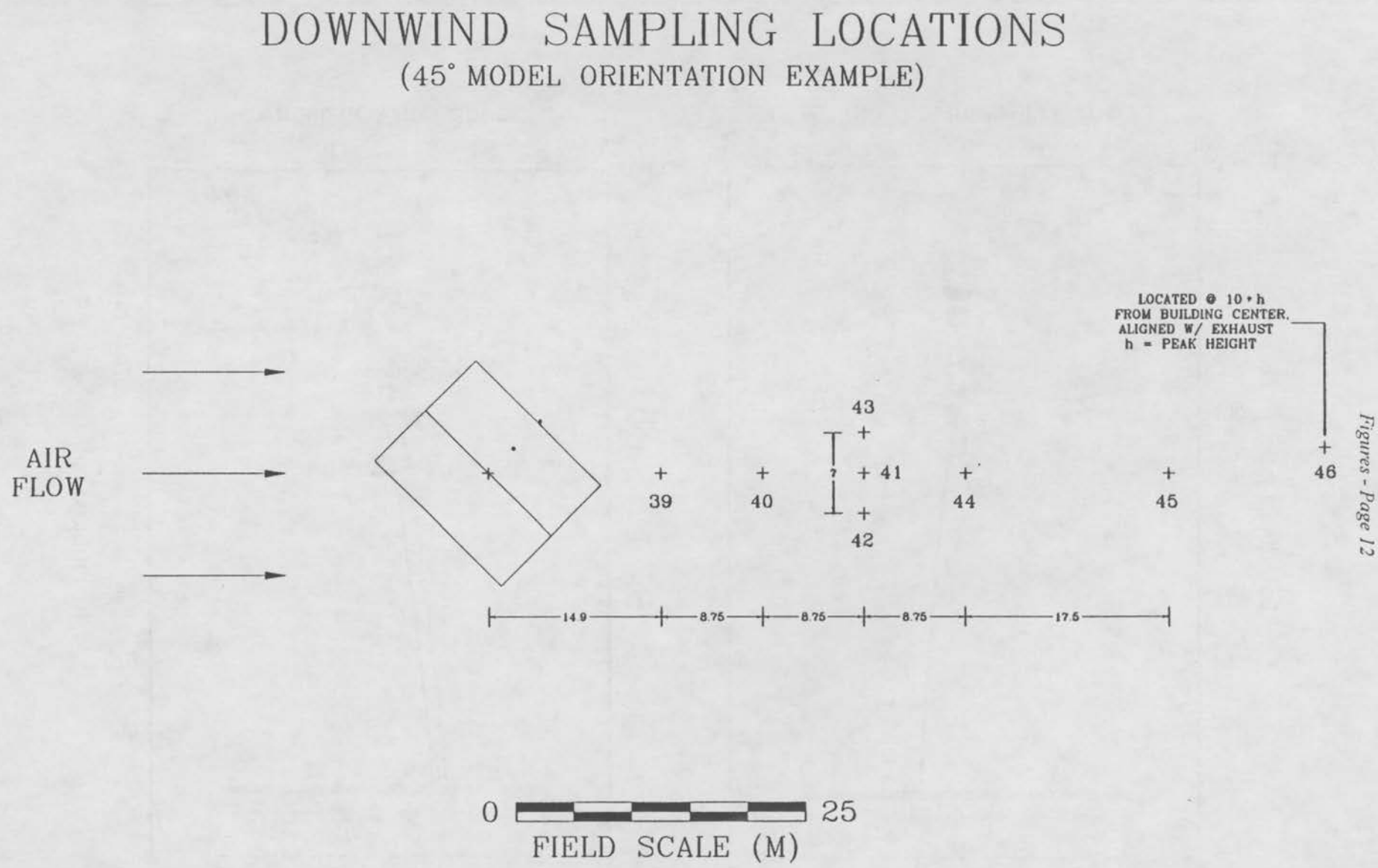

Figure 12 Sampling Locations Downwind of Generic House

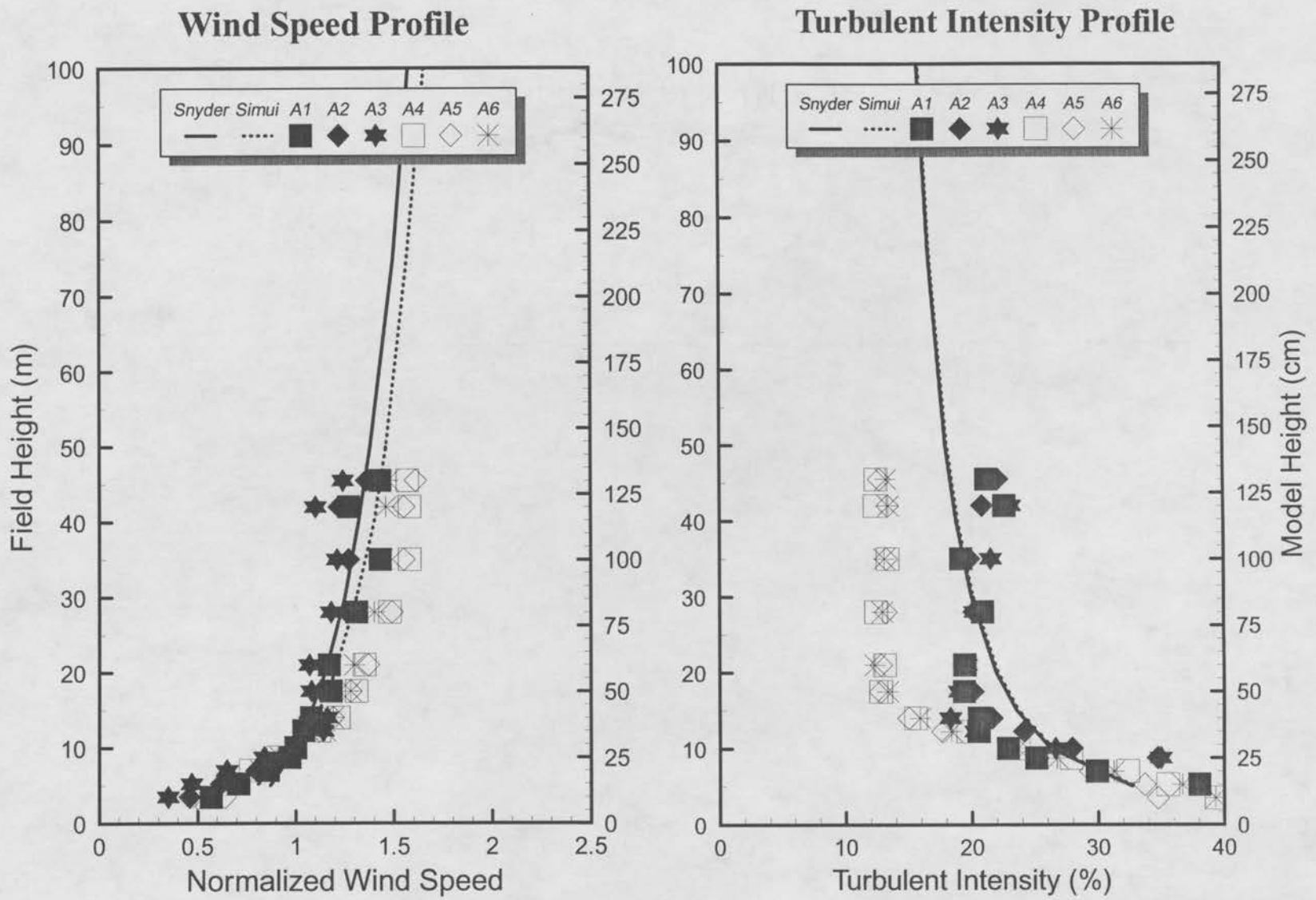

Figure 13 Model Lateral and Downwind Velocity Profile Comparisons

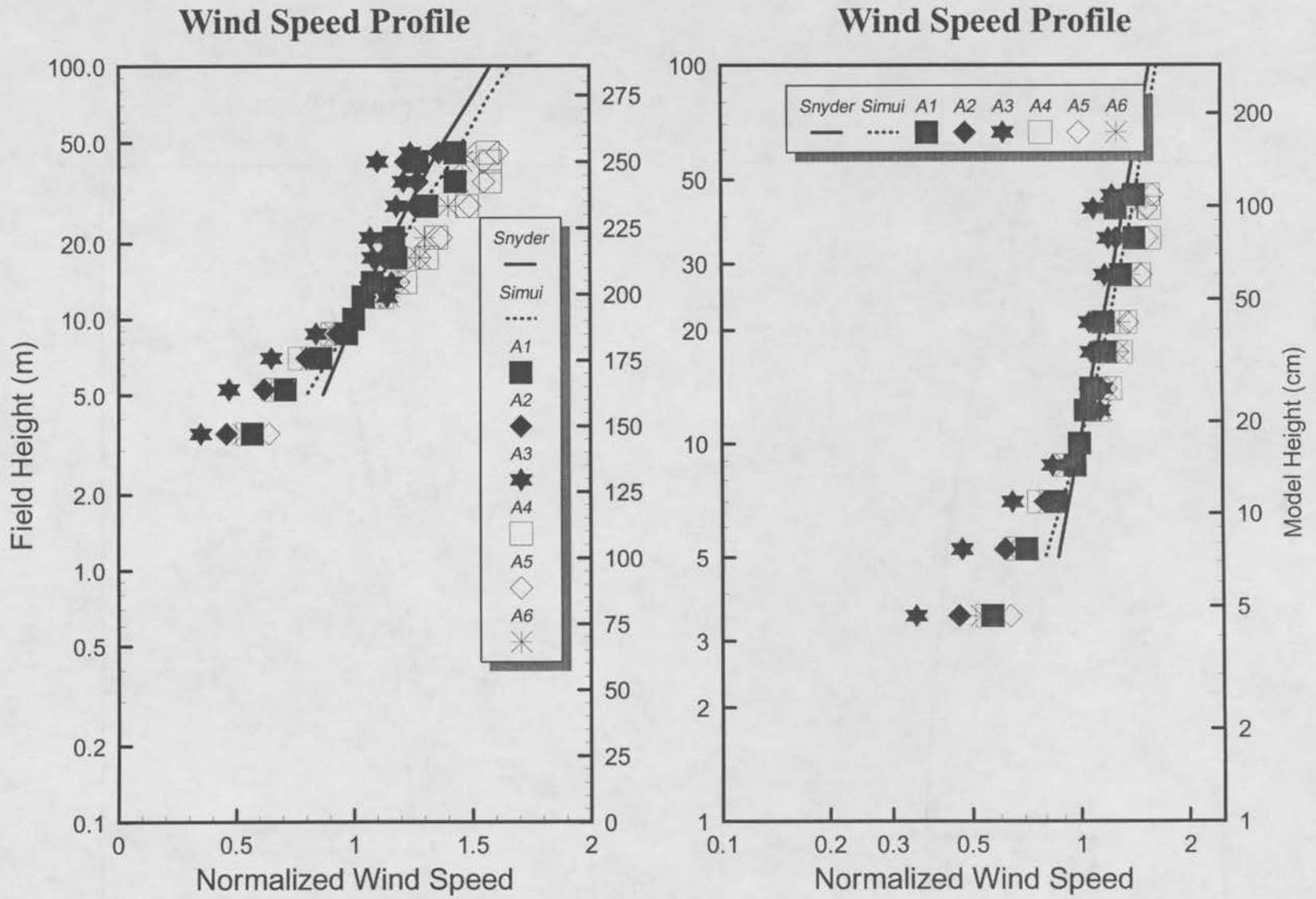

Figure 14 Model Lateral and Downwind Velocity Profile Comparisons; log coordinates

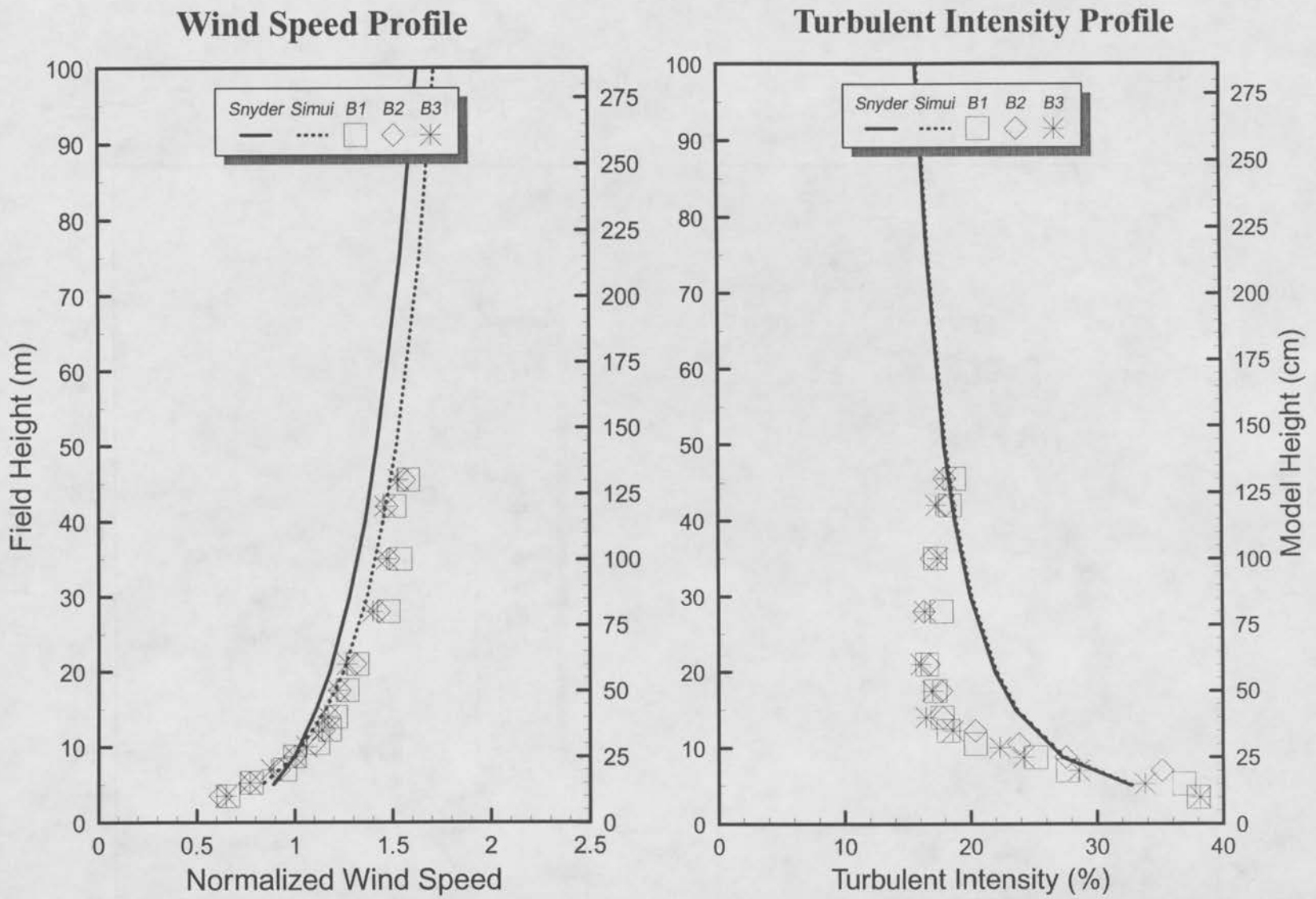

Figure 15 Model Reynolds Number Velocity Profile Comparisons

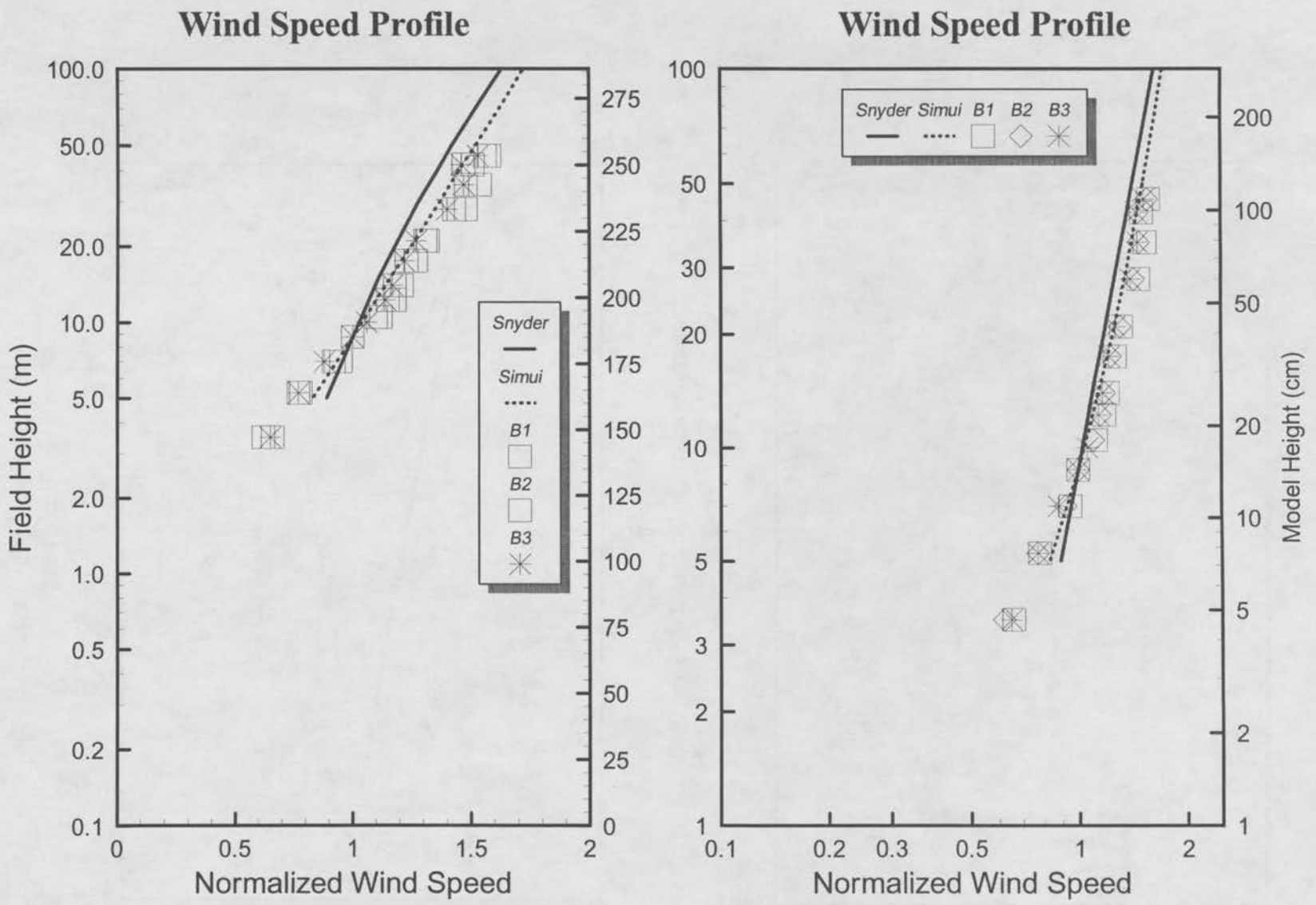

Figure 16 Model Reynolds Number Velocity Profile Comparisons; log coordinates

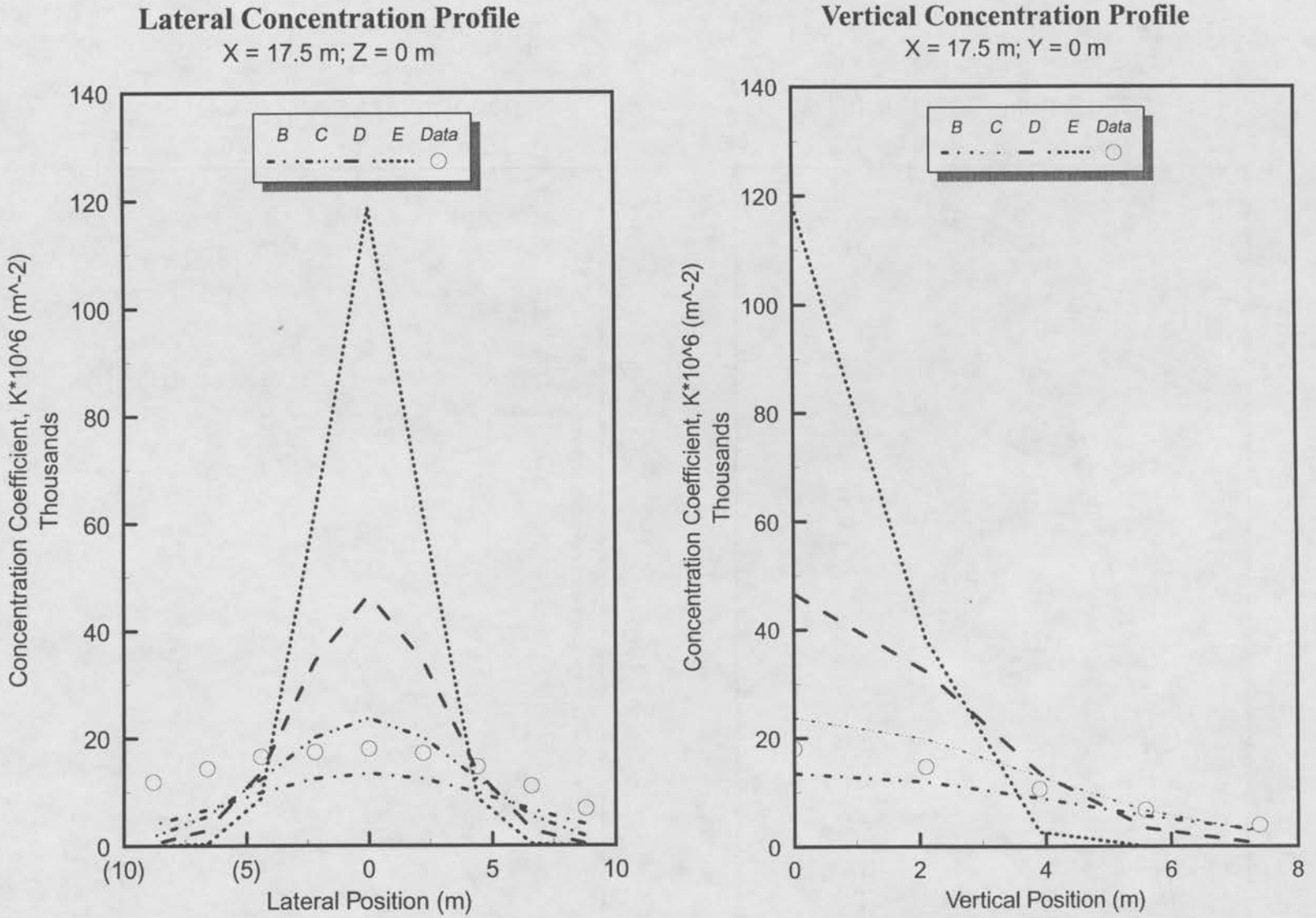

Figure 17 ADCT Test Conc. Profiles; 50cm upwind of model

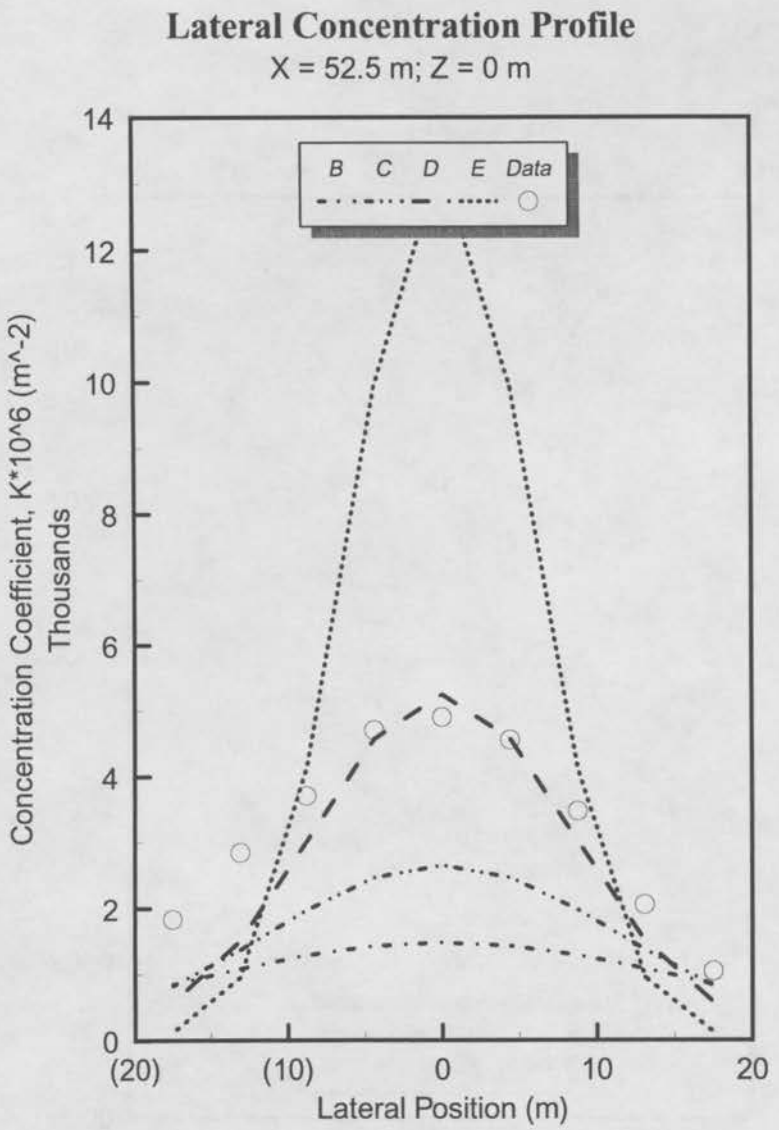

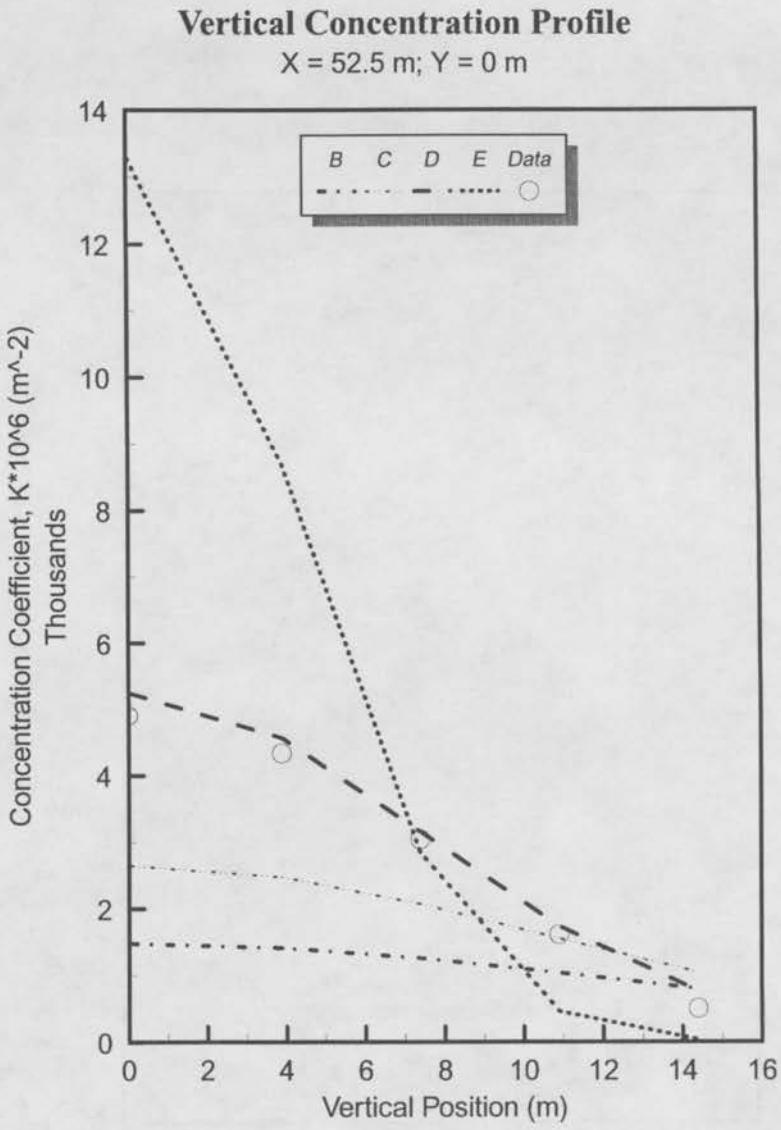

Figure 18 ADCT Test Conc. Profiles; 50cm downwind of model

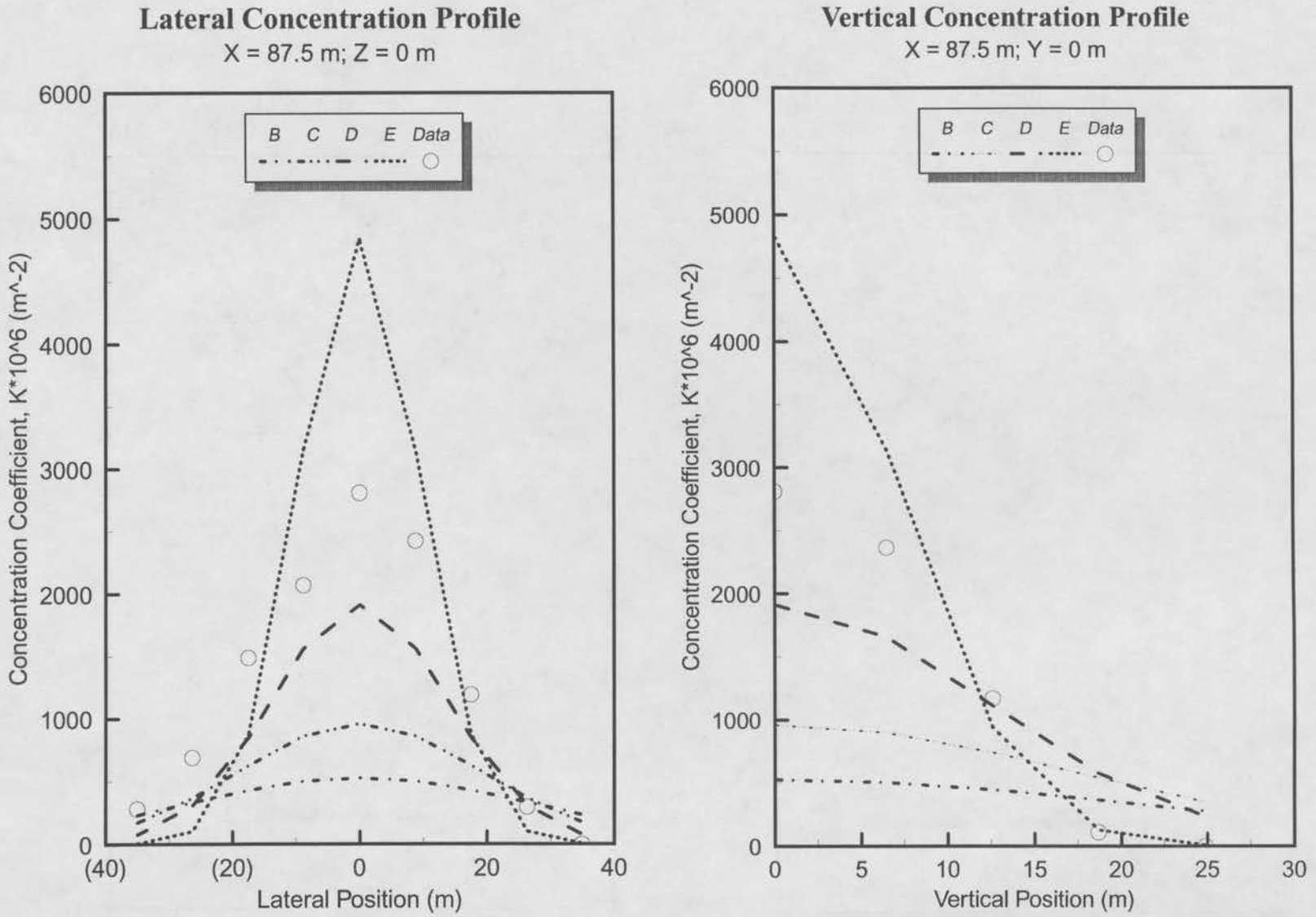

Figure 19 ADCT Test Conc. Profiles; 150cm downwind of model

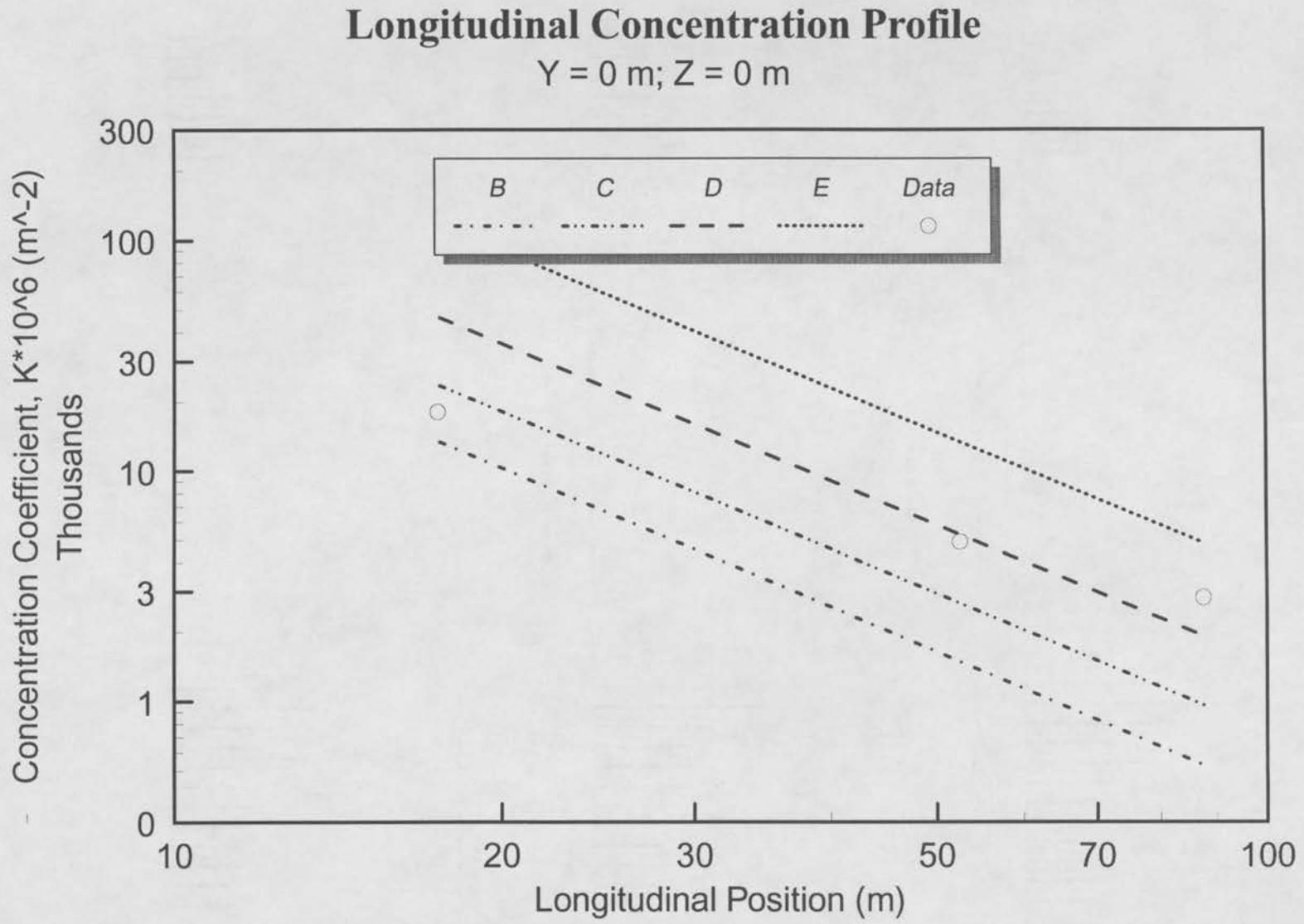

Figure 20 ADCT Test Conc. Profiles; centerline, ground level

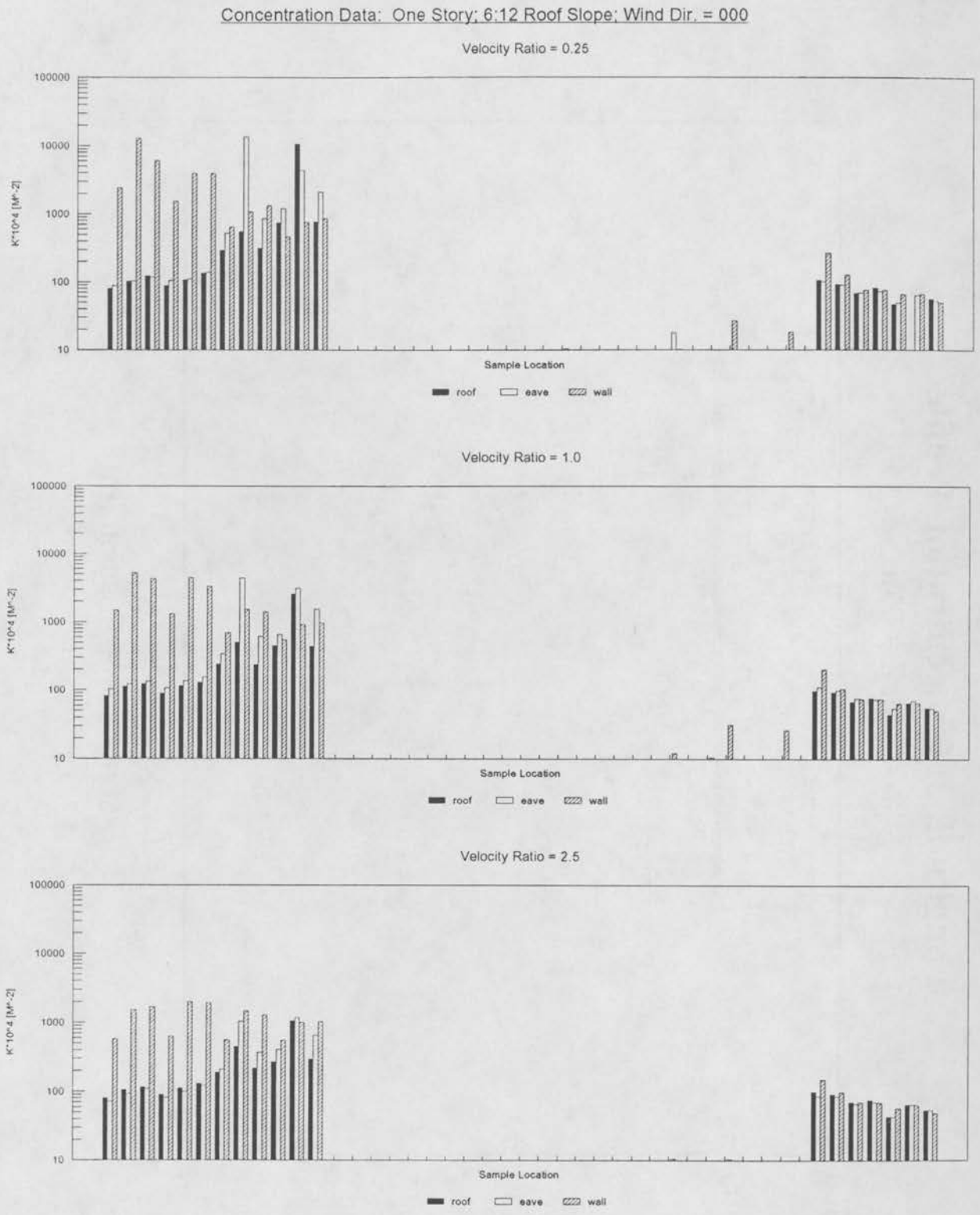

Figure 21a Exp. Conc. Comparisons of Roof, Eave, Wall Releases

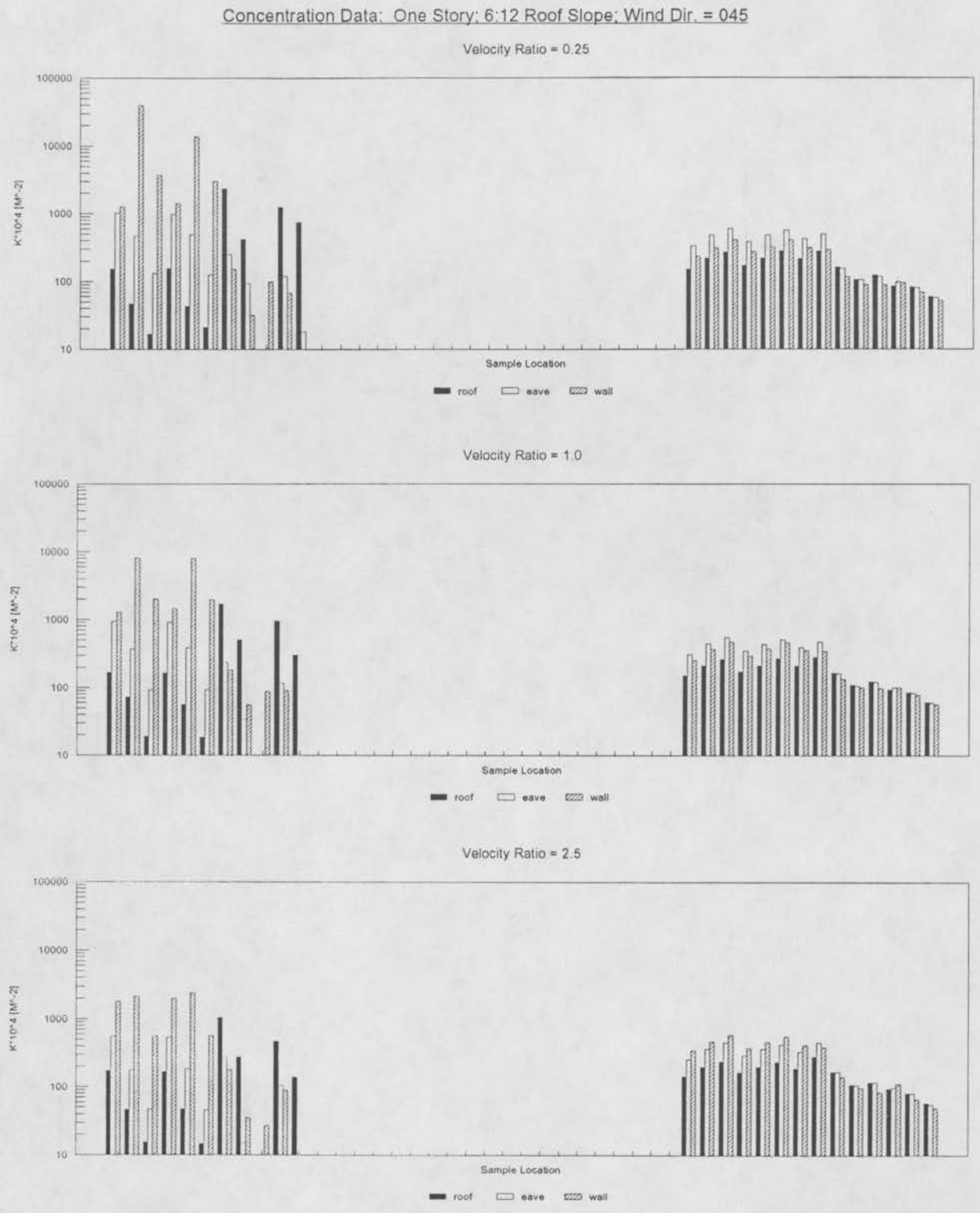

Figure 21b Exp. Conc. Comparisons of Roof, Eave, Wall Releases

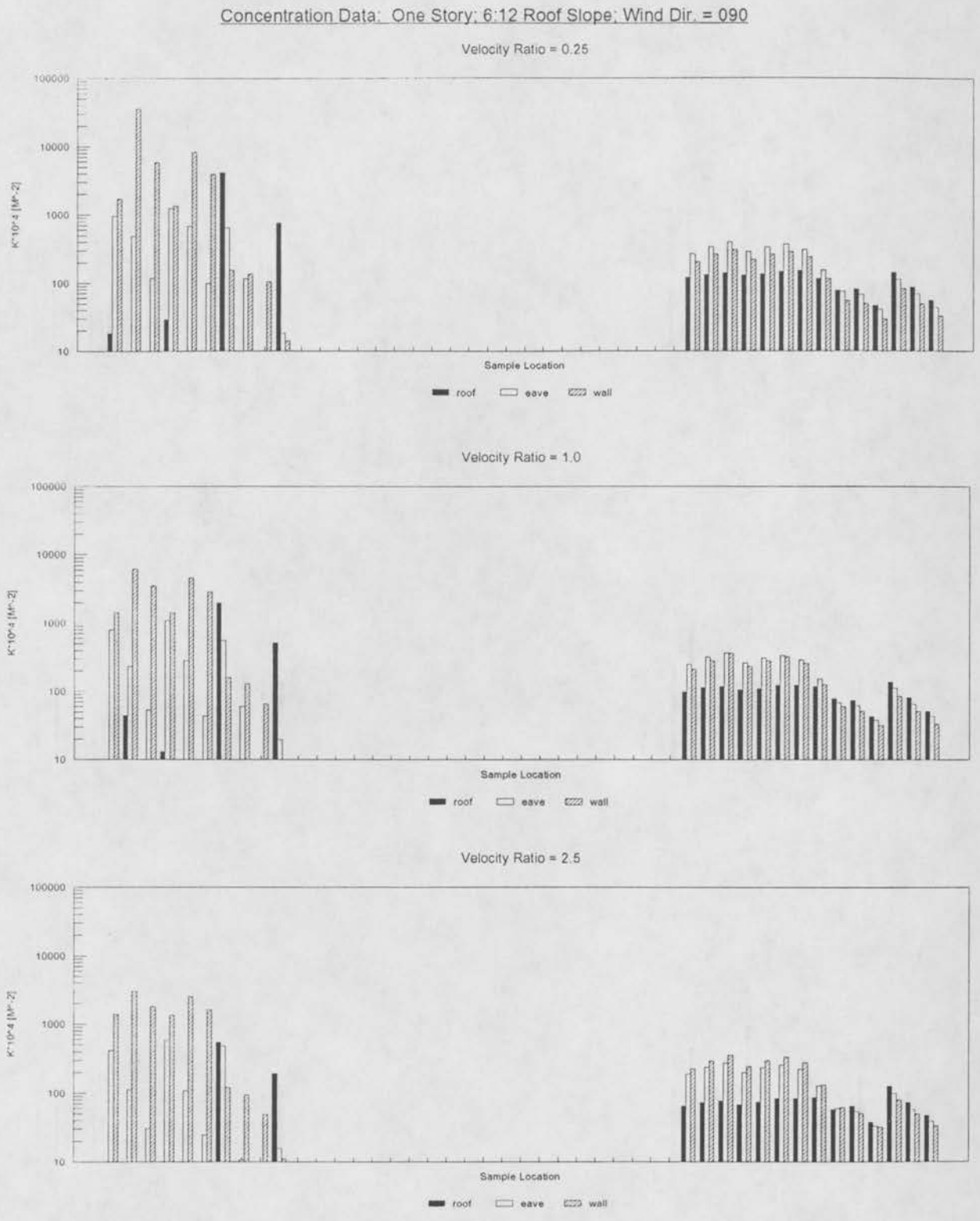

Figure 21c Exp. Conc. Comparisons of Roof, Eave, Wall Releases

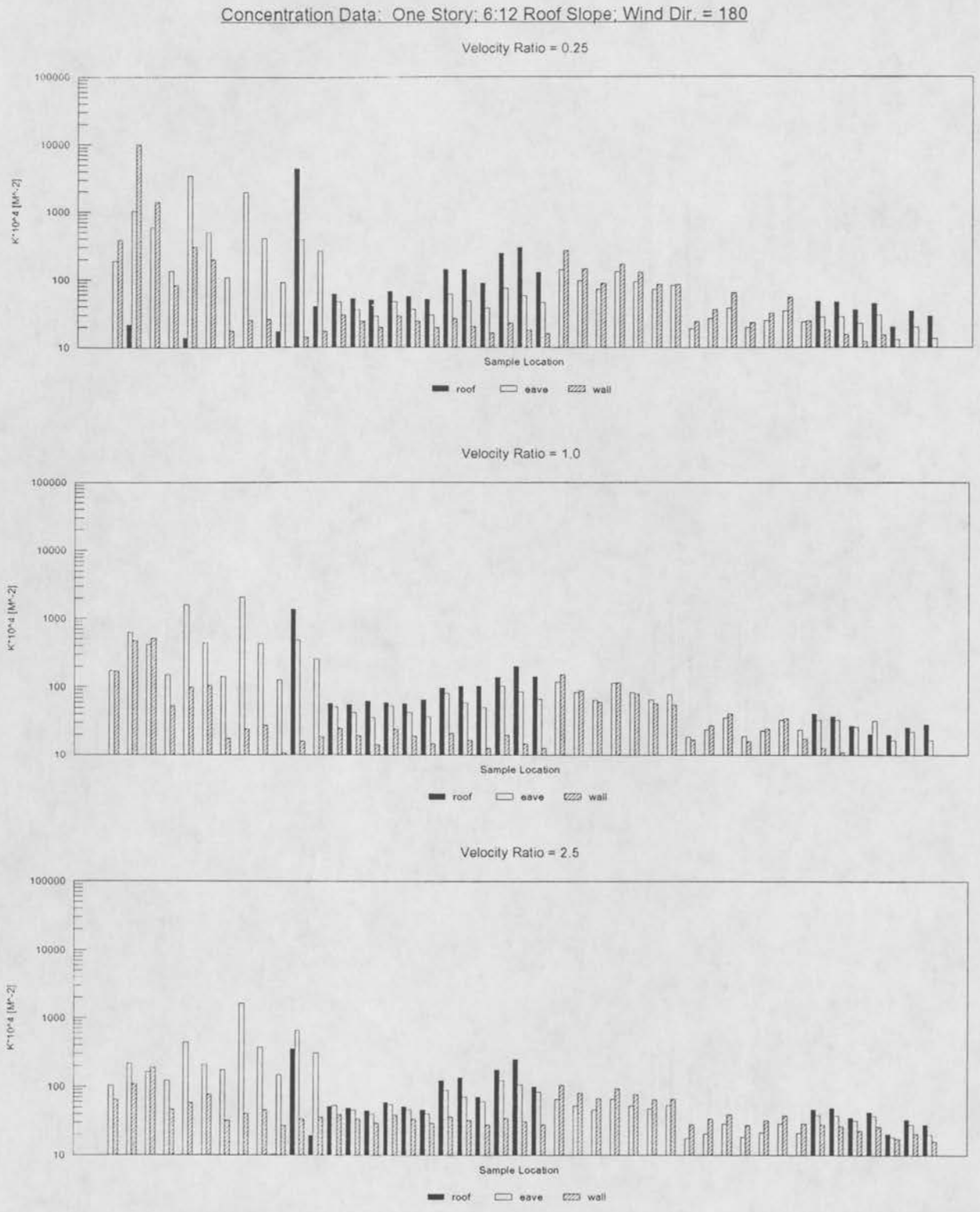

Figure 21d Exp. Conc. Comparisons of Roof, Eave, Wall Releases

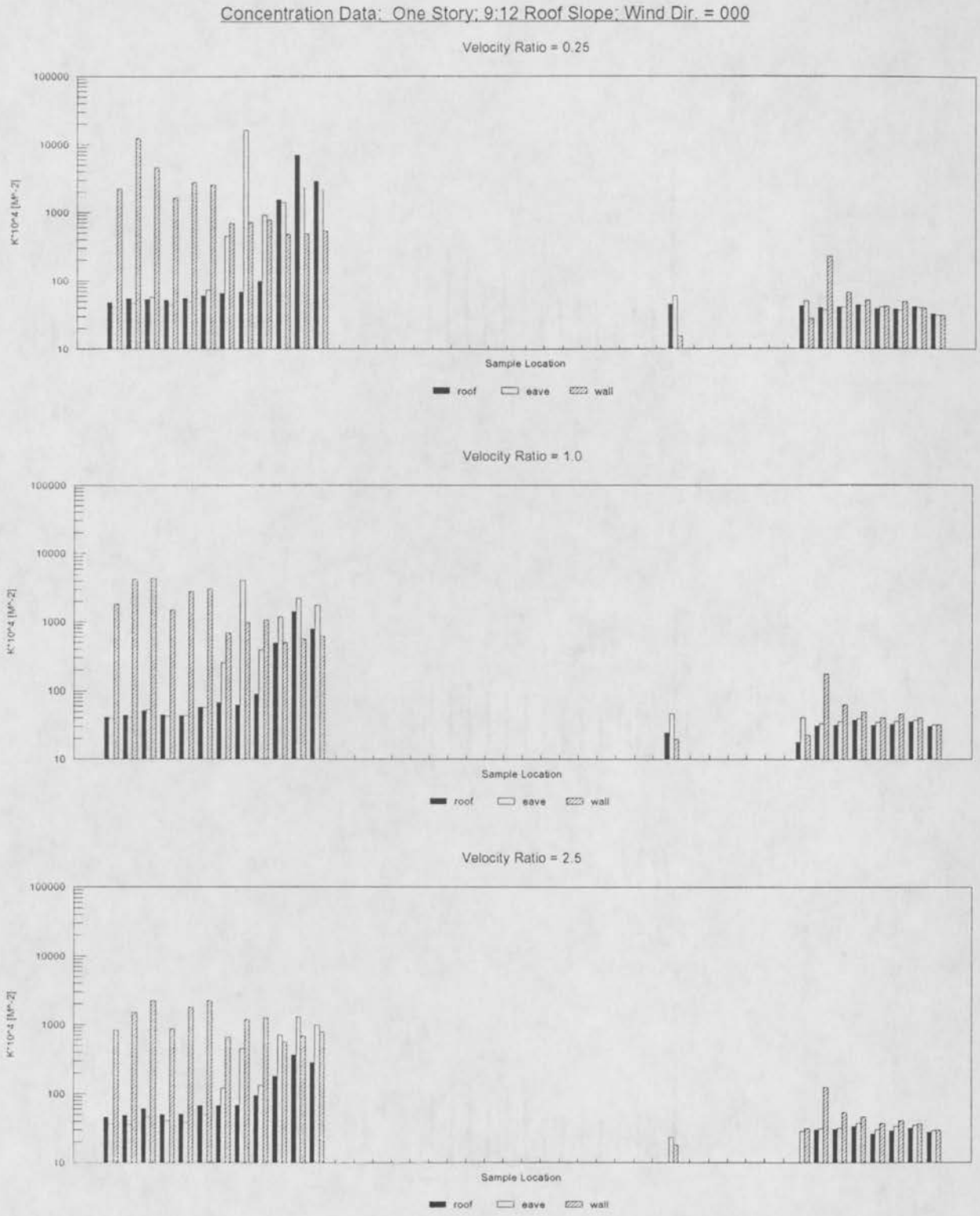

Figure 21e Exp. Conc. Comparisons of Roof, Eave, Wall Releases

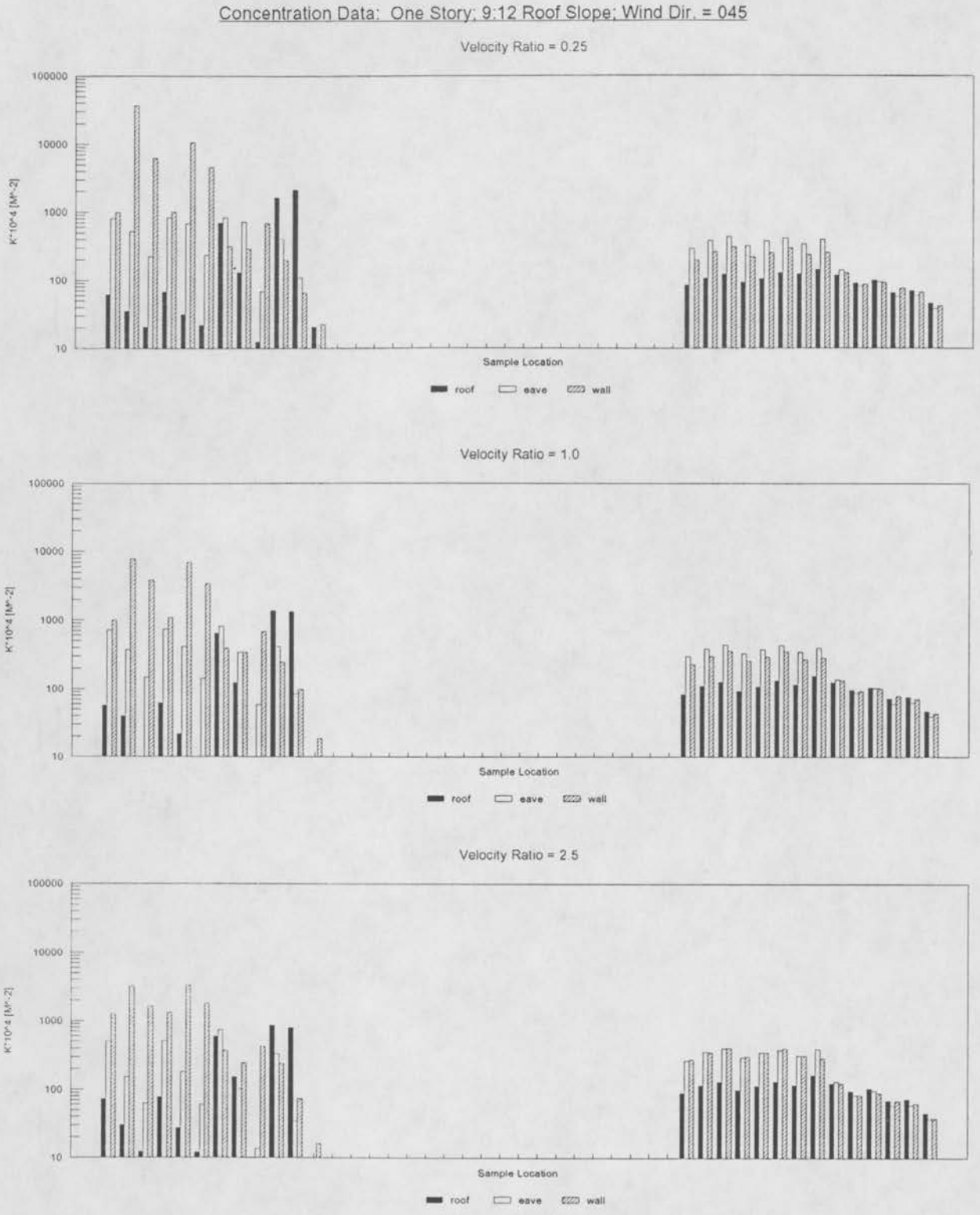

Figure 21f Exp. Conc. Comparisons of Roof, Eave, Wall Releases

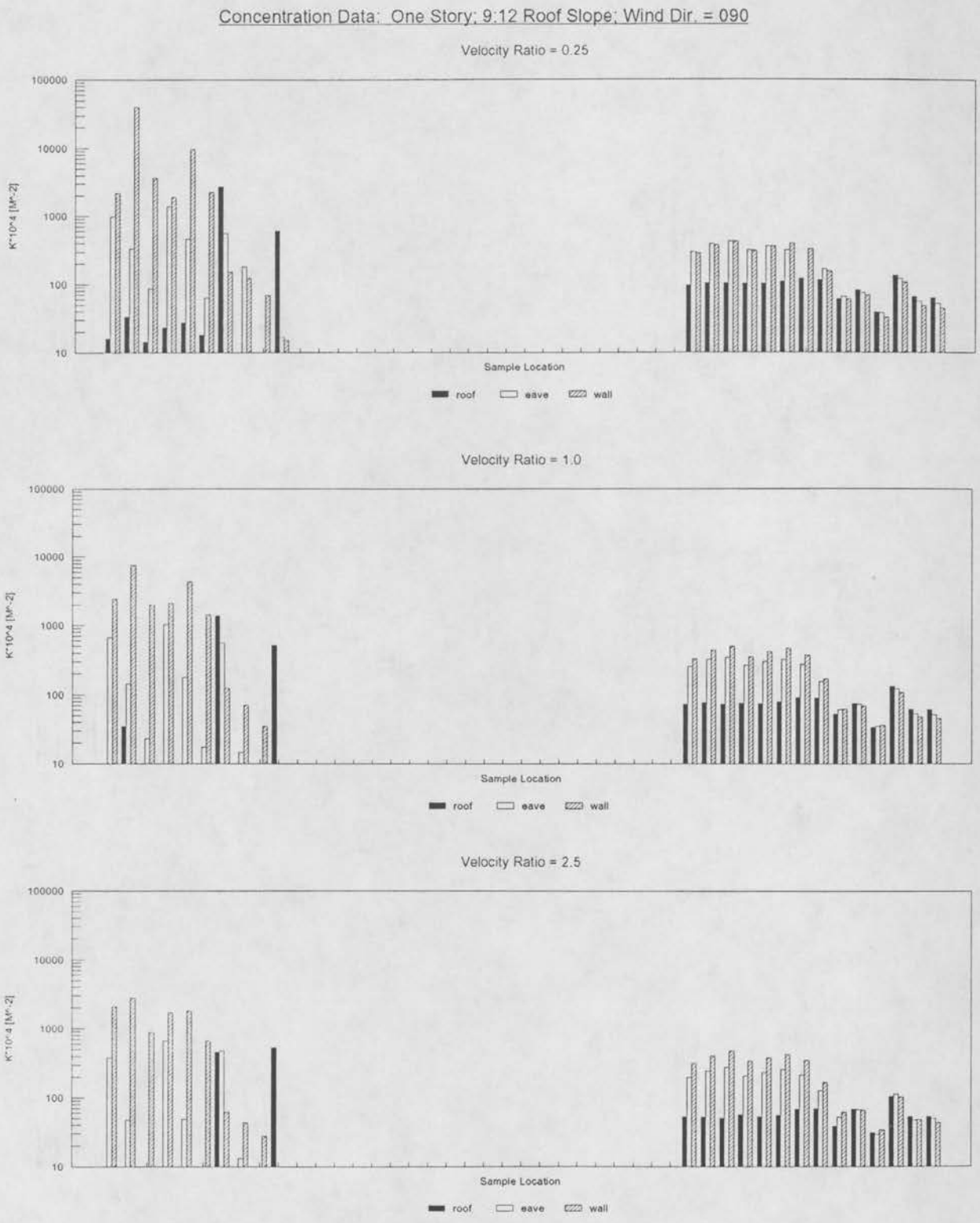

Figure 21g Exp. Conc. Comparisons of Roof, Eave, Wall Releases

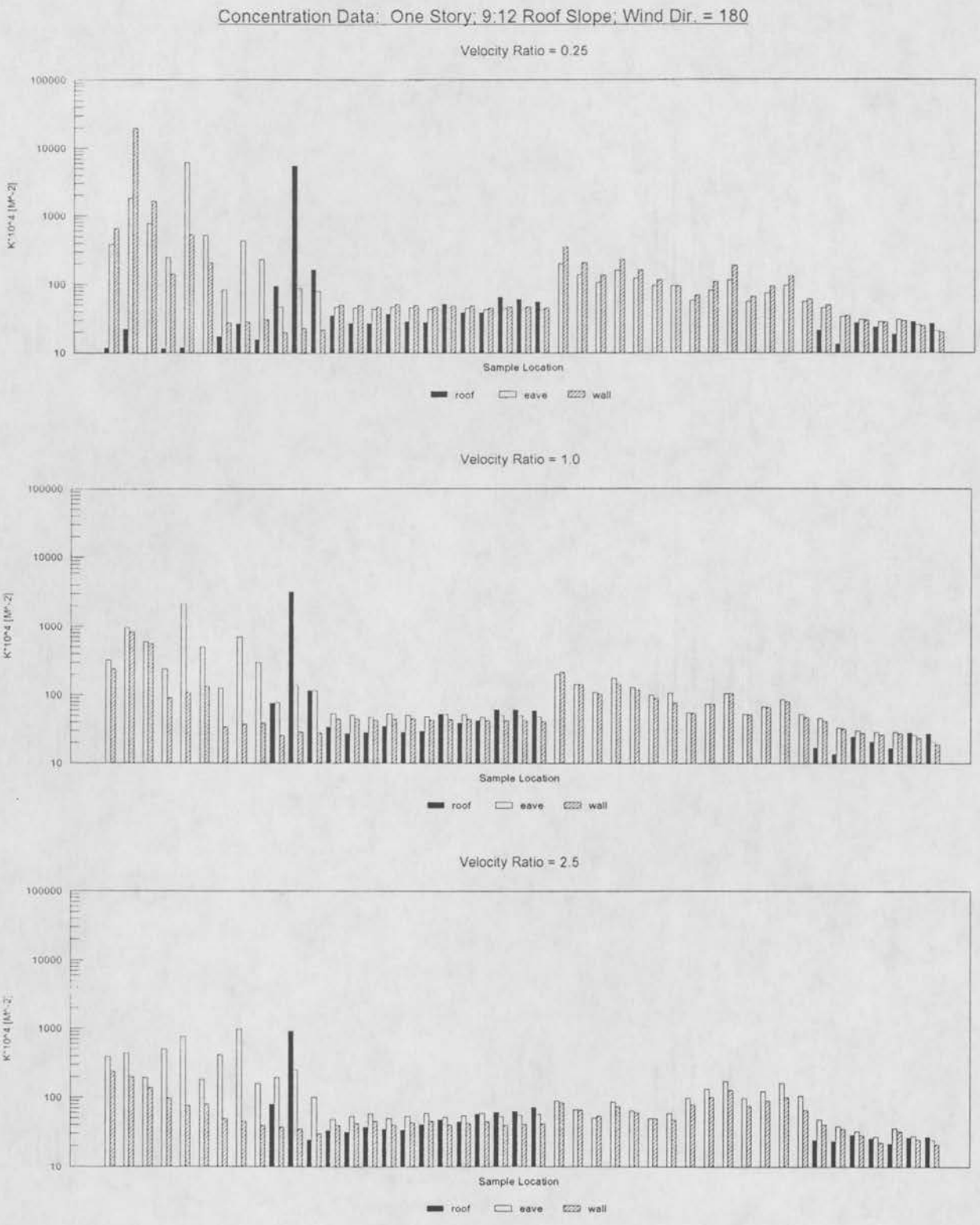

Figure 21h Exp. Conc. Comparisons of Roof, Eave, Wall Releases

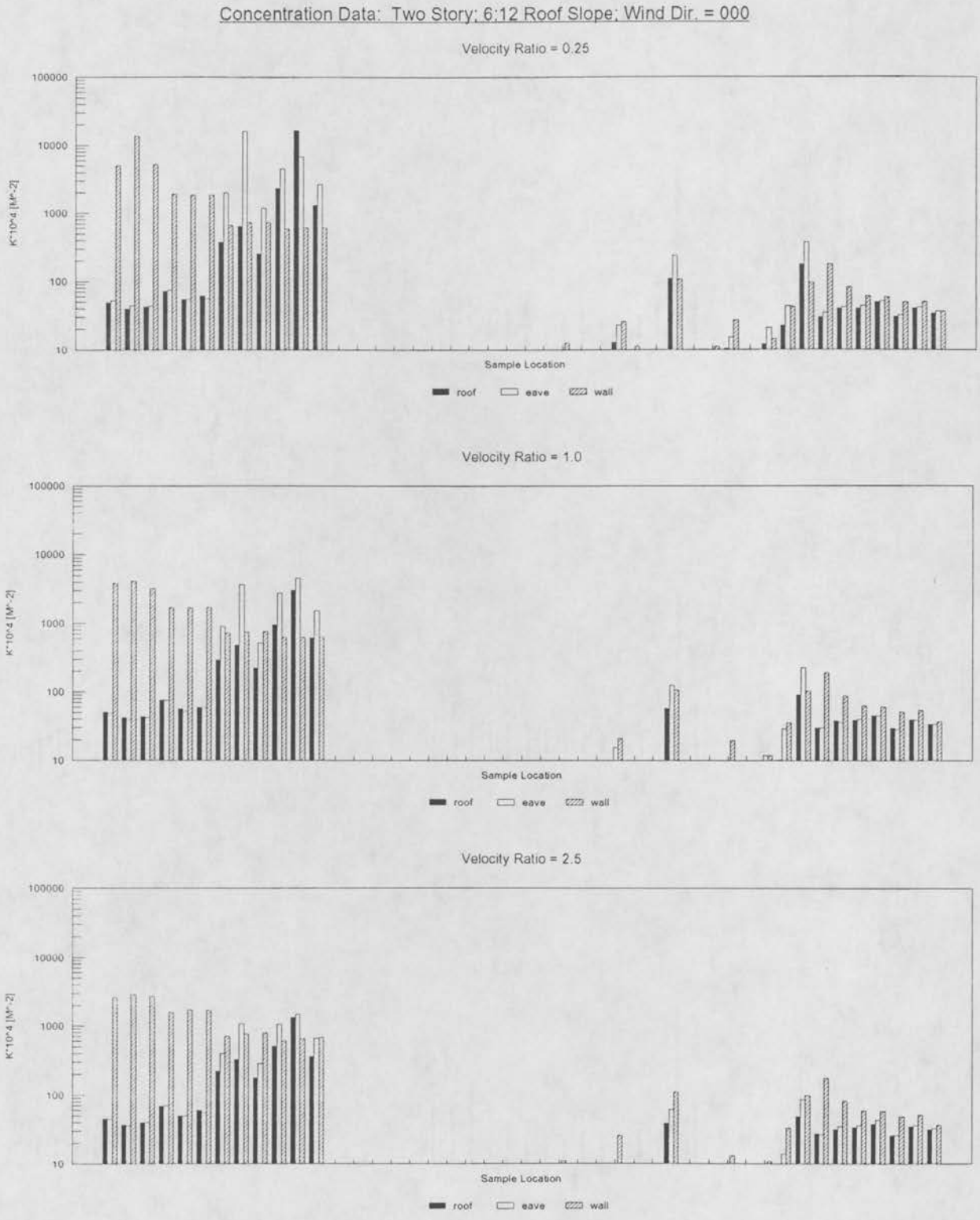

Figure 21i Exp. Conc. Comparisons of Roof, Eave, Wall Releases

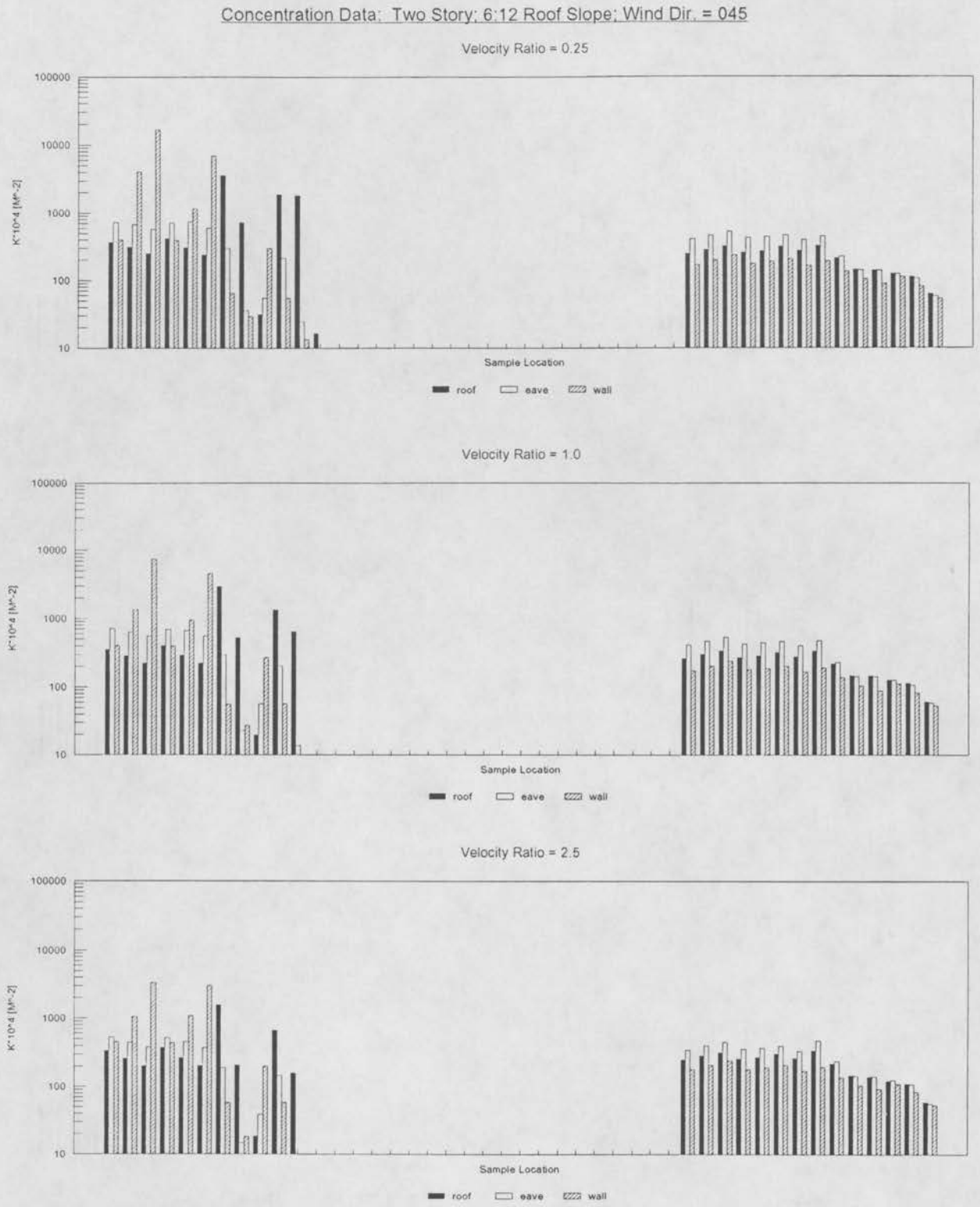

Figure 21j Exp. Conc. Comparisons of Roof, Eave, Wall Releases

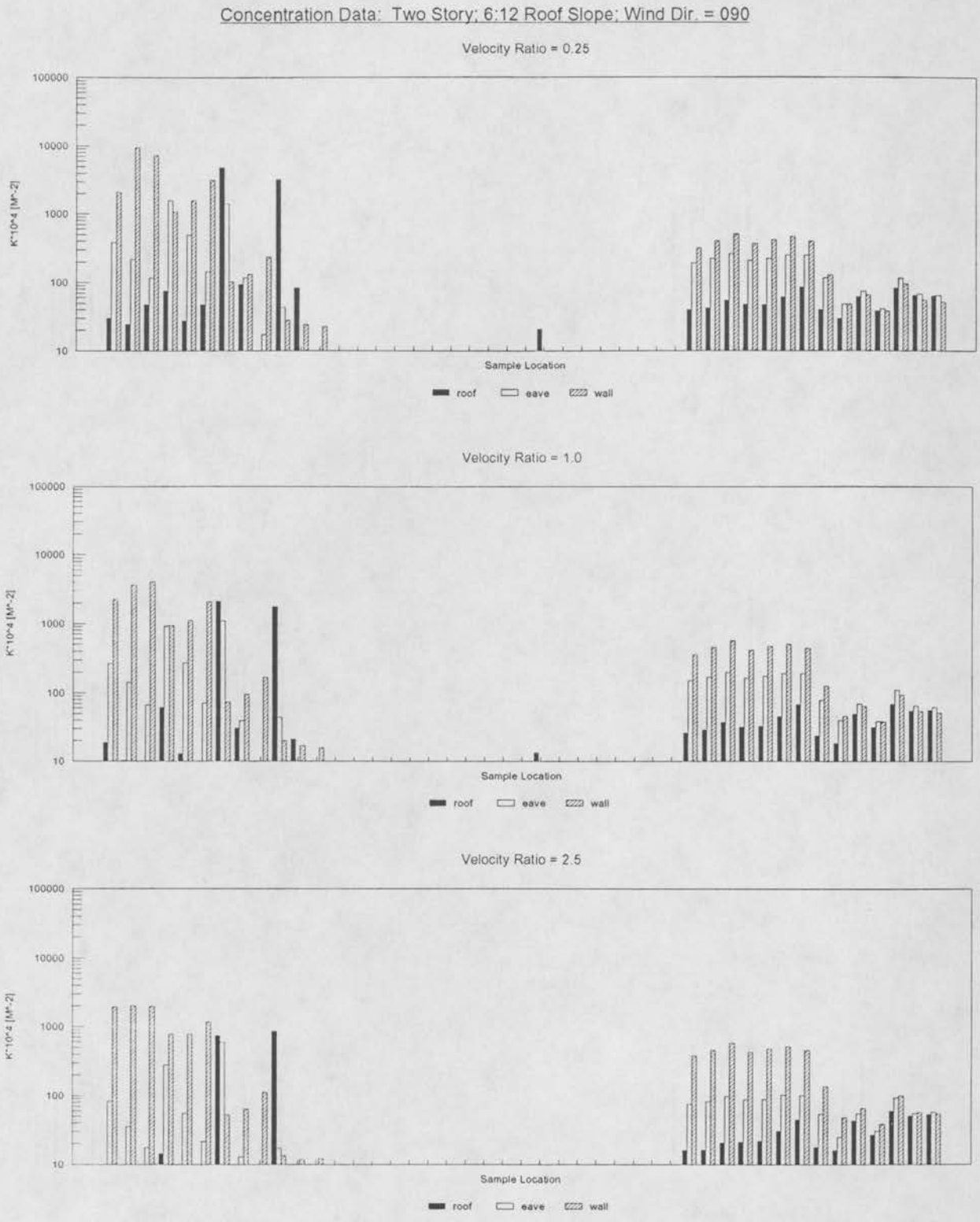

Figure 21k Exp. Conc. Comparisons of Roof, Eave, Wall Releases

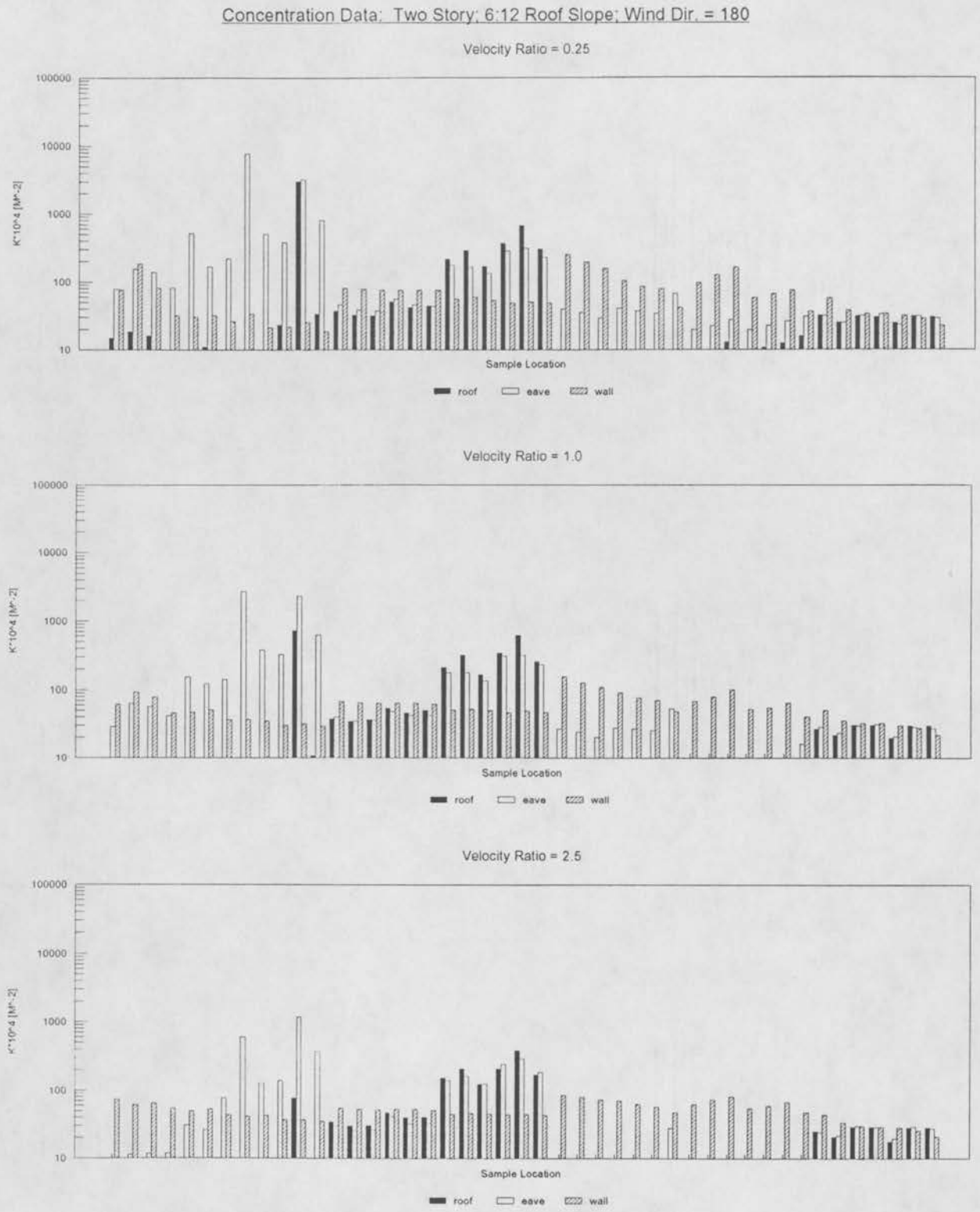

Figure 21l Exp. Conc. Comparisons of Roof, Eave, Wall Releases

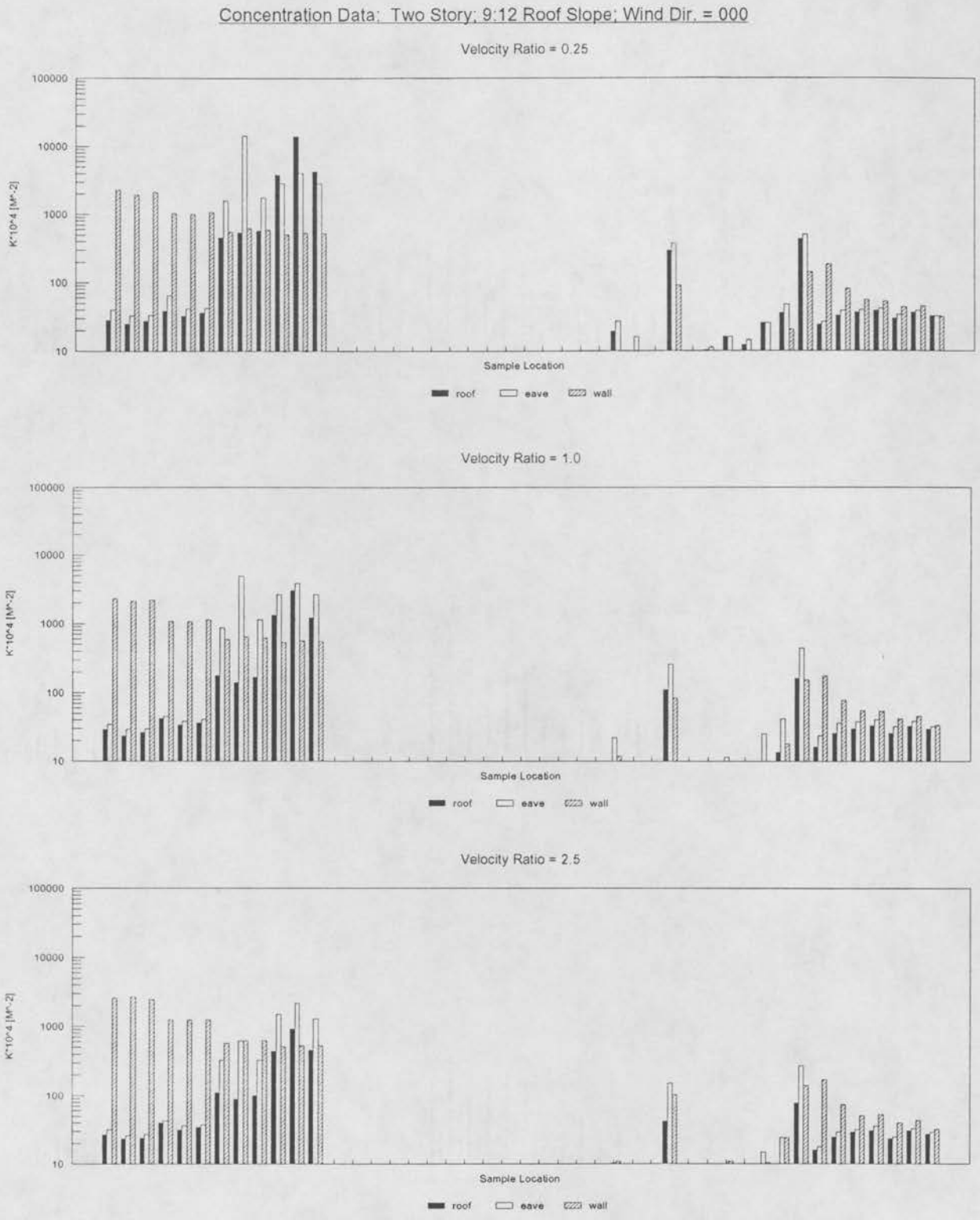

Figure 21m Exp. Conc. Comparisons of Roof, Eave, Wall Releases

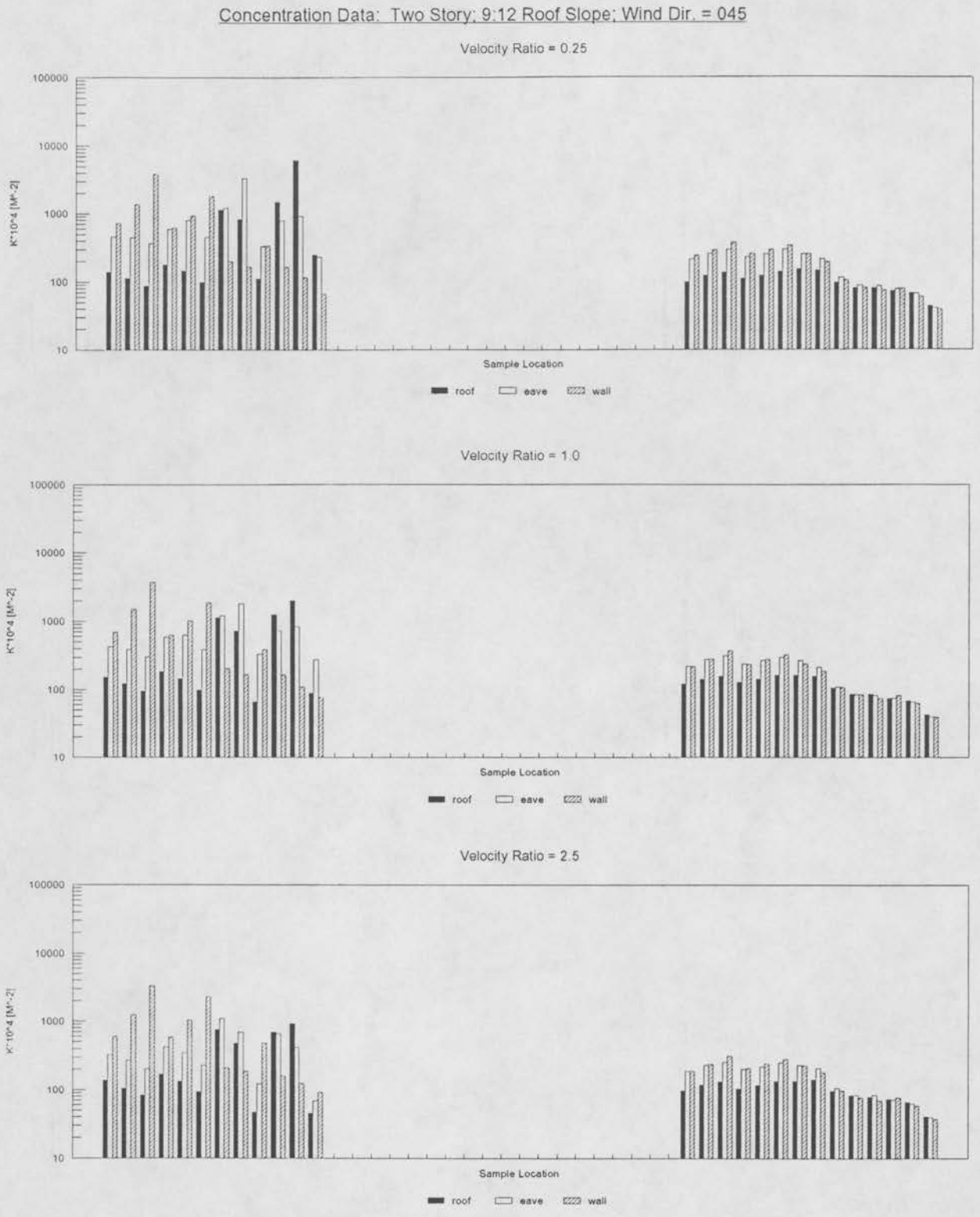

Figure 21n Exp. Conc. Comparisons of Roof, Eave, Wall Releases

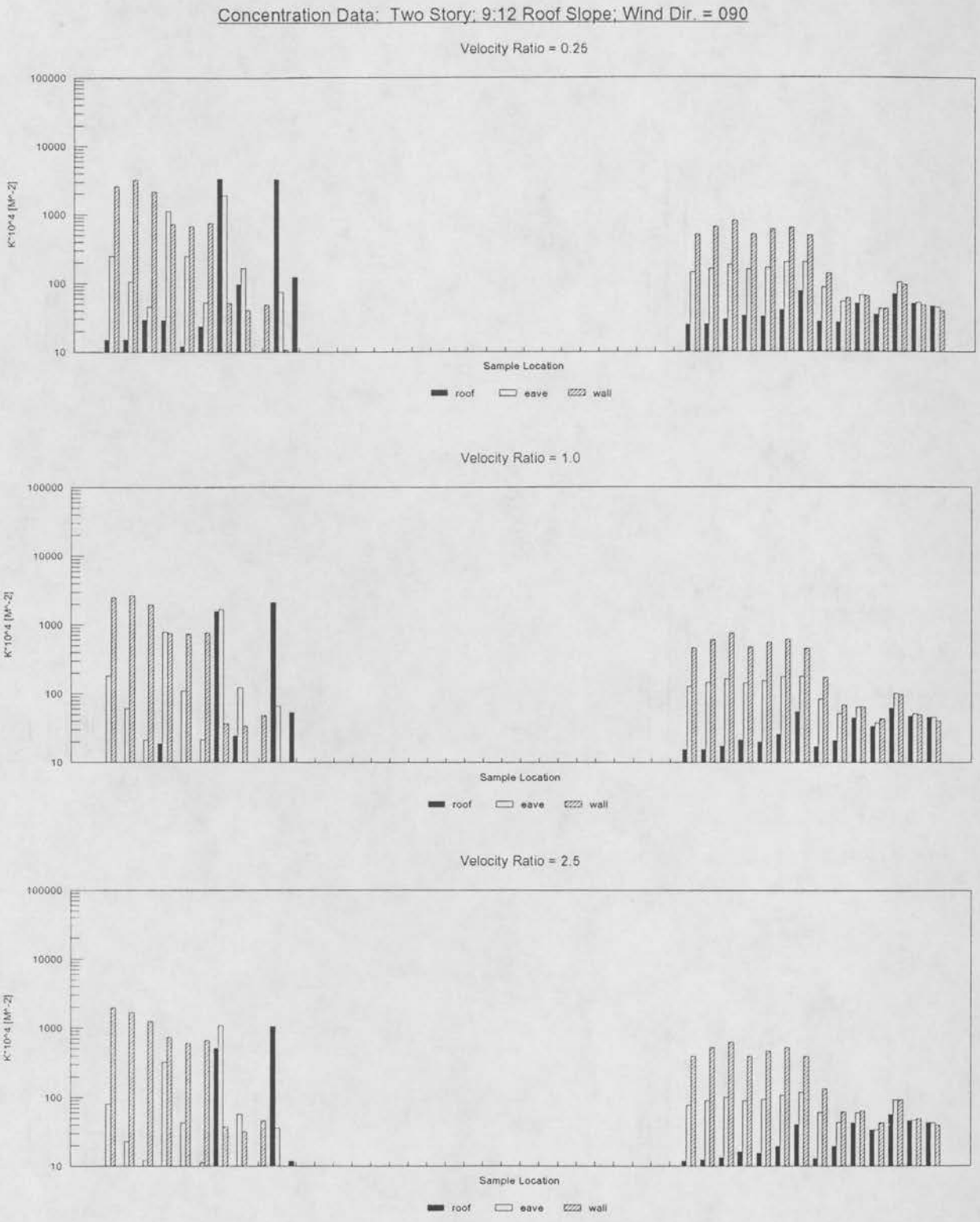

Figure 21o Exp. Conc. Comparisons of Roof, Eave, Wall Releases

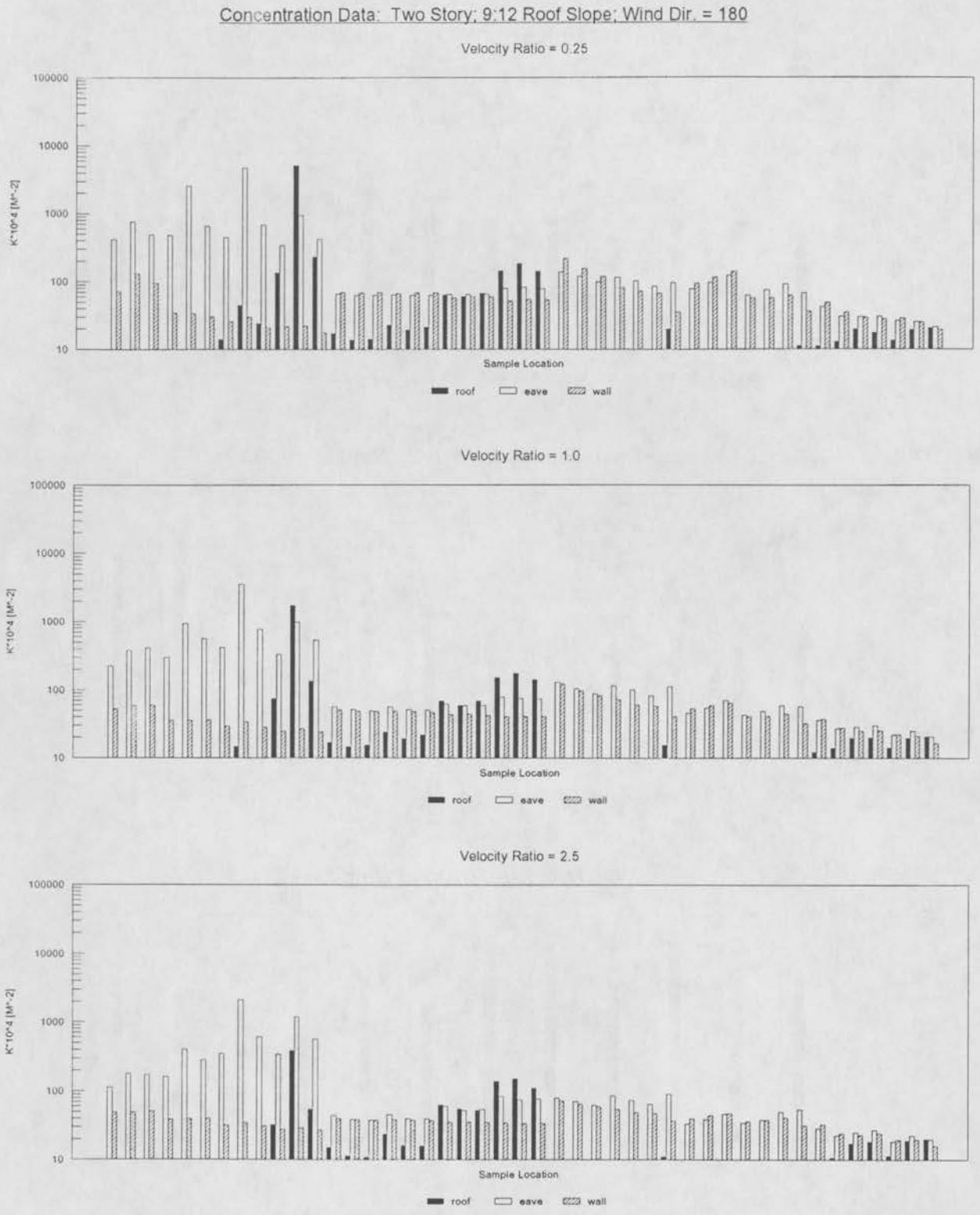

Figure 21p Exp. Conc. Comparisons of Roof, Eave, Wall Releases

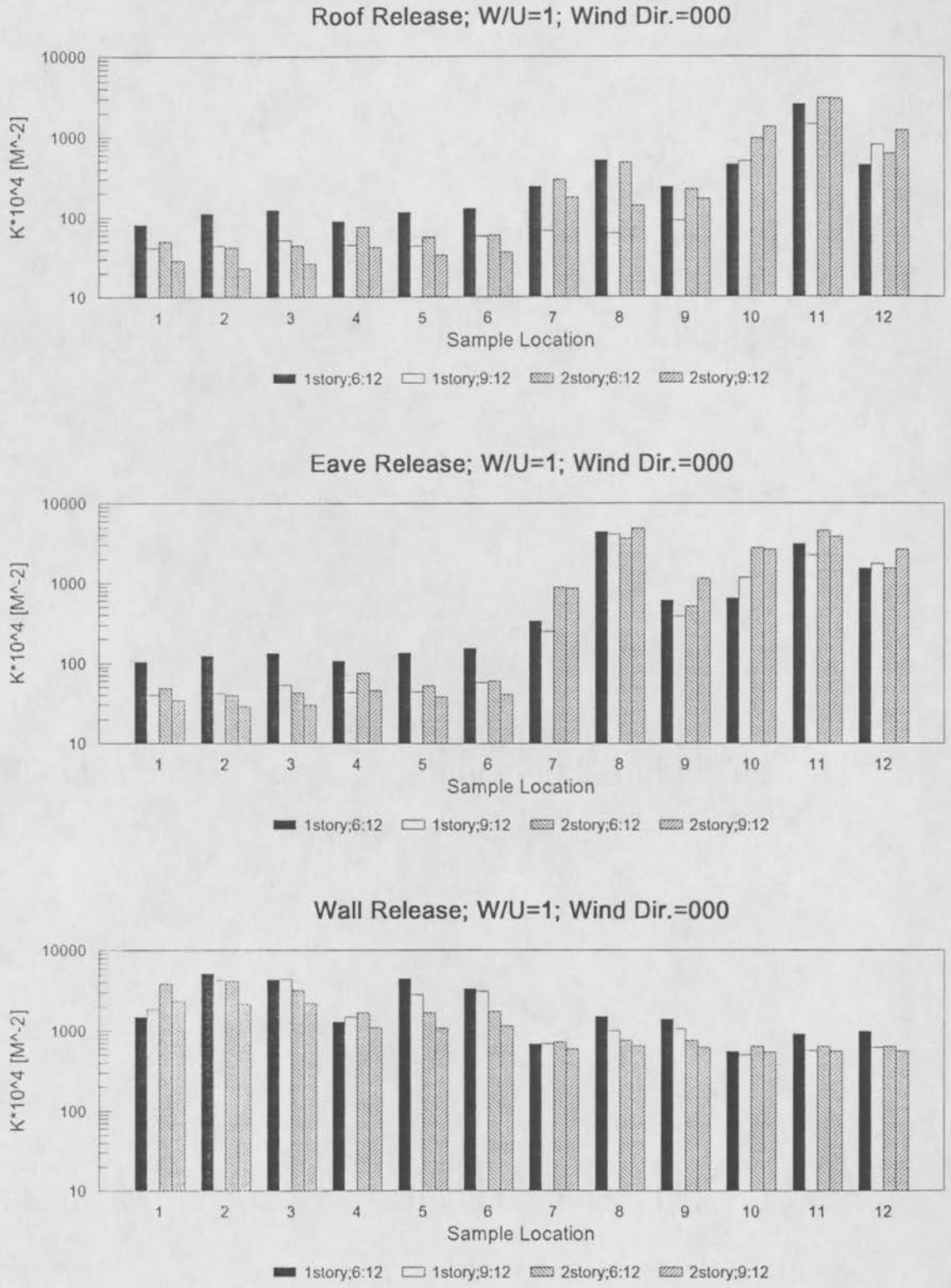

Figure 22 Exp. Conc. Comparisons of House Shape; W/U=1, winddir.=000

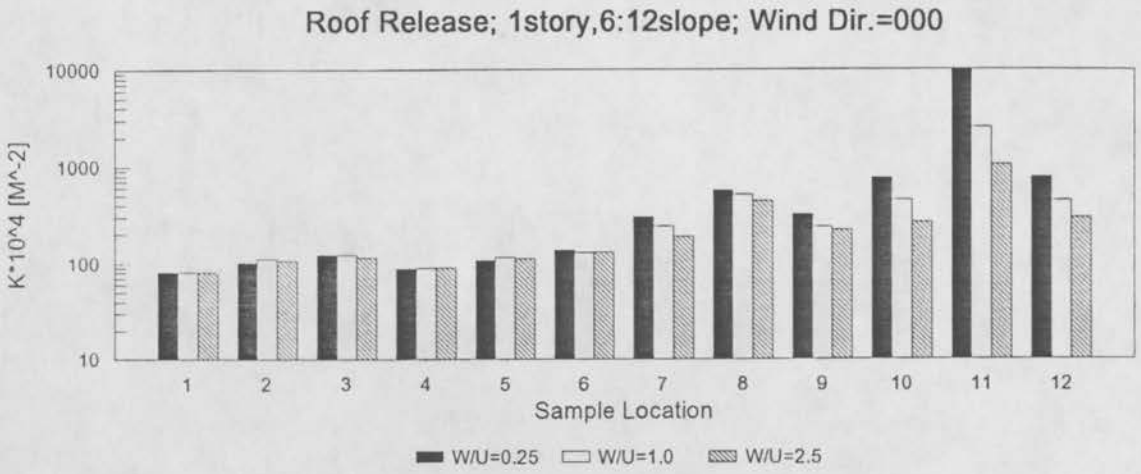

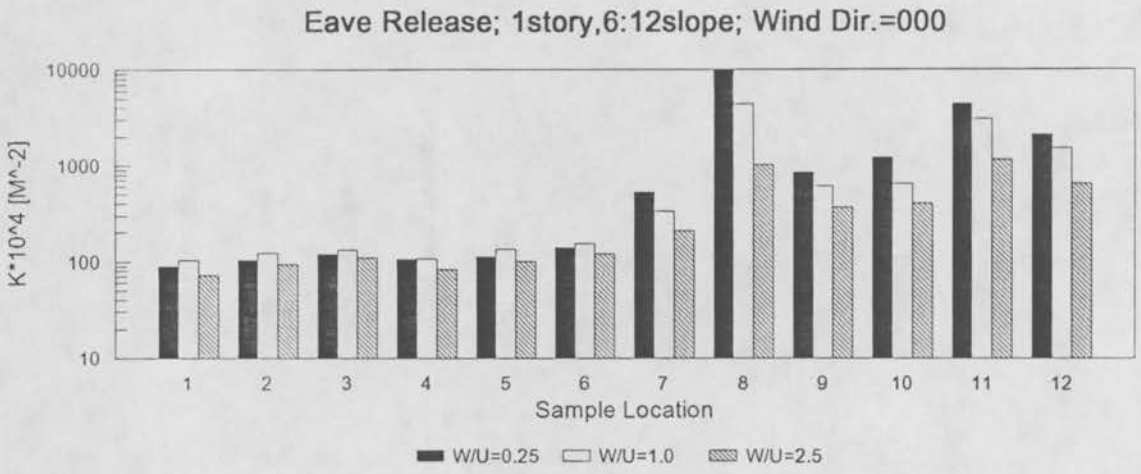

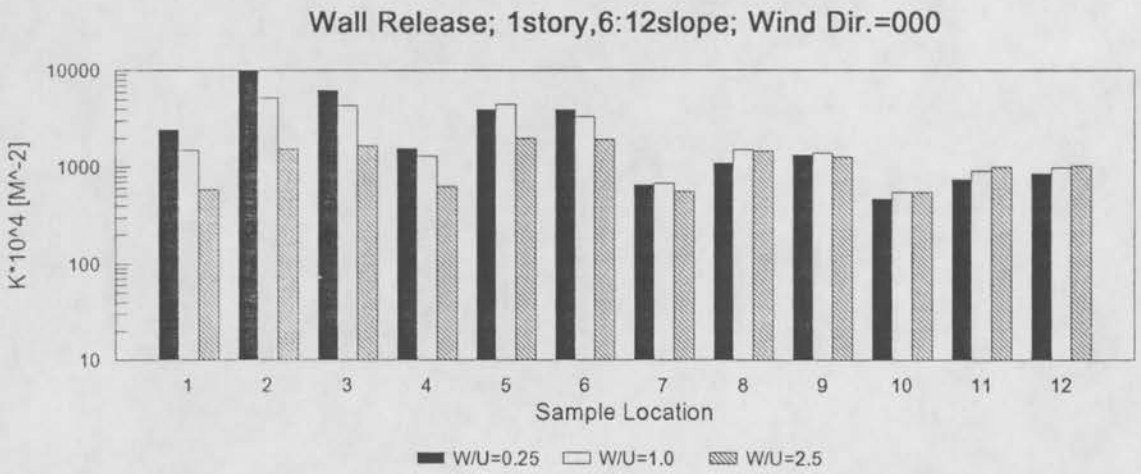

Figure 23 Exp. Conc. Comparisons of Exit Vel. Ratio; one story, 6:12 slope, winddir.=000

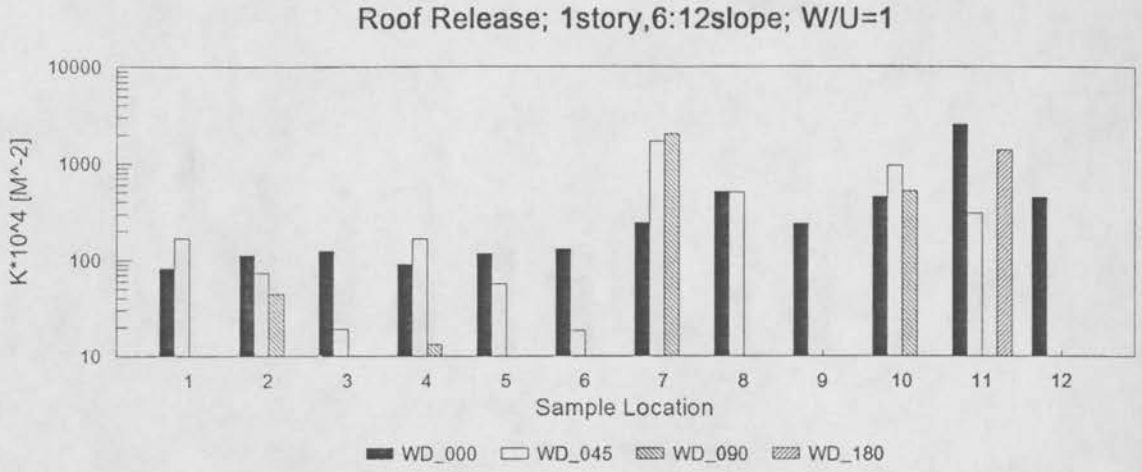

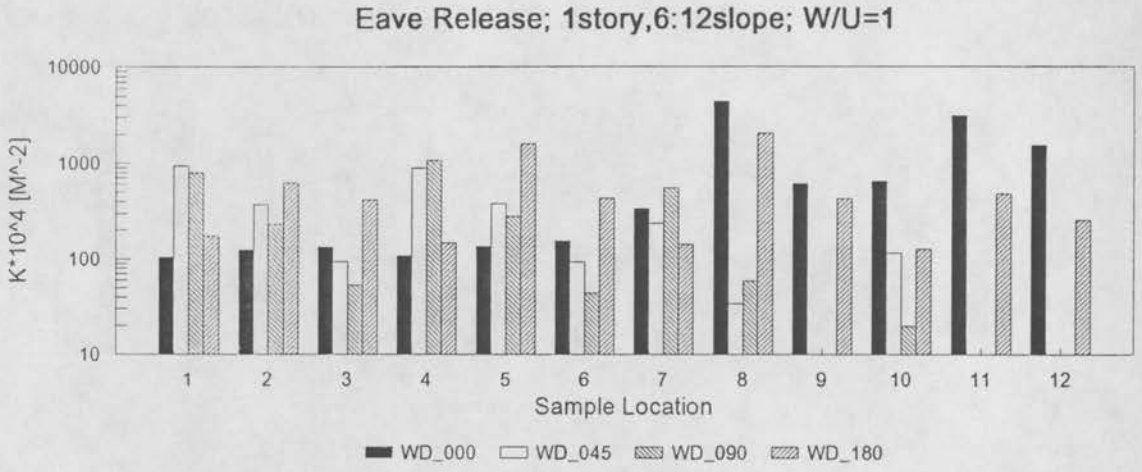

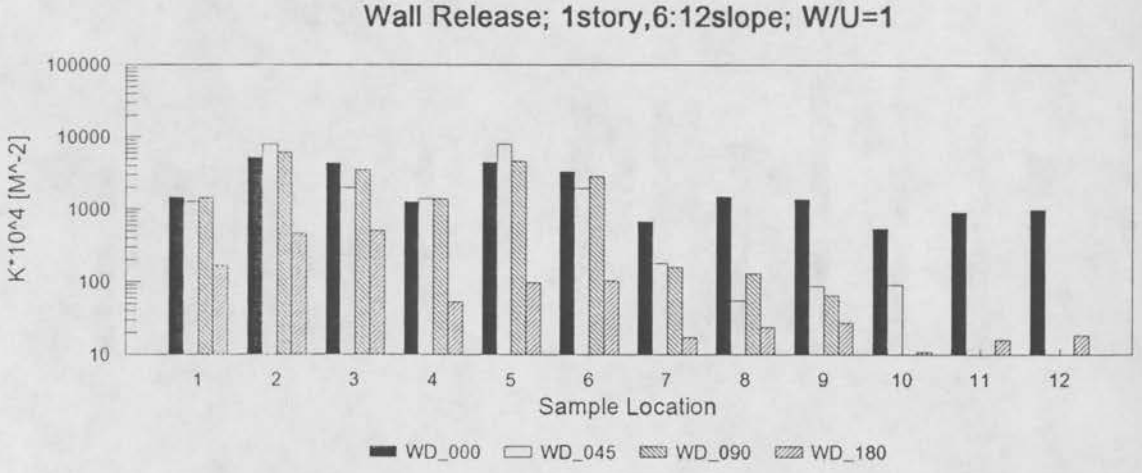

Figure 24 Exp. Conc. Comparisons of Wind Direction; one story, 6:12 slope, W/U=1

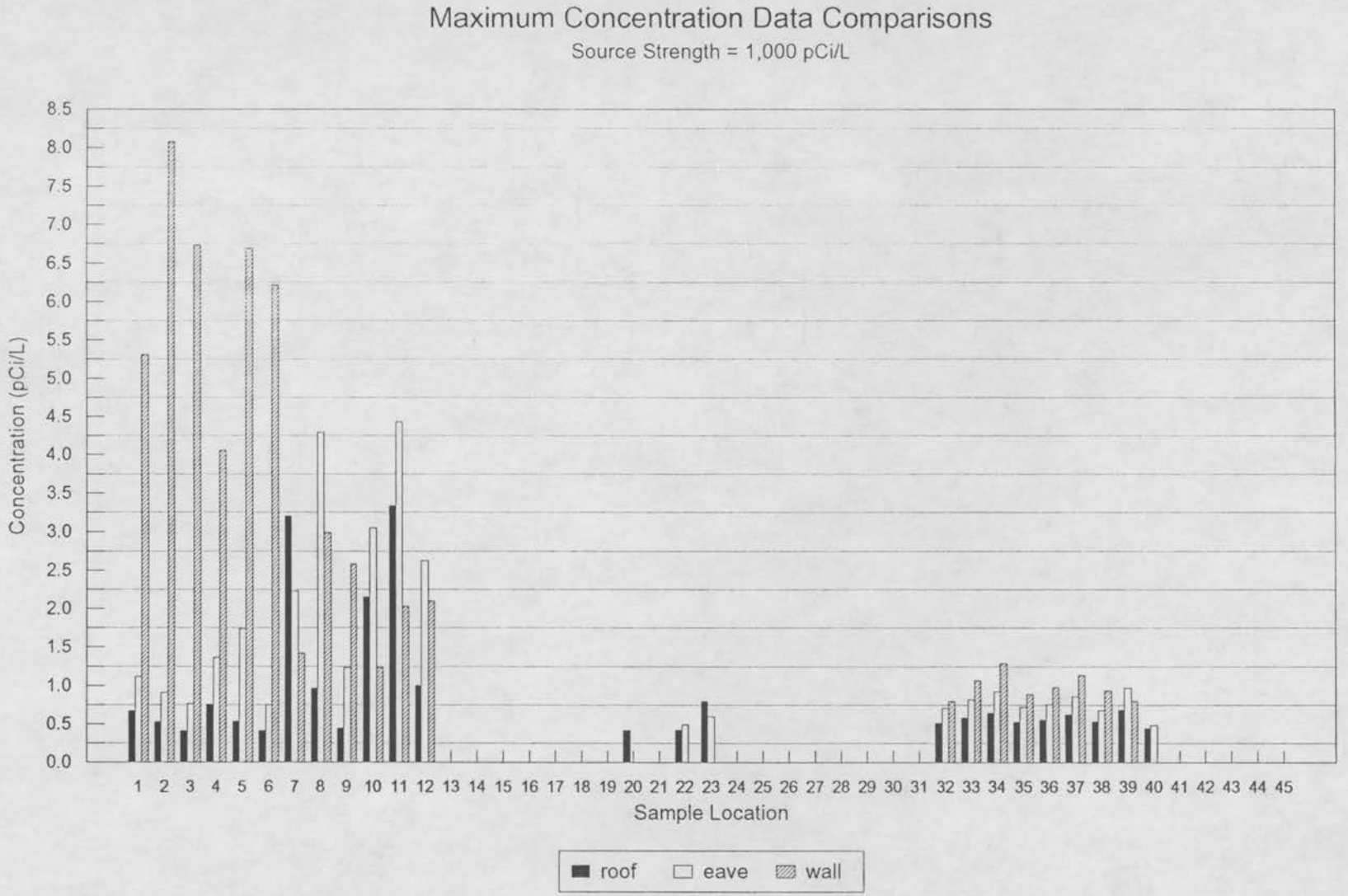

Figure 25 Exp. Maximum Conc. Comparisons; Source Strength = 1,000 pCi/L

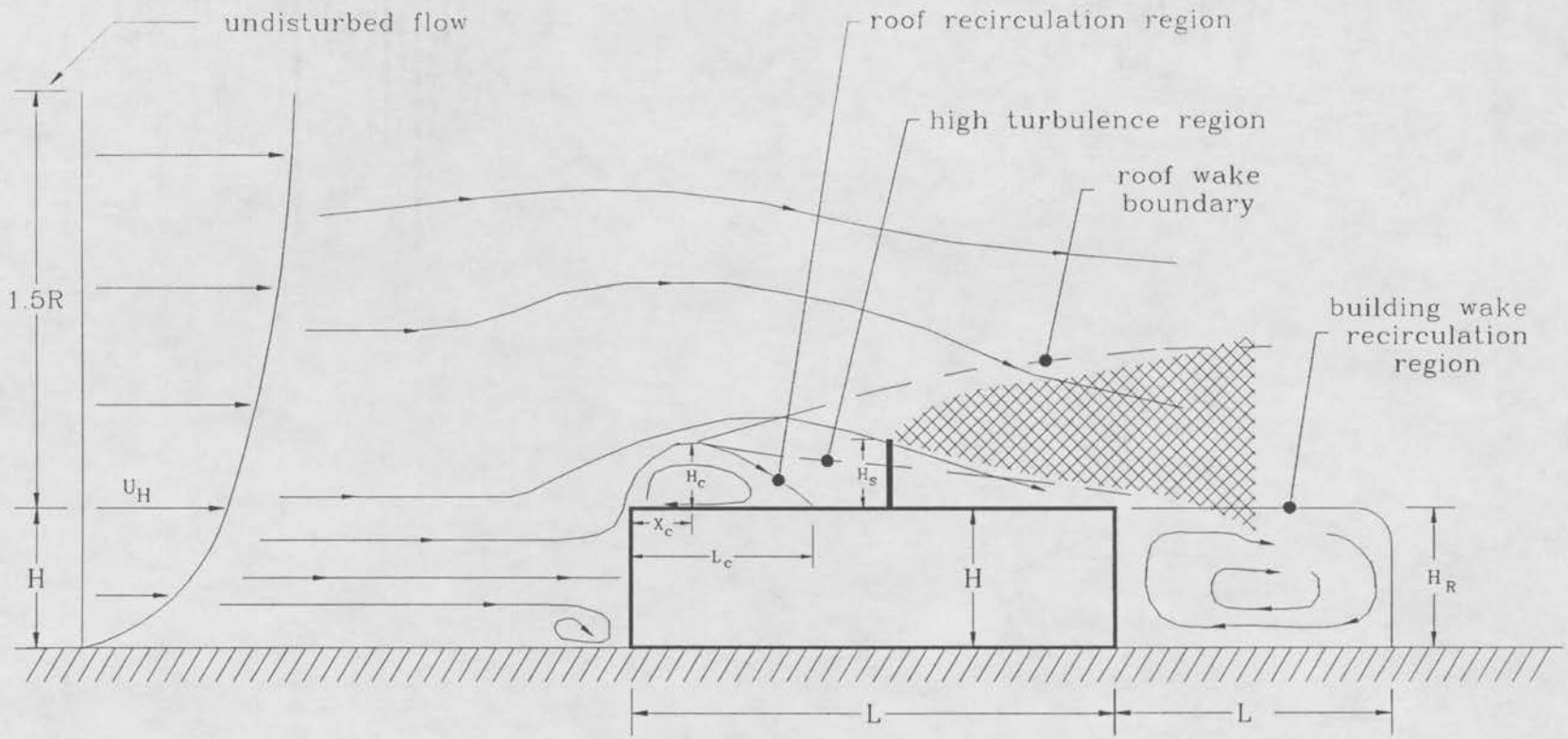

Figure 26 Schulman Model Definition Picture (adopted from Wilson (1979))

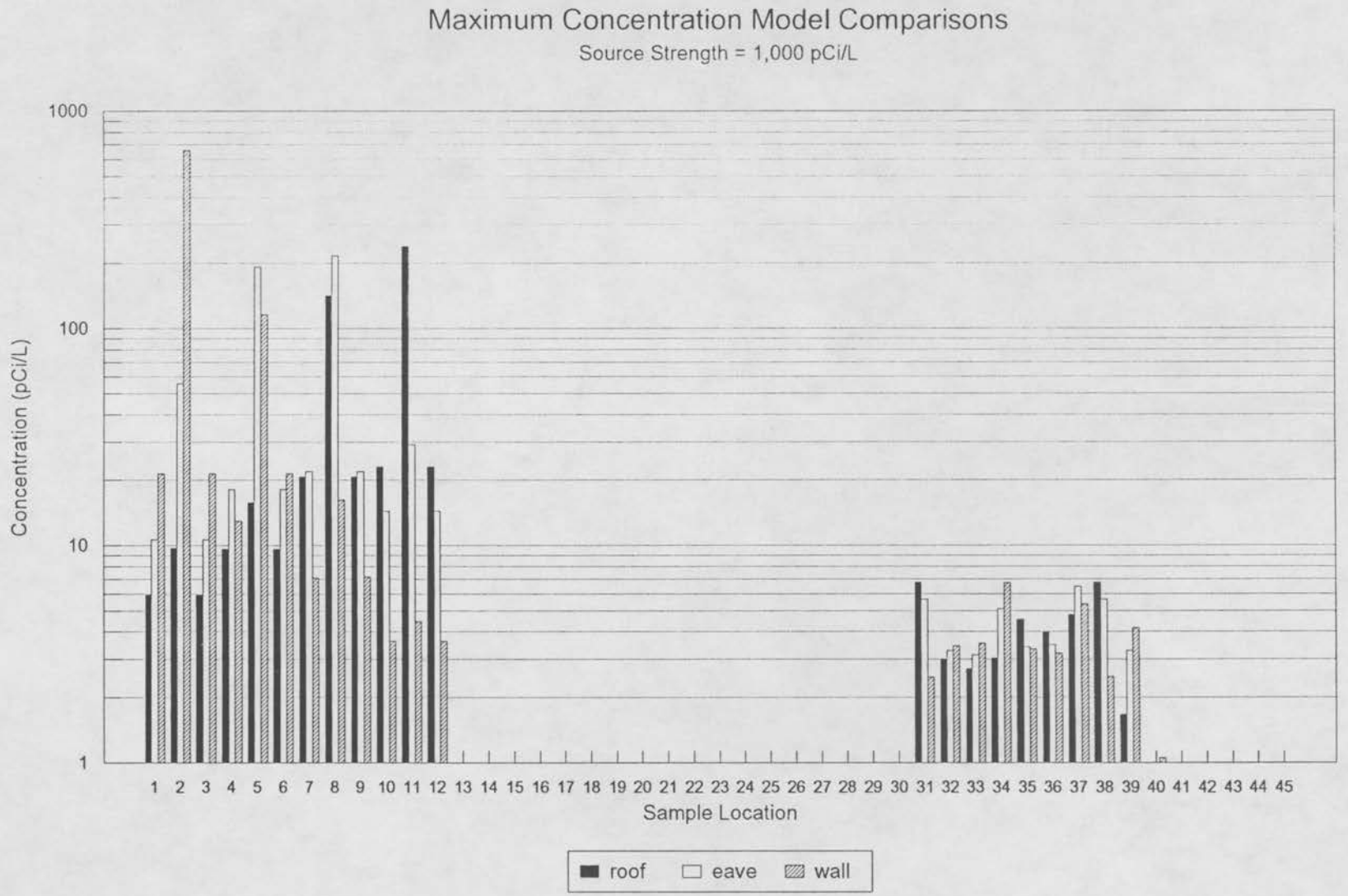

Figure 27 Schulman and Huber Model's Maximum Conc. Comparisons; Source Strength = 1,000 pCi/L

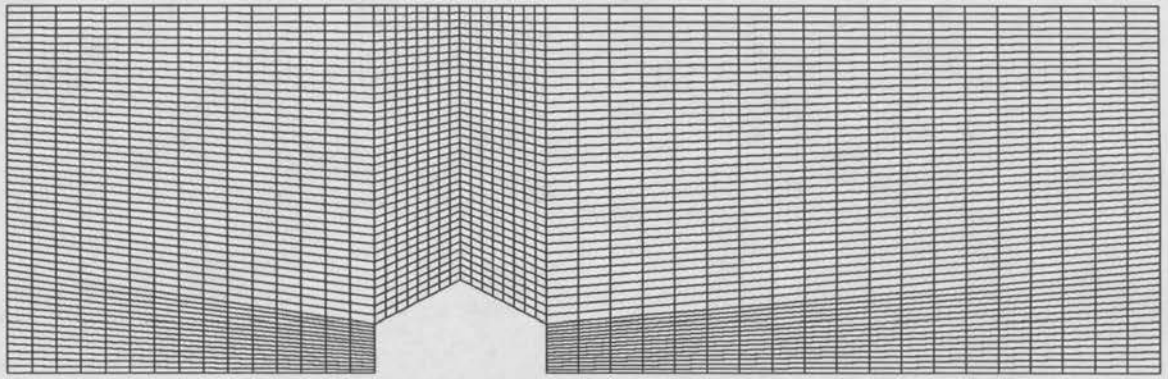

Figure 28 Uniform grid for 6:12 slope roof one-story house with 51 x 51 grid nodes. Inlet has piecewise-linear velocity profile, constant turbulence characteristics. Outlet is a constant pressure boundary, and top is a symmetry plane. Walls are rough surfaces.

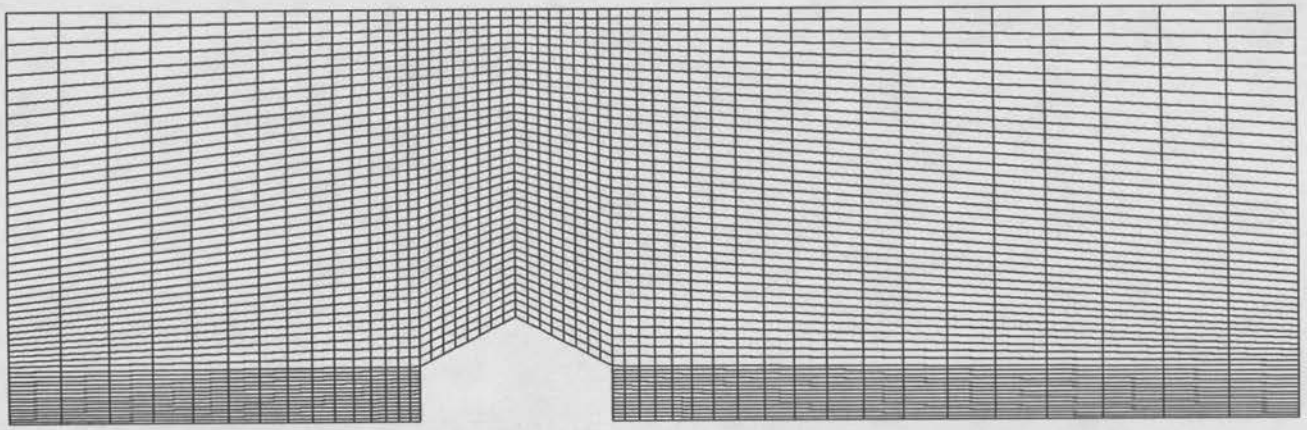

Figure 29 Adapted grid for 6:12 slope roof one-story house with 51 x 51 grid nodes.

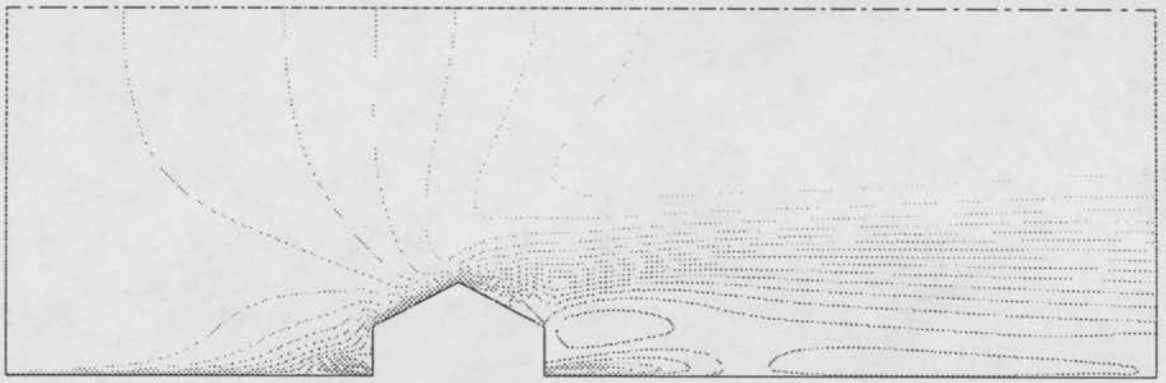

Figure 30 Longitudinal velocity, U, isocontours about 6:12 slope roof one-story house. Note up and down-wind jets from inlets near ground and recirculating regions.

Figure 31 Stream function contours about 6:12 slope roof one-story house.

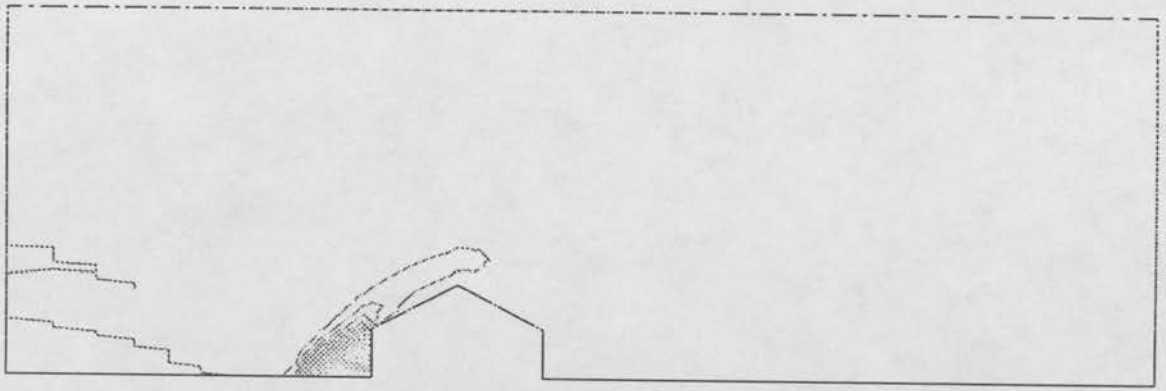

Figure 32 IsoConc. contours for upwind ground-level inlet for 6:12 roof slope one-story house.

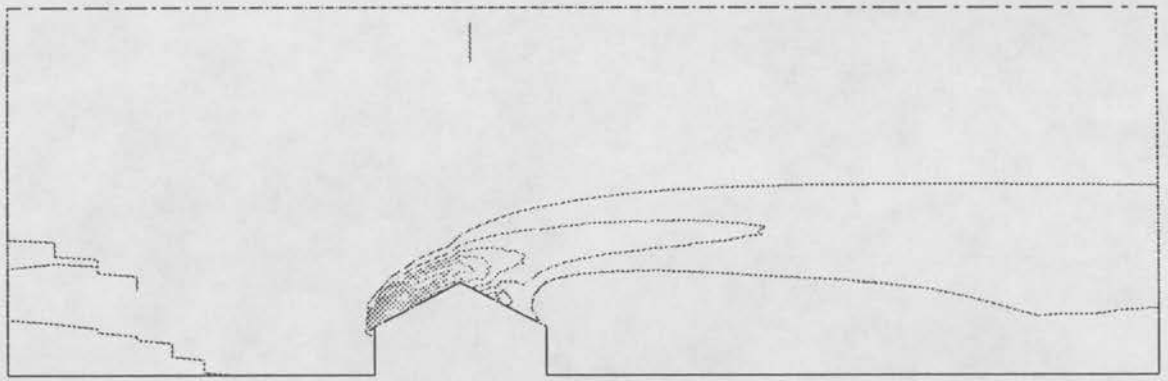

Figure 33 IsoConc. contours for upwind eave inlet for 6:12 roof slope one-story house.

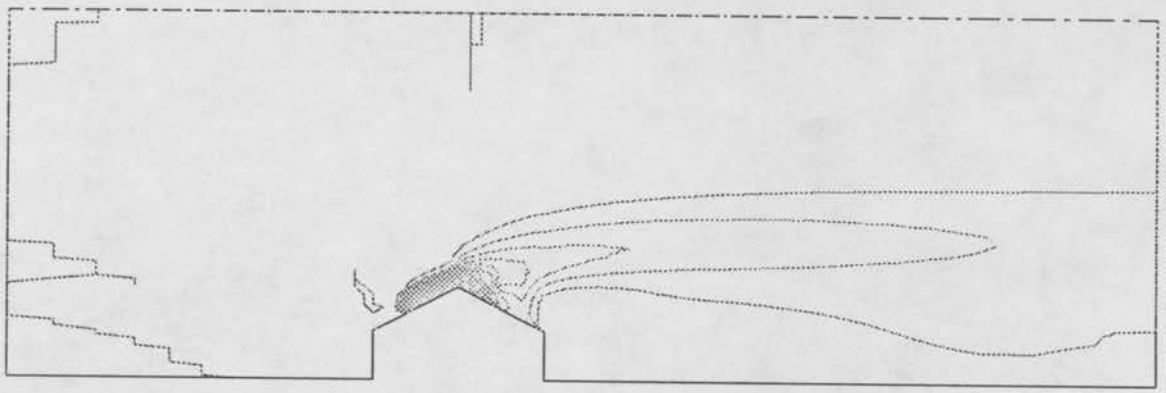

Figure 34 IsoConc. contours for upwind mid-roof inlet for 6:12 slope roof one-story house

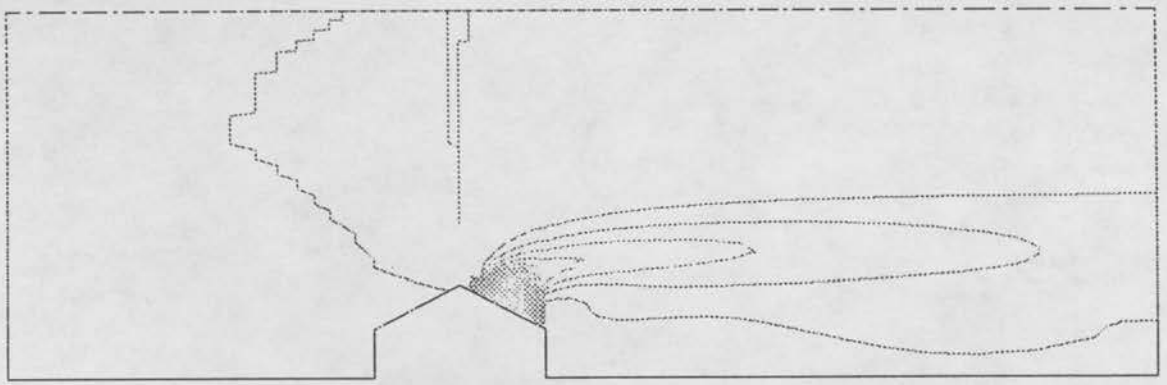

Figure 35 IsoConc. contours for down-wind mid-roof inlet for 6:12 roof slope one-story house.

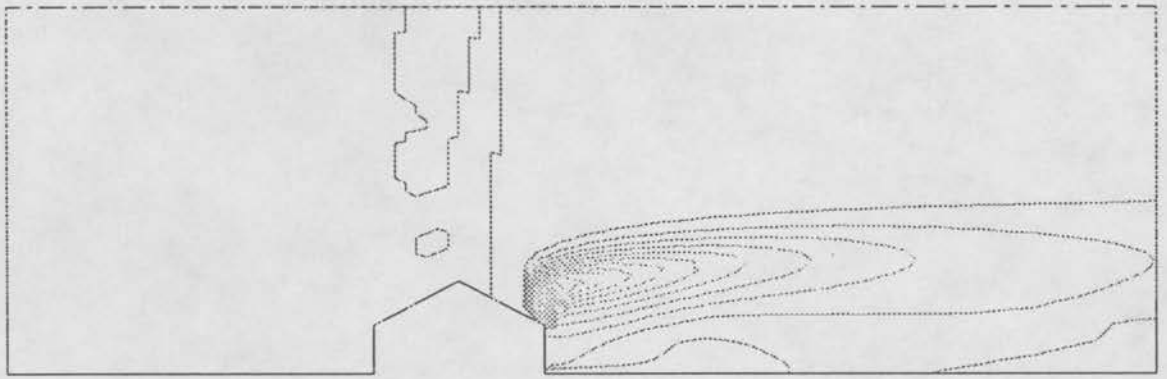

Figure 36 Conc. contours for down-wind roof eave inlet for 6:12 roof slope one-story house. Note effect of mid-roof inlet limiting upwind extend of this plume.

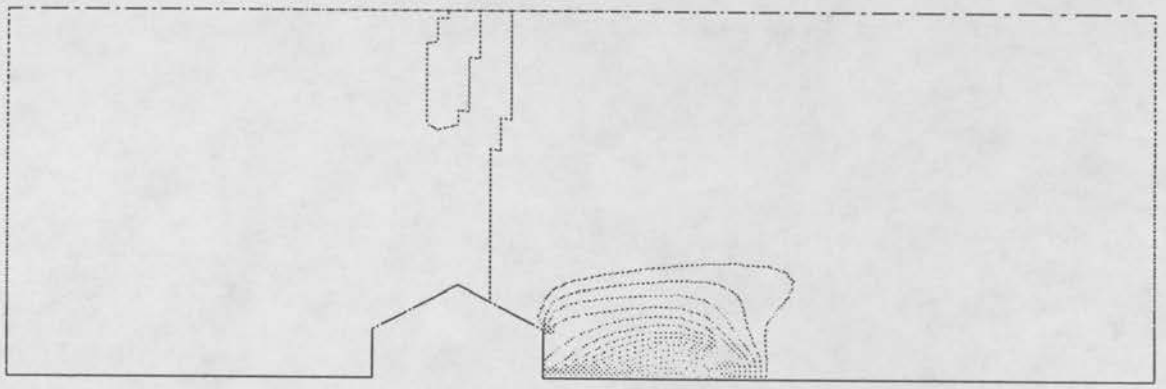

Figure 37 IsoConc. contours for down-wind ground-level inlet for 6:12 slope roof one-story house. Note downwind penetration of jet against upwind circulating separation cell.

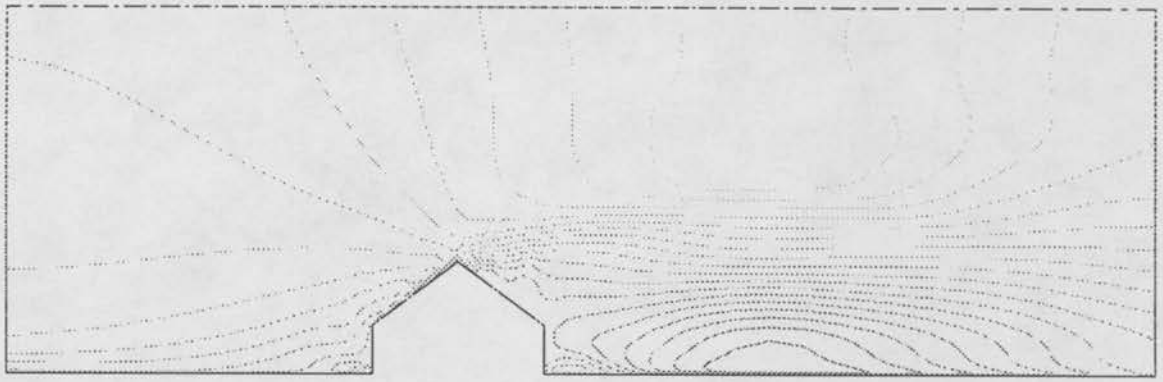

Figure 38 Longitudinal velocity, U, isocontours about 9:12 slope roof one-story house. Note up and down-wind jets from inlets near ground and recirculating regions.

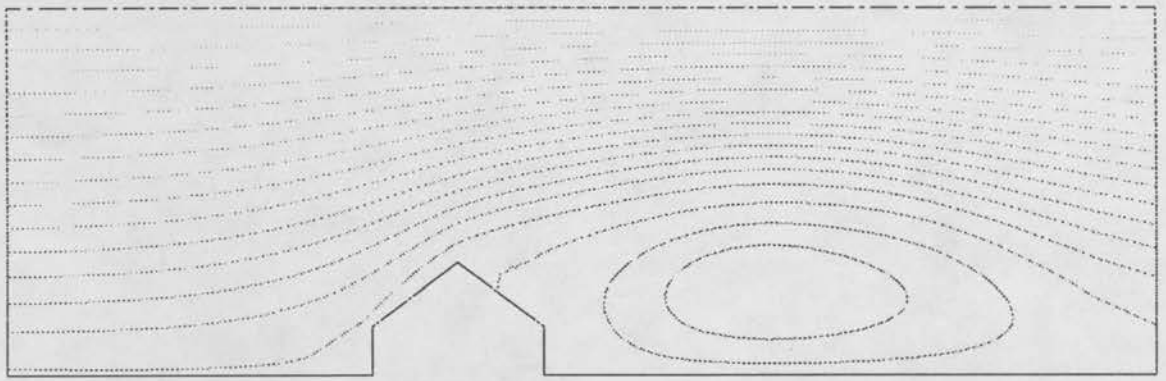

Figure 39 Stream function contours about 9:12 slope roof one-story house

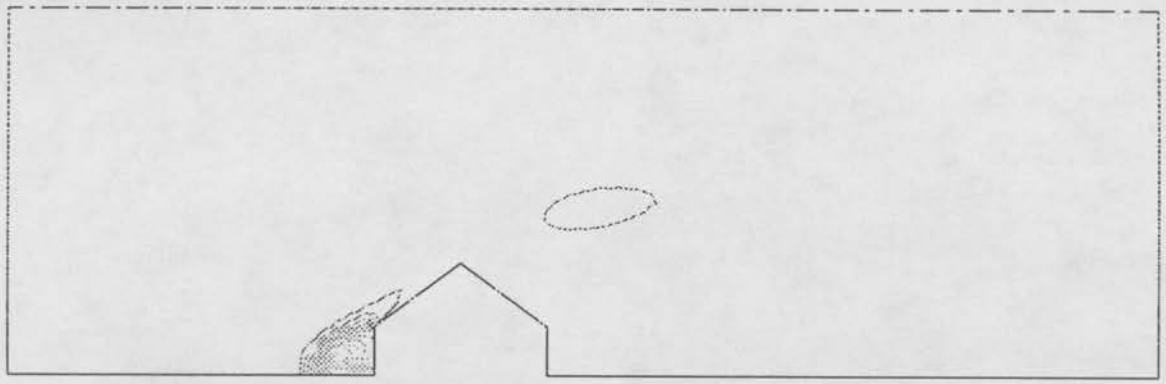

Figure 40 IsoConc. contours for upwind ground-level inlet for 9:12 slope roof one-story house

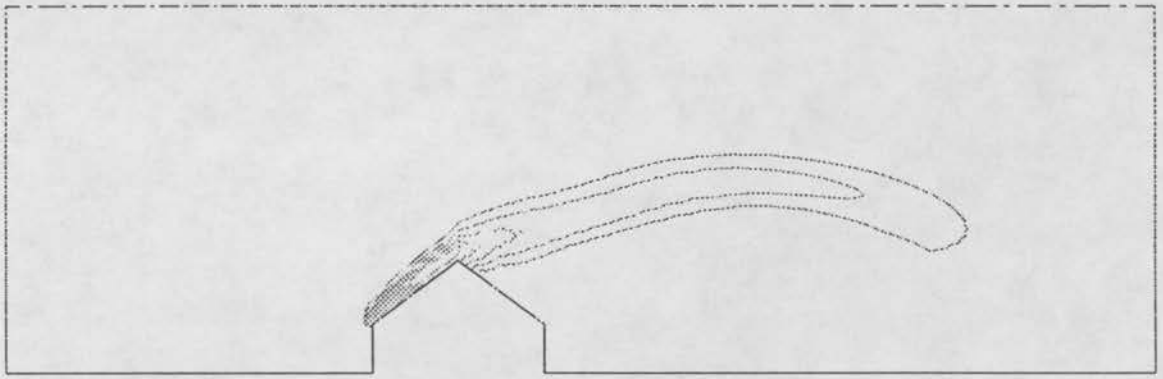

Figure 41 IsoConc. contours for upwind eave-height inlet for 9:12 slope roof one-story house

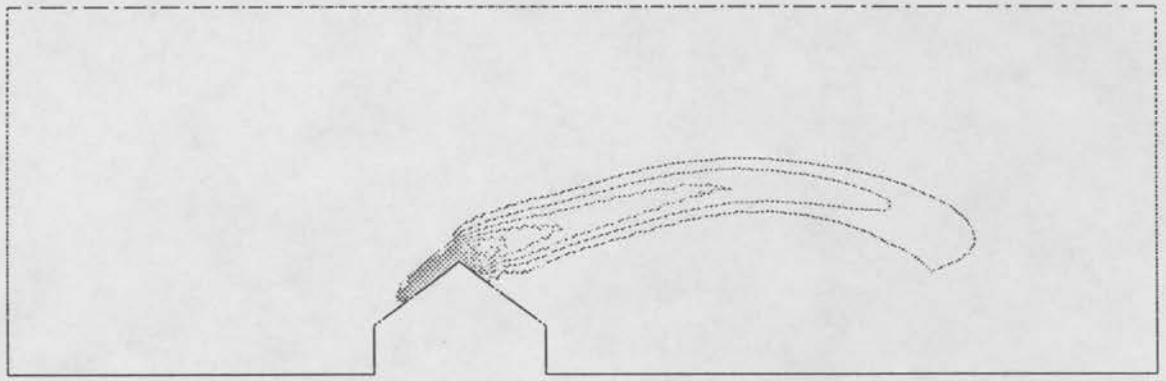

Figure 42 IsoConc. contours for upwind mid-roof inlet for 9:12 slope roof one-story house

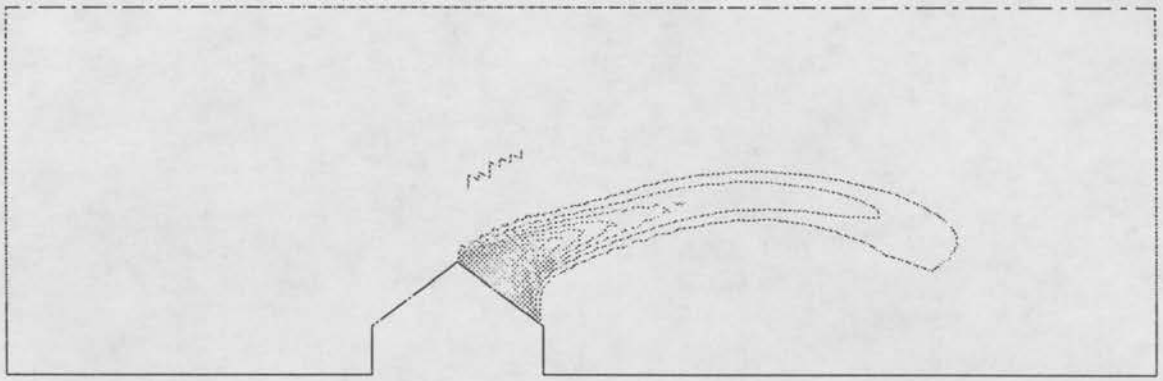

Figure 43 IsoConc. contours for downwind mid-roof inlet for 9:12 slope roof one-story house

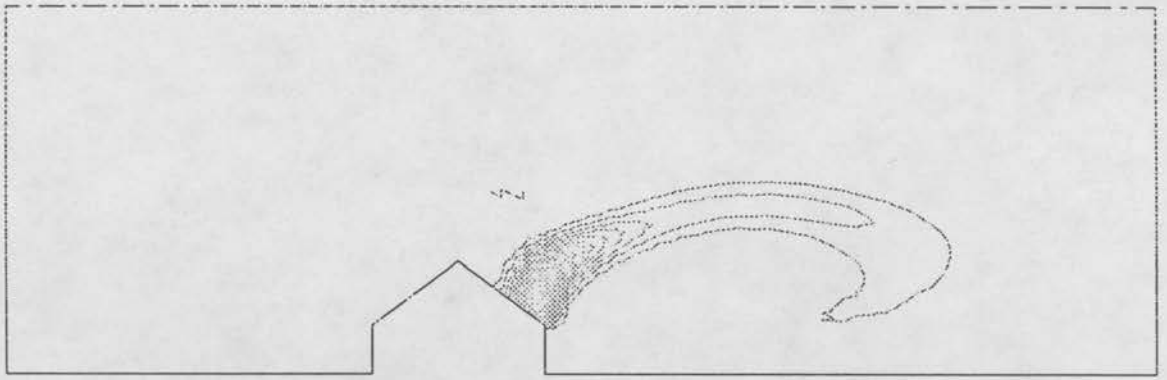

Figure 44 IsoConc. contours for downwind eave-height inlet for 9:12 slope roof one-story house

Figure 45 IsoConc. contours for downwind ground-level inlet for 9:12 slope roof one-story house

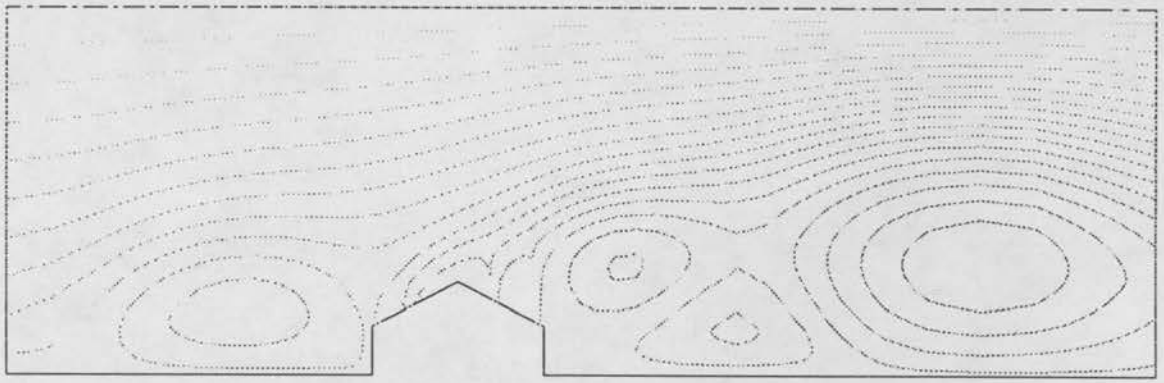

Figure 46 Stream fuction contours for 6:12 roof slope one-story house using RNG k-epsilon turbulence model.

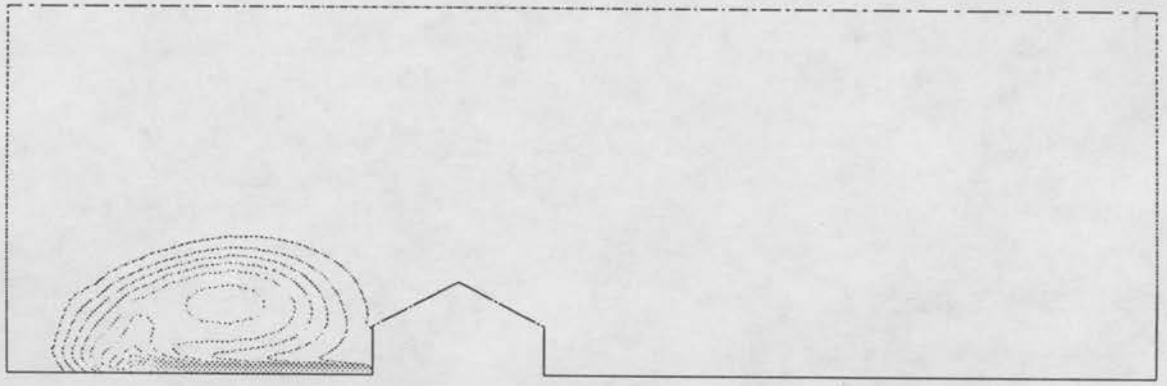

Figure 47 IsoConc. contours for upwind ground-level inlet for 6:12 slope roof one-story house calculated by RNG k-epsilon turbulence model.

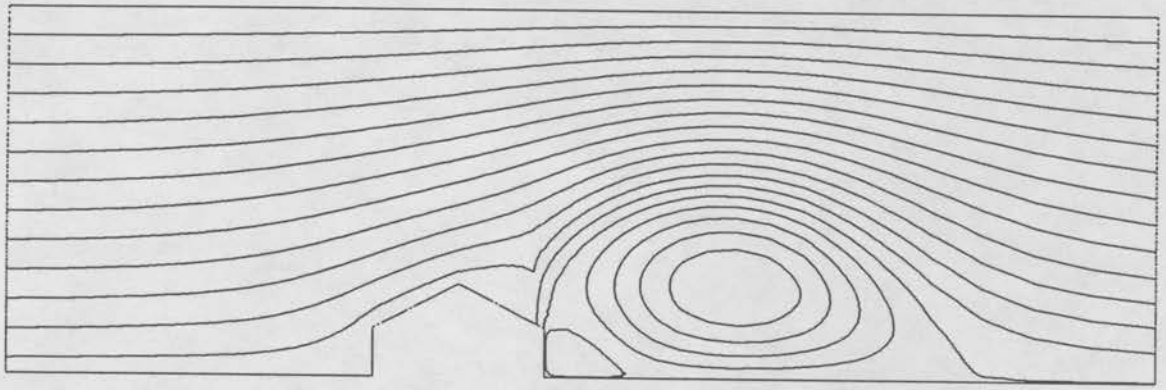

Figure 48 Stream fuction contours for 6:12 roof slope one-story house using RNG k-epsilon turbulence model. Only downwind eave-height inlet active.

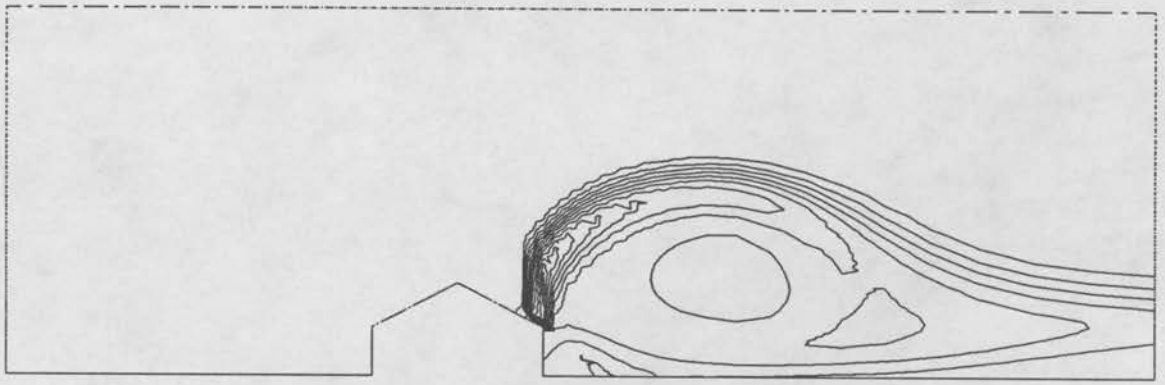

Figure 49 IsoConc. contours for downwind eave-height inlet for 6:12 slope roof one-story house calculated by RNG k-epsilon turbulence model. Only downwind eave-height inlet active.

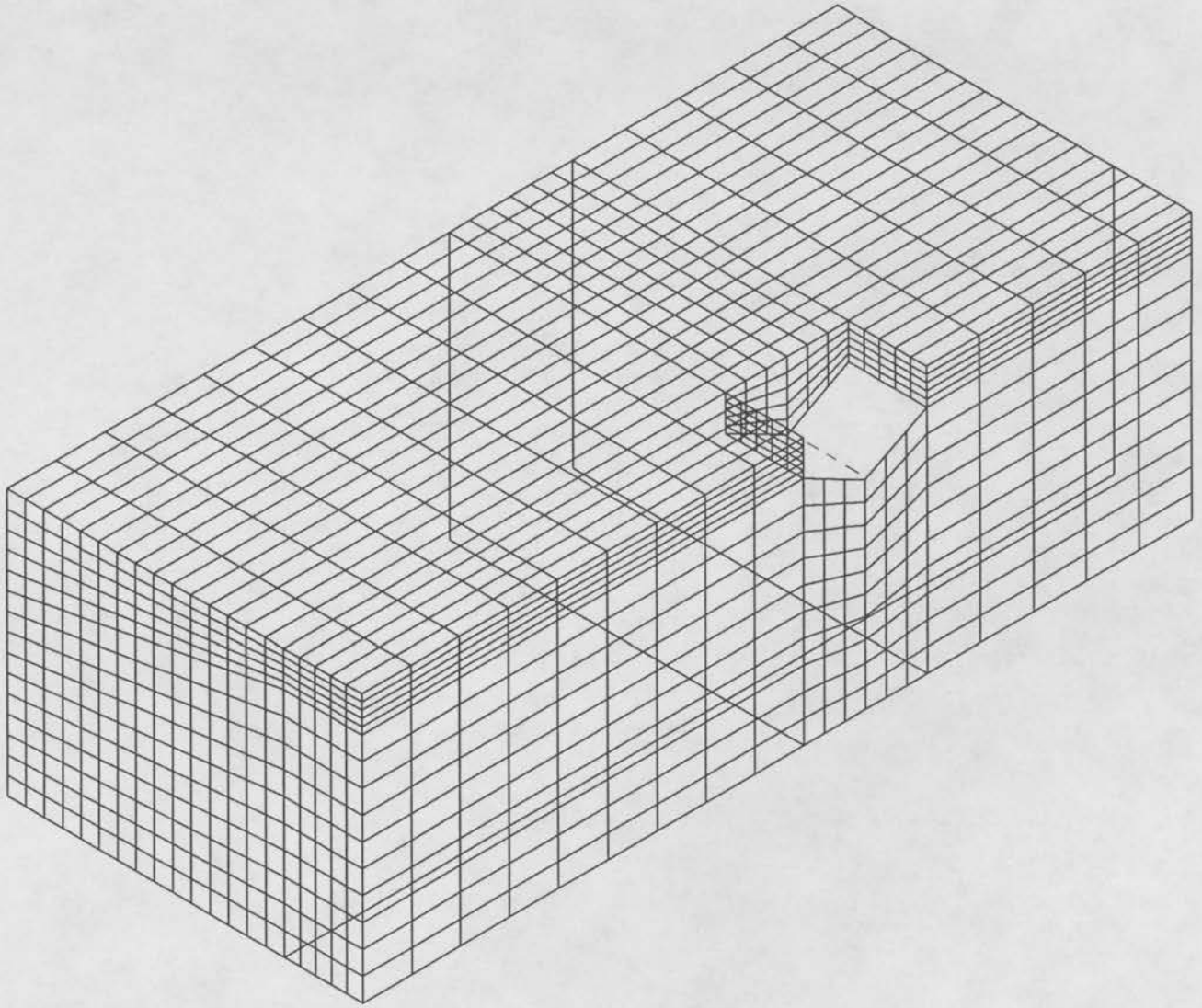

Figure 50 Three-dimensional boundary-fitted grid used to evalute the 6:12 roof-slope one-story house. House is split by a vertical symmetry plane. The top and front side boundaries are also symmetry planes. Grid size 21x16x21.

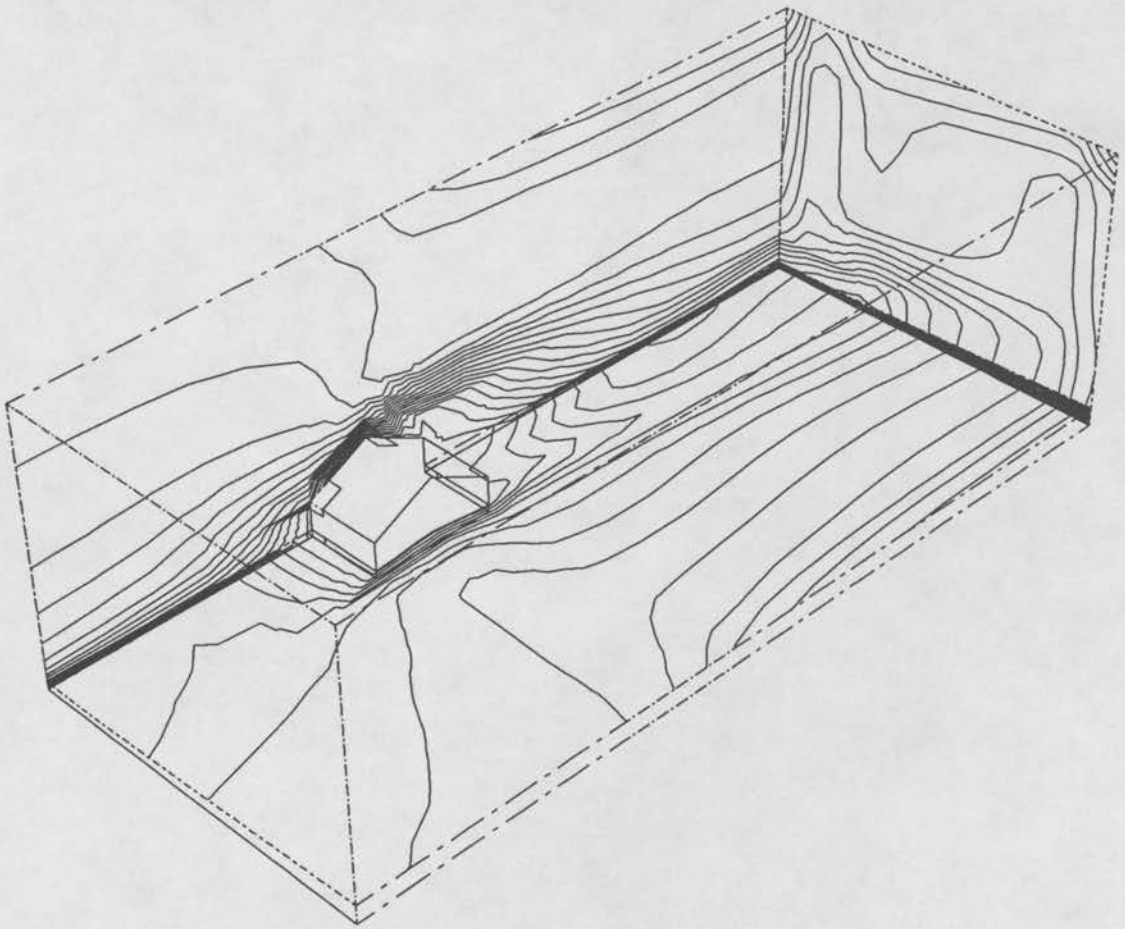

Figure 51 Longitudinal velocitiy, U, isocontours for 6:12 roof slope one-story house.

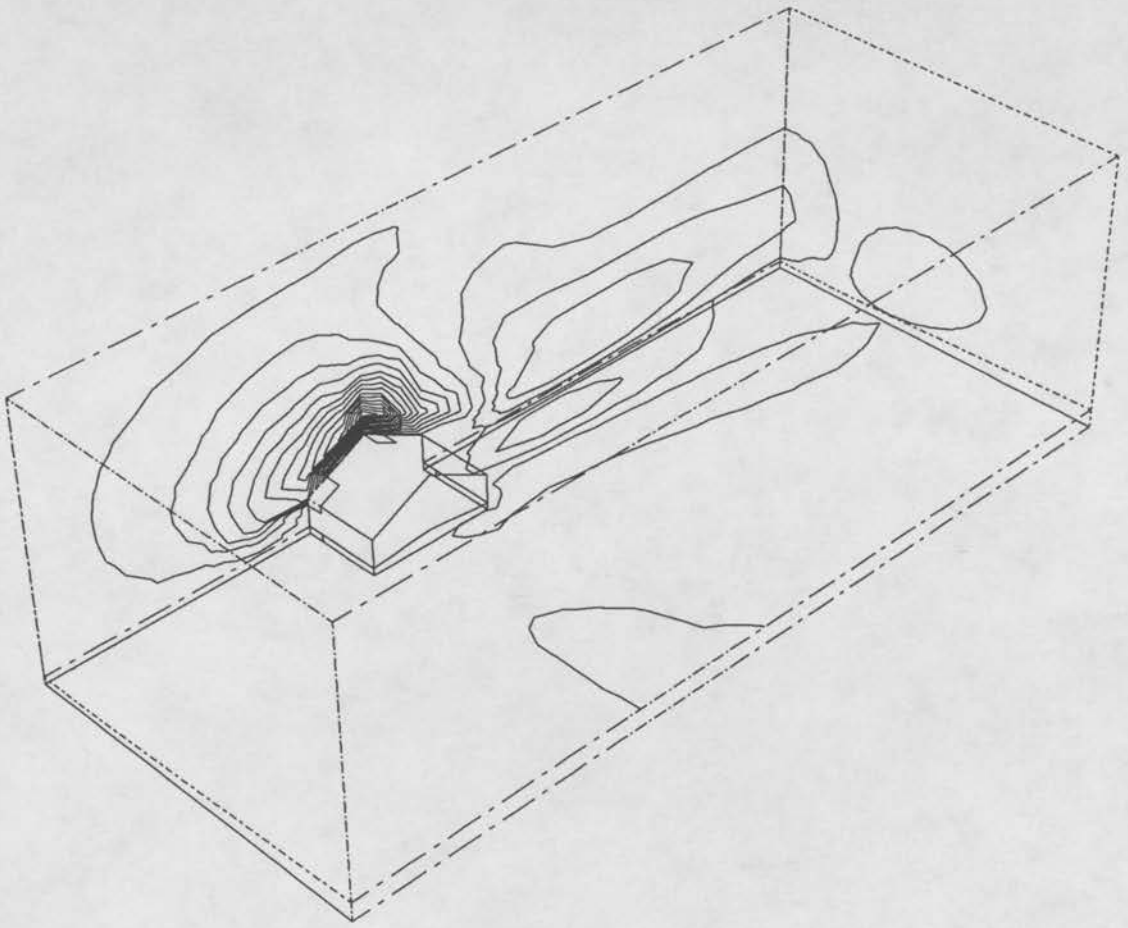

Figure 52 Lateral velocity, V, isocontours for 6:12 roof slope one-story house.

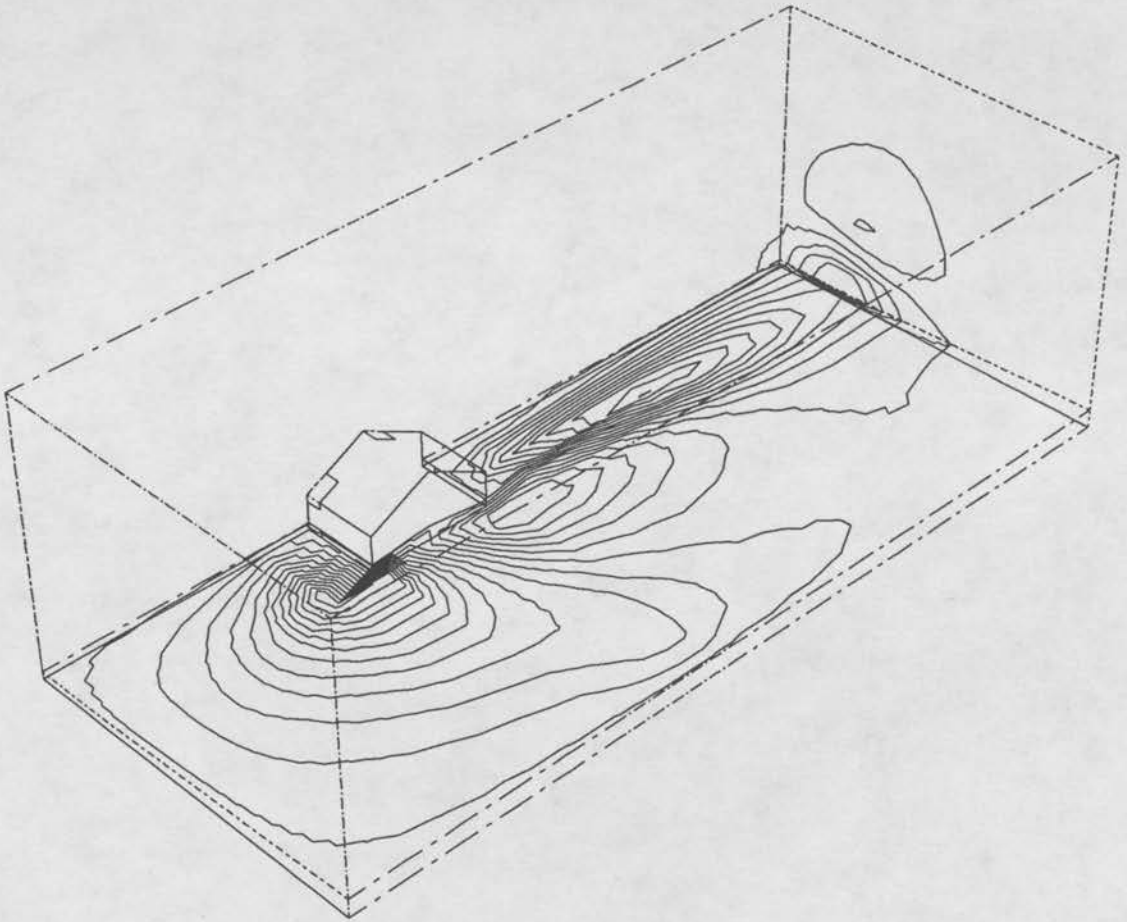

Figure 53 Vertical velocity, W, isocontours for 6:12 roof slope one-story house.

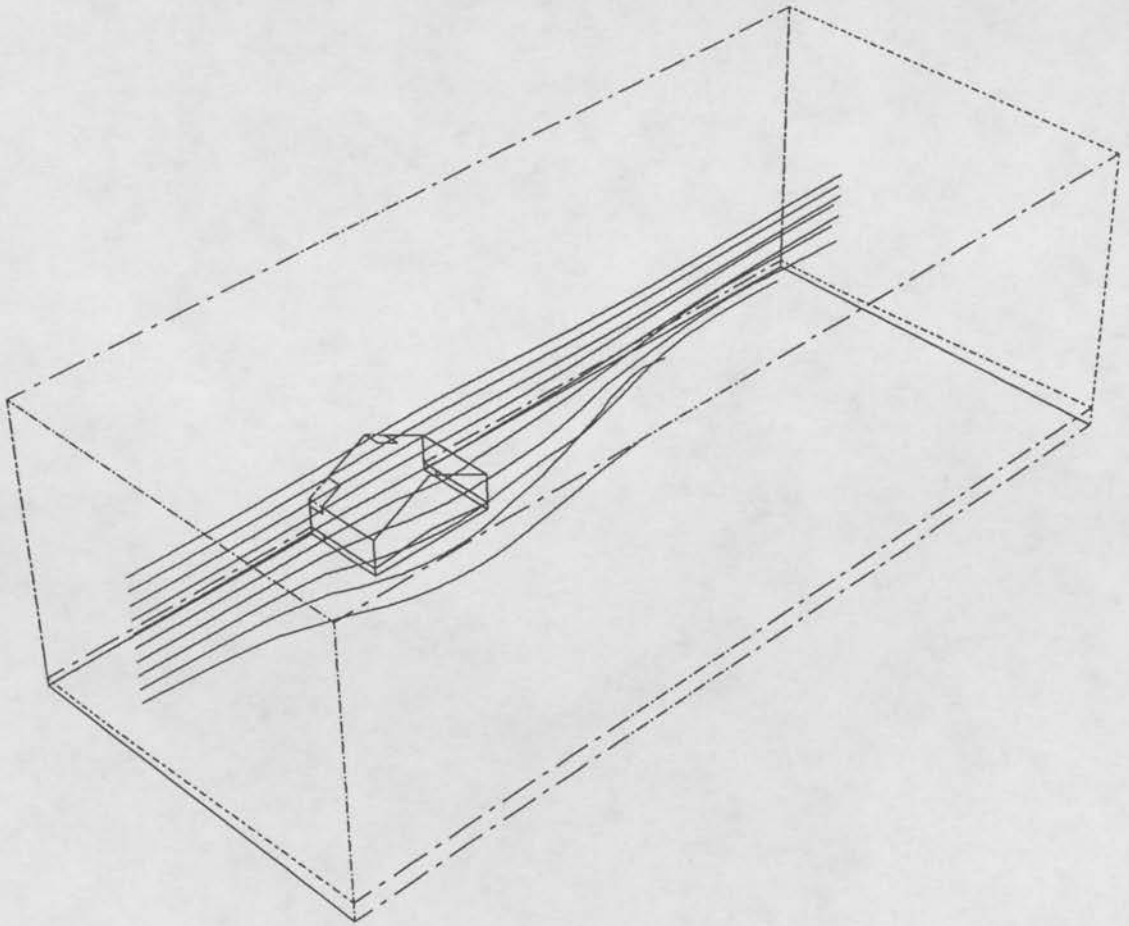

Figure 54 Streaklines from particles released upstream and 20 m from central symmetry plane over 6:12 roof slope one-story house.

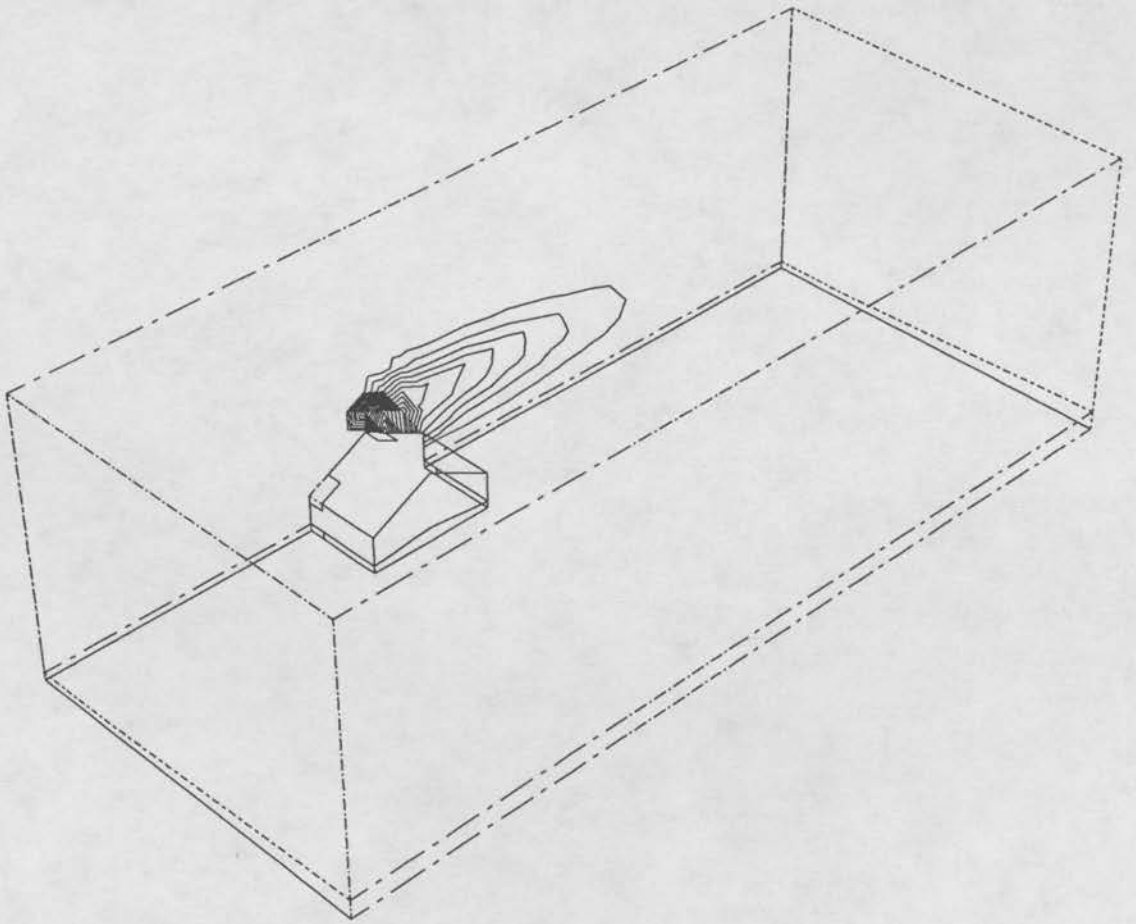

Figure 55 IsoConc. contours from downwind mid-roof inlet for 6:12 roof slope one-story house.

APPENDIX A:
VIDEO TAPE ENCLOSURE

APPENDIX B:
QUALITY ASSURANCE PLAN

1 QUALITY ASSURANCE OBJECTIVES

Data Quality Objectives (DQO) may be defined as requirements which specify an acceptable level of uncertainty regarding the collection of data characterizing a set of measurements. The uncertainties associated with DQOs incorporate a number of errors which are commonly known to occur in most measurement methods. Such errors may be due to the use of different sampling or measurement methods, variations in equipment calibration and response, spatial and temporal distribution of contaminants, etc. The main DQO for this project was to be able to detect tracer gas concentrations equal to 0.01% to 0.001% of the source concentration with a confidence of ± 15%. In the QA plan the data quality indicators (DQIs) goals were set as shown in Table 1.

Current EPA guidance (QAMS 005/80) requires that projects must address five data quality objectives (DQOs): precision, bias, completeness, representativeness, and comparability.

1.1 Precision and Bias

The uncertainty analysis of the experimental results is necessary for the results to be used to their fullest value. The uncertainty is calculated from

$$U = \sqrt{P^2 + B^2}$$

where P is the precision limit and B is the bias limit.

The precision limit, P, about a nominal result is the 95 percent confidence estimate of the band within which the mean of many such results would fall. The bias limit, B, is an estimate of the magnitude of the fixed, constant error. Precision and bias will be assessed by duplicating measurements.

The uncertainty DQOs for the concentration and velocity measurements (hot-film anemometer and pitot-static tube technique) performed for this project is presented in Table B-1. The GC/FID is sufficiently sensitive to reliably detect tracer gas concentrations of 0.01% to the order of ± 3% and 0.001% to the order of about ± 15%. The accuracy of the hot film was within the limits mentioned in the QA plan which was less than 10%.

1.2 Completeness of Data Acquisition

Since the goal of this project is to achieve the highest degree of completeness, all measurement devices were logged at the time of use on this project. The loss of any data may be due to recorder errors, empty paper rolls, thermal drift, and an operator error

Fortunately very few data were lost in the concentration tests (sampling point 44 in run D01 is an example). In some cases the tests were repeated if the loss of data had major effect. Almost no data loss occurred in the velocity measurements. Table 1 shows the completeness of each measurement parameter.

1.3 Representativeness

Fluid modeling is based on the principle that full-scale and model flows can be related through appropriate simulation parameters. The report contains a discussion of simulation logic, the steps taken to assure that the wind-tunnel boundary layer represents a reasonable approximation to the atmospheric surface layer, and the measurements made to assure that results are Reynolds number independent as suggested in EPA- 450/4-81-003.

Sections 2 and 3 explains the wind tunnel boundary layer configuration and the Reynolds number invariance tests for velocity and concentration. The results show that the wind tunnel configuration is representative of the field boundary layer. The Reynolds number invariance tests for the velocity measurements display errors of about 10%. The concentration tests gave error values in K_p 17% at only a few locations. For most locations on the surface errors fall below 10%.

1.4 Comparability

Measurements made from an isolated source within the simulated atmospheric boundary layer were compared with the characteristic growth of height and width and the decay of concentrations as predicted by Pasquill_Gifford urban dispersion model. The results demonstrate that Pasquill-Gifford C-D behavior was obtained.

1.5 Conclusions

The preceding analysis shows that the DQOs were met except for the normalized concentration measurements representativeness where the error increased from 10% to 17% at some locations due to normal flow intermittency. At plume edges the range of normal concentration uncertainty is always physically large, only at the plume centerline will concentrations produce stable values for a limited experimental data set.

Table 1: Goals for Data Quality Indicators (DQIs)

Measurement Parameter	Precision Accuracy (Bias)	Completeness	Representa-tiveness
Sampling and analysis of tracer gas using GC/FID	± 3%[1,2,3], or 1.5 ppm whichever is greater	≥ 98%[8]	--
Source gas Strength	± 0.5%[5]	--	--
Normalized Concentration	± 5%[1,2,3], or 1.5 ppm whichever is greater	≥ 98%[8]	± 17%[4]
Velocity/ Turbulence measurements with hot-film anemometer	± 10%[6]	≥ 99%[8]	± 5%[4]
Flow measurements using pitot tube	± 5%[7]	≥ 99%[8]	--

Footnotes to Table 1:

1. The DQI in this row address combined sampling plus analytical error.
2. The accuracy of the GC/FID was determined daily by sampling atmosphere containing known concentration of 76.4 ppm tracer gas. A tracer gas of concentration 200 ppm was also used at the beginning each test series.
3. The accuracy of the automated syringe/tube sampling system was determined by running four constant release runs two (replicating) using 0 ppm tracer gas and two using 76.4 ppm tracer gas.
4. See Reynolds Number invariance tests for velocity and concentration (sections 3.1 and 3.3.2).
5. 99.5% tracer gas in the source was used. The source gas is certified through the manufacturer.
6. The accuracy of the hot-film was determined by calibrations, before and after velocity profile measurements, using a pitot tube.
7. The pitot tube velocity measurement system was calibrated through the manufacturer.
8. Very minor data loss occurred during the concentration tests.

APPENDIX C:
FACILITIES AND TECHNIQUES

1 FLUID DYNAMICS AND DIFFUSION LABORATORY

Engineering Research Center (ERC) is located at Foothills Campus of Colorado State University in Fort Collins, Colorado. This ERC has facilities for Agricultural & Chemical Engineering, Civil Engineering, Electrical Engineering and Mechanical Engineering Department including Groundwater Laboratory, Geotechnical Laboratory, Hydraulics Laboratory, Fluid Dynamics and Diffusion Laboratory (FDDL), Thermofluid Laboratory, Laser laboratory, Aerosol Science Laboratory and Heat Transfer Laboratory.

The FDDL is an integral part of the Fluid Mechanics and Wind Engineering Program, and houses facilities with unique research capabilities. Special boundary layer wind tunnels for simulation of atmospheric motions provide a capability for unique research on wind engineering and environmental problems of state, national and international concerns. Modern instrumentation and a variety of flow facilities support fundamental investigations on turbulence and turbulent diffusion. The Fluid Mechanics and Wind Engineering Program was awarded in 1989 from National Society of Professional Engineers for its distinguished research.

Research developed during the first three decades has revolved around basic fluid dynamics - turbulence, heat and mass transfer, boundary layers, jets and wakes, vortex dynamics, and flow separation; physical modeling - winds near the surface of Earth (atmospheric boundary layers), atmospheric diffusion, and mountain and urban winds; basic studies in aerosol mechanics - particle generation techniques, sampling and collection investigations, development of ambient aerosol samplers and fractional systems, behavior of particles in turbulent shear flows, deposition of particles in plant canopies; wind engineering - air pollution control, behavior of smoke plumes from power plant stacks, hazard analysis of liquid natural gas (LNG) storage, industrial aerodynamics, environmental design for urban centers, wind power, heat transfer from buildings, and wind forces on buildings and bridges; turbomachinery - effects of turbulence on the performance of blade cascades; and instrumentation - aerosol and tracer gas concentration sensors and hot wire anemometry. Research in these areas is sponsored primarily by the National Science Foundation, the Office of Naval Research, Project SQUID, the National Aeronautics and Space Administration, the Department of Energy, the Gas Research Institute, the Department of Transportation, the Nuclear Regulatory Commission, the Environmental Protection Agency, and the Electric Power Research Institute.

Research in the Program is complemented by a wide variety of laboratory investigations of wind forces on structures, atmospheric diffusion, and other wind engineering problems associated with the design and planning of major engineering projects. These investigations, sponsored by leading consulting and industrial firms throughout the country, utilize many of the research results

obtained by the Program staff and students and help identify areas that will be productive for new research.

The following figure shows the plan view layout of the FDDL laboratory facilities including the meteorological wind tunnel, environmental wind tunnel and industrial aerodynamics wind tunnel.

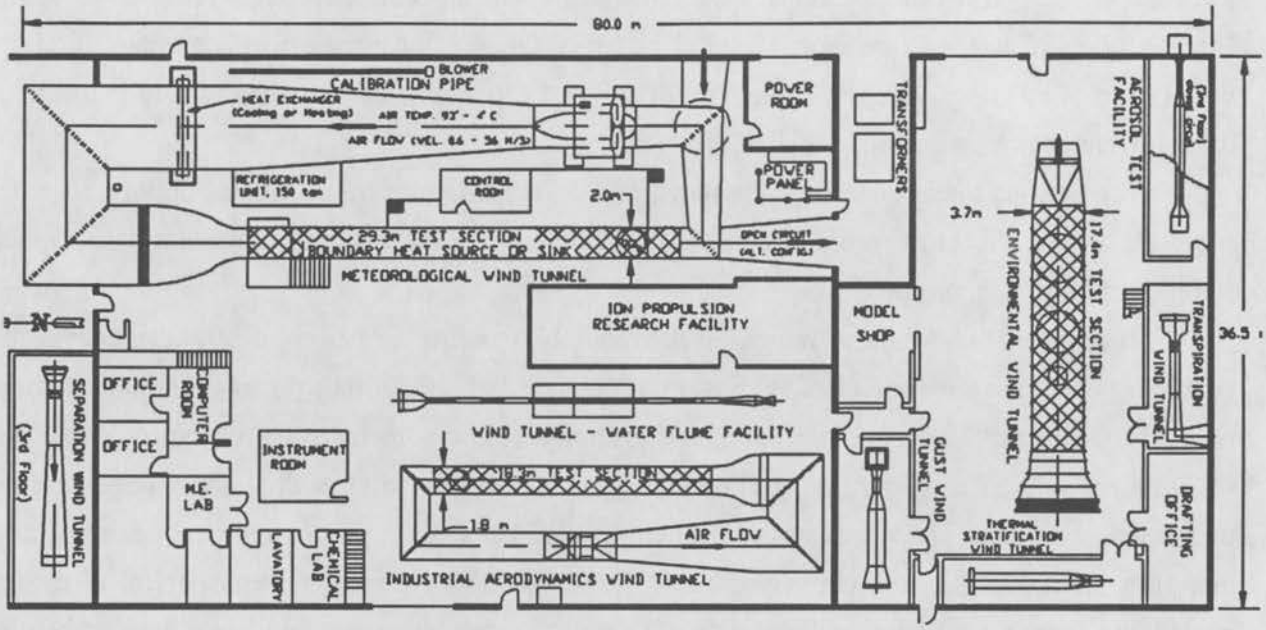

Fluid Dynamics and Diffusion Laboratory Layout

The unique meteorological wind tunnel has an overall length of 200 feet with a 6-foot by 6-foot test or working section 100 feet long. Heating and cooling of air in the 18-foot by 18-foot return flow section of the recirculating tunnel provides extreme flexibility for simulating a wide range of atmospheric thermal stratifications, as well as elevated inversions. This thermal control, coupled with well-controlled flow speeds from 0.0 to 100 miles per hour and a long test section, enables boundary layer flows similar to those found in the real atmosphere to be modeled with accuracy. Thus, this facility provides an ideal medium for fundamental studies on the relationship of mean wind speed and turbulence to surface roughness, thermal stratification and topography. On the other hand, the simulation of natural winds for specific sites provides an ideal means for physical modeling of wind effects on existing or proposed buildings, urban developments, or any other of man's activities on earth's surface.

The FDDL houses an environmental wind tunnel with working section 60 feet long and a cross section of 12 by 8 feet. Using wind speed from 0.5 miles per hour up to 34 miles per hour, this

facility provides excellent capability for investigation of wind effects on large areas. Dispersion of cloud seeding materials over mountain ranges, dispersion of automobile exhaust in new urban developments and existing cities, effects of buildings and topography on power plant plumes, and heat island effects over large urban areas have been investigated successfully in this facility.

The industrial aerodynamics wind tunnel with a working section 60 feet long and 6 feet by 6 feet in cross section provides additional capabilities for basic studies of boundary layer characteristics. Many studies of evaporation from soil and water surfaces, wind pressures on model structures, ventilation of buildings, and the movement of soil and snow by wind have been made in this wind tunnel, which has a speed range of 1 to 70 miles per hour.

A gust wind tunnel equipped with two arrays of oscillating air foils provides opportunities for research on the effects of turbulence scale on the aerodynamics of bluff bodies and aerodynamic stability of long-span bridge decks.

Instrumentation for measurement of flow variables and tracer gas concentrations is available to support either the most advanced studies on turbulence and diffusion or the applied investigations of wind engineering. This instrumentation includes hot wire anemometer system; electronic pressure transducers and meters; aerosol, radioactive gas, and helium and hydrocarbon concentration measurement systems; optical systems; and strain gage balances. Data processing equipment includes analog-to-digital converters connected to PC, AT and 386 type computer, spectral analyzers, probability density analyzers, and a variety of special purpose systems. Additional data processing and numerical analyses are accomplished on the University CDC 170 model 720 digital computer, or the CRAY 1 digital computer of the National Center for Atmospheric Research (NCAR). Recording capabilities are provided by 50 FM magnetic tape channels, 25 digital tape channels, floppy disks, and a variety of motion and still picture cameras.

2 ENVIRONMENTAL WIND TUNNEL DESCRIPTION

This wind tunnel, especially designed to study atmospheric flow phenomena, incorporates special features such as an adjustable ceiling, a rotating turntable and a long test section to permit adequate reproduction of micrometeorological behavior. Mean wind speeds of 0.1 to 15 m/sec in the EWT can be obtained. A boundary-layer thickness up to 1.5 m can be developed over the downwind portion of the EWT test section by using vortex generators at the test section entrance and surface roughness on the floor. The flexible test section on the EWT roof is adjustable in height to permit the longitudinal pressure gradient to be set at zero.

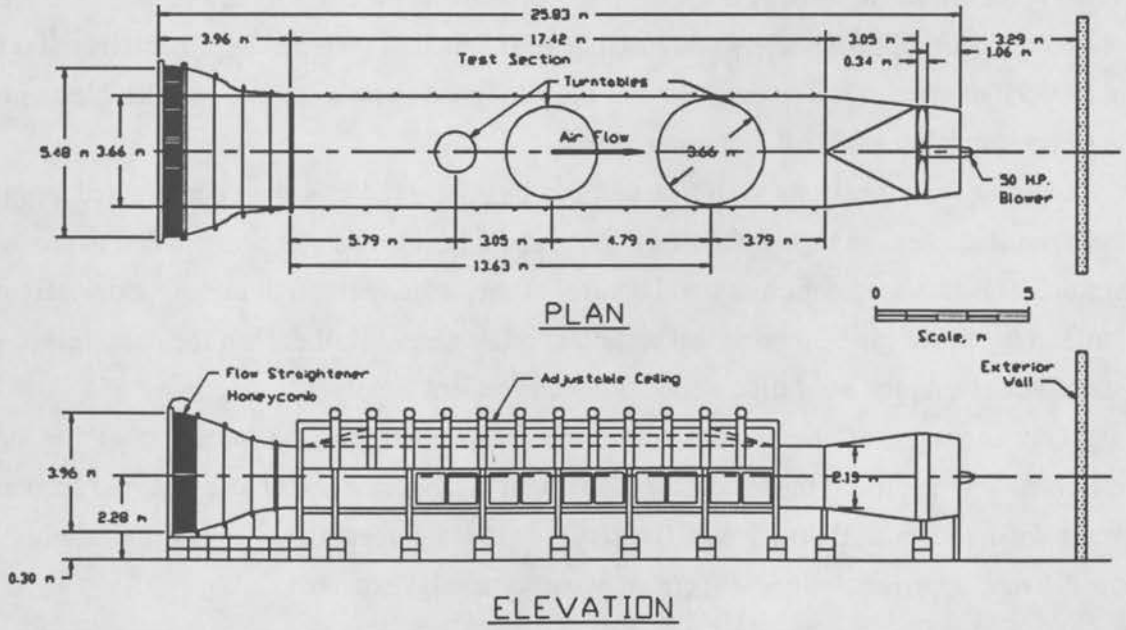

Environmental Wind Tunnel Schematic

3 WIND SPEED MEASUREMENT DESCRIPTION

3.1 Velocity Standards

3.1.1 *CSU Mass Flow System*

The velocity standard used in the present study consisted of a Omega Model FMA-78P4 mass controller and a profile conditioning section designed and calibrated by the Fluid Dynamics and Diffusion (FDDL) staff at Colorado State University (CSU). The mass flow controller sets mass flow rate independent of temperature and pressure. The profile conditioning section forms a flat velocity profile of very low turbulence at the position where the hot-film-probe is located. Incorporating a measurement of the ambient atmospheric pressure, temperature and a profile correction factor permits the calibration of velocity at the measurement station from 0.1 - 2.0 m/s to within ± 5 percent and from 2.0 - 4.7 m/s to within ± 3 percent. This calibration nozzle is mounted on two computer controlled rotary tables for precise flow angle calibrations of multi-film probes.

3.1.2 *TSI Calibrator*

The TSI Model 1125 Velocity Calibrator System is designed to calibrate hot wire and hot film sensors over wide ranges of velocities. It is primarily for air but can also be modified for use in water and other fluids. In air the velocity range is from approximately 0.1 m/s to 305 m/s. This wide range can be covered using manometers with a range of 0.5 inch of water to approximately 400 inch of water (30 inch of mercury). The calibrator has been designed to be as simple and flexible as possible, while still maintaining good calibration accuracy.

In using the calibrator for air, the unit can be connected to a shop compressed air line. An On-Off line valve, pressure regulator, needle valve, and a heat exchanger are installed in line with the calibrator. This arrangement gives good control of the velocity through the calibrator. Essentially the same arrangement can be used for calibrating in other gases. Rather than the compressed air line the source can be a tank of bottled gas or other convenient supply.

The accuracy of the system is primarily dependent on the accuracy of the pressure measurement. When using the inside chambers with the exterior nozzle in place, the accuracy is ± 2 percent down to 3 m/s. Below 3 m/s, the accuracy is ± 5 percent down to approximately 0.1 m/s. Below 0.1 m/s, approximately ± 10 percent accuracy can be expected.

3.1.3 *Pitot Probe*

Pitot-static probes are used as a velocity standard during the calibration of the different hot film systems and to provide the reference upwind velocity measurement. The principles of operation

of pitot-static probes are described in any fundamental text on fluid mechanics and will not be discussed in detail here. The operational relationship for these probes is $U = (2g_c\Delta P/\rho)^{1/2}$, where U = velocity, g_c = gravitational conversion constant, ΔP = difference between static and stagnation pressures, and ρ is the air density. ρ is calculated from ideal gas law and ΔP is measured using a Datametrics Electronic Manometer. The pitot-static probe measurements are accurate to within ± 2 percent of the actual velocity.

3.2 Single-Hot-Film Probe Measurements

Single-hot-film (TSI 1220 Sensor) measurements are used to document the longitudinal turbulence levels. During calibration the probe voltages are recorded at several velocities covering the range of interest. These voltage-velocity (E,U) pairs are then regressed to the equation $E^2 = A + BU^c$ via a least squares approach for various assumed values of the exponent c. Convergence to the minimum residual error was accelerated by using the secant method to find the best new estimate for the exponent c.

The hot-film-probe is mounted on a vertical traverse and positioned over the measurement location in the wind tunnel. The anemometer's output voltage is digitized and stored within an IBM AT computer. This voltage time series was converted to a velocity time series using the inverse of the calibration equation; $U = [(E^2 - A)/B]^{1/c}$. The velocity time series is then analyzed for pertinent statistical quantities, such as mean velocity and root-mean-square turbulent velocity fluctuations. The computer system moves the velocity probe to a vertical position, acquire the data, then moves on to the next vertical positions, thus obtaining an entire vertical velocity profile automatically.

Error Statement

The calibration curve yields hot film anemometer velocities that were always within 2 percent of the known calibrator velocity. Considering the accumulative effect of calibrator, calibration curve fit and other errors the model velocity time series should be accurate to within 5 percent.

3.3 Cross-Film Probe Measurements

Cross-film measurements are used to document longitudinal, lateral and vertical turbulence levels along with cross-component correlations such as Reynolds stresses.

During the calibration of the TSI 1241 X-film probe it is placed at the nozzle of the calibrator with the probe support axis parallel to air flow. In this position the angle between each sensor and the flow vector is 45°. Thus, the yaw angles for each sensor are 45°. The voltage from each anemometer channel are digitized for several velocities covering the range of interest. These voltage-velocity pairs (E_i, U_i; i = 1,2), at a fixed angle, are fit to the equation

$$E_{i,j}^2 = A_i + B_i'(U_j)^{ci} \; ; \; i = 1,2; \; j = 1,n$$

where $B_i' = B_i(\cos^2\phi_i + k^2\sin^2\phi_i)^{ci/2}$

ϕ_i = yaw angle between velocity vector and film i

k = yaw factor

n = number of the calibration points

via a least squares fit with the secant method to find the best new estimate of exponent, c_i.

Note that if the yaw factor, k, equals zero then a sample cosine law dependence of the heat flux exists. To determine the yaw factor, k, the air velocity is set at a constant value, and the probe is rotated about its third axis so that voltage samples are taken for a wide range of yaw angle variation on both films. These voltage-yaw angle pairs, (E_i, ϕ_i; i = 1,2) are regressed to the equation

$$B_i' = (E_{i,j}^2 - A_i)/U^{ci} = B_i(\cos^2\phi_{i,j} + k_i^2\sin^2\phi_{i,j})^{ci/2}$$

where i = 1,2 and j = 1,n

via a least squares approach with the secant method to find the best new estimate for the yaw factor, k_i. A_i, B_i, c_i and k_i for both films are thus obtained. For the reduction algorithm used, k must be equal for both films and not a function of velocity. Providing that both films have similar aspect ratio, then both k_i values should be of similar magnitude; hence, setting them equal does not introduce large errors. Once a value for k is specified then a least squares fit will determine the optimal values for B_i. Once the value of k is determined for a specific probe, it is no longer necessary to perform further angle calibrations.

Given the calibration constants A_i, B_i, and c_i, then the equations

$$E_i^2 = A_i + B_i(V_{eff,i})^{ci} \; ; \; i = 1,2;$$

where $V_{eff,i} = V(\cos^2\phi_i + k^2\sin^2\phi_i)^{1/2} \; ; \; i = 1,2;$

$V_{eff,i}$ = effective cooling velocity for film i, and

V = total velocity vector approaching sensor array

are defined. To take measurements with this calibrated X-film probe, both anemometer signals and the temperature signal are digitized and stored on a disk file within an IBM AT computer. These voltage time series are converted to u and v (or w) velocity time series using the following algorithm proposed by Brunn [1978],

$$u = (V_{eff,1} + V_{eff,2})/[2(\cos^2\alpha + k^2\sin^2\alpha)^{1/2}],$$

$$v \text{ (or } w) = (V_{eff,1} - V_{eff,2})/[(\cos^2\alpha + k^2\sin^2\alpha)^{1/2} A \tan\alpha],$$

where $A = \cos^2\alpha(1-k^2)/[\cos^2\alpha(1 - k^2) + k^2]$,

$\alpha = 45°$,

$V_{eff,i} = [E_i^2 - A_i^*)/B_i^*]^{1/ci}$,

$A_i^* = A_i T_{factor}$, $B_i^* = B_i T_{factor}$,

$T_{factor} = (T_{sensor} - T_{environment})/(T_{sensor} - T_{calibration})$.

Error Statement

The accuracy of X-film velocity measurements and associated reduction algorithms can be estimated by directing different known mean velocity vectors at the probe. Tests at calibration temperature determine that the mean velocity magnitude is generally within ±5 percent of the calibration value. The error in angle calculation was approximately ±2° for angular deviations of 15° or less and somewhat larger than this for greater deviations. Considering cumulative effect of calibrator, calibration curve fit and temperature correction errors, the model longitudinal velocity time series should be accurate to within ±10 percent. The lateral or vertical velocity time series errors are greater than those of the longitudinal component but should be accurate to within ±15 percent.

3.4 Velocity Measurement System

A flow-logic chart of velocity calibration system, velocity measurement system, and the positioning system with the wind tunnel is displayed in the following figure.

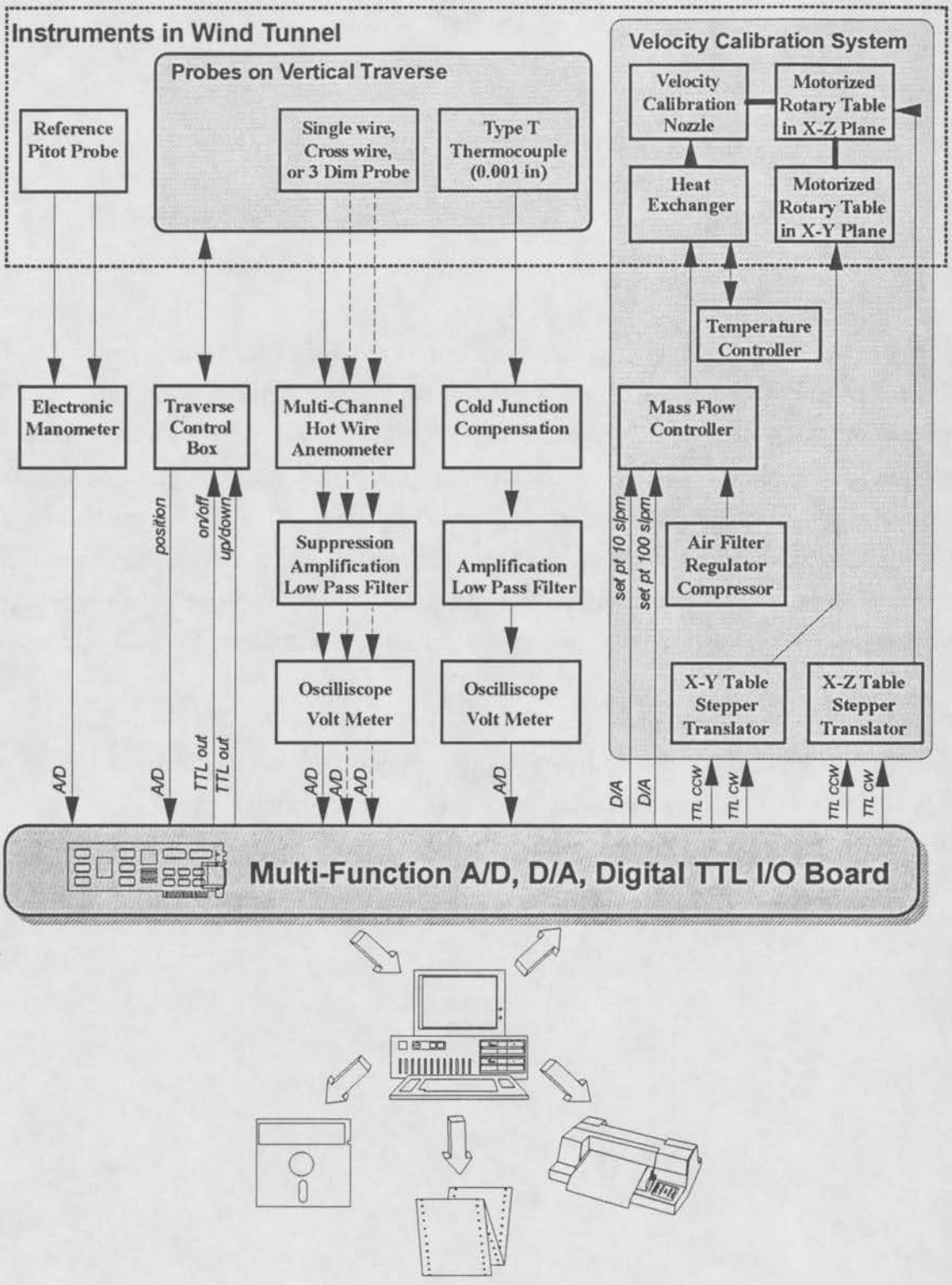
Instruments in Wind Tunnel
Probes on Vertical Traverse
Reference Pitot Probe
Single wire, Cross wire, or 3 Dim Probe
Type T Thermocouple (0.001 in)
Velocity Calibration System
Velocity Calibration Nozzle
Motorized Rotary Table in X-Z Plane
Heat Exchanger
Motorized Rotary Table in X-Y Plane
Temperature Controller
Electronic Manometer
Traverse Control Box
Multi-Channel Hot Wire Anemometer
Cold Junction Compensation
Mass Flow Controller
position
on/off
up/down
Suppression Amplification Low Pass Filter
Amplification Low Pass Filter
set pt 10 slpm
set pt 100 slpm
Air Filter Regulator Compressor
Oscilliscope Volt Meter
Oscilliscope Volt Meter
X-Y Table Stepper Translator
X-Z Table Stepper Translator
A/D
TTL out
D/A
TTL CCW
TTL CW
Multi-Function A/D, D/A, Digital TTL I/O Board

4 FLOW VISUALIZATION TECHNIQUES

4.1 Smoke Generator System

A visible plume is produced by passing the metered simulant gas through a Rosco Model 8215 Fog/Smoke Machine located outside the wind tunnel and then out of the model stack. The plume is illuminated with high intensity back lighting. The visible plumes for each test are recorded on VHS video cassettes with a Panasonic Omnivision II camera/recorder system. Run number titles are placed on the video cassette with a title generator.

4.2 Video Image Analysis System

Digital image processing and computer aided enhancement methods provide a means to modernize and significantly improve the conventional smoke wire technique. The visible behavior of the smoke line is now recorded on by a high-resolution television camera system on VCR tape. The analog images may be transformed into digital arrays, and the images can then be enhanced and manipulated by a computer system.

The hardware components of the FDDL Video Image Processing System (VIPS) are presented in the figure on the following page. The image capturing part of the system includes a SVHS camcorder and a four-head one-half inch tape VCR recorder. These images may be edited into convenient sequences using a dual-monitor, dual-SVHS VCR recorder editing system. Unfortunately, most VCR systems can not be controlled well enough to maintain adequate picture registration when advancing frame-by-frame under computer control. Hence, the edited VCR tape must be additionally recorded onto a video disk. Currently this transfer is being accomplished at another laboratory.

Computer control may be used to command a video-disk player to project each individual video frame to a high-resolution video monitor. We use a high-resolution image capturing board installed in a PC-386 compatible microcomputer to digitize the image. A standard NTSC video signal (30 frames/sec) can be digitized with 8-bit precision. The board we use produces an intensity field of 512 x 512 pixels at 256 possible grey levels. Given the image interweaving typical of an NTSC signal the frames can be split to provide images at 60 frames/sec.

Once the video picture is digitized, the image may be enhanced by a) subtracting the background, b) overlaying a coordinate system, c) enhancing front, center, or back edge of the image, or d) assigning colors to different intensity levels. One can also extract edge pixel locations to calculate velocities or combine images to provide animation.

Often it is appropriate to print or restore enhanced images. The FDDL VIPS includes hardware to project the image to a RGB or VGA monitor; store the digital image to floppy or hard

disks, streaming tapes, optical digital disk, or on network file-servers; or print to a laser printer or color slide maker. Alternatively, a VGA-to-NTSC hardware card can reformulate the signal to record to a conventional VCR or a color video printer.

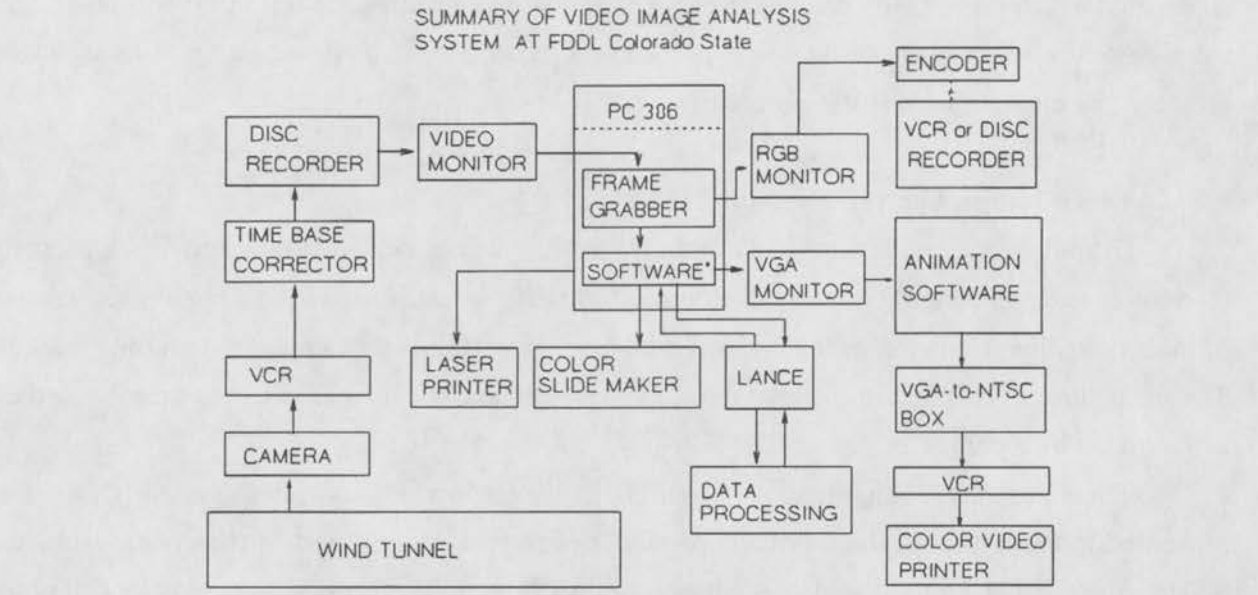

Video Image Analysis System

5 CONCENTRATION MEASUREMENT DESCRIPTION

The experimental measurements of concentration were performed using a Hewlett Packard gas-chromatograph and a sampling systems designed by Fluid Dynamics and Diffusion Laboratory staff.

5.1 Gas Chromatograph

A gas chromatograph (Hewlett-Packard Model 5710A) (GC) with flame ionization detector (FID) operates on the principle that the electrical conductivity of a gas is directly proportional to the concentration of charged particles within the gas. The ions in this case are formed by the burning a mixture of hydrogen and the sample gas in the FID. The ions and electrons formed pass between an electrode gap and decrease the gap resistance. The resulting voltage drop is amplified by an electrometer and passed to a Hewlett-Packard Model 3390A integrator. When no effluent gas is flowing, a carrier gas (nitrogen) flows through the FID. Due to certain impurities in the carrier, some ions and electrons are formed creating a background voltage or zero shift. When the effluent gas enters the FID, the voltage increase above this zero shift is proportional to the degree of ionization or correspondingly the amount of tracer gas present. Since the chromatograph used in this study features a temperature control on the flame and electrometer, there is very low drift of the zero shift. Even given any zero drift, the HP 3390A, which integrates the effluent peak, also subtracts out the zero drift.

The lower limit of measurement is imposed by the instrument sensitivity and the background concentration of tracer within the air in the wind tunnel. Background concentrations are measured and subtracted from all data.

5.2 Sampling System

The tracer gas sampling system consists of a series of fifty 30 cc syringes mounted between two circular aluminum plates. A variable-speed motor raises a third plate, which lifts the plunger on all 50 syringes, simultaneously. Computer controlled valves and tubing are connected such that airflow from each tunnel sampling point passes over the top of each designated syringe. When the syringe plunger is raised, a sample from the tunnel is drawn into the syringe container. The sampling procedure consists of flushing (taking and expending a sample) the syringe three times after which the test sample is taken. The draw rate is variable and generally set to be approximately 6 cc/min.

The sampling system is periodically calibrated to insure proper function of each of the valves and tubing assemblies. To calibrate the sampler each intake is connected to a manifold. The manifold, in turn, is connected to a gas cylinder having a known concentration of tracer gas. The gas

is turned on, and a valve on the manifold is opened to release the pressure produced in the manifold. The manifold is allowed to flush for about one minute. Normal sampling procedures are carried out during calibration to insure exactly the same procedure is reproduced as when taking a sample from the tunnel. Each sample is then analyzed for tracer gas concentration. Percent error is calculated, and "bad" syringe/tube systems (error > 2 percent) are not used or repaired.

Test Procedure

The test procedure consisted of:

1) Setting the proper tunnel wind speed,
2) Releasing the metered mixtures of source gas from the plant stack,
3) Withdrawing samples of air from the tunnel designated locations, and
4) Analyzing the samples with a FID.

The samples were drawn into each syringe over an ~200 second (adjustable) time period and then consecutively injected into the GC.

The procedure for analyzing the samples from the tunnel is:

1) Introduce the sample into the GC which separates the ethane tracer gas from other hydrocarbons,
2) The voltage output from the chromatograph FID electrometer is sent to the HP 3390A Integrator,
3) the HP 3390A communicates the measured concentration in ppm to an IBM computer for storage, and
4) These values, χ_{mea}, along with the response levels for the background χ_{bg} and source χ_{source} are converted into source normalized model concentration by the equation:

$$\chi_m = (\chi_{mea}-\chi_{bg})/(\chi_{source}-\chi_{bg})$$

5) Field equivalent concentration values are related to model values by the equation:

$$\chi_p = \frac{\chi_m}{\chi_m + (1-\chi_m)[V(T_a/T_s)]_m/[V(T_a/T_s)]_p}$$

where $V = Q/U_H L^2$,

and L is the characteristic length scale. When there is no distortion in the model-field volume flux ratio, V, and the plumes are isothermal this equation reduces to $\chi_p = \chi_m$.

Error Statement

Background concentrations, χ_{bg}, (the result of previous tests within the laboratory), are measured to an accuracy of 20 percent. The larger measured concentrations, χ_{mea}, are accurate to 2 percent. The source gas concentration, χ_{source}, is known to within 10 percent. Thus the source normalized concentration for $\chi_{mea} >> \chi_{bg}$ is accurate to approximately 3 percent. For low concentration values, $\chi_{mea} > \chi_{bg}$, the errors are larger.

5.3 Concentration Measurement System

A flow-logic chart of the source gas release, gas sampling, and concentration measurement systems is displayed in the following figure.

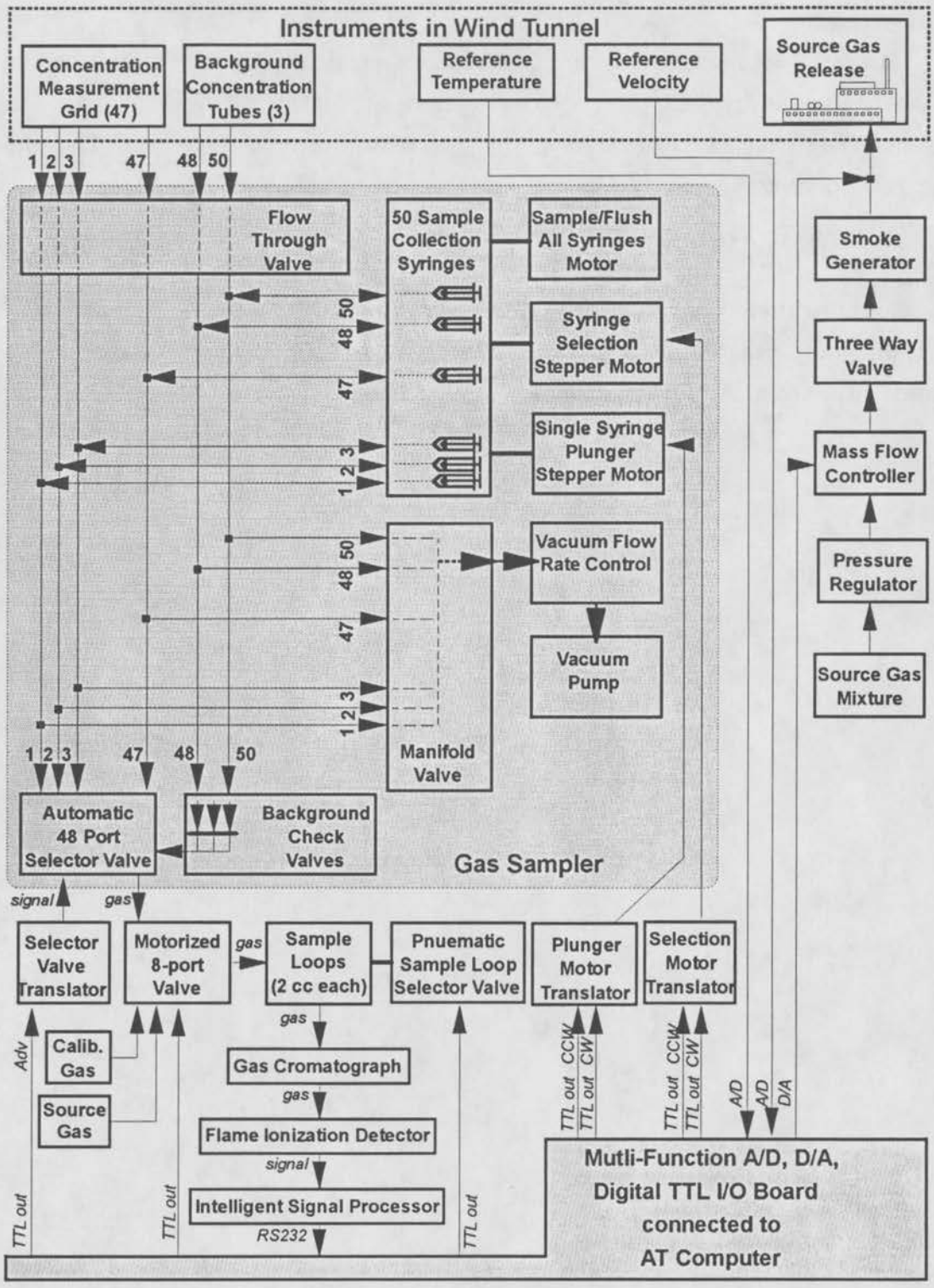

Concentration Sampling and Measurement System Schematic

APPENDIX D:
MODELING TECHNICAL DISCUSSION

1 MODELING OF PLUME DISPERSION

To obtain a predictive model for a specific plume dispersion problem, one must quantify the pertinent physical variables and parameters into a logical expression that determines their inter-relationships. This task is achieved implicitly for processes occurring in the atmospheric boundary layer by the formulation of the equations of conservation of mass, momentum and energy. These equations with site and source conditions and associated constitutive relations are highly descriptive of the actual physical interrelationship of the various independent variables (space and time) and dependent variables (velocity, temperature, pressure, density, concentration, etc.).

These generalized conservation statements subject to the typical boundary conditions of atmospheric flow are too complex to be solved by present analytical or numerical techniques. It is also unlikely that one could create a physical model for which exact similarity exists for all the dependent variables over all the scales of motion present in the atmosphere. Thus, one must resort to various degrees of approximation to obtain a predictive model. At present, purely analytical or numerical solutions of boundary layer, wake, and plume dispersion are unavailable because of the classical problem of turbulent closure (Hinze, 1975). However, boundary layer wind tunnels are capable of physically modeling plume processes in the atmosphere under certain restrictions. These restrictions are discussed in the next sections.

2 FLUID MODELING OF THE ATMOSPHERIC BOUNDARY LAYER

The atmospheric boundary layer is that portion of the atmosphere extending from ground level to a height of approximately 1000 meters within which the major exchanges of mass, momentum, and heat occur. This region of the atmosphere is described mathematically by statements of conservation of mass, momentum and energy (Cermak, 1975). The mathematical requirements for rigid laboratory/atmospheric-flow similarity may be obtained by fractional analysis of these governing equations (Kline, 1965). This methodology scales the pertinent dependent and independent variables by size and then casts the equations into dimensionless form by dividing by one of the coefficients (the inertial terms in this case). Performing these operations on such dimensional equations yields dimensionless parameters commonly known as:

Reynolds number $\quad Re = (UL/\nu)_r \quad = \quad \dfrac{\text{Inertial Force}}{\text{Viscous Force}}$

Bulk Richardson # $\quad Ri = [(Lg\Delta T/T)/U^2]_r \quad = \quad \dfrac{\text{Gravitational Force}}{\text{Inertial Force}}$

Rossby number	$Ro = (U/L\Omega)_r$	=	$\frac{\text{Inertial Force}}{\text{Coriolis Force}}$
Prandtl number	$Pr = [\nu/(k/\rho C_p)]_r$	=	$\frac{\text{Viscous Diffusivity}}{\text{Thermal Diffusivity}}$
Eckert number	$Ec = [U^2/C_p \triangle T]_r$		

2.1 Exact Similarity

For exact similarity between flows which are described by the same set of equations, each of these dimensionless parameters must be equal for both flow systems. There must also be similarity between the surface-boundary conditions and the approach flow wind field. Surface-boundary condition similarity requires equivalence of the following features:

a. Surface-roughness distributions,
b. Topographic relief, and
c. Surface-temperature distribution.

If all the foregoing requirements are met simultaneously, all atmospheric scales of motion ranging from micro- to mesoscale could be simulated within the same flow field. However, all of the requirements cannot be satisfied simultaneously by existing laboratory facilities; thus, a partial or approximate simulation must be used. This limitation requires that atmospheric simulation for plume dispersion must be designed to simulate most accurately those scales of motion which are of greatest significance for the transport and dispersion of plumes.

2.2 Partial Simulation of the Atmospheric Boundary Layer

For many fluid modeling situations several of the aforementioned parameters are unnecessarily restrictive and may be relaxed without causing a significant loss in similarity between model and field fluid flow. The Rossby number magnitude controls the extent to which the mean wind direction changes with height. The effect of Coriolis-force-driven lateral wind shear on wind flow is only significant when heights are of the same order of magnitude as the boundary layer height. The Eckert number (in air $Ec = 0.4\ Ma^2\ (T_r/\triangle T_r)$, where Ma is the Mach number) is the ratio of energy dissipation to the convection of thermal energy. Both in the atmosphere and the laboratory flow, the wind velocities and temperature differences are such that the Eckert number is very small; hence, it is neglected. Prandtl number equality guarantees equivalent rates of momentum and heat transport.

Since air is the working fluid in both the atmosphere and the laboratory, Prandtl number equality is always maintained.

The approach flow Richardson number (Ri) and Reynolds number (Re) determine the kinematic and dynamic structure of turbulent flow within a boundary layer. This influence is apparent in the variations that occur in the spectral distribution of turbulent kinetic energies with changing Ri and changing Re.

The Reynolds Number

Reynolds number (Re) equality implies $U_m = (L_p/L_m)U_p$. Re equality at a significantly reduced length scale would cause the model's flow velocity to be above sonic; hence, its equality must be distorted. A reduced Re changes only the higher frequency portion of an Eulerian-type description of the spectral energy distribution. Unfortunately, there is no precise definition as to which portion of an Eulerian Spectrum is dominant in dispersing ground-level or elevated plumes over moderate travel distances.

Most investigators use a minimum Reynolds number requirement based on rough-walled pipe measurements; i.e., $Re = u_* z_o/\nu > 2.5$, where u_*, the friction velocity, and z_o, the roughness length, are derived from a log-linear fit to a measured mean velocity profile. The value 2.5 is an empirically determined constant. At Re below 2.5, it is observed that the mean velocity profiles in turbulent pipe flow lose similarity in shape and deviate from the universal curve of a rough wall turbulent boundary layer. For Re above 2.5, it is observed that the surface drag coefficient (and thus the normalized mean velocity profile) is invariant with respect to increasing Re. For Re between 0.11 and 2.5, the velocity profiles are characteristic of smooth wall turbulent boundary layers. For values below 0.11, the growth of a laminar sublayer on the wall is observed to increase with decreasing Re.

Extrapolation of results from pipe flow measurement to flat plate boundary layers may cause a shift in the magnitude of the minimum Re requirement, but it is generally felt that this shift is small. Precise similarity in the universal form of mean wind shear may be necessary for invariance with respect to the surface drag coefficient, but this does not necessitate that precise similarity must exist for the invariance of the wind field and dispersion. It is the distribution of turbulent velocities which has the greatest effect on the wind field and dispersion. It is the mean wind shear, however, which generates the turbulent velocities. It is possible that the specification of a minimum Re of 2.5 is overly conservative. The criteria, $Re > 2.5$, for example, is not applicable for flow over complex terrain or building clusters.

The Richardson Number

Although most wind-tunnel investigations are conducted with neutrally stratified boundary layers, there are circumstances when the stratification of the atmosphere must be considered. In particular, air pollution and dispersion problems are often critical during stratified conditions. Unstable stratification may be expected to mitigate hazards by accelerating plume dilution, whereas stable stratification may permit high concentrations to persist. The stability state of the atmosphere is typically characterized by the Richardson number.

The atmospheric gradient Richardson number can be computed from averaged quantities through the equation

$$Ri = g/T\ (\Gamma_d - \Gamma)\ [1 + 0.07/B]\ [(\partial u/\partial z)^2 + (\partial v/\partial z)^2]$$

where Γ and Γ_d are the actual and dry adiabatic potential temperature lapse rates, and $B = [C_p(T_2-T_1)]/[(Z_2-Z_1)(Q_2-Q_1)]$ is the Bowen ratio of sensible to latent heat flux at the surface. The Ri number can be taken to represent the ratio of the relative importance of convective and mechanical turbulence. Negative Ri numbers of large value indicate strong convection and weak mechanical turbulence; zero Ri numbers imply purely mechanical turbulence. Positive Ri numbers less than some critical value, $Ri_{critical}$, suggest the presence of mechanical turbulence damped by the density-induced buoyancy forces; for larger positive Ri numbers, turbulence essentially disappears, since the stratification overpowers production by wind shear. The critical Richardson number has a value near 0.25.

2.3 Performance of Prior Fluid Modeling Experiments

Meroney et al. (1978) summarized experimental data available from field and laboratory studies for neutral airflow over hills, ridges, and escarpments. Wind-tunnel model measurements were performed to study the influence of topography profile, surface roughness and stratification on the suitability of various combinations of these variables. Detailed tables of velocity, turbulence intensity, pressure, spectra, etc., were prepared to guide numerical model design and experimental rule of thumb restrictions. Cases included hill slopes from 1:2 to 1:20, neutral and stratified flows, two- and three-dimensional symmetric ridges, six alternate hill and escarpment shapes, and a variety of windward versus leeward slope combinations to evaluate ridge separation characteristics. The laboratory data were validated by comparison with field measurements for flow in the Rakaia Gorge, New Zealand, and over Kahuku Point, Oahu, Hawaii, (Meroney et al., 1978; Chien, Meroney and Sandborn, 1979).

Local heating and cooling of coastline or hill surfaces are the driving mechanisms for sea-land breezes, and anabatic and katabatic winds which may inhibit or enhance airflow over the land surface.

Early laboratory work includes simulations of urban heat islands by Yamada and Meroney (1971) and Sethuraman and Cermak (1973), simulation of flow and dispersion at shoreline sites by Meroney et al. (1975a), and simulation of dispersion effects of heat rejected from large industrial complexes by Meroney et al. (1975b).

Meroney (1980) compared three model/field investigations of flow over complex terrain, suggested performance envelopes for realizable modeling in complex terrain, and discussed recent laboratory studies which provide data for valley drainage flow situations. Not all of the model/field comparison experiments performed in the past were successful. Many early studies had model approach flow velocity exponents near zero, were modeled as neutral flows when the field observed strong stratification effects, or simulated unrealistic boundary layer depths, integral scales, or turbulence intensities which did not match their atmospheric counterpart. But few studies claimed unreasonable correlation, and some were strongly self-critical. Nonetheless, most studies accomplished their prestated limited objectives. It would appear that the simulation hypothesis developed in the last few years is appropriate for physical modeling of flow over complex terrain when appropriate care is taken to simulate the approach flow conditions and to maintain simulation parameters equal between model and prototype.

Arya and Plate (1969), Arya (1975) performed velocity, temperature, and turbulence measurements in the lowest 15 percent of a 70 cm deep boundary layer over a smooth surface, where conditions ranged from unstable to moderately stable ($-0.3 < z/L_{mo} < 0.3$). Free stream flow speeds varied from 3 to 9 m/s, and temperature differences were about 40°C across the boundary layer. Cermak, Shrivastava and Poreh (1983) reported mean velocity and turbulence measurements made for a variety of simulated atmospheric boundary layers over different surface roughness. Free stream flow speeds varied from 2.4 to 3.0 m/s and temperature differences were from 150°C to -80°C across the boundary layer. Poreh and Cermak (1984) reproduced unstable lapse conditions including mixed layers and elevated inversions. They reproduced the characteristics of convective boundary layer turbulence measured in the atmosphere.

Diffusion studies made by Chaudhry and Meroney (1973) in stable boundary layers investigated previously by Arya (1969) have shown agreement of experimental results with Lagrangian similarity theory. Horst (1979) tested Lagrangian similarity predictions of crosswind-integrated ground concentration against the Prairie Grass diffusion experiment (Barad, 1958) and an experiment at Idaho Falls (Islitzer and Dumbauld, 1963). He reported good agreement for all stabilities at distances x/z_o out to $2*10^5$. Poreh and Cermak (1984, 1985) released plumes in their modeled mixing layer. Their plumes exhibited the plume lofting typical of ground sources and the descent typical of elevated sources, predicted from water tank experiments by Willis and Deardorff (1974, 1976, 1978) and numerically by Lamb (1982).

Staff at the Fluid Mechanics Laboratory at the Ecole Centrale de Lyon have studied unstable wind-tunnel boundary layers and compared them with the atmospheric boundary layer (Schon and Mery, 1971). Flow speeds were typically 2 to 4 m/s and the floor temperature was maintained 50°C above ambient. Comparisons with the Kansas data (Haugen et al., 1971) were quite satisfactory, but longitudinal turbulence intensities exhibited a slight Reynolds number dependence, and spectral energy was too low in the high frequency portions of the spectra. The most unstable flow they studied had a Monin-Obukhov scale length of about -1 m at model scales, or -500 to -1000 when scaled to the atmosphere.

3 PHYSICAL MODELING OF BLUFF BODY AERODYNAMICS

The interaction of an approach wind field with bluff bodies or structures constructed on the earth's surface is broadly termed "Building Aerodynamics." In a review article on this subject, Meroney (1982) discusses the character of bluff body flow about rectangular buildings and cylindrical cooling towers. Defects in velocity profiles can easily persist from 10 to 15 building heights downwind. Field and laboratory measurements of plume dispersion about the Rancho Seco Nuclear Power Station in Sacramento, California, confirm that cooling tower wake effects persist for significant downwind distances under a variety of stratification conditions (Allwine, Meroney and Peterka, 1978; Kothari, Meroney and Bouwmeester, 1981).

3.1 Simulation Criteria

Often atmospheric turbulence may cause only weak effects compared to the turbulence generated by buildings, obstacles, and terrain. Yet the magnitude of the perturbations depends upon the incident flow turbulence scale and intensity, details of the obstacle shape and surface roughness, and size of the obstacle compared to the boundary layer depth. Geometrical scaling implies that the ratio of the building height to length scale must be matched and, of course, that all other building length scales be reduced to this same ratio.

Several questions should be considered when modeling flows which include surface obstacles:

a. What size obstacles should be disregarded?
b. What detail or roughness on an obstacle need be included?
c. To what upwind distance should all obstacles be included?
d. At what point does the size of a modeled obstacle become too big for the wind tunnel (i.e., blockage effects)?
e. What is the effect on the flow field of mismatching obstacle and approach flow length scales?

f. What is the minimum allowable model obstruction Reynolds number?

Obstacle sizes to be disregarded:

Boundary layer studies of rough surfaces reveal that if protuberances are of a size k, such that $u_*k/\nu < 5$, they will have little effect on the flow in a turbulent boundary layer. Thus, assuming a laboratory wind speed of 1 m/s and a typical friction coefficient,

$$C_f/2 = (u_*/u)^2 = 0.0025,$$

obstacles of size less than 2 mm would go unnoticed.

Required obstacle surface detail or roughness:

Another question that always arises is "How much detail is required for the building or obstacle model? The answer is, of course, dependent upon the size of the protuberance compared to the plume and the dominant eddies of mixing. If the obstruction is large enough to modify the separated wake over the main obstacle, then it must be included. Often an equivalent obstacle surface roughness suffices. Snyder (1981) concludes a generic surface roughness criterion might be $u_*k/\nu > 20$. For a 1 m/s laboratory flow this results in model roughness elements equal to about 6 mm. But since the exterior flow is usually highly turbulent, the body typically includes a highly unsteady wake, and the u_* value to be used should be that acting on the building surface, rather than that of the approach flow. Hence, even this roughness may be unnecessarily large.

Upstream fetch to be modeled:

Suppose there is another building, tree line, fence, cooling tower, or obstacle some distance, s, upstream of a meteorological measurement location; is it necessary to include this obstacle in the wind-tunnel model? Hunt (1974) showed that the velocity deficit in the wakes of cubes and cylinders is given approximately by:

$$DU_{mx}/U(h) = A\ (s/h)\text{-}3/2$$

downwind of the separation bubble, where DU_{mx} is the maximum mean velocity deficit created by the obstacle, h is the height of the obstacle, S is the distance downstream of the obstacle, and A is a constant dependent upon the obstacle shape, orientation, boundary layer thickness, etc. Typically, A = 2.5, but it may range from 1.5 to 5.0. If we desire that the velocity at the spill site be within 3 percent of its undisturbed value, Snyder (1981) recommends that any upstream obstacle as high as s/20 be included upstream in the model of the spill site. If the obstacle's width is much greater than its height (for example, a fence or ridge), one should include it in the physical model if its height is greater than s/100.

Blockage effects:

Because of the influence of wind-tunnel walls on the behavior of the flow past models, it is desirable to use small models or big tunnels, or both. On the other hand, larger models are not only easier to work with, but they may be needed for similarity reasons to achieve large enough Reynolds numbers. It is possible to identify three different types of effects of wind-tunnel constraints. The first is the simple "solid blockage" effect which arises because the fluid stream is unable to expand laterally as it normally would in unconfined flow. The second effect, called "wake blockage", results because the accelerated flow between an obstacle and the tunnel walls continues to "pinch" the wake flow region and reduce its normal lateral rate of growth. The third effect is produced by the growth of boundary layers on the tunnel walls which produce "wall boundary interference." Tunnel blockage can cause separation and reattachment locations to vary, produce higher velocities, larger wake turbulence, and modify the dispersion patterns in the vicinity of obstructions.

The ratio of the cross-sectional area of a model obstacle to that of the tunnel is called the "blockage ratio", BR. Mass continuity produces an average velocity speed-up of $S = BR/(1-BR)$. Although wind tunnels with adjustable ceilings can compensate to some extent by raising the roof locally; this is not a perfect solution to the problem. Measurements on building and cooling tower models placed in different size wind-tunnel test sections reveal major changes in the character of pressure distributions, separation, and wake growth in the presence of flow restricted by wind-tunnel side walls (Farell et al., 1977).

Blockage corrections, which are conventionally applied in aeronautical tunnels, cannot usually be applied to the typical asymmetric model configuration placed against the wall of a meteorological wind tunnel (Ranga Raju and Singh, 1976). Conventional wisdom now suggests the "rule of thumb" that blockage ratios greater than five percent should be avoided.

Simulation of the flow over sharp-edged obstacles:

A number of authors have discussed flow studies about simple cubical or rectangular sharp-edged obstacles. An extensive review about such flow fields and the subsequent character of diffusion near obstacles has been provided by Hosker (1984). Peterka, Meroney and Kothari (1985) describe typical flow deviations which result from the presence of a sharp-edged building.

Consider the main features of the flow around a sharp-edged building. Typically, when the approach flow is normal to the building face, the flow separates from the ground upwind of the building and produces a "horseshoe"-shaped vortex which wraps around the base of the building. The surface streamline reattaches on the front of the building, and fluid parcels move up and down the building's forward face. An elevated streamline flows over the obstacle, dips down behind, and stagnates on the surface at the end of the recirculating cavity immediately downwind of the building.

Sometimes separation streamlines from the forward building edges reattach to the same face, yet in other cases the streamlines enter the downwind cavity and mingle with the other recirculating fluid. Air which enters the cavity departs through turbulent mixing across the dividing streamlines, mingles with downwind-pointing vortices and is ejected laterally out of the cavity, or leaves suddenly during an exhalation when the entire cavity appears to collapse and then reform.

When a building is oriented obliquely to the wind, flow over the front side walls does not separate, but strong recirculation occurs on the downwind faces. Flow over the roof often produces counter-rotating "delta-wing" vortices which increase mixing over the top and in the wake of the building. These vortices can cause reattachment of the flow in the middle of the roof and serious plume downwash in the near wake. Other features of the flow near the building include vertical vortices produced by the vertical corners of the building.

Golden (1961) measured the concentration patterns above the roof of model cubes in a wind tunnel. Two sizes of cubes were used to vary the Reynolds number from 1000 to 94,000. The concentration isopleths in the fluid above the cube roof showed only slight variations over the entire range of Reynolds numbers studied. The maximum concentration on the roof itself was found to vary strongly with Reynolds numbers less than 11,000, but to be invariant with Reynolds numbers between 11,000 and 94,000. Frequently, modelers quote Golden's experiments as justification for presuming dispersion invariance when obstacle Reynolds numbers exceed 11,000. However, Golden's "11,000 rule" is limited to the measurement of concentrations at only one point on the roof of smooth-walled cubes placed in a uniform approach flow of very low turbulent intensity. It is probably quite conservative because the shear and high turbulence in a simulated atmospheric boundary layer are likely to further reduce the critical Reynolds number. Indeed, Halitsky (1968) observed that for dispersion in the wake region, no change in isoconcentration isopleths from passive gas releases was found to occur for values of Reynolds number as low as 3300.

Flow around sharp-edged obstacles will remain kinematically similar at very low Reynolds numbers. Wake width variation will be minimal, and obstacle generated turbulence scales and intensity will only vary slowly as Reynolds number decreases. Gas clouds dispersing in this environment will remain similar at very low model speeds.

Simulation of flow over rounded obstacles:

Flow around a smooth cylinder is Reynolds number dependent. This dependence reflects changes in the nature of the boundary layer that forms over the cylinder and its behavior in the vicinity of the flow separation. At low Reynolds numbers, the boundary layer is laminar, and separation occurs easily under the influence of even modest positive pressure gradients. At higher Reynolds numbers, the boundary layer becomes turbulent and flow separation is delayed; i.e., the flow can

move farther along a curved surface without separation. At prototype scales, obstacles are large enough that only turbulent separation occurs. However, model flows are usually at such low Reynolds numbers that the local boundary layer growing over a curved surface would be laminar. Most modelers attempt the reproduction of full- scale similarity around curved surfaces by artificially roughening the model surface to force transition to turbulence in these laminar boundary layers. This can be done by providing the surface with special (or artificial) roughness elements, for example, sandpaper, thin wires, or grooves. The height of the roughness, k, should be such that $Uk/\nu > 400$ and $k/R < 0.01$, where U is the mean wind speed at obstacle height, and R is the characteristic obstacle radius of curvature. Szechenyi (1975) studied flows about rough circular cylinders and determined that as Reynolds number decreases, roughening the surface becomes less effective. Fage and Warsap (1929) considered the effect of increasing the surface roughness of cylinders on their drag coefficient. Eventually, even ridiculously large roughness is ineffective.

Niemann and Ruhwedel (1980) compared pressures and forces about a 1:333 scale model to a full-scale hyperbolic cooling tower shell. They roughened their model with vertical ribs of height 0.09 mm and width 0.77 mm, producing a roughness coefficient of $k/2R = 0.0006$ and roughness Reynolds number, $Re_k > 270$. They found meridional forces on the cooling tower model and prototype were similar. Model Reynolds numbers were between $4.5*10^5$ and $6.0*10^6$, and this corresponding to $U_m > 45$ m/s. But again these speeds are much higher than is appropriate for current measurements.

Halitsky et al. (1963) examined dispersion about a smooth-model nuclear reactor containment building (a hemisphere fitted on a vertical cylinder) and found a critical Reynolds number greater than 79,000. (Yet this critical Reynolds number was for flow very close to the vessel wall. The behavior of concentration isopleths further downwind is likely to be less Reynolds number dependent.)

Although the details of fluid motions around rounded obstacles vary significantly with Reynolds number, the gross features of the flow do not change. Even small models at low wind speeds will produce horseshoe-shaped ground vortices, elevated pairs, and regular vortex shedding. If the internal boundary layer over the obstacle is laminar, then the wake region will be broader and less intense.

3.2 Performance of Prior Fluid Modeling Experiments

A number of studies have been performed in the Colorado State University Fluid Dynamics and Diffusion Laboratory to establish the effect of buildings and meteorological masts on flow fields. Hatcher et al. (1977) examined flow and dispersion in stratified flow downwind of the Experimental Organic Cooled Reactor, Idaho Falls; Allwine et al. (1978) studied the Rancho Seco Reactor,

Sacramento; Kothari et al. (1979) studied the Duane Arnold Energy Center, Iowa. In each case field measurements were compared to laboratory measurements with good agreement. Specific effects of the structure of a meteorological mast on instrumentation response were reported by Hsi and Cermak (1965).

4 PHYSICAL MODEL OF PLUME MOTION

In addition to modeling the turbulent structure of the atmosphere in the vicinity of a test site it is necessary to properly scale the plume source conditions. One approach would be to follow the methodology used in Section 1; i.e., writing the conservation statements for the combined flow system followed by fractional analysis to find the governing parameters. An alternative approach, the one which will be used here, is that of similitude (Kline, 1965). The method of similitude obtains scaling parameters by reasoning that the mass ratios, force ratios, energy ratios, and property ratios should be equal for both model and prototype. When one considers the dynamics of gaseous plume behavior the following nondimensional parameters of importance are identified (Halitsky, 1969; Skinner and Ludwig, 1978; Synder, 1981)[1].

$$\text{Mass Flux Ratio } (M) = \frac{\text{mass flow of plume}}{\text{effective mass flow of air}} = \frac{(\rho WA)_g}{(\rho UA)_a} = \frac{\underline{\text{at the source}}\ \rho_s Q}{\rho_a U_a L^2}$$

$$\text{Momentum Ratio } (F) = \frac{\text{inertia of plume}}{\text{effective inertia of air}} = \frac{(\rho W^2 A)_g}{(\rho U^2 A)_a} = \frac{\rho_s Q^2}{\rho_a U_a^2 L^4}$$

$$\text{Densimetric Froude No. relative to the inertia of air } (\mathrm{Fr}) = \frac{\text{effective inertia of air}}{\text{buoyancy of plume}} = \frac{(\rho U^2 A)_a}{g(\rho_g - \rho_a)V_g} = \frac{U_a^2}{Lg(\rho_s - \rho_a)/\rho_a}$$

$$\text{Densimetric Froude No. relative to inertia of the plume } (\mathrm{Fr}_s) = \frac{\text{inertia of plume}}{\text{buoyancy of plume}} = \frac{(\rho W^2 A)_g}{g(\rho_g - \rho_a)V_g} = \frac{Q^2}{L^5 g(\rho_s - \rho_a)/\rho_a}$$

[1] The scaling of plume Reynolds number is also a significant parameter. Its effects are invariant over a large range. This makes it possible to accurately model its influence by maintaining model tests above a minimum plume Reynolds number requirement.

$$\text{Flux Froude No. } (Fr_{flux}) = \frac{\text{momentum flux of air}}{\text{buoyancy momentum flux of plume}} = \frac{(\rho U^2 A)_a}{Qg(\rho_g-\rho_a)(L/U_a)} = \frac{U_a^3 L}{Qg(\rho_g-\rho_a)/\rho_a}$$

$$\text{Volume Flux Ratio } (V) = \frac{\text{volume flow of plume}}{\text{effective volume flow of air}} = \frac{(WA)_g}{(UA)_a} = \frac{Q}{U_a L^2}$$

It is necessary to maintain equality of the plume's specific gravity, ρ_g/ρ_a, over the plume's entire lifetime to obtain simultaneous simulation of all of these parameters. Unfortunately a requirement for equality of the plume gas specific gravity for plume with significant buoyancy differences (i.e. ρ_g not equal ρ_a) leads to several complications in practice. These are:

1) Equality of the source gas specific gravity between a model and its atmospheric equivalent leads to a wind speed scaling from $(U_m/U_p)^2 = L_m/L_p$. For a significant range of atmospheric wind speeds this relationship leads to wind- tunnel speeds at which there is a possible loss of the Reynolds number invariance in the approach flow.

2) A thermal plume in the atmosphere is frequently simulated in the laboratory by an isothermal plume formed from a gas of appropriate molecular weight. Under certain situations of specific heat capacity mismatch, this practice will lead to a variation of the equality of plume density as the plume mixes with air.

It is important to examine each modeling situation and decide if an approximation to complete plume behavior may be employed without a significant loss in the similarity of the modeled plume structure.

5 REFERENCES

Allwine, K. J., Meroney, R. N., and Peterka, J. A. (1978), "Rancho Seco Building Wake Effects on Atmospheric Diffusion: Simulation in a Meteorological Wind Tunnel," FDDL Report No. CER77-78KJA-RNM-JAP25, Colorado State University, Fort Collins, Colorado.

Arya, S. P. S., and Plate, E. J. (1969), "Modeling of the Stably Stratified Atmospheric Boundary Layer," J. Atmos. Sci., Vol. 26, No. 4, pp. 656-665.

Ayra, S. P. S. (1975), "Buoyancy Effects in a Horizontal Flat-Plate Boundary Layer," J. Fluid Mech., Vol. 68, Pt. 2, pp. 321-343.

Barad, M. L., Ed. (1958), Project Prairie Grass: A Field Program in Diffusion, Geophysical Research Papers, No. 59, Vols. I and II, Report AFCRC-TR-58-235, Air Force Cambridge Research Center.

Brunn, (1978), "Multi-Probes and Higher Moments," Proceedings of the Dynamic Flow Conference 1978, pp. 943-961.

Cermak, J. E. (1975), "Applications of Fluid Mechanics to Wind Engineering--A Freeman Scholar Lecture," J. of Fluids Engineering, Vol. 97, pp. 9-38.

Cermak, J. E., Shrivastava, P. K., and Poreh, M. (1983), "wind-tunnel Research on the Mechanics of Plumes in the Atmospheric Surface Layer," Civil Engineering Department Report CER83-84JEC-PKS-MP12, Colorado State University, Fort Collins, CO, Annual Progress Report to U.S. Dept. of Army Contract DAAK11-82-K-0004, 140 pp.

Chaudhry, F. H. and Meroney, R. N. (1973), "A Laboratory Study of Diffusion in Stably Stratified Flow," Atmos. Envir., Vol. 7, pp. 443-454. Chien, H. C., Meroney, R. N., and Sandborn, V. A. (1979), "Sites for Wind-Power Installations: Physical Modeling of the Wind Field Over Kahuku Point, Hawaii," FDDL Report No. CER79-80HCC-RNM-VAS25, Colorado State University, Fort Collins, Colorado.

Chien, Meroney, R. N. and Sandborn (1979), "Sites for Wind-Power Installations: Physical Modeling of the Wind Field Over Kahuku Point, Hawaii," FDDL Report No. CER79-80HCC-RNM-VAS25, Colorado State University, Fort Collins, Colorado.

Fage, A. and Warsap, J. H. (1929), "Effects of Turbulence and Surface Roughness on Drag of Circular Cylinders," U.K., ARC R&M 1283.

Farell, C., Carrasquel, S., Guven, O., and Patel, V. C. (1977), "Effect of Wind-Tunnel Walls on the Flow Past Circular Cylinders and Cooling Tower Models," J. of Fluids Engineering, Vol. 99, pp. 470-479.

Golden, J. (1961), "Scale Model Techniques," M.S. Thesis, Dept. of Met. and Ocean., New York University, 42 pp.

Halitsky, J., Colden, J., Halpern, P., and Wu, P. (1963), "Wind Tunnel Tests of Gas Diffusion from a Leak in the Shell of a Nuclear Power Reactor and from a Nearby Stack," N.Y.U. Meteorol. and Oceanog. Geophys. Sciences Lab. Report 63-2 (New York Univ., College of Engineering, New York.)

Halitsky, J. (1968), "Gas Diffusion Near Buildings," Meteorology and Atomic Energy, 1968, editor D. H. Slade, Atomic Energy Commission, Ch. 5-5, pp. 221-256.

Halitsky, J. (1969), "Validation of Scaling Procedures for Wind Tunnel Model Testing of Diffusion Near Buildings," Geophysical Sciences Laboratory, Report No. TR-69-8, New York University, New York.

Hatcher, R. V. and Meroney, R. N. (1977), "Dispersion in the Wake of a Model Industrial Complex," Joint Conf. on Applications of Air Pollution Meteorology, Proceedings, Am. Meteorol. Sco., Salt Lake City, Utah, 29 November - 2 December, 1977, pp. 343-346.

Haugen, D. A., Kaimal, J. C., and Bradley, E. F. (1971), "an Experimental Study of Reynolds Stress and Heat Flux in the Atmospheric Surface Layer," Quart. J. Roy. Meteorol. Soc., Vol. 97, pp. 168-180.

Hinze, J. O. (1975), Turbulence, McGraw-Hill, New York, 2nd. edition, 790 pp.

Horst, T. W. (1979), "Lagrangian Similarity Modeling of Vertical Diffusion from a Ground Level Source," J. Appl. Meteorol., Vol. 18, pp. 733-740.

Hosker, R. P., Jr. (1984), "Flow and Diffusion Near Obstacles," Atmospheric Science and Power Production, DOE/TIC-27601, pp. 241-326.

Hsi, G., and Cermak, J. E. (1965), "Meteorological-Tower Induced Wind Field Perturbations," Prepared under U.S. Army Research Grant DA-AMC-28-043-64-G-9, Fluid Mechanics Program Report No. CER65GH-JEC49, Colorado State University, Fort Collins, Colorado.

Hunt, J. C. R. (1974), "Wakes Behind Buildings," presented at the Aeronautical Research Council's Atmospheric Environment Committee Meeting, Oct. 23, ARC Report 35601, Atmos. 229, Aeronautical Research Council of Great Britain, Her Majesty's Stationery Office, London.

Islitzer, N. F. and Dumbauld, R. K. (1963), "Atmospheric Diffusion Deposition Studies over Flat Terrain," INt. J. Air Water Pollut., Vol. 7 (11-12), pp. 999-1022.

Kline, S. J. (1965), Similitude and Approximation Theory, McGraw-Hill Book Company, New York, 229 pp.

Kothari, K. M., Meroney, R. N., Bouwmeester, (1981), "An Algorithm to Estimate Field Concentrations Under Nonsteady Meteorological Conditions from Wind Tunnel Experiments," Jornal of Applied Meteorology, Vol. 30, pp. 92-101.

Kothari, K. M., Meroney, R. N. and Peterka, J. A. (1979), "Nuclear Power Plant Building Works Effects on Atmosphere Diffusion," EPRI Report No. 1891, CER79-80KMK-RNM-JAP28, 109 pp.

Lamb, R. G. (1982), "Diffusion in the Convective Boundary Layer," Chapter 5, Atmospheric Turbulence and Air Pollution Modeling, Nieuwstadt and van Dop, editors, D. Reidel Publishing Company, Dordrecht, Holland, pp. 159-230.

Meroney, R. N. (1980), "Wind-Tunnel Simulations of the Flow Over Hills and Complex Terrain," J. of Industrial Aerodynamics, Vol. 5, pp. 297-321.

Meroney, R. N. (1982), "Turbulent Diffusion Near Buildings," Engineering Meteorology, Chapter 11, pp. 481-521.

Meroney, R. N., Cermak, J. E., and Garrison, J. A. (1975a), "Wind-Tunnel Study of Stack Gas Dispersal at Lansing Power Station, Units 1, 2, 3, and 4," FDDL Report No. CER74-75RNM-JEC-JAG28, Colorado State University, Fort Collins, Colorado.

Meroney, R. N., Cermak, J. E., and Garrison, J. A. (1975b), "Wind-Tunnel Study of Stack Gas Dispersal at Lansing Power Station, Units 1, 2, 3, and 4," FDDL Report No. CER74-75RNM-JEC-JAG29, Colorado State University, Fort Collins, Colorado.

Meroney, R. N., Sandborn, V. A., Bouwmeester, R. J. B., Chien, H. C., and Rider, M. (1978), "Sites for Wind-Power Installations: Physical Modeling of the Influence of Hills, Ridges and Complex Terrain - Part II: Executive Summary," Dept. of Energy Report RLO/2438-77/3, 90 pp.

Niemann, H. J. and Ruhwedel, J. (1980), "Full-scale and Model Tests on Wind-induced, Static and Dynamic Stresses in Cooling Tower Shells," Eng. Struct., Vol. 2, pp. 81-89.

Peterka, J. A., Meroney, R. N. and Kothari, K. (1985), "Wind Flow Patterns About Buildings," J. of Wind Engineering and Industrial Aerodynamics, Vol. 21, pp. 21-38.

Poreh, M. and Cermak, J. E. (1984), "Wind Tunnel Research on the Mechanics of Plumes in the Atmospheric Surface Layer, Part II," Annual Report to U.S. Dept. of Army, Chemical Systems Laboratory, Aberdeen Proving Ground, Maryland, Colorado State University Civil Engineering Department Report CER84-85MP-JEC47, 45 pp.

Poreh, M. and Cermak, J. E. (1985), "Study of Neutrally Buoyant Plumes in a Convective Boundary Layer with Mean Velocity and Shear," Symposium on Turbulence and Diffusion, Nov. 12-15, 1985, Boulder, Colorado, pp 119-122.

Ranga Raju, K. G. and Singh, V. (1976), "Blockage Effects on Drag of Sharp Edged Bodies," J. of Industrial Aerodynamics, Vol. 1, pp. 301-309.

Schon, J. P. and Mery, P. (1971), "A Preliminary Study of the Simulation of Neutral Atmospheric Boundary Layer Using Air Injection in a Wind Tunnel," Atmos. Enviro., Vol. 5, No. 5, pp. 299-312.

Sethuraman, S., and Cermak, J. E. (1973), "Stratified Shear Flows Over a Simulated Three-Dimensional Urban Heat Island," Project Themis Technical Report No. 23, CER73-74SS-JEC4, Colorado State University, Fort Collins, Colorado.

Skinner, G. T. and Ludwig, G. R. (1978), "Physical Modeling of Dispersion in the Atmospheric Boundary Layer," Calspan Advanced Technology Center, Calspan Report No. 201, May.

Snyder, W. H. (1981), "Guidelines for Fluid Modeling of Atmospheric Diffusion," EPA Report EPA-600/8-81-009, 185 pp.

Szechenyi, E. (1975), "Supercritical Reynolds Number Simulation for Two dimensional Flow over Circular Cylinders," J. Fluid Mech., Vol. 70, pp. 529-542.

Willis, G. E. and Deardorff, J. W. (1974), "A Laboratory Model of the Unstable Planetary Boundary Layer," J. Atmos. Sci., Vol. 31, pp. 1297-1307.

Willis, G. E. and Deardorff, J. W. (1976), "A Laboratory Model of Diffusion into the Convective Planetary Boundary Layer," Quart. J. Roy. Meteorol. Soc., Vol. 102, pp. 427-445.

Willis, G. E. and Deardorff, J. W. (1978), "A Laboratory Study of Dispersion from an Elevated Source Within a Modeled Convective Planetary Boundary Layer," Atmos. Envir., Vol. 12, pp. 1305-1311.

Yamada, T. and Meroney, R. N. (1971). "Numerical and Wind-Tunnel Simulation of Response of Stratified Shear Layers to Nonhomogeneous Surface Features," CER7071TY-RNM62, Colorado State University, also (AD-730-953).

6 NOMENCLATURE FOR APPENDIX

A,B,C	Constants
BR	Blockage ratio
C_p	Specific heat capacity at constant pressure
h	Height of the obstacle
g	Gravitational acceleration
k	Roughness length
L	Length
Q	Flow rate
S	Distance downstream of the obstacle
T	Temperature
U	Wind velocity
u_*	Friction velocity
x	Distance
Z	Height above ground
z_o	Roughness length

Greek Characters

ρ	Air density
Γ	Abiabatic potential temperature lapse rate
κ	Thermal conductivity
μ	Dynamic viscosity
ν	Kinematic viscosity
ρ	Density
χ	Fraction of a gas component
Ω	Angular velocity of earth - $0.726*10^{-4}$ rad/s

Dimensionless Parameters

Ec	Eckert number
Ma	Mach number
Re	Reynolds number
Ri	Bulk Richardson number
Ro	Rossby number
Pr	Prandtl number
V	Volume flux ratio ($Q/U_H L^2$)